Volume 8, Number 4

Special Issue: University of Miami Workshop
on High-Temperature Superconductivity,
Part I of II

August 1995

JOUSEH 8(4) 391–534 (1995)

ISSN 0896-1107

Journal of Superconductivity

PLENUM PRESS • New York and London

DISCLAIMER NOTICE

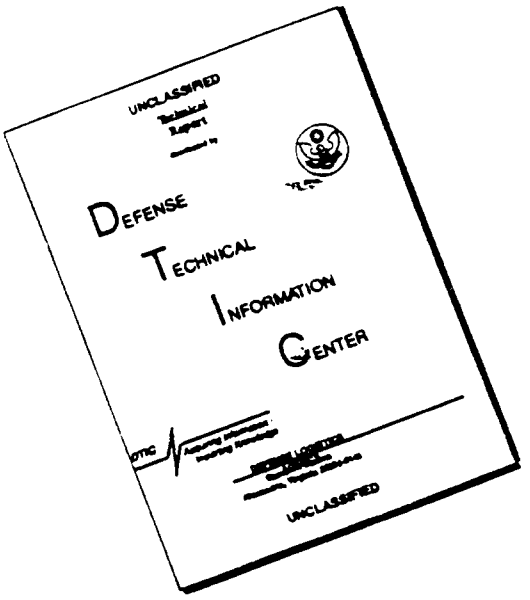

THIS DOCUMENT IS BEST QUALITY AVAILABLE. THE COPY FURNISHED TO DTIC CONTAINED A SIGNIFICANT NUMBER OF PAGES WHICH DO NOT REPRODUCE LEGIBLY.

JOURNAL OF SUPERCONDUCTIVITY

Journal of Superconductivity is an international forum for the publication of high-quality, peer-reviewed original papers and review articles on *all* aspects of the **science** and **technology** of superconductivity. *Journal of Superconductivity* is devoted *solely* to this subject area, publishing papers and reviews on significant developments in the field of superconductivity—both basic research and applications. Topics include (but are not limited to): new materials, new mechanisms, new phenomena, basic properties, technological properties, and small-scale and large-scale applications.

Journal of Superconductivity is published bimonthly at 71 Winterstoke Road, Bristol BS3 2NT, England, by Plenum Publishing Corporation, 233 Spring Street, New York, N.Y. 10013. In 1995, Volume 8 (6 issues) will be published. *Journal of Superconductivity* is abstracted or indexed in Automatic Subject Citation Alert, Cambridge Scientific Abstracts, Chemical Abstracts, Current Contents, High Temperature Superconductors, Metals Abstracts, Science Citation Index, Scisearch, and World Aluminum Abstracts.

Journal of Superconductivity participates in the Copyright Clearance Center (CCC) Transactional Reporting Service. The appearance of a code line at the bottom of the first page of an article in this journal indicates the copyright owner's consent that copies of the article may be made for personal or internal use. However, this consent is given on the condition that the copier pay the flat fee of $7.50 per copy per article (no additional per-page fees) directly to the Copyright Clearance Center, Inc., 222 Rosewood Drive, Danvers, Massachusetts 01923, for all copying not explicitly permitted by Sections 107 or 108 of the U.S. Copyright Law. The CCC is a nonprofit clearinghouse for the payment of photocopying fees by libraries and other users registered with CCC. Therefore, this consent does not extend to other kinds of copying, such as copying for general distribution, for advertising or promotional purposes, for creating new collective works, or for resale, nor to the reprinting of figures, tables, and text excerpts. 0896-1107/95 $7.50

Advertising inquiries should be addressed to Advertising Sales, Plenum Publishing Corporation, 233 Spring Street, New York, N.Y. 10013—telephone (212) 620-8495 and fax (212) 647-1898.

Subscription inquiries and subscription orders should be addressed to the publisher at Subscription Department, Plenum Publishing Corporation, 233 Spring Street, New York, N.Y. 10013 or faxed to the Subscription Department at its number (212) 807-1047, or may be telephoned to the Subscription Department's Journal Customer Service at (212) 620-8468, -8470, -8472, or -8082. Subscription rates:
Volume 8, 1995 (6 issues) $295.00 (outside the U.S., $345.00).

Second-class postage paid at Jamaica, N.Y. 11431. Postmaster: Send address changes to *Journal of Superconductivity*, Plenum Publishing Corporation, 233 Spring Street, New York, N.Y. 10013. Air freight and mailing in the USA by Publications Expediting, Inc., 200 Meacham Avenue, Elmont, N.Y. 11003.

Printed in Great Britain.

JOURNAL OF SUPERCONDUCTIVITY

Volume 8, Number 4 **August 1995**

Special Issue: University of Miami Workshop on High-Temperature Superconductivity, Part I of II

CONTENTS

University of Miami Workshop on High-Temperature Superconductivity:

Physical Properties and Mechanisms

Coral Gables, FL
January 5-11, 1995

Edited By:

J. Ashkenazi, S. E. Barnes, J. L. Cohn, F. Zuo
University of Miami
Coral Gables, FL

Sponsored by:

Office of Naval Research (Grant No. N00014-95-1-0273),
University of Miami

Journal of Superconductivity, Vol. 8, No. 4, 1995

δ-Influence on the Pressure-Effect on T_c of $HgBa_2CuO_{4+\delta}$ and the Inverse Parabolic T_c-Relation

C. W. Chu,[1] Y. Cao,[1] Q. Xiong,[1] and Y. Y. Xue[1]

Received 5 January 1995

We have observed a δ-independent linear pressure effect on T_c of $HgBa_2CuO_{4+\delta}$ under hydrostatic pressures up to 1.7 GPa for $\delta \leq 0.30$ but a nonlinear effect for $\delta > 0.30$. These results, together with previous doping data, show a possible non-rigidity of the electron bands of the compounds, based on which previous phenomenological models of the pressure effect on T_c are built, and thus suggest only a restricted universality for the inverse parabolic relation between T_c and charge carriers per CuO_2-layer. In other words, factors in addition to charge carriers can affect high temperature superconductivity.

KEY WORDS: high temperature superconductivity, pressure effect

1. INTRODUCTION

Immediately after the discovery of high temperature superconductivity (HTSy), extensive efforts were devoted to the search for systematic trends of the evolution of HTSy with various physical parameters. These trends form a useful basis for the development of a comprehensive microscopic theory of HTSy and for the continued quest for high temperature superconductors (HTSr's) with a higher transition temperature (T_c). One of the trends observed in the layered cuprates is the universal relationship between T_c and the number of charge carriers per CuO_2-layer (n). It is known as the inverse parabolic universal relation [1] $T_c(n) = T_c^{max}[1-a(n-n_{op})^2]$, where T_c^{max} is the maximum T_c of the cuprate with an optimal n (n_{op}). In other words, HTSy occurs only over a limited doping region for $(n_{op} - 1/\sqrt{a}) < n < (n_{op} + 1/\sqrt{a})$. Compounds with $n < n_{op}$ are known as underdoped, $n > n_{op}$ as overdoped and $n = n_{op}$ as optimally doped. The $T_c(n)$ above with constants $a = 82.6$ and $n_{op} = 0.16$ describes a wide variety of high temperature superconducting (HTSg) compounds systems examined [1] and therefore has been considered universal [1].

High pressure has been employed extensively [2] to obtain information about the occurrence of HTSy and to provide tests and to impose constraints on the universal T_c-relations and HTSy models. Most of the experiments were made on optimally doped compounds with a small but non-negligible pressure effect on their T_c (dT_c/dP). Only a few were done on non-optimally doped samples. The results can be described by the phenomenological model on $T_c(P)$ based on the combined pressure effects on n [3] and T_c^{max} [4], which give rise to an ever-decreasing dT_c/dP with increasing n due to the former effect superimposed on a constant dT_c^{max}/dP, consistent with the inverse parabolic universal relation $T_c(n)$ [1]. Unfortunately, the large ultrahigh pressure-induced T_c-enhancement detected [5] in $HgBa_2Ca_{m-1}Cu_mO_{2m+2+\delta}$ [Hg-12(m--1)m] is too large to be accounted for by the phenomenological model on $T_c(P)$ [3,4].

Recently, a large T_c-variation was achieved [6] in the newly discovered $HgBa_2CuO_{4+\delta}$ (Hg-1201) by anion-doping only without introducing possible chemical complications [7] by the combined cation- and anion-dopings adopted usually to acquire the similarly large T_c-change in other HTSg-system. The T_c of Hg-1201 varies with δ as $T_c(\delta) = 97[1-26(\delta-0.22)^2]$ throughout the doping range of $0.03 \leq \delta \leq 0.4$ examined. In contrast to the expected similar parabolic relation of $T_c(n)$ over the same δ-range due to the usual linear dependence of n on δ, such a behavior was observed [6] only over a limited range of $\delta \leq 0.3$, *i.e.* $T_c(n) = 97[1-50(n-0.16)^2]$, for $0.02 \leq n \leq 0.23$ only. The deviation of $T_c(n)$ from the parabolic

1. Department of Physics and Texas Center for Superconductivity at the University of Houston, Houston, Texas 77204-5932

0896-1107/95/0800-0393$07.50/0

dependence has been attributed to the possible new oxygen site being filled at high δ. It should be noted that n here was determined from the thermoelectric power measurements as was previously done [1]. Although the n_{op} = 0.16 for Hg-1201 is the same as for other HTSg compound systems, superconductivity takes place at a lower n ~ 0.02 in Hg-1201 than that of ~ 0.05 according to the universal inverse parabolic T_c(n)-relation.

We have therefore tested the universal T_c(n) proposed by investigating the δ-dependence of the hydrostatic pressure effect on T_c of Hg-1201 with 0.07 ≤ δ ≤ 0.39 up to 1.7 GPa. We find a constant linear pressure effect on T_c for δ < 0.30 and a nonlinear effect for δ ≥ 0.30. The results raise questions concerning the universality of the inverse parabolic T_c(n)-relation [1] and the phenomenological T_c(P)-models [3,4]. The results suggest that the dopant affects T_c through channels in addition to varying n, and that the electron-bands of HTSr's may be less rigid than previously thought. Some of the results to be discussed have been recently submitted for publication elsewhere [8].

2. EXPERIMENTAL

The Hg-1201 samples investigated here were prepared by the controlled solid-vapor reaction technique [9]. The excess oxygen content δ was varied by annealing the Hg-1201 compound at a temperature between 240° and 500° C in an oxygen atmosphere of pressure ranging from 10^{-8} to 500 bar. Detailed sample synthesis steps to achieve various dopings have been published previously [6].

The structure and phase purity were characterized by powder X-ray diffraction, employing a Rigaku D-MAX/BIII diffractometer. The T_c at ambient was determined both resistively by the four-lead method using a Linear Research LR-400 bridge, and magnetically using a Quantum Design SQUID magnetometer. Under pressure, the T_c was measured mostly resistively and for a few by the ac susceptibility technique. The hydrostatic pressure environment was generated by the modified Be-Cu clamp technique [10] inside a Teflon cup using the 3M fluorinert as the pressure medium. The pressure was measured with a superconducting Pb-manometer situated next to the sample inside the Teflon cell and the temperature by a chromel-alumel thermocouple above 30 K or a Ge-thermometer below 30 K.

3. RESULTS AND DISCUSSION

All Hg-1201 samples investigated are single-phase within the resolution of ~ 4% of our X-ray diffraction. The superconducting transition is narrow for the optimally doped sample with a width of ~ 1 K° and is broadened with a width of ~ 10 K° for the heavily underdoped sample, or ~ 5 K° for the heavily overdoped sample. The midpoint transition temperature (T_c), where the resistivity drops by 50% during the transition, is shown as a function of δ in Fig. 1. The value of δ is determined according to the T_c(δ)-curve previously obtained [6], once the T_c is measured.

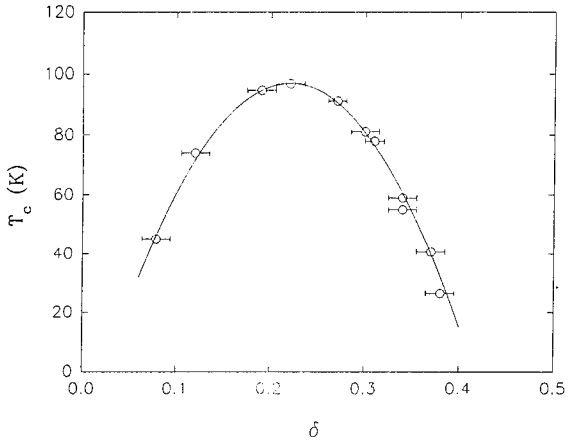

Fig. 1. T_c(δ) for the Hg-1201 examined.

Under pressure, the superconducting transition width increases slightly for the sample with $\delta = \delta_O$ = 0.22 but remains constant for those with δ ≠ 0.22. The onset, midpoint, and the offset temperatures of a sample respond to pressure in a similar general fashion. Therefore, we shall consider below only the pressure effect on the midpoint transition temperature T_c of the samples with different δ's. The results are summarized in Fig. 2a for the underdoped (Nos. 1-3) and the optimally doped (No. 4) samples, and in Fig. 2b for the overdoped ones (Nos. 5-11). The numbers in these figures stand for the sequential order of increasing δ in the samples. They are, respectively, 0.07, 0.12, 0.19, 0.22, 0.27, 0.30, 0.31, 0.34, 0.36, 0.37, and 0.39. It is evident that pressure enhances T_c linearly for samples with δ < 0.30 and that it affects T_c nonlinearly for those with δ ≥ 0.30. The data can be fitted as $T_c(P) = T_c(0) + \alpha P + \beta P^2$ and the linear pressure terms α and the quadratic pressure term β can be obtained. They are displayed in Figs. 3a and 3b for different δ's. α is a constant of 2.0±0.2 K/GPa for δ ≤ 0.27, decreases rapidly to 0 near δ = 0.30 and turns

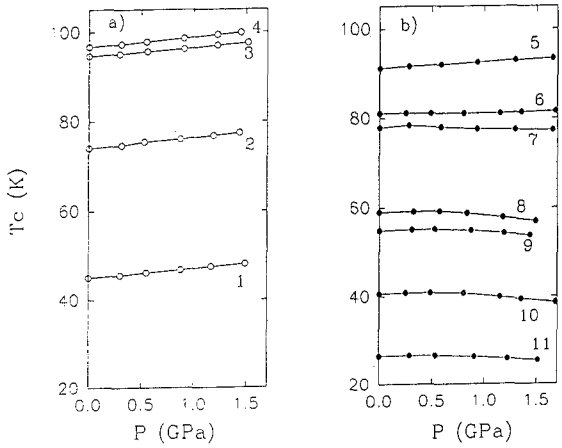

Fig. 2. $T_c(P)$ for Hg-1201: (a) underdoped (Nos. 1-3) and optimally doped (No. 4); and (b) overdoped (Nos. 5-11).

back to 1.0±0.2 K/GPa at $\delta \sim 0.33$ before it falls off again for $\delta > 0.33$. β is almost 0±0.02 K/GPa^2 for $\delta < 0.30$, starts to drop rapidly near $\delta \sim 0.30$ and decreases to 0 at -1.7±0.5 K/GPa^2 at $\delta = 0.33$ before it rises again. Clearly, both α and β exhibit a drastic change near $\delta \sim 0.3$.

According to a general inverse quadratic relation $T_c(n) = T_c^{max}[1-a(n-n_{op})^2]$, one obtains

$$dT_c/dP = [1-a(n-n_{op})^2](dT_c^{max}/dP) - T_c^{max}(n-n_{op})^2(da/dP) - 2aT_c^{max}(n-n_{op})(dn/dP) + 2aT_c^{max}(n-n_{op})(dn_{op}/dP) \quad (1)$$

where (dT_c^{max}/dP) represents the change in T_c^{max}, (da/dP) the change in the range for HTSy to occur, (dn/dP) the charge transfer, and (dn_{op}/dP) the change in n_{op}, all induced by pressure. By retaining only the (dn/dP)-term on the basis of a rigid band model, one obtains the familiar phenomenological model [3], *i.e.* $dT_c/dP = -2aT_c^{max}(n-n_{op})(dn/dP)$. It predicts a linearly n-dependent dT_c/dP which is positive for samples in the underdoped region, negative in the overdoped region, and zero for the optimally doped sample. The observed non-zero dT_c/dP for the optimally doped sample prompted the addition of a constant (dT_c^{max}/dP) term, which corresponds to the n-independent part of the (dT_c^{max}/dP)-term in Eq. (1), to the charge-transfer term and led to the modified phenomenological model [4], *i.e.* $dT_c/dP = dT_c^{max}/dP - 2aT_c^{max}(n-n_{op})(dn/dP)$. This models accounts for

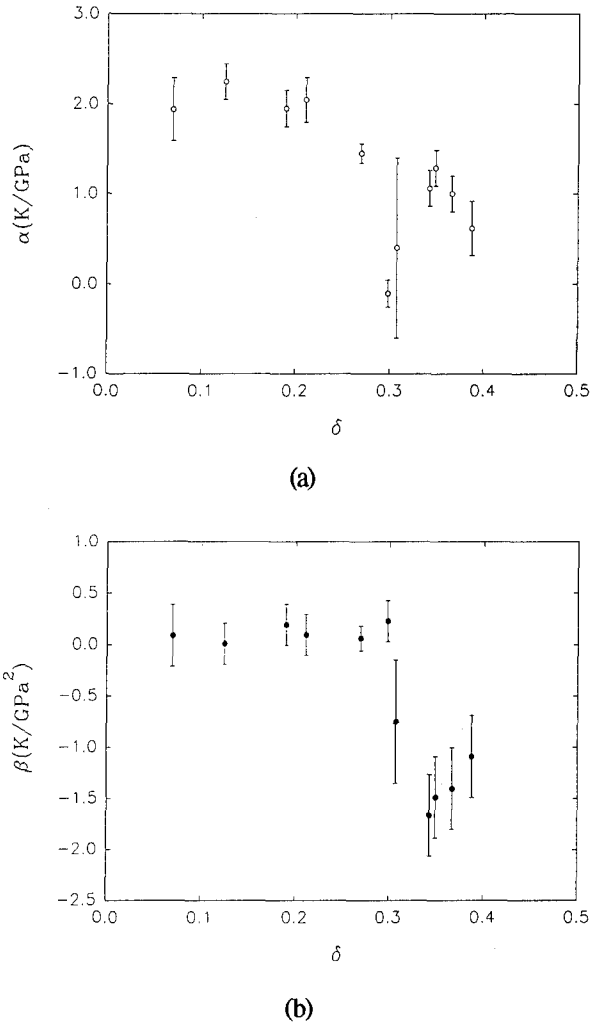

Fig. 3. The δ-effect on $T_c(P) = T_c(0) + \alpha P + \beta P^2$: (a) the linear pressure dependent term and (b) the quadratic pressure dependent term.

the non-zero dT_c/dP for the optimally doped HTSr's and the linearly n-dependent dT_c/dP in the original phenomenological model, as shown schematically in Fig. 4. Unfortunately, the model in either form cannot account for the δ (or n) dependence of dT_c/dP of Hg-1201, nor can it explain the large pressure induced T_c-enhancement observed in Hg-12(m-1)m under very high pressure [5].

From Eq. (1), we find the n-effect on dT_c/dP as

$$\partial(dT_c/dP)/\partial n = 2(n-n_{op})[-a(dT_c^{max}/dP) - T_c^{max}(da/dP)] - 2aT_c^{max}[(dn/dP) - (dn_{op}/dP)] \quad (2)$$

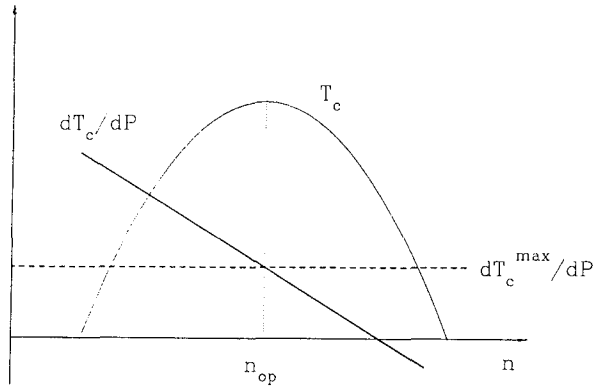

Fig. 5. The schematic n-dependence of dT_c/dP by the previous phenomenological models [3,4] based on the rigid inverse parabolic $T_c(n)$ relation [1] shown.

For Hg-1201, with $\delta < 0.30$, we observed $\partial(dT_c/dP)/\partial n = 0$. Therefore $(dn/dP) = (dn_{op}/dP)$ at $n = n_{op}$. This shows that n_{op} also shifts with pressure if the pressure induces a charge-transfer, giving rise to a non-zero dT_c/dP for an optimally doped HTSr. The pressure induced shifts in n_{op} and a imply that the electron bands of Hg-1201 and other members of the homologous series Hg-12(m-1)m (based on new data to be published [11]) are not rigid under pressures. The inverse parabolic relation itself may thus be valid only under a set of more restrictive conditions than originally envisioned.

The sudden change in α and β for samples with $\delta \sim 0.30$ (or $n \sim 0.22$) under pressure below 1.7 GPa coincides with the onset of deviation of $T_c(n)$ from the inverse parabolic-behavior. The deviation has been ascribed to the occupation of extra O-sites in addition to the usual O(3)-sites for the heavily doped samples [6]. Our recent oxygen effusion spectrum experiment [12] on heavily doped Hg-1201 and thermopower measurements [13] on an irradiation HTSr provide supporting evidence for the proposition. Hence, the observation suggests that the so-called charge-reservoir layers (which include HgO_δ in the present case) in HTSr may play roles additional to providing carriers.

ACKNOWLEDGMENTS

This work is supported in part by NSF Grant No. DMR 91-22043, USAFOSR Grant No. F49620-93-1-0310 by BMDO, EPRI, the State of Texas through the Texas Center for Superconductivity at the University of Houston, and the T. L. L. Temple Foundation.

REFERENCES

1. M. R. Presland *et al.*, Physica C 176, 95 (1991) and references therein; and T. Schneider and H. Keller, Phys. Rev. Lett. 69, 3374 (1993).
2. See, for example, J. S. Schilling and S. Klotz, in *Physical Properties of High Temperature Superconductors III*, ed. by D. M. Ginsberg (World Scientific, Singapore, 1992), p. 84.
3. N. Mori *et al.*, J. Phys. Soc. Jpn. 59, 3839 (1990); J. G. Lin *et al.* Physica C 175, 627 (1991); C. W. Chu *et al.*, *Frontiers of High Pressure Research*, ed. H. D. Hochheimer and R. D. Etters (Plenum Press, New York, 1991), p. 383; and R. J. Wijngaarden *et al.*, *ibid.*, p. 399.
4. J. J. Neumier and H. A. Zimmerman, Phys. Rev. B 47, 8386, (1993).
5. C. W. Chu *et al.*, Nature 365, 323 (1993); L. Gao *et al.*, Phys. Rev. B 50, 4260 (1994).
6. Q. Xiong *et al.*, Phys. Rev. B 50, 19346 (1994).
7. T. Egammi, Solid State Commun. 63, 1019 (1987).
8. Y. Cao *et al.*, submitted to Phys. Rev. B.
9. R. L. Meng *et al.*, Physica C 216, 21 (1993).
10. C. W. Chu, Phys. Rev. Lett. 33, 1283 (1974).
11. F. Chen *et al.*, to be published.
12. A. Hamed *et al.*, to be published.
13. F. Chen *et al.*, to be published.

Journal of Superconductivity, Vol. 8, No. 4, 1995

Antiparamagnon in d-wave superconductors

Hyekyung Won[1] and Kazumi Maki[2]

Received 31 January 1995

We have shown recently two dimensional *t-J* model gives an excellent description of dynamical spin fluctuation as seen by inelastic neutron scattering from $La_{1.86}Sr_{0.14}CuO_4$ by Mason et al and from $YBa_2Cu_3O_{6+x}$ by Rossat-Mignod et al. In this comparison d-wave superconductor is indispensable. Further the strong spin fluctuation (i.e. antiparamagnon) gives rise to almost T-linear resistance and large almost T-independent thermoelectric power as observed in high T_c cuprates.

KEY WORDS: Antiparamagnon, d-wave superconductor, inelastic neutron scattering

1. Introduction

Now an overwhelming number of experiments [1-6] appear to support the notion of d-wave superconductor in high T_c cuprates. Here we shall first review our theory on spin fluctuation within two dimensional *t-J* model [7]. We obtain the dynamical spin correlation function within RPA, which describes semi-quantitatively in terms of d-wave superconductor recent inelastic neutron scattering data both from $La_{1.86}Sr_{0.14}CuO_4$ (LSCO) by Mason et al [8] and $YBa_2Cu_3O_{6+x}$ (YBCO) by Rossat-Mignod et al [9]. More specifically a) for small chemical potential μ ($|\mu|<1.91\ T$), the antiparamagnon spectrum has a single peak at (π, π) (i.e. commensurate) while for larger chemical potential $|\mu|$ it becomes incommensurate with four separate peaks at $(\pi \pm q_o, \pi)$ and $(\pi, \pi \pm q_o)$. b) It is well known that the antiparamagnon in YBCO is commensurate while in LSCO it is incommensurate. So we may map both YBCO and LSCO to the *t-J* model with $-\mu \leq 200K$ and $-\mu \cong 435.5K$ respectively [7]. c) In the commensurate region $Im\chi(0, \omega)$ develops a spin gap $Eg=2|\mu|$ at low temperature, where $\vec{q}$ in $\chi(\vec{q}, \omega)$ is measured from $\vec{Q} = (\pi, \pi)$. d) In the incommensurate region $Im\chi(\vec{q}, \omega)$ has the gapless region, which includes the edge of square formed by connecting four incommensurate peaks $(\pm q_o, 0)$ and $(0, \pm q_o)$. Therefore our theory not only gives natural interpretation of the spin gap observed in YBCO, but also describes large spin scattering seen in LSCO at $T=4K$. On the contrary s-wave superconductor gives spin gap Eg larger than $2\Delta(0)$ irrespectively whether the antiparamagnon is commensurate or incommensurate resulting in too large energy gap in YBCO and no spin scattering in LSCO at low temperatures.

2. Dynamic Spin Susceptibility

Following Tanomoto et al [10] let us consider the *t-J* model. However unlike [10], we assume that the non-double occupancy condition simply renormalizes t the transfer integral. Then the dynamical spin susceptibility is given by

$$\chi(\vec{q}, \omega) = \chi_o(\vec{q}, \omega)\left(1 + J(\vec{Q}+\vec{q})\,\chi_o(\vec{q}, \omega)\right)^{-1} \quad (1)$$

where

$$\begin{aligned} J(\vec{Q}+\vec{q}) &= J(\cos(\pi + q_x) + \cos(\pi + q_y)) \\ &= -J(\cos q_x + \cos q_y) \end{aligned} \quad (2)$$

and $\chi_o(\vec{q}, \omega)$ is obtained as [7]

$$\chi_o(q, \omega) = 2N_0[\Lambda_s - F(\vec{q}, \omega)] \quad (3)$$

$$\Lambda_s = \begin{cases} \ln\dfrac{(8\gamma|t|)}{\pi T} & \text{for } T > T_c \\ \displaystyle\int_0^{4|t|} dE \left\langle JRe\frac{1}{\sqrt{E^2 - \Delta^2|f|^2}}\right\rangle \tanh\left(\frac{\beta}{2}E\right)/\langle J\rangle & \end{cases} \quad (4)$$

and

$$F = \left\langle J\frac{\eta^2 - \frac{1}{4}\omega^2}{\Delta^2|f|^2} f(\eta, \omega)\right\rangle / \langle J\rangle \quad (5)$$

and $f(\eta, \omega)$ is the generalized superfluid density [11] and

[1]Physics Department Hallym University, Chunchon 200-702, South-Korea
[2]Department of Physics & Astronomy, University of Southern California, Los Angeles, CA 90089-0484

0896-1107/95/0800-0397$07.50/0

$\langle\cdots\rangle$ means average over ϕ and

$$\eta = 2t\left(\sin\left(\frac{1}{2}q_x\right) \pm \sin\left(\frac{1}{2}q_y\right)\right)\sin(2\phi) - \mu \qquad (6)$$
$$f = \cos(2\phi)$$

and

$$J = \left(1 - \left(\frac{1+\mu/4t}{1-\mu/4t}\right)^2 \cos^2(2\phi)\right)^{-\frac{1}{2}} \qquad (7)$$

and η is the parameter describing the degree of imperfect nesting and +sign in Eq (6) has to be taken in the first and third quadrant while -sign in the second and forth in the k_x-k_y plane. Here J in Eq (7) is the Jacobian, which was put to unity in [7]. Though the Jacobian is not so important in t-J model, it will play more important role in t-t'-J model. In the following analysis we take the renormalized value of t as t=50 *meV* consistent with specific heat data [11]. In the normal state $T \geq T_c$, Eq (5) is further simplified as

$$F(\hat{q}, \omega) = \frac{1}{2}\langle J\left[\psi\left(\frac{1}{2} + \frac{i\left(\eta + \frac{\omega}{2}\right)}{2\pi T}\right)\right.$$
$$\left. + \psi\left(\frac{1}{2} - \frac{i\left(\eta - \frac{\omega}{2}\right)}{2\pi T}\right)\right]\rangle / \langle J\rangle - \psi\left(\frac{1}{2}\right) \qquad (8)$$

with

$$ImF(\hat{q}, \omega) = \frac{\pi}{2} sh\left(\frac{\omega}{2T}\right)\langle J\left(ch\frac{\eta}{T} + ch\frac{\omega}{2T}\right)^{-1}\rangle / \langle J\rangle \quad (9)$$

and $\psi(z)$ is the di-gamma function.

Then making use of Eq (1) $Im\chi(\hat{q}, \omega)$ is readily constructed. We show in Fig. 1 $Im\chi(\hat{q}, \omega)$ at T=33K for two q scans [Q_g scan, $\hat{q} = (q + \frac{1}{2} q_o, q - \frac{1}{2} q_o)$ and Q_γ scan, $\hat{q}(\hat{q}, q)$]. Here we took μ = - 435.5K which produces four peaks in $Im\chi(\hat{q}, \omega)$ at $\pm(q_o, o)$ and $o, \pm q_o$ with $q_o = 0.245\pi$ appropriate for $La_{1.86}Sr_{0.14}CuO_4$. Indeed the present $Im\chi(q, \omega)$ reproduces quite well inelastic neutron scattering data by Mason et al [8]. Also it is readily shown that $\chi(q, o)$ has a single peak (i.e commensurate) when $|\mu|$<1.91 T while has four separate peaks (incommensurate) when $|\mu|$<1.91 T. This behavior of paramagnon provides us a nice scenario for the phase diagram for YBCO [12] that the peak in T_c at $YBa_2Cu_3O_{6.94}$ corresponds to the crossover point when paramagnon changes from commensurate to incommensurate. Unfortunately, however, we discover that the

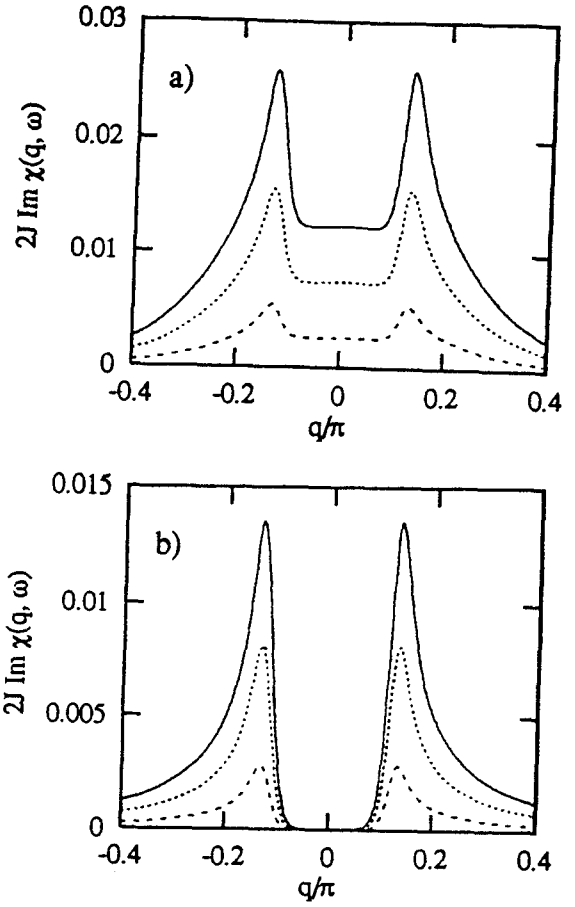

Fig. 1. $2JIm\chi(\hat{q}, \omega)$ for two q scans at T=T_c(=33K) and for ω=6*meV* (–), 3.5*meV* (····), and 1.2*meV* (---). a) Q_δ scan and b) Q_γ scan

crossover point shift to $|\mu|$=1.55 T when we study $Im\,\chi(\hat{q}, \omega)$ instead of $\chi(\hat{q}, o)$ [13]. Therefore this may be the first indication that t-J model is not adequate for YBCO.

At T=0K, on the other hand, Eq (5) reduces to

$$F(\hat{q}, \omega) = \langle J\left[\frac{\eta^2 - \frac{1}{4}\omega^2}{\Delta^2|f|^2 + \eta^2 - \frac{1}{4}\omega^2}\right]^{\frac{1}{2}}$$
$$\times\, arcsh\left(\frac{\left[\eta^2 - \frac{1}{4}\omega^2\right]^{\frac{1}{2}}}{\Delta|f|}\right)\rangle / \langle J\rangle \qquad (10)$$

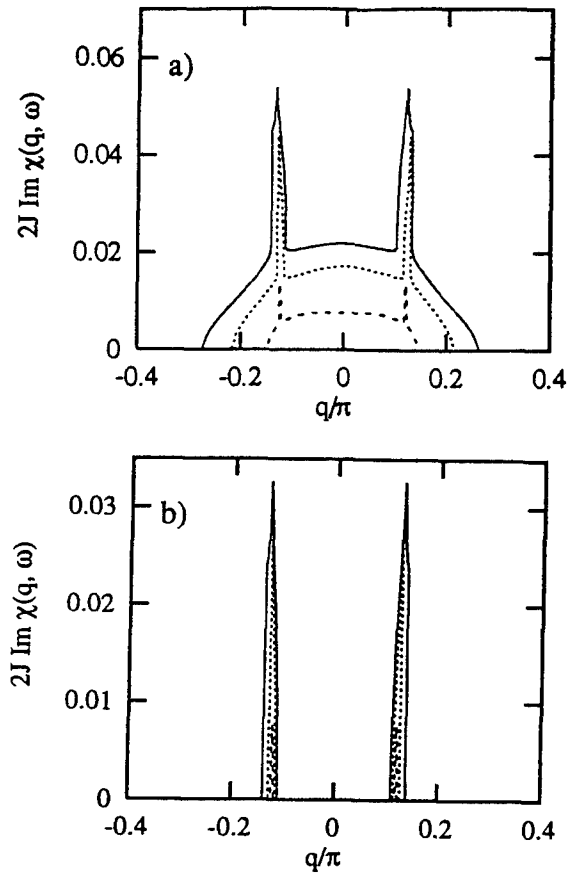

Fig. 2. $2JIm\chi(\dot{q}, \omega)$ for two q scans at $T=0K$ and for the same set of ω as in Fig. 1. a) Q_δ scan and b) Q_γ scan.

with

$$ImF = \frac{\pi}{2}\langle J\left[\frac{\frac{1}{4}\omega^2 - \eta^2}{\frac{1}{4}\omega^2 - \eta^2 - \Delta^2|f|^2}\right]^{\frac{1}{2}} \times \theta\left(\frac{1}{4}\omega^2 - \eta^2 - \Delta^2|f|^2\right)\rangle / \langle J\rangle \qquad (11)$$

Again we show in Fig. 2 $Im\ \chi(\dot{q}, \omega)$ for two $\dot{q}$ scans as in Eq (1). The presence of the gapless region in the commensurate antiparamagnon on the edge of square formed by connecting $(\pm q_o, o)$ and $(o, \pm q_o)$ is consistent again with the experimental result by Mason et al [8]. A similar result is obtained by Tanomoto et al [14] within somewhat different approximation scheme.

In the commensurate regime (i.e. $|\mu|<1.91\ T_c$) on the other hand, Eq (11) predicts an energy gap $Eg = 2|\mu|$ in the antiparamagnon spectrum. Similar energy gap is obtained independently in t-t'-J model by Lavagna et al [15]. In Fig. 3 we show $Im\ \chi(o, \omega)$ at $T=0K$ for t-J model with $-\mu=2meV$ and $14meV$ corresponding $YBa_2Cu_3O_{6+x}$ with x=0.51 (with $T_c=47K$) and x=0.92 (with $T_c=91K$) respectively.

It is of interest to see that the shape of Fermi surface reflects in $Im\ \chi(o, \omega)$ at $T=0K$. The Jacobian somewhat sharpen the peak in the underdoped region. Also from the relation $Eg=2|\mu|$ we obtain an empirical formula $\mu = 345\,(x - 0.45)\,K$ for YBCO [12].

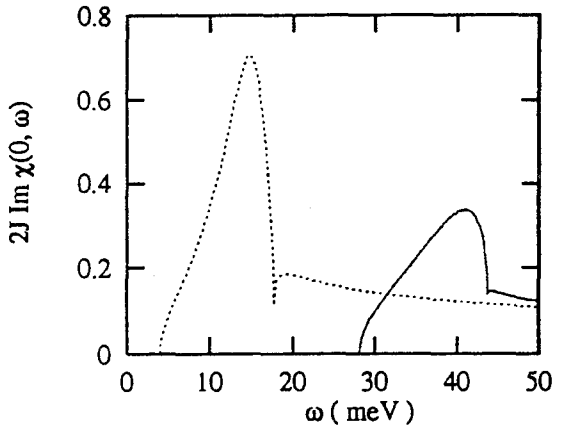

Fig. 3. $2Im\ \chi(o, \omega)$ of $YBa_2Cu_3O_{6+x}$ at $T=0K$ as function of ω for x=0.51 (---) and 0.92 (–).

3. Conclusion

We have seen that 2D t-J model treated with RPA describes quite well inelastic neutron scattering data from a monocrystal of $La_{1.86}Sr_{0.14}CuO_4$ and monocrystals of $YBa_2Cu_3O_{6+x}$. Even in the normal state the spectral function is quite different from the one commonly used in phenomenological treatment [16] and reflects the shape of Fermi surface through η. We have shown also the antiparamagnon gives rise to the nuclear spin lattice relaxation rate observed both in commensurate region and incommensurate region quite well [12]. Further the exchange of antiparamagnon gives rise to finite renormalization of quasi-particle mass with $Z\cong4$ [17], which is consistent with earlier theoretical analysis [18, 19] (i.e. Fermi liquid behavior) but almost T linear normal resistivity [17] and large almost T independent thermoelectric power. In Fig. 4 we plotted the thermoelectric power Q as function of $T/|\mu|$. Except the low temperature region $\left(T \le \mu^2/4t\right)$, Q is the universal function of $T/|\mu|$ within t-J model. Here we give Q in the region of incommensurate antiparamagnon and the result appears to describe rather well the thermoelectric power observed in LSCO

by Uchida et al [20]. In the region of commensurate

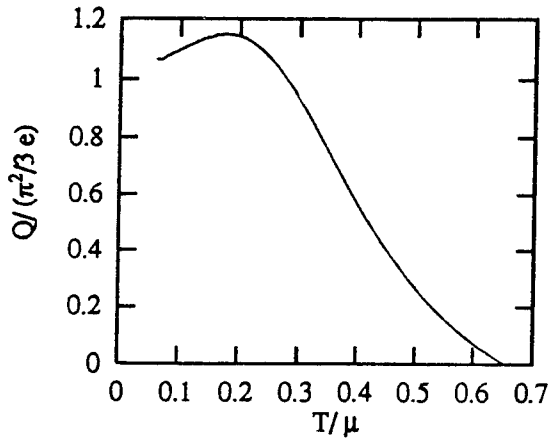

Fig. 4. $3eQ/\pi^2$ where Q is the thermoelectric power is plotted as function of T/μ for incommensurate region ($T/\mu < 0.65$).

antiparamagnon like YBCO on the other hand, it appears that t-J model is inadequate to describe the thermoelectric power observed by Cooper et al [21]. We may now list a few short-coming of t-J model when applied to YBCO. a) it predicts the commensurate-incommensurate transition around $x = 0.85$, while no such transition is seen in inelastic neutron scattering. b) t-J model cannot give a pseudogap seen in the normal state, while t-t'-J model does [15]. c) Q in the commensurate region in t-J model is quite different from the one observed in YBCO [21]. On the other hand in t-t'-J model there is no commensurate-incommensurate transition in the interesting parameter region of μ [10]. So it is of great interest to see if t-t'-J model gives Q compatible with the one observed in YBCO. The origin of T-linear resistivity may be understood in analogy to the Nesting Fermi liquid theory of Virosztek and Ruvalds [22]. Of course in the Nesting Fermi liquid theory only the Born term is considered, while paramagnon exchange corresponds the total T matrix. Nevertheless the analytical structure of the quasiparticle lifetime is very similar to the antiparamagnon model except for the imperfect nesting parameter η, which plays the crucial role in our analysis.

Therefore it is of great interest to study the superconducting order parameter and the superconducting transition temperature within antiparamagnon exchange model.

ACKNOWLEDGEMENTS

We thank Thom Mason and Jean Rossat-Mignod for enlightening discussions on their inelastic neutron scattering data, which gave the initial impetus to this work. In course of the present work we benefitted from discussions and correspondences with H. Fukuyama, M. Lavagna and F. Ohkawa

The present work is in part supported by NSF under grant number DMR92-18371.

REFERENCES

1. Z.-X. Shen et al, *Phys. Rev Lett.* **70**, 1553 (1993).
2. W.N. Hardy, D.A. Bonn, D.C. Morgan, R. Liang, and K. Zhang, *Phys. Rev. Lett.* **70**, 3999 (1993).
3. D.A. Wollman, D.J. Van Harlingen, W.C. Lee, D.M. Ginsberg and A.J. Leggett, *Phys. Rev. Lett.* **71**, 2134 (1993).
4. T.P. Devereaux, D. Einzel, D. Stadlober, R. Hackl, P.H. Leach and J.J. Neumeier, *Phys. Rev. Lett.* 72, 396 (1994).
5. C.C. Tsuei, J.R. Kirtley, C.C. Chi, Loo See Yun-Jahnes, A. Gupta, T. Shaw, J.Z. Sun and M.B. Ketchen, *Phys. Rev. Lett* **73**, 593 (1994).
6. D.A. Brawner and H.R. Ott, *Phys. Rev. B.* **50**, 6530 (1994).
7. K. Maki and H. Won, *Phys. Rev. Lett.* 72, 1758 (1994); H. Won and K. Maki, *Phys. Rev. B.* 49, 15305 (1994).
8. T.E. Mason, G. Aeppli, S.M. Hayden, A.P. Ramirez and H.A. Mook, *Phys. Rev. Lett* **71**, 919 (1993).
9. J. Rossat-Mignod, L.P. Regnault, P. Bourges, C. Vettier, P. Barlet and J.Y. Henry, *Physica B* **186-188**, 1 (1993).
10. T. Tanamoto, H. Kohno and H. Fukuyama, *J. Phys. Soc. Jpn.* **61**, 1886 (1992), **62**, 717 (1993).
11. J.W. Loram et al., *Physica C* **162~164**, 493 (1989); J.W. Loram et al., *Phys. Rev. Lett.* **71**, 1741 (1993).
12. H. Won and K. Maki, *Physica B* (in press)
13. H. Won and K. Maki, unpublished.
14. T. Tanamoto, H. Kohno and H. Fukuyama, *J. Phys. Soc. Jpn.* **62**, 1455 (1993), **63**, 2739 (1994).
15. M. Lavagna and G. Stemmann, *Phys. Rev. B* 49, 4235 (1994); G. Stemmann, C. Pépin and M. Lavagna, *Phys. Rev. B* **50**, 4075 (1994).
16. B.W. Statt and A. Griffin, *Phys. Rev. B* 46, 3199 (1992); *Phys. Rev. B* 48, 619 (1993); P. Montheaux and D. Pines, Phys. Rev. B 47, 6069 (1993).
17. K. Maki and H. Won, *Physica B* (in press).
18. W. Stephan and P. Horsch, *Phys. Rev. Lett.* **66**, 2253 (1991).
19. K.W. Becher, R. Eder and H. Won, *Phys. Rev. B* 45, 4864 (1992).
20. S. Uchida, K. Tamasaku, K. Takenaka and H. Takagi, *J. Low Temp. Phys.* 95, 109 (1994).
21. J.R. Cooper and A. Carrington, *Advances in Superconductivity V* (Springer-Verlag Tokyo 1993) 95; S.D. Obertelli, J.R. Cooper and J.L. Tallon, *Phys. Rev. B* 46, 14928 (1992).
22. A. Virosztek and J. Ruvalds, *Phys. Rev. B* 42, 2258 (1990); C.T. Rieck, W.A. Little, J. Ruvalds and A. Virosztek, *Solid State Commun.* **88**, 395 (1993).

Journal of Superconductivity, Vol. 8, No. 4, 1995

D-wave Superconductivity in the Nearly Antiferromagnetic Fermi Liquid

J.P. Carbotte,[1] D. Branch,[1] and C. O'Donovan[1]

Received December 10, 1994

Self consistent calculations, based on the 2 dimensional Hubbard model, indicate that the nearly antiferromagnetic Fermi liquid may be a superconductor with $d_{x^2-y^2}$ symmetry. The recent observation of a large anisotropy of the in plane penetration depth has been widely interpreted as evidence that a significant part of the condensate in $YBa_2Cu_3O_{7-\delta}$ resides in the chains. This introduces orthorhombic symmetry. Calculations, which remain within a single tight binding band model but with different nearest neighbour hopping in a- and b-directions, can account for the penetration depth anisotropy and also explain the observed size of the D.C. Josephson current between $YBa_2Cu_3O_{7-\delta}$ and Pb in c-axis tunnelling.

KEY WORDS: $d_{x^2-y^2}$, tunnelling, antiferromagnetic fluctuations

There exists an extensive theoretical literature on the possible existence of a gap with $d_{x^2-y^2}$ symmetry for the superconductivity of the 2 dimensional copper oxide planes. [1] D-wave superconductivity is also supported by many recent experiments. They are too numerous to quote here, [2] but include the penetration depth [3] and the angular resolved photo emission. [4] These experiments, however, are not sensitive to the sign of the gap but only to the zeros. Perhaps a more direct measurement of $d_{x^2-y^2}$ symmetry, sensitive to a change in sign of the gap, is the SQUID experiment of Wollman et al. [5]

The approach to the superconductivity in the copper oxide planes, taken by Lenck, Carbotte and Dynes, [6] is to calculate, from first principles but in a definite approximation, the spin and charge susceptibility for a tight binding band and use this susceptibility as the kernels in the self energy equations for the electrons. While a simple approximation for the susceptibilities is made, the calculations are carried out self consistently. Once the value of on site Coulomb repulsion (U) is fixed, the only remaining parameter in the theory is the nearest neighbour hopping parameter $\bar{t}$ and the filling factor. Within this two parameter model (U and $\bar{t}$) for a given choice of filling factor n, the irreducible susceptibility is calculated from the simple product of two fully dressed Green's functions and U is introduced in a random phase approximation to describe the Stoner enhancement of the irreducible susceptibility. The enhanced susceptibility then determines the critical temperature T_c through the self energy equations. The generalized self energy equations involve three coupled nonlinear integral equations for a renormalization parameter, for the energy shift and for the pairing. They are solved numerically using a fast Fourier transform technique. [6] Similar calculations have been reported by Chien-Hua Pao and N.E. Bickers [7] using instead a numerical technique inspired by renormalization group ideas, and by Monthoux and Scalapino [8] using a different approximation for the interaction kernels in the self energy equations.

Lenck, Carbotte and Dynes [6] have found superconducting solutions. The filling was fixed at n=0.84. For a value of the Hubbard U=4.28 in units of the hopping parameter $\bar{t}$, they obtained a value of critical temperature of $T_c \cong 0.016\,\bar{t}$ which exhibited pure $d_{x^2-y^2}$ symmetry for the gap. This symmetry comes out

[1]Department of Physics and Astronomy
McMaster University, Hamilton,
Ontario, Canada L8S 4M1

0896-1107/95/0800-0401$07.50/0

of the numerical work and was not imposed on the system. The value for $T_c=0.016\ \bar{t}$ compares very favourably with the value found by C-H Pao and Bickers [7] using different numerical methods and a slightly different form for the potentials in the Eliashberg equations. Monthoux and Scalapino [8] who have also found superconducting solutions in the model studied here. Of course, in none of these works, is the problem solved completely since some approximation must be made for the effective potential and many terms are left out of the perturbation series. While it might be hoped that the self consistency imposed on the computations might reduce the effects of these omissions, the calculations by their very nature remain approximate, and while they are an indication for superconductivity, the do not prove it.

Our results for the self consistent susceptibility are shown in Fig. 1 for $T\cong 0.91\ T_c$. What is plotted is the imaginary part of the susceptibility divided by frequency ω in the limit of small ω. Only the region of $\underline{k}$-space near (π,π) is shown. Clear incommensurate peaks are seen which are of about the observed height as compared with the background value found in experiments on $La_{1.86}Sr_{0.14}CuO_4$ by Mason et al. [9] Also, the absolute value of $[\Im m\chi_s/\omega]$ at the peaks is of order $18x10^{-3}$ $(meV)^{-2}$ in units of $\mu_B{}^2$ where μ_B is the Borh magneton. This is almost precisely the value observed at T_c by Mason et al. [9,10] As the temperature is lowered to $T=.6\ T_c$, however, the entire pattern is reduced by an order of magnitude and the background becomes much more prominent as compared to the peak heights. This is in contrast to experiment in which no distortion of peak height with respect to background is observed and also the magnitude of the magnetic response in going from 35K to 4.5K is observed to drop by 60%, i.e. by a factor of 2.5 rather than the factor of 10 calculated in reference (6). In considering the absolute size of the susceptibility at T_c, we note that the corresponding Stoner enhancement factor in the incommensurate peaks is very large, indicating that we are near the antiferromagnetic transition. Superconductivity is found to occur only in this narrow region of phase space. For example, for our calculation at $T=0.91\ T_c$ with the Hubbard U set at 4.288, the critical value of $U(U_c)$ for the antiferromagnetism is calculated to be 4.3048. This implies a Stoner factor of about 175. This huge enhancement factor is required in order to get agreement with the measured absolute value of the susceptibility in La Sr Cu O.

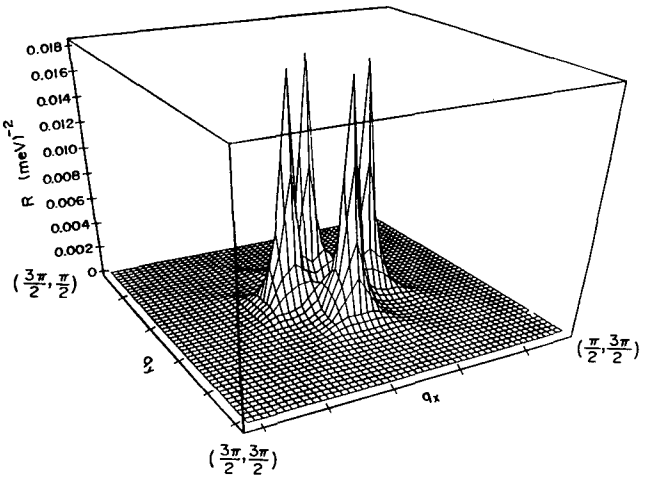

Fig. 1. R is the imaginary part of the spin susceptibility divided by ω. It is given as a function of momentum (k_x,k_y) around the incommensurate peak displaced from (π,π) for $T=.91\ T_c$. This figure applies equally well to any small ω and not just the limit $\omega\to 0$.

Recently, the penetration depth and microwave absorption have been measured separately for the a- and b- direction of the CuO_2 plane and found to display a very significant anisotropy. [11,12] For example, the zero temperature penetration depth in the a- direction was found to be 1600 Å and in the b- direction 1030 Å for $YBa_2Cu_3O_7$. This large measured anisotropy has been taken to be due to the CuO chains and as an indication that a considerable amount of the condensate resides on the CuO chains. To simulate the existence of chains as well as plane, we use a tight binding band but with anisotropic first nearest neighbour hopping. This ensures that the a- and b- directions are distinct while retaining a single 2-dimensional copper oxide band. For such an anisotropic band structure, we write down and solve numerically, by a fast Fourier transform technique, the BCS gap equations with pairing interaction due to the exchange of antiferromagnetic spin fluctuations. For the spin susceptibility, which determines the pairing, we employ the simple form suggested by Millis, Monien and Pines. [13] It is much simpler to use than the self consistent susceptibility described previously and is phenomenological in origin. The form is determined from consideration of NMR data. In this work, it is taken over unmodified.
Lenck and Carbotte [14] have already solved numerically, the BCS gap equation for a model dispersion with tetragonal symmetry and MMP

susceptibility. They found that the solution for the gap contained a single irreducible representation of the crystal lattice group with $d_{x^2-y^2}$ symmetry. Of course, the numerical solutions involve many higher harmonics within this representation but much of the physics can be understood using the simple function $\Delta(\underline{K}) \cong \Delta_0(t)\frac{1}{2}[\cos(K_x a)-\cos(K_y a)]$. When anisotropy is included in the first nearest neighbour hopping, the solutions for the gap $\Delta(\underline{K})$ become more complicated. When we projected our solutions onto the various irreducible representations of the tetragonal group, we found that they contained a mixture of $d_{x^2-y^2}$, isotropic S_0wave, and extended S-wave (S_x) representation. Of course, as for the d-wave part, the extended S_x wave part consists of a $[\cos(K_x a)+\cos(K_y a)]$ plus many higher harmonics. A reasonable, although certainly not exact, representation of our solutions, however, is obtained by keeping only lowest harmonics in each representation.

In Fig. 2, we show the penetration depth $\lambda_{xx}^{-2}(T)$ and $\lambda_{yy}^{-2}(T)$ for an MMP superconductor as a function of temperature. A second nearest neighbour hopping parameter was included appropriate to YBCO and the filling was $<n>=0.88$. The magnitude for T_c, is 94.0 K. The nearest neighbour hopping anisotropy parameter was taken to be 25%, which led to a 29% admixture of extended S-wave plus constant part into the mainly D-wave gap on solution of the BCS equation. From the figure, we conclude that the ratio $\lambda_{xx}^{-2}(T=0)/\lambda_{yy}^{-2}(T=0)$ is around 2 as in the experiments of Zhang et al.[11] We note also that both penetration depths λ_{xx}^{-2} and λ_{yy}^{-2} show a linear temperature variation at low T as is observed, although over the entire temperature range the agreement is not so good. In particular, the slope near T_c is smaller in our calculations than is observed. Simple BCS models of the kind used here seem not to be able to reproduce the detailed observations particularly near T_c. They omit, of course, any effect of fluctuations which could become important in this temperature region.

In a recent experiment, Sun et al. [15] have observed a D.C. Josephson current to flow between YBCO and Pb for a c-axis tunnel function with current perpendicular to the planes. The authors point out that this is unexpected if YBCO is a pure d-wave superconductor. But in our anisotropic effective mass, model a- and b- directions are not equivalent and the gap does not have pure $d_{x^2-y^2}$ symmetry so that a Josephson current can flow even for incoherent tunnelling. For a

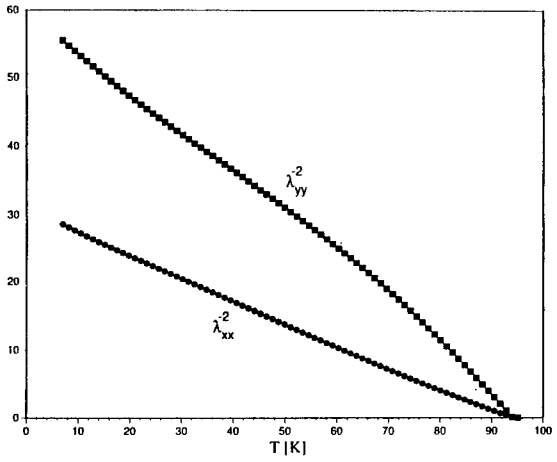

Fig. 2. Comparison of the temperature variation of the penetration depth (in arbitrary units) for x and y direction for the case with second nearest neighbour hopping appropriate for YBCO filling $n=0.94$, $T_c=94K$ and effective mass anisotropy parameter and $\delta=0.25$. These results are based on complete numerical solutions of the BCS gap equation for the MMP model susceptibility. The anisotropy in $\lambda_{ii}^{-2}(0)$ is about a factor of 2 as measured experimentally.

25% anisotropy between a- and b- direction first nearest neighbour hopping parameters, we have computed the maximum D.C. Josephson current of a YBCO-I-Pb function and show our results in Fig. 3 (solid dots). Also shown for comparison are the standard results for a Pb-Pb function (solid squares) The temperature dependence predicted for the anisotropic orthorhombic case is not so different from the standard isotropic gap result. The resulting RJ(0) product where R is the junction resistance and J(0) is the zero temperature value of the maximum current was 0.9 meV. This is close to the measured value.

Self consistent calculations of spin and charge fluctuations in a narrow tight binding band with nearest neighbour hopping and Hubbard U can give superconducting solutions. In the calculation of the self energy, some definite approximation must be adopted for the computation of the susceptibility kernels. Using a random phase approximation for the treatment of the Stoner enhancement of the irreducible susceptibilities which are calculated as a simple product of two self consistent Green's functions without vertex corrections, does give a superconducting solution with $d_{x^2-y^2}$ symmetry (including, of course, many high order

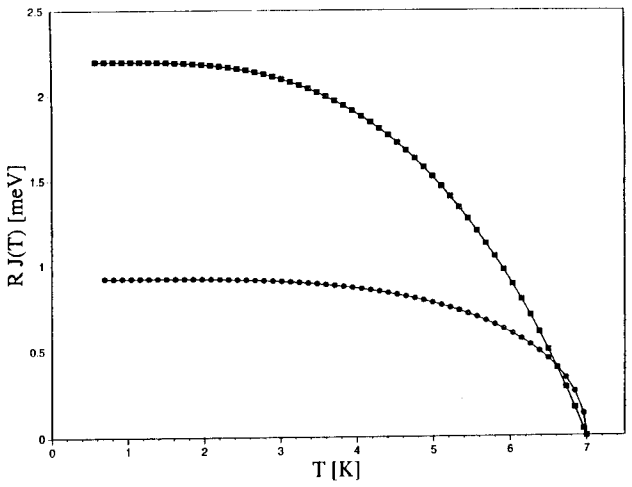

Fig. 3. The maximum D.C. Josephson current (solid dots) as a function of temperature calculated from full numerical solutions of the BCS gap equation with spin susceptibility taken to be the MMP model. The anisotropy in nearest neighbour hopping is 25% so that the penetration depth shows a factor of 2 anisotropy between a- and b- in plane value as measured in experiments. Also shown for comparison are the standard results (solid squares) for a Pb-Pb junction.

harmonics in this irreducible representation) of the tetragonal group for Hubbard U very near the antiferromagnetic phase transition boundary. While such calculations are suggestive of a possible superconducting instability in the Hubbard model, they certainly do not prove that this is the case since the approximations used may prove to be inadequate for the values of U considered. Recent experiments on the in plane penetration depth in high quality single crystals of $YBa_2Cu_3O_{7-\delta}$ have discovered a large anisotropy between a- and b- directions inconsistent with tetragonal symmetry and a pure $d_{x^2-y^2}$ gap. For a single electronic band with different first nearest neighbour hopping in a- and b- direction, we find that the numerical solutions of the BCS gap equations using, for simplicity, the phenomenological susceptibility of Millis, Monien and Pines, yields a gap which is an admixture of a main $d_{x^2-y^2}$ component but with a minority component having extended S-wave symmetry including a small constant part. Our solutions can easily account for the measured penetration depth anisotropy. Additionally, they provide a possible explanation for the magnitude of D.C. Josephson current measured between YBCO and Pb in c-axis oriented functions.

ACKNOWLEDGEMENT

Research supported in part by the Natural Sciences and Engineering Research Council of Canada (NSERC) and by the Canadian Institute for Advanced Research (CIAR).

REFERENCES

1. P. Monthoux and D. Pines, *Phys. Rev.* **B47**, 9124 (1993).
2. J.F. Annett and N. Goldenfeld, *Jour. Low Temp. Phys.* **81**, 197 (1992).
3. W.N. Hardy, D.A. Bonn, D.C. Morgan, Ruixing Liang and Kuan Zhang, *Phys. Rev. Lett.* **70**, 3999 (1993).
4. Z.K. Shen, D.S. Dessau et al., *Phys. Rev. Lett.* **70**, 1553 (1993).
5. D.A. Wollman, D.J. Van Harlingen, W.C. Lee, D.M. Ginsberg and A.J. Leggett, *Phys. Rev. Lett.* **71**, 2134 (1993).
6. St. Lenck, J.P. Carbotte and R.C. Dynes, *Phys. Rev.* **B50**, 10149 (1994).
7. Chien-Hua Pao and N.E. Bickers, *Phys. Rev. Lett.* **72**, 1870 (1994).
8. P. Monthoux and D. Scalapino, *Phys. Rev. Lett.* **72**, 1874 (1994).
9. T.E. Mason, G. Aeppli, S.M. Hayden, A.P. Ramirez and H.A. Mook, *Phys. Rev. Lett.* **71**, 919 (1993).
10. T. Mason (private communication).
11. K. Zhang, D.A. Bonn, S. Kamal, R. Liang, D.J. Baar, W.N. Hardy, D. Basov and T. Timusk (preprint).
12. D.N. Basov, R. Liang, D.A. Bonn, W.N. Hardy, D. Dabrowski, M. Quijada, D.B. Tanner, J.P. Rice, D.M. Ginsberg and T. Timusk (preprint).
13. A.J. Millis, H. Monien and D. Pines, *Phys. Rev.* **B42** 167 (1990).
14. St. Lenck and J.P. Carbotte, *Phys. Rev.* **B49**, 4176 (1994).
15. A.G. Sun, D.A. Gajewki, M.B. Maple and R.C. Dynes, *Phys. Rev. Lett.* **72**, 2267 (1994).

Journal of Superconductivity, Vol. 8, No. 4, 1995

Existence of both *s* and *d*-wave solutions of Eliashberg equations

G. Santi[1], T. Jarlborg[1], M. Peter[1] and M. Weger[2]

Received 31 January 1995

We solve Eliashberg equations in the case of strong anisotropic electron-phonon coupling and low energy cutoff. In a simplified model representing the Fermi Surface of $(CuO_2)_n$ planes, we exhibit a *d*-wave solution as well as a generalized *s*-wave one.

KEY WORDS: Eliashberg equations, electron-phonon.

1. Introduction

The basic mechanism of high-temperature superconductivity is not yet known. Possibilities are the BCS phonon-mediated interaction, exchange of paramagnons, or some other Coulomb interaction, described for example by the t-J model, or the Pines theory [1]. It is frequently argued that when the superconducting gap parameter Δ has a *d*-wave symmetry [2], this implies a Coulomb mechanism, while a phonon-mediated interaction causes an *s*-wave (or extended *s*-wave) symmetry of Δ [3]. This argument is based on a long experience with the phonon-mediated mechanism, since the work of BCS, Gorkov, Nambu and Eliashberg [4]. The electron-phonon interaction in normal metals is local in ordinary space [5] and consequently the $\boldsymbol{k}$-dependence of the interaction $D(\boldsymbol{k},\boldsymbol{k}', i\omega - i\omega') = g^2(\boldsymbol{k},\boldsymbol{k}')\,2\omega_{ph}/\left[(\omega-\omega')^2+\omega_{ph}^2\right]$ is weak and usually averaged over the FS [6]. This locality is due to strong screening; $g(\boldsymbol{k},\boldsymbol{k}')$ is proportional to the ion-electron potential given by [7] $V(\boldsymbol{k},\boldsymbol{k}') = 4\pi e^2/\left[(\boldsymbol{k}-\boldsymbol{k}')^2+\kappa_{TF}^2\right]$ and the Thomas-Fermi screening parameter κ_{TF} is large, and therefore V is nearly isotropic. In normal metals, $\kappa_{TF}^2 = 0.66\, r_s\, k_F^2$, where r_s ($\approx$3) is the average distance between electrons in units of the Bohr radius. In the high-T_c cuprates, the oxide background has a very large dielectric constant $\varepsilon_0 = 60$ [8], therefore $\kappa_{TF}^2 = 4\pi e^2 n(E_F)/\varepsilon_0$ is much smaller, and a typical value is $\kappa_{TF} \approx 0.3 k_F$. Consequently V is very anisotropic, with predominantly forward scattering. This favors superconductivity with *d*-wave symmetry of Δ, even for the phonon-mediated process.

In the present work, we present solutions of the Eliashberg equations, generalized for an interaction $D(\boldsymbol{k},\boldsymbol{k}', i\omega - i\omega')$ with a strong $\boldsymbol{k}$-dependence, for an electron-phonon matrix element $g(\boldsymbol{k},\boldsymbol{k}')$ proportional to $V(\boldsymbol{k},\boldsymbol{k}')$. We find that there are solutions with *d*-wave and *s*-wave symmetries that are nearly degenerate in energy, and thus small changes in the parameters cause a crossover between the two symmetries, without a large change in T_c.

In previous publications [9] we solved the generalized Eliashberg equations for an electron-phonon coupling $g(\boldsymbol{k},\boldsymbol{k}')$ possessing a cutoff at an energy ξ_{ph} close to the energy ω_0 at which the dielectric constant $\varepsilon(\omega)$ of the background falls significantly, i.e. about 10-20 meV [6]. We found that this small cutoff $\xi_{ph} < \omega_{ph}$, where $\omega_{ph} \approx 40$ meV is the energy of the phonons responsible for the pairing, changes the nature of the solutions of the Eliashberg equations in a very essential way. The well-known relationship $Z = 1 + \lambda$ (for the renormalization at the FS) and $h/2\pi\tau = 2\pi\lambda k_B T$ (the Hopfield relation between the electron-phonon scattering rate τ^{-1} and the McMillan constant λ) no longer hold, even approximately; thus a very large λ ($\approx$10) gives rise to a value of Z of about 2-3, and a very small τ^{-1}. We found that we can account for the high value of T_c, the insensitivity to the very strong Coulomb interaction, the suppression of the isotope effect, the large value of $2\Delta(0)/T_c$, the zero-bias-anomaly, and several other features of the superconductivity of the cuprates, as well as some other exotic superconduc-

[1] Département de la Physique de la Matière Condensée, Université de Genève, CH-1211 Genève 4, Switzerland

[2] Racah Institute of Physics, Hebrew University, Jerusalem, Israel

0896-1107/95/0800-0405$07.50/0

tors, such as the organics. We developed a computer program that solves the generalized Eliashberg equations, incorporating the strong $\boldsymbol{k}$-dependence. The present calculation is a continuation of this work.

2. Description of the model

In our calculations, we consider a simple model of the Fermi surface (FS). It is divided into 3 pieces, in which FS piece number 2 has a different coupling from pieces 1 and 3. This choice is made to remind of the FS of BiSCO, so that number 2 corresponds to the rounded corners while 1 and 3 correspond to the planar sections [11]. The tetragonal crystal symmetry is such that pieces 1 and 3 are equivalent. We restrict ourselves to a 2-dimensional momentum space, thus the momentum can be defined as $\boldsymbol{k} \equiv (k_\perp, k_\parallel)$ where $k_\perp$ is the component perpendicular to the FS and $k_\parallel$ the parallel one.

The gap equation that we solve self-consistently can be written as [12] (in the Matsubara representation where $\omega_n = (2n+1)\pi T$)

$$\Phi(\boldsymbol{k}, i\omega_n) = -T\sum_{n'}\int\int d^2k' G(\boldsymbol{k}', i\omega_{n'}) \times [D(\boldsymbol{k}, \boldsymbol{k}', i\omega_n - i\omega_{n'}) - \mu(\boldsymbol{k}, \boldsymbol{k}')]\ \Phi(\boldsymbol{k}', i\omega_{n'}) \quad (1)$$

where G is the renormalized electronic Green function, D is the phononic one and μ represents the Coulomb potential. We consider an electron-phonon interaction that is cut off in $k_\perp$, i.e. the coupling falls to zero for $|\xi(k_\perp) - \xi(k'_\perp)| > \xi_{ph}$ [13]. This cutoff ξ_{ph} is small except for the FS piece corresponding to the corner. Indeed, since the density of states is larger there (we are near a Van Hove singularity), the elastic scattering rate τ_{el}^{-1} being therefore larger too, and since the cutoff ξ_{ph} must be greater than τ_{el}^{-1}, ξ_{ph} cannot be so small [9]. Another essential feature of our coupling is that it decreases rapidly with $k_\parallel - k'_\parallel$, i.e. the coupling is very weak between two different FS pieces. This follows from the small value of κ_{TF}. Morover, in order to simplify the calculations, we choose the phonon spectrum as an Einstein spectrum of frequency ω_{ph}. The Coulomb repulsion is chosen to have a similar behavior with a cutoff ξ_c and being peaked in $k_\parallel$ (but not so sharply as the electron-phonon interaction).

Since eq.(1) has to be solved self-consistently, we have to choose the initial values for $\Phi(\boldsymbol{k}, i\omega_n)$. We will show that 2 different initial conditions lead to 2 different solutions of the Eliashberg equations even with exactly the same coupling parameters. As we said above, we take 3 FS pieces that are labelled with the discretized $k_\parallel$ coordinate: $q = 1, 3$ for the two planar sections and $q = 2$ for the corner. The s-wave like initial condition is simply

$$\Phi_0^{(s)}(\boldsymbol{k}, i\omega_n) = 1 \qquad \forall \boldsymbol{k}, n \quad (2)$$

wheras the d-wave like one is

$$\Phi_0^{(d)}(\boldsymbol{k}, i\omega_n) = \begin{cases} -1 & \text{if } q = 1 \\ 0 & \text{if } q = 2 \\ 1 & \text{if } q = 3 \end{cases} \qquad \forall k_\perp, n \quad (3)$$

3. Results

The corresponding solutions of the Eliashberg equations are shown in Fig.1. We immediately see that the initial symmetry is preserved. Since we take only a few FS pieces in account, it is more convenient to use a matrix notation to denote the (q, q') dependence of the parameters. The $(k_\perp, k_\perp')$ part is defined through the cutoff matrices ξ_{ph} and ξ_c. The strength of electron-phonon interaction is given by the matrix of McMillan [14] constants λ_{ph} and the coulomb repulsion is defined by μ. The parameters we used for these calculations are:

$$\lambda_{ph} = \begin{bmatrix} 5 & 0.25 & 0.05 \\ 0.25 & 1 & 0.25 \\ 0.05 & 0.25 & 5 \end{bmatrix}, \quad \xi_{ph} = \begin{bmatrix} 0.4 & 2 & 4 \\ 2 & 2 & 2 \\ 4 & 2 & 0.4 \end{bmatrix}$$
$$\mu = \begin{bmatrix} 3 & 0.75 & 0.25 \\ 0.75 & 3 & 0.75 \\ 0.25 & 0.75 & 3 \end{bmatrix}, \quad \xi_c = \begin{bmatrix} 2 & \infty & \infty \\ \infty & 2 & \infty \\ \infty & \infty & 2 \end{bmatrix} \quad (4)$$

Fig.2 shows the density of states (DOS) of the quasiparticles in the two cases considered. We can see that both of these DOS roughly reproduce the measured DOS with ARPES [15] or STM [16]. Indeed the difference between the d-wave and the s-wave DOS is very small and they could equally well explain experimental data.

We considered a situation where the non-diagonal coupling was very small. Following the discussion of Combescot [3], one can think that this is due to the weakness of the coupling. Indeed, we found that the solution possesses s-wave symmetry as soon as the non-diagonal coupling is strong enough. This occurs approximately when the non-diagonal terms of the electron-phonon coupling λ_{ph} become equal to the corresponding terms in the coulomb repulsion μ, and this is completely independent of the choice of the initial condition $\Phi_0^{(s)}$ or $\Phi_0^{(d)}$.

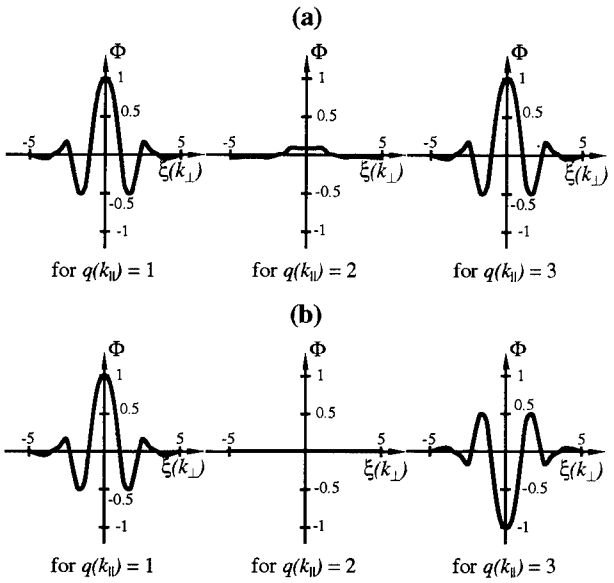

Fig. 1. Gap parameter $\Phi(\boldsymbol{k}, i\omega_n)$ for $n = 0$ as function of $\xi(k_\perp)$ and $q(k_\parallel)$ for **(a)** s-wave case and **(b)** d-wave case. The temperature is $T = 0.016$ (all energies are in units of ω_{ph}).

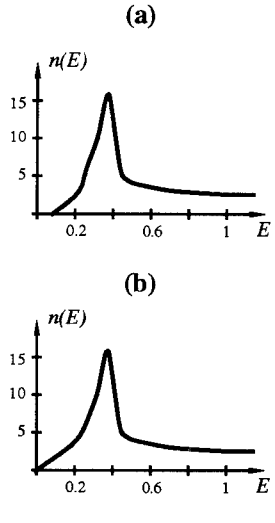

Fig. 2. DOS $n(E)$ of the quasiparticles (approximated as in [9]) as function of their energy E in the case of **(a)** s-wave and **(b)** d-wave (all energies are in units of ω_{ph}).

The solution with the lowest free energy will be the stable one, and it is likely that this is also the one with the highest T_c. This is because high T_c is correlated with a large gap, which in turn lowers the energy more than a small gap. We calculated T_c and found the same temperature of $T_c \approx 0.135\ \omega_{ph}$ in both cases. There seems then at first sight to be a degeneracy in the two symmetries. This is not surprising as long as the coupling is very weak between different FS pieces. In this case the gap equation is in practice decoupled between the different FS pieces and the sign of the gap of one FS with large local coupling can take any value independent of the phase of the gap at neighboring FS pieces.

4. Discussion

We find solutions of the Eliashberg equations with s- and d-wave symmetry are nearly degenerate. This result can also be understood qualitatively within the framework of the weak-coupling limit, where the gap equation is given by [10]:

$$\Delta(k_\parallel) = \frac{1}{\int dk_\perp dk_\parallel} \int \frac{dk'_\parallel}{v(k'_\parallel)} \Delta(k'_\parallel) \ln\left(\frac{2\omega_{ph}}{\Delta(k'_\parallel)}\right) \times [V(k_\parallel - k'_\parallel) - \mu^*(k_\parallel - k'_\parallel)] \tag{5}$$

We consider now an isotropic Coulomb interaction μ^*, an isotropic Fermi velocity $v(k'_\parallel)$, and an anisotropic phonon-mediated interaction $V(k_\parallel - k'_\parallel)$ that vanishes for a scattering angle $(k_\parallel - k'_\parallel)/k_F$ larger than $\Delta\theta$. There is a solution with s-wave symmetry, with: $\Delta_s = 2\omega_{ph} e^{-1/(\lambda - \mu^*)}$, where $\lambda = n(E_F) V_0$, $V_0 = \int V(k_\parallel - k'_\parallel)\, dk_\parallel dk'_\parallel / \int dk_\parallel dk'_\parallel$. There is also a solution with d-wave symmetry, with nodes at $\theta = k_\parallel / k_F = \pm\pi/4, \pm 3\pi/4$. If $\Delta\theta < \pi/4$, then at $\theta = 0$, $\Delta_d = 2\omega_{ph} e^{-1/\lambda}$. We illustrate Δ_s and Δ_d as function of θ in Fig.3a. We plot Δ_s, Δ_d as function of $\Delta\theta$ in Fig.3b, for the "normal" case in which $\mu^* < \lambda$, but μ^* not very small, and for the case in which μ^* is very small. We see that when $\Delta\theta < \pi/4$, and also $\mu^* \ll 1$, the solutions with s- and d-wave symmetry are nearly degenerate.

In our case, $\Delta\theta \approx (\kappa_{TF}/k_F)^2 \approx 0.1$, therefore the condition that there is virtually no scattering for $\theta > \pi/4$ is well satisfied. For a "normal" metal, where $\kappa_{TF} > k_F$, this is not the case. As for μ^*, we estimate for the cuprates that $\mu^* \approx 0.3 - 0.4$, since the bare μ is very large, and $\ln(E_F/\omega_{ph})$ is not very large because of the large value of ω_{ph}. Thus the condition $\mu^* \ll 1$ is not satisfied. However, we saw [9] that because of the small cutoff ξ_{ph}, μ^* has to be replaced by μ^{**} given by: $\mu^{**} = \mu / \{1 + \mu \ln[(E_F/\omega_{ph})(E_F/\xi_{ph})]\}$, and μ^{**} is very small (≈ 0.1). Thus the two conditions for the near-degeneracy are indeed satisfied. This is not the case in the theory of Monthoux et al [1], where the d-wave solution is due to the very large value of $\mu(1, 3)$, and no solution with s-wave symmetry is present.

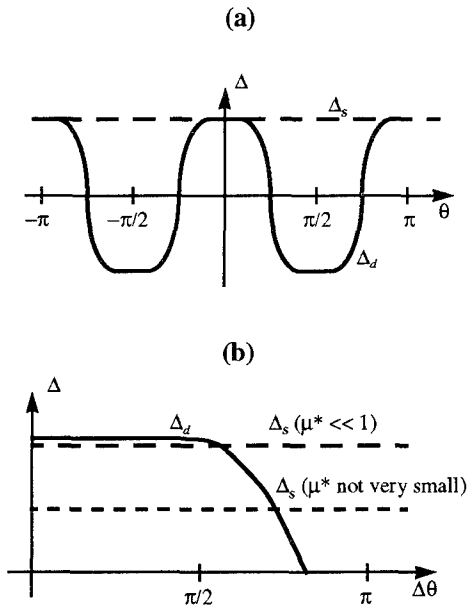

Fig. 3. General shape of the gap parameters Δ_s (dashed line) and Δ_d (plain line) as function of **(a)** the angle θ, and **(b)** $\Delta\theta$ determining the angular range of the interaction.

5. Conclusion

The conventional belief that the phonon-mediated (BCS) mechanism gives rise to solutions with *s*-wave symmetry, depends on a nearly-isotropic electron-ion potential. This is the case in "normal" metals, where the screening parameter κ_{TF} is large. In the cuprates, and some other "exotic" superconductors, κ_{TF} is very small because of the large static polarizability of the oxygen background, and therefore the potential is extremely anisotropic, giving rise to predominantly forward scattering. We found that this causes solutions of the Eliashberg equations with *s*- and *d*-wave symmetry to be nearly-degenerate, so that a small change in parameters (such as the elastic scattering rate due to defects) can cause a cross-over between the two symmetries without a large change in T_c. This seems to be in accord with experiment.

We wish to acknowledge B. Barbiellini for discussions and his contributions on earlier stage of this work, and one of us (M. W.) wants to thank G.M. Eliashberg for stimulating discussions.

References

1. Monthoux, A. Balatsky, D. Pines, *Phys. Rev. B* **46**, 14803 (1992)
2. D.A. Wollman, D.J. Van Harlingen, W.C. Lee, D.M. Ginsberg, A.J. Leggett, *Phys. Rev. Lett.* **71**, 2134 (1993); A. Mattai, Y. Gim, R.C. Black, A. Amar, F.C. Wellstood, preprint; D.A. Brawner and H.R. ott, *Phys. Rev. B* **50**, 6530 (1994)
3. R. Combescot, *Phys. Rev. lett.* **67**, 148 (1991)
4. G.M. Eliashberg, *Soviet. Phys. JETP* **11**, 696 (1960); *Soviet. Phys. JETP* **12**, 1000 (1961)
5. J. Appel and W. Kohn, *Phys. Rev. B* **4**, 2162 (1971)
6. M. Peter, J. Ashkenazi, M. Dacorogna, *Helv. Phys. Acta* **50**, 267 (1977)
7. J. Bardeen, *Phys. Rev.* **52**, 688 (1937)
8. J. Humlicek, A.P. Lityinchuk, W. Kress, B. Lederle, C. Thomsen, M. Cardona, H.U. Habermeier, I.E. Trofimov, W. Konig, Physica C 206, 345 (1993)
9. M. Weger, B. Barbiellini, M. Peter, *Z. Phys. B* **94**, 387 (1994); M. Weger, B. Barbiellini, T. Jarlborg, M. Peter, G. Santi, (to be published)
10. V.L. Pokrovskiĭ and M.S. Ryvkin, *Soviet. Phys. JETP* **16**, 67 (1963)
11. D.S. Dessau et al, *Phys. Rev. Lett.* **71**, 2781 (1993)
12. This equation is one of a set of three coupled equations since we consider a mass renormalization Z as well as a band renormalization X, both entering with the gap parameter Φ in the electronic Green function [9].
13. This is what we call the "strip" form in ref. [9].
14. W.L. McMillan, *Phys. Rev.* **167**, 331 (1968)
15. Z.X. Shen et al, *Phys. Rev. Lett.* **70**, 1553 (1993)
16. B. Barbiellini, Ø. Fischer, M. Peter, Ch. Renner and M. Weger, *Physica C* **220**, 55 (1994)

Journal of Superconductivity, Vol. 8, No. 4, 1995

Exchange-Correlation Effects on the Superconductivity of a Layered Two-Dimensional System

Y.M. Malozovsky[1+] and S.M. Bose[1]

The effects of the Hubbard exchange-correlation term G(k) on the normal and superconducting state properties of a layered 2D system has been investigated. It is shown that it can induce a metal-insulator phase transition when the condition $p_F \approx 1/c$, where c is the interlayer separation, is satisfied. For lower carrier densities, the plasmon-mediated superconductivity is suppressed, whereas at higher densities superconductivity can exist with T_c having a bell-shape dependence on the carrier density.

KEY WORDS: exchange-correlation, plasmons, bell-shape T_c

Among potential nonphonon mechanisms of high-T_c superconductivity the plasmon exchange model has been studied by various authors [1-3]. In recent related papers [4,5], we have shown that in the standard Fermi-liquid approach in the RPA, the electron-plasmon interaction in a layered 2D electron gas may lead to results which are similar to the phenomenology of 'marginal' Fermi-liquid model in both normal and superconducting states [6,7]. In this paper we introduce the exchange-correlation effects in the Hubbard approximation and show that it can induce a metal-insulator phase transition at a certain carrier density and suppress plasmon-mediated superconductivity near this phase transition. For higher carrier densities superconducting transition temperature T_c has a bell-shape dependence on the carrier density [8].

The local field factor is related to the Landau Fermi-liquid interaction and has the form [9]

$$G(\mathbf{k}) = -\frac{Z(0)}{2V(\mathbf{k})}\left\langle f^{\uparrow\uparrow}_{\mathbf{p},\mathbf{p}'} + f^{\uparrow\downarrow}_{\mathbf{p},\mathbf{p}'}\right\rangle, \quad (1)$$

where $Z(0) = Z(\mathbf{p},\omega)\,|_{\omega=0,\ |\mathbf{p}|=p_F} = 1 - \partial\Sigma(\mathbf{p},\omega)/\partial\omega\,|_{\omega=0,\ |\mathbf{p}|=p_F}$ is the well-known Fermi-liquid renormalization parameter. It has also been shown that [10]

$$\left\langle f^{\uparrow\uparrow}_{\mathbf{p},\mathbf{p}'}\right\rangle \approx 2\,\frac{\delta\Sigma^{ex}(\mathbf{k})}{\delta n_s}, \quad (2)$$

In a layered two-dimensional (2D) metal, with cylindrical topology of the Fermi surface, the exchange part of the self-energy can be written as [11]

$$\Sigma^{n}_{ex}(\mathbf{p}) = 2\sum_{\mathbf{k}}\int_{-\infty}^{\infty}\frac{d\omega}{2\pi}\,V(\mathbf{p}-\mathbf{k})\times \mathrm{Im}\,G(\mathbf{k},\omega)\,n_F(\omega), \quad (3)$$

where $n_F(\omega) = [\exp(\omega/T) + 1]^{-1}$ is the Fermi distribution function, and G is the normal electron Green's function which is determined by

$$G(\mathbf{p},\omega) = [\omega Z(\mathbf{p},\omega) - \xi_{\mathbf{p}}]^{-1}, \quad (4)$$

where $\xi_{\mathbf{p}} = \varepsilon_{\mathbf{p}} - \varepsilon_F$ is the energy measured relative to the Fermi energy with $\varepsilon_{\mathbf{p}} = p^2/2m^*$ being the 2D single-particle energy. In Eq. (2) V(k) is the bare Coulomb interaction in a layered crystal which has the well-known form [8]

$$V(\mathbf{k}) = V_0(k_{||})\,\frac{\sinh c\,k_{||}}{\cosh c\,k_{||} - \cos ck_z} = V_0(k_{||})\,f(\mathbf{k}), \quad (5)$$

where c is the separation between successive layers of a layered 2D metal, and

[1]Department of Physics and Atmospheric Science, Drexel University, Philadelphia, PA 19104

[+]Present address: Department of Physics, Southern University and A&M College, P.O. Box 10559, Baton Rouge, LA 70813

0896-1107/95/0800-0409$07.50/0

$V_0(k_{||}) = 2\pi e^2/k_{||}\kappa$ is the Coulomb interaction in a pure 2D case with κ as the dielectric constant of the background lattice.

Combining Eqs. (1), (2), (3), and (4) we arrive at the following Hubbard-like expression for the local field factor in a layered system [11]

$$G(\mathbf{k}) = \frac{k}{2\, f(\mathbf{k})\sqrt{k^2 + p_F^2}}, \tag{6}$$

We wish to use the Eliashberg equations for a layered system derived in reference 5, in which the kernel of interaction has the form

$$S(\Omega,\omega) = -\frac{1}{(2\pi)^3}\int_{Y(\omega)/v_F}^{2p_F} [\, F(k,\omega) + F(k,-\omega)] \times \bar{S}(k,\Omega)kdk \tag{7}$$

with $k=k_{||}$, and

$$\bar{S}(k,\omega) = \frac{c}{2\pi}\int_{-\pi/c}^{\pi/c} dk_z V^2(\mathbf{k}) \times [\,1 - G(\mathbf{k})]\, \mathrm{Im}\,\chi(\mathbf{k},\omega), \tag{8}$$

is the average of the kernel of interaction over k_z. In Eqs. (7) and (8)

$$F(k, \pm\omega) = \left[v_F^2 k^2 - \left(\frac{k^2}{2m^*} \pm Y(\omega) \right)^2 \right]^{-1/2},$$

and

$$\chi(\mathbf{k},\omega) = \tilde{\chi}(\mathbf{k},\omega)/[1 - V(k)\,\tilde{\chi}(\mathbf{k},\omega)],$$

with

$$\tilde{\chi}(\mathbf{k},\omega) = \chi_0(\mathbf{k},\omega)\Gamma(\mathbf{k},\omega) = \frac{\chi_0(\mathbf{k},\omega)}{1 + V(\mathbf{k})G(\mathbf{k})\chi_0(\mathbf{k},\omega)}, \tag{9}$$

where $\chi_0(\mathbf{k},\omega)$ is the usual Lindhard response function in a pure 2D case and

$$Y(\omega) = Z(\omega)\, \mathrm{Re}\sqrt{\omega^2 - \Delta^2(\omega)}.$$

Let us first we consider the contribution of plasmon excitations. Following the method of reference 5, it can be shown that the average kernel of interaction in region of plasmon excitation is

$$\bar{S}_{pl}(k,\omega) = -\frac{V_0(k)\omega^2}{\sqrt{(\omega_+^2 - \omega^2)(\omega^2 - \omega_-^2)}}, \tag{10}$$

In Eq. (10)

$$\omega_+^2 \approx \omega_p^2(k)\coth\frac{ck}{2} + \frac{3}{4}\left(1 - \frac{2}{3}\alpha\right) v_F^2 k^2, \tag{11}$$

is the pure optical plasmon frequency, and

$$\omega_-^2 \approx \omega_p^2(k)\tanh\frac{ck}{2} + \frac{3}{4}\left(1 - \frac{2}{3}\alpha\right) v_F^2 k^2, \tag{12}$$

is the proper acoustic plasmon frequency with $\omega_p^2(k) = e^2 v_F p_F k/\kappa$ being the plasmon frequency for a pure 2D system; $a^*_B = \kappa/e^2 m^*$ is the effective Bohr radius and $\alpha = e^2/v_F\kappa$ is the inter-electron interaction constant.

Substituting Eq. (10) into Eq. (7) we find that for a layered system ($p_{Fc} \geq 1$), the kernel for the electron-plasmon interaction is

$$S_{pl}(\Omega,\omega') \approx \frac{\alpha\Omega}{2\pi^2\sqrt{\omega_{pl}^2 - \Omega^2}} \times K\left[\sqrt{1 - (\gamma - \alpha/2 + 3/4)Y^2(\omega')/\Omega^2}\right], \tag{13}$$

$$\sqrt{\gamma - \alpha/2 + 3/4}\; Y(\omega') \leq \Omega \leq \min\{\omega_{pl}, \sqrt{\gamma - \alpha/2 + 3/4}\;\varepsilon_F\},$$

where $K(x)$ is the complete elliptic integral of the first kind and $\gamma = c/2a^*_B$ is the interlayer plasmon coupling constant, $\omega_{pl} = (4\pi e^2 n_s/\kappa m^* c)^{1/2} = \omega_c/\sqrt{\gamma}$ is the bulk plasmon frequency for a layered 2D system, and $\omega' Z(\omega') \leq \varepsilon_F$.

It has been shown that the contribution from the single-particle excitations and bare Coulomb interaction to the equation for the gap has the form [5]

$$Z_{cl}\Delta_{cl} = -\int_0^\infty d\omega' \mathrm{Re}\left\{\frac{\Delta(\omega')}{\sqrt{\omega'^2 - \Delta^2(\omega')}}\right\} \times \mu(\omega')\, \tanh\frac{\omega'}{2T}, \tag{14}$$

where

$$\mu(\omega) = \frac{c}{(2\pi)^3}\int_{-\pi/c}^{\pi/c} dk_z \int_{Y(\omega)/v_F}^{2p_F} kdk \times [\, F(k,\omega) + F(k,-\omega)]\, V_{scr}(\mathbf{k}), \tag{15}$$

is the screened Coulomb repulsion parameter with

$$V_{scr}(k) = \frac{V(k)}{1 - V(k)\,[1 - G(k)]\,\chi_0(k_{\|},0)}, \quad (16)$$

as the screened Coulomb potential in a layered 2D metal. The averaging over k_z in Eq. (15) with the use of Eq. (16) gives the expression for the screened Coulomb repulsion parameter near $\omega \approx 0$ as $\mu(0) = \alpha\mu_s/\pi$ where

$$\mu_s = \int_0^1 \frac{dx}{\sqrt{1 - x^2}} \times \frac{1}{\sqrt{x^2\Phi^2(x) + 2\alpha x\Phi(x)\coth \zeta x + \alpha^2}}, \quad (17)$$

with $\Phi(x) = 1 - \alpha/\sqrt{1+4x^2}$, and $\zeta = 2p_F c$. In the strong coupling $\alpha >> 1$(low density) limit when $\zeta = 2p_F c \to 2$ we get

$$\mu_s \sim \frac{1}{\alpha\sqrt{5}} \ln \frac{4\sqrt{5p_F c}}{\sqrt{p_F(c + a^*_B) - 1}}, \quad (18)$$

which shows that the Coulomb repulsion parameter increases infinitely for $p_F(c + a^*_B) \to 1$. It will be seen later that the system undergoes a metal-insulator phase transition when the condition $p_F (c + a^*_B) = 1$ is satisfied.

Now we can evaluate the electron-plasmon interaction constant using the result of our previous paper [5]

$$\lambda_{pl}(\omega) = 4 \int_0^{\infty} \frac{d\Omega}{\Omega} S_{pl}(\Omega,\omega), \quad (19)$$

Substituting Eq. (13) into Eq. (19) we find the electron-plasmon interaction constant as

$$\lambda_{pl}(\omega) \approx \frac{\alpha\beta}{\pi} \ln (\Omega_0/\omega Z(\omega)), \text{ where}$$

$$\Omega_0 \propto \begin{cases} \omega_{pl}/\sqrt{\gamma - \alpha/2 + 3/4}, & \xi > 1, \\ \varepsilon_F, & \xi < 1, \end{cases} \quad (20)$$

and $\beta = \min\{\xi,1\}$, $\xi = \frac{\varepsilon_F}{\omega_{pl}}\sqrt{\gamma - \alpha/2 + 3/4}$. Thus in the vicinity of the instability (the metal-insulator phase transition) we have

$$\lambda_{pl} \sim \beta = \xi \approx \frac{\varepsilon_F}{\omega_{pl}} \sqrt{\gamma(1 + a^*_B/c - 1/cp_F)} \to 0$$

when $p_F (c + a^*_B) \to 1$, i.e., the electron-plasmon interaction constant drops rapidly in this region.

Next let us consider the renormalization parameter $Z(\omega)$ which includes contributions of both plasmon and single-particle excitations. It can be shown using the results of our previous paper [5] that the renormalization parameter can be written as

$$Z(\omega) = 1 + \bar{\lambda}_{pl}(\omega,T) + \frac{\alpha}{\pi}(1 - \mu_s), \quad (21)$$

where μ_s is defined by Eq. (17) and

$$\bar{\lambda}_{pl}(\omega,T) \approx \begin{cases} \frac{\alpha}{\pi}\beta \ln(\Omega_0/\omega), & \omega >> T, \\ \frac{\alpha}{\pi}\beta \ln(\Omega_0/T), & \omega << T, \end{cases} \quad (22)$$

is the temperature dependent electron-plasmon interaction constant. It follows from Eq. (21) that when μ_s is finite and less than the plasmon contribution, the quasi-particles are well defined with $Z(\omega)>1$. In the vicinity of the instability, however, μ_s increases infinitely, the renormalization parameter $Z(\omega)$ decreases rapidly and thus quasi-particle cannot exist. The instability (infinite increase of μ_s) corresponds to the metal-insulator phase transition which in this case manifests itself as a drop in the quasi-particle density of states at the Fermi surface. Thus, the exchange-correlation correction in a layered 2D system gives rise to the metal-insulator phase transition when the condition $p_F (c + a^*_B) = 1$ is satisfied. The dependence of the renormalization parameter on doping density (p_F^2) is schematically represented in the Fig. 1.

Following the method described in reference 5 the equation for the superconducting transition temperature is

$$T_c \approx 1.13\,\omega_0 \exp(-1/\lambda_{eff}), \quad (23)$$

where

$$\lambda_{eff}^{-1} \approx \frac{\pi\mu^*}{\alpha\beta} + \sqrt{\left(\frac{\pi\mu^*}{\alpha\beta}\right)^2 + \frac{2\pi}{\alpha\beta} + a^2 - b}\ , \quad (24)$$

Here a^2 and b are two constants of approximately equal magnitude, and $\mu^* = \mu(0)/[1+\mu(0)\ln(\omega_\infty/\omega_0)]$ is the reduced Coulomb repulsion parameter where ω_∞ is the cutoff frequency of the Coulomb repulsion, which is of order of ε_F, and $\omega_0 \approx \Omega_0$ is the cutoff frequency of the electron-plasmon interaction.

We now study Eq. (23) in two different limits: $p_F c >> 1$ and $p_F c \geq 1$. First, let us consider the case when $p_F c >> 1$ where we have $\omega_0 \approx \Omega_0 \approx \omega_c/\gamma \sim v_F/c << \varepsilon_F$ and $\alpha<<1$, and we get

$$T_c \sim \frac{v_F}{c} \exp\left(-\lambda_{eff}^{-1}\right),$$

where $\lambda_{eff}^{-1}>>1$ (since α is small and β is finite). Thus, in this case T_c will diminish with the increase of $p_F c$. In the case $p_F c \geq 1$ we have $\omega_0 \sim \varepsilon_F$, and $\beta \approx 1$ and T_c takes the form

$$T_c \sim \varepsilon_F \exp(-1/\lambda_{eff})$$

where λ_{eff}^{-1} is finite. This case which represents strong intra- and inter-plane couplings ($\alpha>>1$ and $p_F c \geq 1$) gives the maximum possible T_c which scales with the Fermi energy ε_F. However, in the vicinity of the metal insulator phase transition ($p_F c=1$), where μ_S increases and $\lambda_{pl} \sim \beta \approx \xi << 1$ decreases rapidly, Eq. (23) also leads to the sharp drop of T_c since $\lambda_{eff}^{-1}>>1$, because $\mu_s >> 1$(see Eq. (18)), and $\xi << 1$ (see Eq. (20)). Thus, exchange-correlation corrections strongly suppress plasmon mediated superconductivity in the vicinity of the metal-insulator phase transition.

Our calculation shows that in a layered 2D system, in the presence of Hubbard-type local field correction, the plasmon mediated superconductivity can explain the bell-shaped dependence of T_c on the carrier density [8] as schematically shown in Fig. 1, and that the metal-insulator phase transition takes place when the Fermi momentum is approximately equal to the inverse interlayer spacing. Our estimation of the doping parameter x at the metal-insulator phase transition ($p_F c \approx 1$) for the LaSrCuO compounds with $c \approx 6.6$Å, and $a \approx 3.8$Å (where a is the in-plane lattice constant for Cu) gives $x = a^2 n_s = a^2/2\pi c^2 \approx 0.053$, which is in good agreement with experimental values for the doping parameter for the insulator-superconductor transition.

In conclusion, in this paper we have shown that the Hubbard-type exchange-correlation corection can induce metal-insulator phase transition in a layered 2D electron gas and lead to the bell-shaped dependence on doping density of the transition temperature of the plasmon mediated superconductivity .

REFERENCES

1. V.Z. Kresin, Phys. Lett. **122A**, 434 (1987); Phys. Rev. B **35**, 8716 (1987); V.Z. Kresin and H. Moravitz, ibid. **37**, 7854 (1988).
2. J. Ruvalds, Phys. Rev. B **35**, 8869 (1987); Y. Ishii, and J. Ruvalds, *ibid.* **48**, 3455 (1993).
3. S.M. Bose and P.Longe, J. Phys. : Condens. Matter **2**, 2491 (1990); P. Longe and S.M. Bose, *ibid.* **4**, 1811 (1992).
4. Y.M. Malozovsky, S.M. Bose, and P.Longe, Phys. Rev. B **47**, 15242 (1993).
5. Y.M. Malozovsky, S.M. Bose, P.Longe, and J.D. Fan, Phys. Rev. B **48**, 10504 (1993).
6. C.M. Varma, P.B. Littlewood, S. Schmitt-Rink, E. Abrahams, and A.E. Ruckenstein, Phys. Rev. Lett. **63**, 1996 (1989).
7. P.B. Littlewood and C.M. Varma, Phys. Rev. B **46**, 405 (1992).
8. H. Zang and H. Sato, Phys. Rev. Lett. **70**, 1697 (1993).
9. D. Pines and P. Nozières, *The Theory of Quantum Liquids* (W.A. Benjamin, Inc., NY, 1966).
10. T.M. Rice, Annals of Phys. **31**, 100 (1964); T.K. Lee *et al*, Phys. Rev. Lett. **35**, 1048 (1975).
11. A.A. Abrikosov, L.P. Gorkov, and I.E. Dzyaloshinski, *Method of Quantum Field Theory in Statistical Physics* (Prentice-Hall, New Jersey, 1964).
12. M. Jonson, J. Phys. C **9**, 3055 (1976).

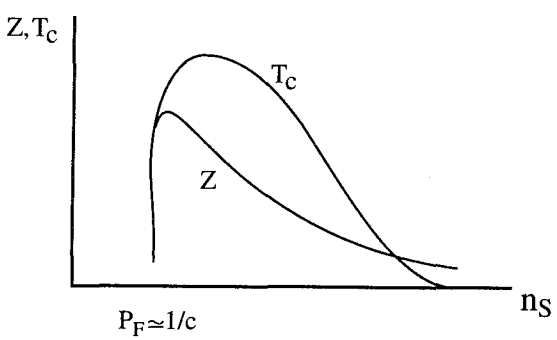

Fig. 1. Schematic diagram of the renormalization parameter $Z(\omega,T)$ and the transition temperature T_c on the carrier density n_s.

Journal of Superconductivity, Vol. 8, No. 4, 1995

Intrinsic Paramagnetic Centers in 1-2-3 Superconductors

M.A.Teplov[1], O.N.Bakharev[1,2], H.B.Brom[2], A.V.Dooglav[1], A.V.Egorov[1], E.V.Krjukov[1], O.B.Marvin[1], I.R.Mukhamedshin[1], V.V.Naletov[1], A.G.Volodin[1], D.Wagener[3], and J.Witteveen[2]

Received 31 January 1995

The ^{169}Tm "enhanced" NMR in $TmBa_2Cu_3O_{6+x}$ (x=0.5, 0.6) at temperatures below 4.2K and the ^{63}Cu(1) NQR in $YBa_2Cu_3O_{6.5}$ at temperatures above 4.2K are used to study properties of intrinsic paramagnetic centers incorporated into superconducting materials. The spin-lattice relaxation of thulium and copper nuclei reveals three types of paramagnetic centers to be present in oxygen-deficient 1-2-3 superconductors, those are (1) two-level ones with a spin S=1/2, localized outside CuO_2 bilayers, (2) singlet-ground-state paramagnetic centers with an integer spin S≥1 in CuO_2 bilayers, and (3) exchange copper-oxygen clusters with a half-integer spin S≥5/2, localized in a nearest neighborhood of CuO_x basal plane at boundaries of superconducting OrthoII microdomains.

KEY WORDS: 1-2-3 superconductors; NMR; NQR; spin-lattice relaxation; paramagnetic centers.

1. INTRODUCTION

Specific heat measurements at Lawrence Berkeley Laboratory on a variety of $YBa_2Cu_3O_{6+x}$ ($YBCO_{6+x}$) samples have revealed correlations between a number of sample-dependent parameters that suggest that the volume fraction of superconductivity is strongly sample dependent and that the nonsuperconducting (NSC) regions are associated with a low concentration of Cu^{2+} magnetic moments [1]. The principal goal of this paper is to clarify the origin of the paramagnetic centers (PCs) in 1-2-3 compounds using magnetic resonance methods. The "enhanced" NMR of ^{169}Tm nuclei (spin I=1/2, 100% natural abundance) in $TmBCO_{6+x}$ (x=0.5, 0.6) and ^{63}Cu(1) NQR in $YBCO_{6.5}$ were studied at low temperatures. The nuclear spin-lattice relaxation (NSLR) data suggests that all PCs are localized in NSC regions between superconducting (SC) mesoscopic domains of OrthoII structure.

2. THULIUM AND COPPER RELAXATION AT LOW TEMPERATURES

The ^{169}Tm NMR, "enhanced" by a hyperfine interaction of the nuclei with 4f-electrons, is very sensitive to the structure of the crystal lattice [2]. Five different combinations of "filled" and "empty" nearest-neighbor CuO chain fragments in $TmBCO_{6+x}$ form five types of rare-earth centers K_i (i=0,1,2,3,4 denote the number of "filled" chains, i=0,2,4 corresponding to Tetra, OrthoII, and OrthoI structures, respectively) in relative amounts well consistent with a model of two-dimensional ordering of the chains in CuO_x basal planes. The Tm spectra are described by the Hamiltonian $\mathcal{H}=-\hbar\Sigma\gamma_i H_i I_i$, whose parameters $|\gamma_b/2\pi|$ and $|\gamma_c/2\pi|$ at T≤4.2K have the following values: 68(1) and 22.0(5) MHz/T in OrthoI phase, 61(1) and 25.6(5) MHz/T in OrthoII phase, and 53(1) and 30.5(5) MHz/T in Tetra phase [3]. The particular feature of these spectra used in our studies is that the parameter $|\gamma_a/2\pi|$ remains at the value 53(1) MHz/T for all types K_i of Tm^{3+} centers. Consequently, at the condition H/ν=0.0189 T/MHz the resonant effect of the rf field is felt mainly by those $TmBCO_{6+x}$ crystallites whose a-axes are nearly parallel to field H. The principal features of the Tm NMR in samples aged at room temperature for more than 1 year are as follows [4]. The Tm NSLR is governed by PCs at boundaries between SC and NSC mesoscopic plate-like domains. The mean size of CuO chain fragments (or SC domains in the b-direction) has been estimated to vary from $6b_0$ (24Å) to $12b_0$ (48Å) for x's ranging from 0.5 to 0.8, and the PC concentration n vs. x has been deduced (Fig.1). The most interesting

[1]Kazan State University, 420008 Kazan, Russia
[2]Leiden University, P.O.Box 9506, RA 2300 Leiden, The Netherlands
[3]Universität Bonn, W-5300 Bonn, Germany

0896-1107/95/0800-0413$07.50/0

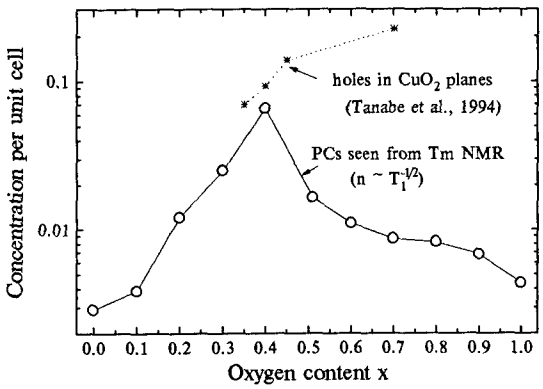

Fig.1. Concentrations of paramagnetic centers (O) and holes in CuO_2 planes (*=Ref.6) vs. oxygen content x.

finding is that the n-value at the transition "semiconductor-superconductor" (x=0.4) reaches the maximum of ~0.07/unit cell [5], which coincides with the critical hole density in CuO_2 planes for both the metallic conduction and superconductivity [6]. The NSLR kinetics in the "aged" samples was found to obey the following equation

$$1 - M_t/M_\infty = \exp(- (t/ T_1)^m)\cdot\exp(-t/ T_1'), \qquad (1)$$

with M_t the magnetization at time t, the T_1 and T_1' the NSLR times, and the quantity m=1/2, typical for three-dimensional systems. The measured relaxation rates $1/T_1'$ at liquid helium temperatures were found to have non-zero values (~$0.5s^{-1}$) only in the overdoped samples (x≥6.94). The kinetics (1) of the "m=1/2"- type, called "Förster's law", is known to be valid in the absence of the nuclear spin-diffusion [7], when nuclear spins relax directly via PCs randomly distributed in a crystal lattice. The diffusionless relaxation is characteristic for $TmBCO_{6+x}$ compounds, since numerous crystal lattice defects result in a large difference between local crystal electric fields and, consequently, between Larmor frequencies of Tm nuclei at neighboring Tm sites. The same defects should be responsible for the distortions of the electric field gradients at copper sites, resulting in a diffusion- limited relaxation of Cu nuclei as well. At liquid helium temperatures the NSLR of both ^{169}Tm and $^{63}Cu(2)$ nuclei in $TmBCO_{6.92}$ sample with a low PC concentration obey Eq.(1) with $1/T_1'=0$ and m=1/2, however, in the case of a high PC concentration (at x=0.5) the power m becomes close to 1/3, the value characteristic for two-dimensional systems [8]. The physical reasons for such a difference in the NSLR behavior in high- and low-PC concentration limits will be discussed elsewhere. Formally, in any case the magnetization can be anticipated to recover according to the Eq.(1) with m=D/6 and the NSLR rate dependent on the PC parameters as follows:

$$1 / T_1 = A_D \frac{\tau_c}{1 + \omega_0^2 \tau_c^2}(1 - P_o^2) \; . \qquad (2)$$

Here D is a dimensionality of the PC distribution, ω_0 is the nuclear resonance frequency, τ_c is a correlation time for the local magnetic field fluctuations created by PCs at nuclei's sites, P_0 is the polarization factor (P_0= tanh($g\mu_B H/2kT$) for the two-level system with S=1/2), the coefficient $A_D \sim n^{6/D}$ being dependent on n and D, and on the strength of dipolar interaction between nuclei and PCs.

3. Tm RELAXATION IN $TmBCO_{6+x}$ (x=0.5 and 0.6)

Since PCs in 1-2-3 compounds are, most likely, induced by a certain type of the crystal lattice defects, i.e., oxygen vacancies, we studied the low temperature NSLR evolution as a function of time of a room-temperature annealing (RTA) of non-equilibrium samples. The samples were prepared from the starting materials with x=0.95 by annealing in air at 700-750 °C followed by fast quenching in liquid nitrogen. The RTA procedure of sample x=0.5 results in the evolution of the Tm NMR spectrum from tetragonal to orthorhombic symmetry and an increase of the critical temperature T_c. The most peculiar features of the Tm NSLR in non-equilibrium samples are as follows [9]: (a) The "m=1/3"-type kinetics observed at 1.5K for the sample x=0.5 aged for $t_{RTA} \leq 1000$ min transform into "m=1/2"-type at $t_{RTA} \geq 10^4$ min. (b) The "1/3"-type kinetics are found for both "as quenched" ($t_{RTA} \approx 30$ min) and the "aged" (t_{RTA}=2 weeks) samples x=0.5 at temperatures above ~2K, however the "1/3"-power in the "aged" sample transforms into "1/2"-power at T<1K. Therefore, the transition from one regime to another can be driven not only by an oxygenation of the sample (x=0.5→0.6) or by the RTA procedure for a long enough time, but can be driven also by the temperature lowering. The latter fact means that the concentration of PC- acceptors starts to decrease at low temperatures. Such effect of a thermal depopulation is well consistent with a model of a singlet-doublet system. Indeed, the effect of the thermal depopulation must occur in the system where the PCs have a non-magnetic (singlet) ground state, separated from an excited magnetic state by an energy gap of ~1K. (c) The experiments with sample x=0.6 confirm the "1/2"-type kinetics in the whole temperature range from 0.7K to 4.2K. (d) The temperature dependence of the NSLR rate obeys the law $T_1^{-1} \sim$ (1-$\tanh^2\delta/2kT$), characteristic for the relaxation via

paramagnetic impurites. However, the energy splitting δ depends on x: in the field of 1.7T we have δ=3.4÷3.6K and 2.3÷2.7K for x=0.5 and 0.6, respectively, the latter value of δ corresponding to the Zeeman splitting $g\mu_B H$ in a two-level system with S=1/2 and g=2.0÷2.4.

Overall, the Tm NSLR data makes it possible to assume two types of PCs to be present in oxygen-deficient $TmBCO_{6+x}$ superconductors, those are singlet-ground-state PCs localized in CuO_2 planes and two-level PCs localized, most likely, outside CuO_2 planes. The concentration of singlet-ground-state PCs is very high in as-quenched samples and decrease drastically during RTA procedure, so that in well-annealed samples the two-level PCs centers remain mainly responsible for the nuclear relaxation at low temperatures.

4. Cu(1) RELAXATION IN $YBCO_{6.5}$

The $^{63}Cu(1)$ NQR spectrum of twofold co-ordinated $Cu^{+}(1)_2$ atoms consists of three lines [10] at 31.4 MHz (copper NQR centers belong to the "empty" chain located between two "filled" CuO chain fragments), 30.9 MHz (one of the neighboring chains is empty), and 30.3 MHz (both heighboring chains are empty). The 30.9 MHz-line has a maximum intensity in as-quenched sample x=0.5, however, during RTA procedure the intensity of the 31.4 MHz-line, corresponding to the growing OrthoII phase, increases at the expense of 30.9 MHz-line. All the results discussed below were obtained at the frequency of 31.4 MHz. In this way the $^{63}Cu(1)$ NQR was used to monitor the formation of SC microdomains of Ortho II phase during RTA procedure. The kinetics of the Cu(1) NSLR at T=4.2K was found to obey Eq. (1) with $1/T_1'=0$ and m=1/3 (two-dimensional distribution of PCs) for any values of the annealing times t_{RTA} up to 8 months. As follows from Eq.(2) with $A_2 \sim n^3$ and measured values of T_1's at T=4.2K (T_1=2ms and 13ms at t_{RTA}=6min and 8 months, respectively), the PC concentration falls down (for ~2 times) during RTA when microdomains of Ortho II phase grow in size. The characteristics of these PCs responsible for the NSLR of Cu(1) nuclei can be seen from the temperature dependence of the NSLR rate (Fig.2). In fact, the kinetics of the Cu(1) NSLR at temperatures above ~20K is described by Eq. (1) with m=1/3 and $1/T_1' \neq 0$. We shall not discuss here the relaxation mechanism accounted for the measured values of the rates $1/T_1'$ shown in lower part of Fig.2, but concentrate on the rate $1/T_1$ governed by PCs. For temperatures above 4.2K the T_1^{-1} vs. T^{-1} dependences for both "as-quenched " (t_{RTA}=20 min) and "aged" (t_{RTA}=4.5

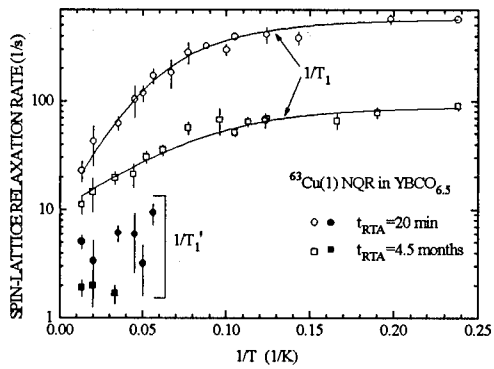

Fig.2. Temperature dependences of Cu(1) NSLR rates $1/T_1$ (O,□) and $1/T_1'$ (●,■) in "as quenched" (O,●) and "aged" (□,■) $YBCO_{6.5}$ samples. Solid lines represent Eqs.(3) with the parameters (4) (lower curve) and (5) (upper curve).

months) samples can be formally described by the Eq.(2) with $P_0=0$ and $A_2=\gamma^2\langle h_t^2\rangle$, where $\gamma/2\pi=11.285$ MHz/T is the gyromagnetic ratio of ^{63}Cu nuclei, and $\langle h_t^2\rangle$ is the mean square of a transverse (perpendicular to the c-axis) fluctuating local field produced by PCs at Cu(1) sites. Having now the Eq.(2) in a standard form [11], one can explain the decrease of the rate $1/T_1$ at high temperatures as a result of shortening of the time τ_c. It was shown earlier in EPR measurements [12] that impurity rare-earth ions (Er and Yb) in $YBCO_{6.85}$ compound are subject to a fluctuating magnetic field of ~16mT from copper ions, independent of the sort of rare-earth ions and directed predominantly along the c-axis. The fluctuation rate of this field at T>6K has been found to increase exponentially with temperature: $W(s^{-1})=3.5\cdot10^{10}\cdot\exp(-25/T)$. Since the relaxation rates $1/T_1$ of Cu(1) nuclei do not depend on temperature at $4.2K \leq T \leq 10K$, in the following we assume the fluctuation rate $1/\tau_c$ to consist of the temperature dependent contribution W and the temperature-independent term W_{ss}, appeared due to a spin-spin interaction of PC-acceptors with each other. Thus, using the equation

$$1/T_1=\gamma^2\langle h_t^2\rangle\tau_c/(1+\omega_Q^2\tau_c^2) \qquad (3a)$$

with

$$1/\tau_c=W+W_{ss}, \qquad (3b)$$

we can describe fairly well the experimental data on the "aged" sample $YBCO_{6.5}$ at the following values of the parameters:

$$\langle h_t^2\rangle^{1/2}=8.7\text{mT}, \qquad W_{ss}=4.4\cdot10^9 s^{-1}. \qquad (4)$$

It is seen in Fig.2 that the temperature dependence of the Cu(1) relaxation in the "aged" sample at temperatures around 77K is somewhat stronger than that corresponding to the activation energy of 25K. This

feature appears to be much more pronounced in the experimental data for the "as-quenched" sample, in which case the best-fit procedure gives the following results (upper curve in Fig.2.):

$W(s^{-1})=3.5\cdot10^{10}\exp(-25/T)+3.4\cdot10^{11}\exp(-77/T)$,

$\langle h_t^2\rangle^{1/2}=24.1$mT, $W_{ss}=5.4\cdot10^9\ s^{-1}$. (5)

Summarizing the results of our analysis, given in Eqs.(3)-(5), we have to notice several peculiar facts.

(a) The energy splittings of 25K and (77-25)≈50K support the idea that PCs felt by Cu(1) nuclei are actually copper-oxygen paramagnetic clusters with a half-integer spin S≥5/2. The splitting of 25÷77K (2÷7 meV) appear to be similar with so-called "energy gaps" in a magnetic excitation spectra of oxygen-deficient $YBCO_{6+x}$ [13].

(b) The "spin-spin relaxation" rate W_{ss} does not depend strongly on the concentration of PCs, whereas the effective fluctuating field $\langle h_t^2\rangle^{1/2}$ at Cu(1) nuclei in OrthoII microdomains in the "as-quenched" sample is almost three times larger than that in the "aged" sample.This fact supports the idea [4] that PCs are localized outside superconducting microdomains. Under the assumption that PCs felt by Cu(1) nuclei are coupled by a purely dipole-dipole interaction, one can use the relation $W_{ss}\sim S(S+1)g^2\mu_B^2/r^3\hbar$ to estimate the distance between PCs. Using $W_{ss}=5\cdot10^9 s^{-1}$, S=5/2, and g=2, we find r~8Å, i.e. the distanse between the "filled" CuO chains in OrthoII phase. This may mean that PCs are localized at the ends of the "filled" CuO chain fragments at boundaries of OrthoII microdomains.

(c) The pre-exponential factors in Eq.(5) are approximately two orders of magnitude larger than those for rare-earth ions having Stark splittings of ~30K. This extremely fast spin-lattice relaxation also supports the idea that we deal with clusters formed by a very strong exchange (superexchange) interaction.

5. CONCLUSION

The Tm and Cu(1) NSLR data suggest that oxygen deficient 1-2-3 superconductors contain three types of intrinsic PCs, those are with half-integer spins S=1/2 and S≥5/2, and with an integer spin S≥1. The latter type of PCs seems to be the most intriguing one, since their concentration reaches a maximum value at the "semiconductor-superconductor" transition (x=0.4) and decreases drastically in "good" superconducting materials. The pentanuclear copper clusters with oxygen holes localized in CuO_2 planes and characterized by a total spin S=2 [14] can be considered as plausible candidates on the role of these PCs.

ACKNOWLEDGMENTS

This work was supported by the Ministry of Science and Technology of Russian Federation, the Scientific Council on HTSC Problem, under Project No. 91001, and the NATO Scientific and Environmental Affairs Division, under Grant HTECH. 930343. Authors are grateful to L.K.Aminov and M.V.Eremin for fruitful discussions.

REFERENCES

1. N.E.Phillips, J.P.Emerson, R.A.Fisher, J.E.Gordon, B.F.Woodfield, and D.A.Wright, *J. of Superconductivity* 7, 251 (1994).
2. L.K.Aminov and M.A.Teplov, *Sov.Phys.Usp.* **28**, 762, (1985).
3. O.N.Bakharev, A.V.Dooglav, A.V.Egorov, H.Lütgemeier, M.P.Rodionova, M.A.Teplov, A.G.Volodin, and D.Wagener, *Appl.Magn.Resonance* **3**, 613 (1992).
4. O.N.Bakharev, A.V.Dooglav, A.V.Egorov, O.B.Marvin, V.V.Naletov, M.A.Teplov, A.G.Volodin, and D.Wagener, *JETP Lett.* **58**, 608 (1993); also, in *Phase Separation in Cuprate Superconductors*, E.Sigmund and K.A.Müller, eds. (Springer-Verlag, Berlin, 1994), p.257.
5. M.A.Teplov, O.N.Bakharev, A.V.Dooglav, A.V.Egorov, E.V.Krjukov, O.B.Marvin, V.V.Naletov, A.G.Volodin and D.Wagener, *Physica C* **235-240**, 265 (1994).
6. K.Tanabe, S.Kubo, F.Hosseini Teherani, H.Asano, and M.Suzuki, *Phys.Rev. Lett.* **72**, 1537 (1994).
7. M.R.McHenry, B.G.Silbernagel, and J.H.Wernick, *Phys.Rev. B* **5**, 2958 (1972).
8. J.Klafter and A.Blumen, *J.Chem.Phys.* **80**, 875 (1984).
9. O.N.Bakharev, J.Witteveen, H.B.Brom, E.V.Krjukov, O.B.Marvin, and M.A.Teplov, *Phys.Rev.B* **51**, 693 (1995).
10. I.Heinmaa, H.Lütgemeier, S.Pekker, G.Krabbes, and M.Buchgeister, *Appl.Magn.Resonance* **3**, 689 (1992).
11. C.P.Slichter, *Principles of Magnetic Resonance*, 3-rd ed. (Springer, Berlin) 1989.
12. I.N.Kurkin, I.Kh.Salikhov, L.L.Sedov, M.A.Teplov, and R.Sh.Zhdanov, *JETP* **76**, 657 (1993).
13. V.Barzykin. D.Pines, A.Sokol, and D.Thelen, *Phys.Rev.B* **49**, 1544 (1994).
14. M.V.Eremin and E.Sigmund, *Solid State Comm.* **90**, 795 (1994).

Journal of Superconductivity, Vol. 8, No. 4, 1995

Electronic Raman Scattering in $YBa_2Cu_4O_8$

S. Donovan,[1] J. Kircher,[1] J. Karpinski,[2] E. Kaldis,[2] and M. Cardona[1]

Received January 5, 1995

We report on the electronic Raman scattering in $YBa_2Cu_4O_8$ and find that, in contrast to the other superconducting cuprates, the continuum in the normal state is strongly temperature dependent in all polarizations. This temperature dependence is found to follow a Bose-Einstein-like form. We conclude that the absence of the Bose-Einstein factor in the electronic continuum is not essential to high-T_c superconductivity, as is sometimes implied. Additionally, we report on the rearrangement of the continuum which occurs below T_c.

KEY WORDS: Electronic Raman Scattering, Normal State, Non-Fermi Liquid behavior

1. INTRODUCTION

The electronic Raman scattering continuum observed in the superconducting cuprates [1,2] exhibits several very unusual properties. In particular, the unexpected frequency and temperature independence of this background have led to a wealth of investigations, both experimental and theoretical, into its origins. A phenomenological Marginal Fermi Liquid (MFL) model was proposed by Varma [3], who showed that a wide variety of the anomalous normal state properties could be understood if the quasiparticle scattering rate was linearly dependent on both frequency and temperature. Virosztek and Ruvalds later showed that this result could be obtained from a microscopic point of view [4]; within their Nested Fermi Liquid (NFL) theory the electronic scattering rate is given by:

$$\tau^{-1} = \alpha[\omega^2 + \beta^2 T^2]^{1/2} \qquad (1)$$

where α and β are determined by the ratio of the Hubbard U to the one-electron bandwidth and β is on the order of 1.

Electronic Raman scattering has been extensively studied in doped semiconductors [5], where, as first pointed out by Platzmann [6], neutral density fluctuations involving carriers from different valleys lead to low-frequency inelastic scattering of light. However, it was found that the experimental results could only be understood if non-k-conserving electronic collisions were considered [7]. In this case, the Raman scattering efficiency is simply given by:

$$\frac{\partial^2 S}{\partial\omega\partial\Omega} = (1+n_\omega)\frac{\omega\tau^{-1}B}{\omega^2+\tau^{-2}} \qquad (2)$$

where $1+n_\omega=[1-\exp(-\omega/T)]^{-1}$ is the Bose-Einstein factor, τ^{-1} the electron scattering rate and B is:

$$B = \frac{e^4}{\pi c^4}N(\epsilon_F) < |\hat{\mathbf{e}}_l \cdot (\mu^{-1} - <\mu^{-1}>) \cdot \hat{\mathbf{e}}_s|^2 > \qquad (3)$$

where μ is the effective mass tensor and $<>$ indicates an average over the Fermi surface.

Combining Eqs. 1 and 2 one finds in the limiting cases of $\omega/T \to \infty, 0$ that $\frac{\partial S}{\partial\omega\partial\Omega} \to \frac{B\alpha}{1+\alpha}, \frac{B}{\alpha\beta}$, thus tending to a constant in either case. Such an analysis has been used extensively to explain the ω, T independence of the electronic continuum. In contrast to the large number of cuprates which display this behavior, the B_{2g} component of the continuum in $Bi_2Sr_2CaCu_2O_8$ exhibits the "usual" Bose-Einstein-like behavior as the temperature is decreased. The origin of this effect is not at all understood and, partly for this reason, we decided to look at the normal state temperature dependence of some of the other cuprates. We will report here our recent measurements performed on $YBa_2Cu_4O_8$ (124) samples.

2. EXPERIMENTAL TECHNIQUES AND CRYSTAL PREPARATION

Single crystals of the 124 superconductor were grown in a (BaO-CaO)-rich flux under high oxygen

[1]Max-Planck-Institut für Festkörperforschung, Postfach 80 06 65, D-70506 Stuttgart, Germany

[2] Laboratorium für Festkörperphysik, ETH Zürich-Hönggerberg, 8093 Zürich, Switzerland

0896-1107/95/0800-0417$07.50/0

pressure (910 bar) at 1380 K. Details of the growth process are published elsewhere [8,9]. In contrast to the one-chain compounds, where impurities from the crucible occupy Cu(I) sites, many impurities in the two-chain compound 124 replace plane-Cu ions since the double chains are more stable. Therefore, the plane properties (and T_c) are more susceptible to impurities in 124 [10]. Unlike the older 124 samples, grown in alumina crucibles, our samples were grown in 1993 in an yttria crucible. The critical temperature of these samples is 79.5 K, which is comparable to that obtained on the best sintered materials and significantly higher than that obtained in the older samples (T_c ~72 K).

The dimensions of the samples are about 1.5 mm × 1 mm × 80 μm; the same samples were used previously for other optical measurements [11]. The as-grown crystals are twin-free, as opposed to $YBa_2Cu_3O_7$ (123) where a thermomechanical detwinning procedure is required.

All spectra presented here were taken using the 514.5 nm line of an Ar^+ laser with the scattered light collected into a SPEX Triplemate spectrometer equipped with a Mepsicron position-sensitive detector. The laser spot size on the sample was ~25 μm. The power was kept below 2 mW and at these levels we were unable to see evidence of sample heating. The samples were mounted on the cold finger of a He flow-through UHV cryostat with a base pressure (300 K) better than $\sim 10^{-7}$ Torr in a near-backscattering geometry (angle of incidence ~ 20°). In this configuration we obtained reproducible spectra even after prolonged periods (days) at low T.

3. RESULTS AND DISCUSSION

The Raman spectra of 124 have been thoroughly investigated; we refer the interested reader to the literature for details [12,13]. The samples mounted in such a way that the *a*, *b*, and *c* axes corresponded to the *x*,*y*, and *z* axes of the lab. As all measurements presented here were made with the light polarized in the CuO_2 planes (i.e. $k \parallel c,z$), we will use an abbreviated Porto notation *jk*, where *j* and *k* signify the polarization directions of the incident and scattered light, respectively, for the polarization configuration. The *x'* and *y'* directions are rotated by 45° about the *z* axis with respect to the *x* and *y* axes. Since we are interested in the electronic background, one must be careful to avoid any stray light and/or luminescence from the sample, cold finger, and/or cryostat windows. We found that all of the phononic features (frequencies and relative intensities) were reproducible at different points on each sample, thus indicating the homogeneity and untwinned nature of the crystals. However, we also observed considerable increases in the intensity of the continuum towards high frequencies at different points on the same sample. These differences presumably originate from luminescent centers at the sample surface. We report here only spectra which display the flat, frequency-independent feature characteristic of the electronic scattering in the HiTc superconductors. Such spectra were reproduced at several different points on the same sample as well as on a separate sample from the same batch.

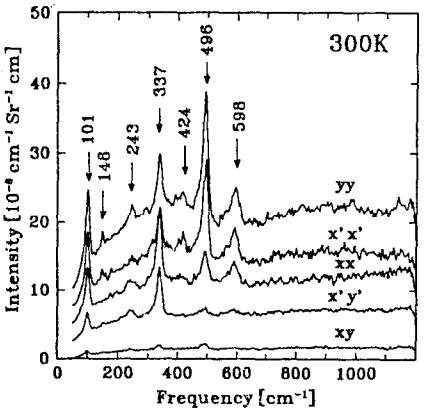

Fig. 1. Absolute Raman scattering efficiency in 124 in 5 different polarization configurations at 300 K. The frequencies of A_g phonons are given. For the sake of clarity consecutive offsets of 0,1,...,4 × 2.5 10^{-6} cm^{-1} Sr^{-1} cm were used for the xy,$x'y'$,...,yy spectra, respectively.

In Fig. 1 we present the absolute Raman efficiency for 124 at 300 K in 5 polarization configurations. The absolute efficiencies were determined by comparison with the known efficiencies [14] of both Si and BaF_2. After corrections for both the optical constants [15] and the instrumental lineshape, the results obtained based on the BaF_2 standard were within 25% of that found with the Si standard. We present the results obtained from the Si standard in Table I below, together with the results of Krantz [16] obtained for 123. A comparison with the values obtained from 124 band structure calculations is not yet possible, but we note that our experimental results agree well (to better than a factor of 2) with the calculations performed for 123 [16,17] in both the absolute value and polarization dependence. This result seems to indicate that the contribution of the second chain band is not that large. A more detailed analysis must await further calculations of the mass fluctuations of 124 entering into Eq. 3.

On the l.h.s. of Fig. 2 we show the spectra

obtained in 5 different polarization configurations at 300 K (upper curve, dashed) and 90 K (lower curve, solid). The spectra are displayed up to 1200 cm^{-1} and were corrected for spectrometer response. Their most striking feature is the large observed temperature dependence of the continuum. As mentioned above, previous measurements on a variety of cuprates [1,13]

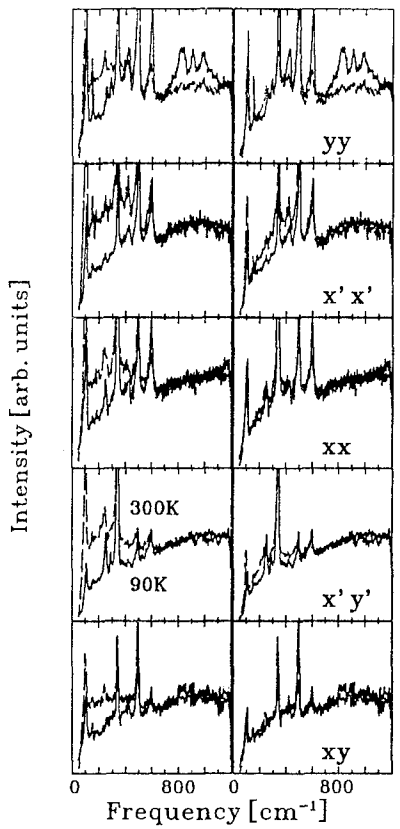

Fig. 2. The Raman scattering efficiency in 124 shown in 5 different polarization configurations at both 300 K (dashed) and 90 K. The 5 panels on the left hand side of the figure are as measured, whereas the 5 panels on the right hand side have been corrected with the Bose-Einstein factor $1 + n(\omega)$.

have indicated that, with the exception of the xy configuration of $Bi_2Sr_2CaCu_2O_8$, the background is practically temperature independent. For 124, on the contrary, we find a rather strong temperature dependence below ~500 cm^{-1}. Furthermore, the 90 K spectra can be seen to decrease sharply compared with those at 300 K in *all* polarization configurations. Such a feature is strongly suggestive of the need to correct for the Bose-Einstein factor, as seen in Eq. 2. The Bose-Einstein corrected spectra are displayed in the 5 panels on the right hand side of Fig. 2 and the agreement between the two sets of data (90 and 300 K) is excellent.

We emphasize that while the spectra *are* temperature dependent in the normal state of 124, the very broad, nearly frequency independent behavior of the continuum found in all cuprates was also observed in 124. This feature is clearly still anomalous and cannot simply be described within a Fermi liquid approach. However, as seen from Eqs. 1 and 2 our results can be understood within the NFL if $\beta \ll 1$. As of yet, we do not understand why β appears to differ between the 123 and 124 compounds.

In addition to the clearly Bose-Einstein-like continuum in 124, we find 3 high-frequency polarization-dependent features at low temperatures which have not been previously observed. These features can be easily seen in the 90K yy spectra presented in Fig. 2 and are observed to peak near 826, 908, and 982 cm^{-1}. They are broad compared to the low frequency phonons and two of them peak at frequencies very close to twice the 424 and 496 cm^{-1} phonon frequencies, with the third seen to peak near the sum of these two frequencies. In particular, since the A_g phonon appearing at 424 cm^{-1} in the 300 K spectrum of Fig. 1 has a strongly asymmetric Fano lineshape ($q < 0$), the observed one-phonon peak appears lower in frequency than the fitted bare phonon frequency (in this case the difference is 8 cm^{-1}). At 90 K, the intensity peak occurs at 421 cm^{-1} ($\omega(\text{bare}, 90\text{ K}) = 430\ cm^{-1}$), so that a feature at twice this frequency would peak near 842 cm^{-1}, or about 16 cm^{-1} above the observed maxima. Note, however, that this is well within the 68 cm^{-1} width which, in the case of two-phonon spectra, is due to the phonon dispersion. If the 3 high frequency features originated from 2 phonon processes we would expect features near 842, 917, and 992 cm^{-1}, in good overall agreement with the observed peaks [18].

Finally, we present the spectra obtained on 124 at 10 K, in the superconducting state. In order to emphasize the redistribution of the continuum which occurs below T_c, we have removed the contribution from the phonons by dividing the Bose corrected spectra at 10 K with their 90 K counterparts. The results are displayed in Fig. 3. These ratios are proportional to the 10 K spectra since the normal state spectra are only weakly frequency dependent. However, since the phonon parameters are somewhat temperature dependent in this range, the cancellation is not complete and one is left with sharp spikes in the vicinity of the phonons. Another possibility is to fit the phonons and then to subtract their contribution. However, since the phonons interact strongly with the con-

tinuum one must fit this coupled phonon-continuum excitation over a fairly wide range and we have found

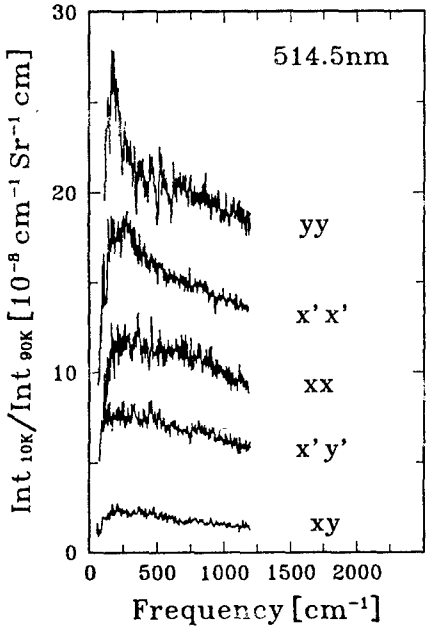

Fig. 3. The ratio of the 10 and 90 K spectra in 124 shown in 5 different polarization configurations normalized to the absolute scattering efficiency. Note that for the sake of clarity consecutive offsets of 0,1,...,4 × 2.5 10^{-8} cm^{-1} Sr^{-1} cm were used for the xy,$x'y'$,...,yy spectra, respectively.

that small deviations of the fit from the data produce large spurious features in the resulting spectra. We have tried both methods on each spectrum, and in the case of mutual agreement (e.g. $x'x'$), we present the data obtained by fitting the phonons, but when discrepancies result, we present just the ratio (e.g. yy). In either case, the results are qualitatively similar to those for several other cuprate superconductors [1]. In particular, no sharp cut-off below a characteristic gap frequency is observed, but a rather broad polarization dependent maximum is found together with an approximately linear decrease down to zero frequency. Furthermore, as seen in other cuprates, the symmetric A_g component (yy) peaks near the maximum of the B_{2g}, but well below the B_{1g} component [20,19]. This will be analyzed in detail in a future publication.

4. CONCLUSIONS

We have presented evidence for the need to correct the electronic continuum in 124 for the Bose factor, in contrast to most of the other cuprates. This suggests that the marginal Fermi Liquid, introduced to explain the lack of a Bose temperature dependence in the Raman continuum, is not an essential component of the mechanism of superconductivity.

Table I. Absolute room temperature Raman efficiencies for electronic scattering at 700 cm^{-1} in 124 with a 514.5 nm laser excitation. These results were based on comparison with the know efficiency of Si and are given in units of 10^{-8} cm^{-1} Sr^{-1} cm. For the purposes of comparison, we include the measured results [16] for 123.

Polarization	$\frac{\partial^2 S}{\partial\omega\partial\Omega}$ 124	$\frac{\partial^2 S}{\partial\omega\partial\Omega}$ 123[a]
yy	10	27
$x'x'$	7.0	17
xx	5.8	14
$x'y'$	4.2	9.0
xy	1.7	3.4

a Ref. [16].

ACKNOWLEDGMENTS

We express our appreciation to K. Syassen for the use of the Mepsicron detector, to Tao Zhou for his help, to H. Hirt and M. Siemers for their expert technical assistance. One of us (S.D.) is indebted to the A.-von-Humboldt Foundation for support.

REFERENCES

1. T. Staufer *et al.*, Solid State Comm. **75**, 975 (1990).
2. D. Reznik *et al.*, Phys. Rev. B **46**, 11725 (1992).
3. C.M. Varma *et al.*, Phys. Rev. Lett. **63**, 1996 (1989).
4. A. Virosztek *et al.*, Phys. Rev. Lett. **67**, 1657 (1991).
5. G. Abstreiter *et al.*, in *Light Scattering in Solids IV*, ed. M. Cardona, G. Güntherodt (Springer, Berlin, 1984).
6. P.M. Platzmann, Phys. Rev. A **139**, 379 (1965).
7. I.P. Ipatova *et al.*, Solid State Comm. **37**, 893 (1981).
8. J. Karpinski *et al.*, Appl. Supercond. **1**, 333 (1993).
9. J. Karpinski *et al.*, in *Materials and Crystallographic Aspects of Hi-Tc Superconductivity*, ed. E. Kaldis (Kluwer 1994), p. 555-583.
10. H. Schwer *et al.*, to be published.
11. J. Kircher *et al.*, Physica C, in press.
12. E.T. Heyen *et al.*, Phys. Rev. B **41**, 11058 (1990).
13. E.T. Heyen *et al.*, Phys. Rev. B **43**, 12958 (1991).
14. M. Cardona, in *Light Scattering in Solids II*, ed. M. Cardona, G. Güntherodt (Springer, Berlin, 1981).
15. J. Kircher *et al.*, Phys. Rev. B **48**, 3993 (1993).
16. M.C. Krantz *et al.*, Phys. Rev. B, in press.
17. O.K. Andersen *et al.*, Physica C **185-189**, 147 (1991).
18. M. Reedyk *et al.*, Phys. Rev. B **50** 13762 (1994).
19. T.P. Devereaux *et al.*, Phys. Rev. Lett. **72**, 396 (1994).
20. M.C. Krantz *et al.*, J. Low Temp. Phys., in press.

Journal of Superconductivity, Vol. 8, No. 4, 1995

Electronic Raman Scattering as a Probe of Anisotropic Electron Pairing

T. P. Devereaux[1]

Received 5 January 1995

A theory for the electronic contribution to Raman scattering in anisotropic superconductors is presented. It is shown that Raman scattering can provide a wealth of polarization-(symmetry-) dependent information which probes the detailed angular dependence of the energy gap. Using a model band structure, the symmetry-dependent Raman spectra are calculated for $d_{x^2-y^2}$ pairing and compared to the data taken on $Bi_2Sr_2CaCu_2O_8$. Favorable agreement with the symmetry-dependent electronic spectra is shown. Further, the impurity dependence of theory is calculated, which provides an unique test of $d_{x^2-y^2}$ pairing.

KEY WORDS: Raman scattering, polarization symmetry, $d-$wave, impurity scattering.

1. INTRODUCTION

The electronic Raman spectra of the cuprates in the superconducting phase shows a remarkable dependence on the incident and scattered photon polarization vectors[1]-[6]. This polarization dependence, which is consistently seen in all the cuprates regardless of the presence of chains and the number of CuO_2 planes, has been recently interpreted as evidence for an order parameter of predominantly $d_{x^2-y^2}$ symmetry[7]. The key to the polarization dependence lies in the coupling of the screened Raman vertex $\delta\gamma(\mathbf{k}) = \gamma(\mathbf{k}) - \langle\gamma(\mathbf{k})\rangle$, and the energy gap $\Delta(\mathbf{k})$. The topology of the nodes of each of the functions leads to a polarization dependence which not only affects the peak positions for each polarization orientation, but also the behavior of the spectra for small frequency shifts. Defining the imaginary part of the Tsuneto function as

$$\lambda''(\mathbf{k},\omega) = \Theta(\omega^2 - 4 \mid \Delta(\mathbf{k}) \mid^2)\tanh(\omega/4T) \times \frac{\mid \Delta(\mathbf{k}) \mid^2}{\sqrt{\omega^2 - 4 \mid \Delta(\mathbf{k}) \mid^2}}, \quad (1)$$

the screened Raman spectra can then be written as

$$\chi''(\omega) \sim \langle \mid \delta\gamma(\mathbf{k}) \mid^2 \lambda(\mathbf{k},\omega)\rangle'' - \left\{ \frac{\langle \delta\gamma(\mathbf{k})\lambda(\mathbf{k},\omega)\rangle^2}{\langle\lambda(\mathbf{k},\omega)\rangle} \right\}'' \quad (2)$$

[1]Department of Physics, University of California, Davis CA 95616

where $''$ denotes taking the imaginary part. The real parts of the Tsuneto function can be obtained from the imaginary part via a Kramers Kronig transformation. The second term of Eq. (2) takes into account the complete screening of intercell charge fluctuations so that only anisotropic charge fluctuations (intracell) remain. This is the expression for the gauge invariant Raman response which has Coulomb screening and the Anderson–Bogoliubov gauge mode taken into account. It does not take into account any vertex corrections resulting from the pairing interaction in other channels other than the pairing channel. The derivation and consequences of the above expression have been put forth in Ref. [7].

2. RAMAN VERTEX

The polarization dependence enters through the coupling of $\delta\gamma(\mathbf{k})$ and the energy gap $\Delta(\mathbf{k})$ under the Fermi surface averaging, and leads to subsequently different frequency dependent Raman spectra for each polarization channel. For non-resonant scattering, the Raman vertex can be expressed in terms of the curvature of the energy band dispersion $\epsilon(\mathbf{k})$,

$$\gamma(\mathbf{k}) = m \sum_{\alpha,\beta} e^{\mathrm{S}}_{\alpha} \frac{\partial^2\epsilon(\mathbf{k})}{\partial k_\alpha \partial k_\beta} e^{\mathrm{I}}_{\beta}, \quad (3)$$

where $\hat{\mathbf{e}}^{\mathbf{S,I}}$ denote the scattered and incident polarization light vectors, respectively, which select elements of the Raman tensor. Thus under the average, the contribution to Raman scattering is due to both

0896-1107/95/0800-0421$07.50/0

(1) a large density of states, and (2) large curvature of the band near the Fermi level. We parameterize our band structure via the standard $t-t'$ model with lattice constant a,

$$\epsilon(\mathbf{k}) = -2t\,[\cos(k_x a) + \cos(k_y a)] + 4t'\cos(k_x a)\cos(k_y a). \quad (4)$$

Here t and t' are the nearest and next nearest neighbor hopping parameters, respectively. This is the anti–bonding band derived from a reduction of a three band model which gives the largest contribution to the density of states at the Fermi level for the cuprate systems and adequately reproduces the observed photoemission data[8].

Recently it has been suggested that the presence of another band, due to, e.g., another CuO_2 plane as in Y 1:2:3, can lead to substantially different results than the case for a single band[9]. This is in conflict with experiments, since the details of the number of planes and chains do not seem to affect the observed spectra[1]- [6]. This has been shown theoretically in Ref. [10], which considers multiband scattering. of two planes, the response can be constructed from the real space wavefunctions in each plane, labelled by $|\,1\rangle$ and $|\,2\rangle$, for planes 1 and 2, respectively. Diagonalizing the Hamiltonian, we arrived at the $\pm$ bands, defined as $|+\rangle = \frac{1}{\sqrt{2}}[|\,1\rangle + |\,2\rangle]$ and $|-\rangle = \frac{1}{\sqrt{2}}[|\,1\rangle - |\,2\rangle]$. For the case of no wavefunction overlap between plane 1 and 2, the combined response can be written as

$$\begin{aligned}\chi_{11}+\chi_{22} &= \frac{1}{2}[\chi_{+,+}+\chi_{-,+}+\chi_{+,-}+\chi_{-,-}] \\ &\quad +\frac{1}{2}[\chi_{+,+}-\chi_{-,+}-\chi_{+,-}+\chi_{-,-}] \\ &= \chi_{-,-}+\chi_{+,+}. \end{aligned} \quad (5)$$

and the response is simply additive. If an overlap exists between planes 1 and 2, then $\chi_{+,-}$ must be kept. Nevertheless, it's prefactor is smaller than the single layer terms by the amplitude for creating an electron-hole pair on different planes, for instance via an intermediate state such as the bridging oxygens. This term depends on the difference of vertices for bands + and −, e.g.[10],

$$\chi_{+,-} \sim [\gamma_+ - \gamma_-]^2. \quad (6)$$

Since the bands $\{+,-\}$ are nearly degenerate for the double layer compounds, again this leads to a small mixing term. Thus the full response is well approximated by the addition of the intraband scattering in each band, in agreement with experiments.

3. CALCULATIONS

Using a gap, $\Delta(\mathbf{k},T) = 0.5\Delta_0(T)[\cos(k_x a) - \cos(k_y a)]$, of $d_{x^2-y^2}$ symmetry, we evaluated the averages in Eq. (2) numerically using a Fermi surface given by the band structure, Eq. (4). Our results for the channel dependent spectra are given in Fig. (1), using the parameters $2t'/t = 1.3$ and $\mu/2t = -0.5$ appropriate for dopings which produce the highest T_c values[11]. We have also performed the calculations for a Fermi surface which is more square-like ($\mu/2t = -0.2$, $t' = 0.1$) and obtain qualitatively the same results shown in Fig. (1). We immediately see that the spectra is extremely polarization dependent, in contrast to the case of isotropic s–wave superconductors which is dominated by the square root divergence at the threshold in each channel. We see that the peak in the Raman spectra lies at different frequencies $\omega_{peak} \sim 2\Delta_0(T), 1.5\Delta_0(T)$ and $1.25\Delta_0(T)$ for the B_{1g}, B_{2g} and A_{1g} channels, respectively. The symmetry dependence is also manifest in the low frequency behavior. The spectra rise slower in the B_{1g} channel ($\sim \omega^3$) than the A_{1g} or B_{2g} channels ($\sim \omega$). The power–laws are insensitive to vertex corrections and arise solely due to topology arguments. The channel dependence of the exponents are unique to a $d_{x^2-y^2}$ pair state. The symmetry dependence of the spectra is a direct consequence of the angular averaging which couples the gap and Raman vertex, and leads to constructive (destructive) interference under averaging if the vertex and the gap have the same (different) symmetry. Thus it has been reasoned that the symmetry which shows the highest peak position gives an unique indication of the predominant symmetry of the gap [7]. These channel-dependent power laws and relative peak positions have been observed in the electronic contribution to Raman scattering in Bi 2:2:1:2 [7, 3], Y 1:2:3 [1], Tl 2:2:n-1:n (for $n = 1, 2, 3$)[4, 6, 5], and Sr doped La 2:1:4[2], and are strong evidence for a d–wave gap of this symmetry as opposed to d_{xy}, d_{xz} or d_{yz} symmetry, which also have nodes on lines on the Fermi surface [7]. The overall height scales with the hopping parameter t for the B_{1g} and A_{1g} channels, and with t' for the B_{2g} channel. Similar results earlier obtained via a truncated Fermi surface harmonic expansion[7] validate the as-

sertion that the shape of the manifold (Fermi surface) has only a minor role on the Raman spectra. The lineshape of the spectra is determined by the topological nodal structure of the coupled energy gap and vertex.

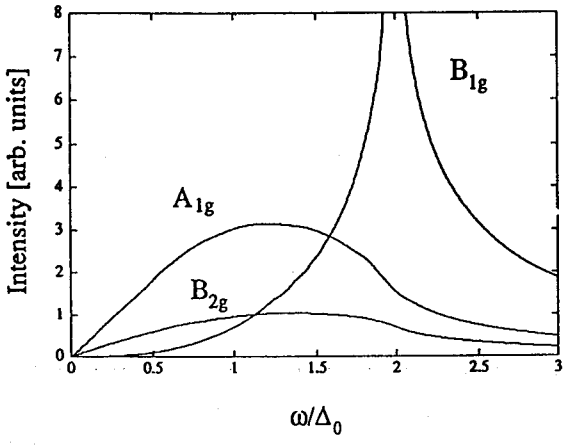

Figure 1. Theoretical channel-dependent Raman spectra for $d_{x^2-y^2}$ pairing.

We fit the data taken on single crystals of as grown $Bi_2Sr_2CaCu_2O_8$ ($T_c = 86K$) obtained in Ref. [3] for all symmetries at $T = 20K$, where a subtraction procedure has been employed to ascertain the A_{1g} signal. The comparison of the theory with experiment is shown in Fig. (2). The parameters used to obtain the best fit to the spectrum are $\Delta_0 = 280$ cm^{-1} and a smearing width of $\Gamma/\Delta_0 = 0.15$. We see immediately that the peak positions in the B_{2g} and A_{1g} channels given by the theory automatically agree with the data once the B_{1g} peak is fixed by setting Δ_0, and the low frequency behavior in each channel is consistent with the power laws predicted by the theory. Lastly, the ratio of the intensity of the spectra in different channels is consistent with magnitude of the Raman vertex derived from the $t - t'$ band structure[12]. All of the experimental features are thus consistent with the theory, at least for $\omega < 1000$ cm^{-1}.

However, like other correlation functions, only $|\Delta(\mathbf{k})|$ could be determined from the fit, and thus it could not be ascertained whether the gap changed sign around the Fermi surface. The theory also fails to predict *any* Raman intensity in the normal state due to phase space restrictions (consequence of the limit $\mathbf{q} \to 0$).

These deficiencies can be remedied by including impurity scattering[13]. Using a T−matrix approach[14], the results of the theory in the Born ($c >> 1$) and unitary ($c = 0$) limits are shown in Figure 3. The impurity scattering smears out the sharp features of the spectra (i.e., the logarithmic divergence of the spectra at the gap edge for the B_{1g} channel) and thus can in part account for the broadening seen in the data at low temperatures. In addition, the anisotropy of the peak positions is maintained (unless the scattering is so large that the normal state behavior is recovered), supporting that the energy gap in the cuprates is *predominantly* of $d_{x^2-y^2}$ symmetry.

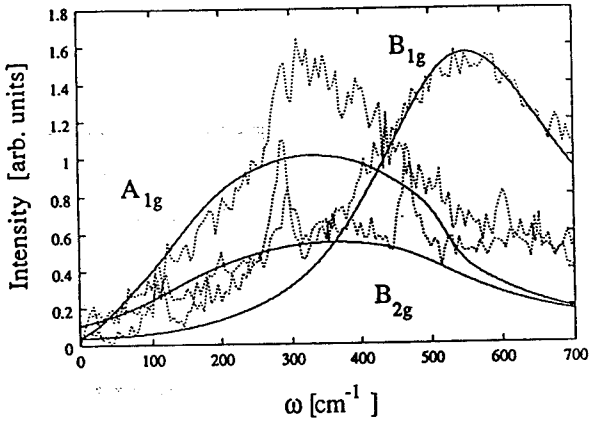

Figure 2. Comparison with the data on Bi 2:2:1:2 (from Ref. [3]). A_{1g} phonons have been subtracted.

To determine further whether the gap is *entirely* of $d_{x^2-y^2}$ symmetry, the impurity dependence of the low frequency behavior of the channel dependent spectra can be exploited. From Figure 3, it is seen that Born impurity scattering yields low frequency exponents that are the same as for clean materials (unless of course $\Gamma \sim \Delta_0$ and the normal state is recovered). However, in the unitary case, while the low frequency behavior remains linear in frequency in the A_{1g} and B_{2g} channels, below a characteristic frequency ω^* the behavior changes from ω^3 to linear in ω for the B_{1g} channel. This is due to a nonzero density of states at the Fermi level, which allows for normal-state-like behavior to be recovered [15]. As in the case of the penetration depth[16], the scale ω^* grows with increasing impurity concentrations. However, the exponent is symmetry dependent (remains 1 for A_{1g} and B_{2g} channels, while *decreases* from 3 to 1 for the B_{1g} channel, which is unlike the penetration depth). This is in marked contrast to the impurity dependence of the spectra for anisotropic s-wave gaps, since in that case,

the exponents for *all* channels would grow as the gap becomes more isotropic for increased impurity scattering [17]. Thus the impurity dependence can be systematically checked to determine whether the gap has accidental or intrinsic zeroes, or more generally, if the gap is anisotropic s-wave with predominantly B_{1g} symmetry, or if it is $d_{x^2-y^2}$ symmetry.

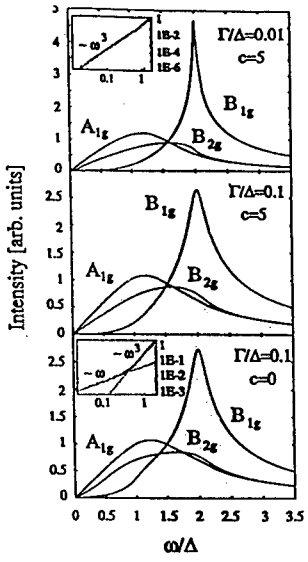

Figure 3. Impurity dependence of the theory for Born and Unitary scattering. Inset: B_{1g} channel.

In conclusion, we have presented a theory for electronic Raman scattering in both clear and dirty unconventional superconductors. An accurate fit to the data can be made from a single-band theory using a gap of $d_{x^2-y^2}$ symmetry.

REFERENCES

1. R. Hackl *et al.*, Phys. Rev. B **38**, 7133 (1988); S. L. Cooper *et al.*, *ibid*, 11934 (1988); X. K. Chen *et al.*, *ibid* **48**, 10530 (1993).
2. X. K. Chen *et al.*, Phys. Rev. Lett (in press).
3. T. Staufer *et al.*, Phys. Rev. Lett. **68**, 1069 (1992).
4. R. Nemetschek *et al.*, Phys. Rev. B **47**, 3450 (1993).
5. A. Hoffmann *et al.*, preprints.
6. A. A. Maksimov *et al.*, Zh. Eksp. Teor. Fiz. **97**, 1047 (1990) [Sov. Phys. JETP **70**, 588 (1990)].
7. T. P. Devereaux *et al.*, Phys. Rev. Lett. **72**, 396 (1994); Phys. Rev. B **50**, 10287 (1994).
8. see, e.g., J. Yu and A. J. Freeman, J. Phys. Chem. Solids **52**, 1351 (1991); A. Zawadowski, Physica Scripta **T27**, 66 (1989).
9. M. Krantz and M. Cardona, Phys. Rev. Lett. **72**, 3290 (1994); [but see T. P. Devereaux *et al.*, *ibid*, 3291 (1994)].
10. A. Zawadowski *et al.*, preprint.
11. X. K. Chen *et al.*, Physica C **227**, 113 (1994) [However, screening was not taken into account in these calculations]; E. J. Nicol *et al.*, Phys. Rev. B **47**, 8131 (1993).
12. The magnitude of the vertex was rescaled by a factor 1.4, 1.5 and 1.75 for the B_{1g}, A_{1g}, and B_{2g} channels, respectively.
13. T. P. Devereaux, preprint.
14. See, e.g., P. J. Hirschfeld, P. Wölfle, and D. Einzel, Phys. Rev. B **37**, 83 (1988).
15. K. Ueda and T. M. Rice, in *Theory of Heavy Fermions and Valence Fluctuations*, edited by T. Kasuya and T. Saso (Springer, Berlin, 1985); L. P. Gorkov, Pis'ma Zh. Eksp. Teor. Fiz. **40**, 351 (1994) [Sov. Phys. JETP **40**, 1155 (1985)].
16. P. Hirschfeld and N. Goldenfeld, Phys. Rev. B **48**, 4219 (1993); F. Gross *et al.*, Z. Phys. B **64**, 175 (1986).
17. L. S. Borkowski and P. J. Hirschfeld, Phys. Rev. B **49**, 15404 (1994).

Journal of Superconductivity, Vol. 8, No. 4, 1995

New Class of Intermetallic Borocarbide Superconductors: Electron-Phonon Coupling and Physical Parameters

Warren E. Pickett[1] and David J. Singh[1]

Received 5 January, 1995

In spite of their layered crystal structure, the new class of intermetallic borocarbide superconductors (typified by $LuNi_2B_2C$) have three-dimensional conduction with anisotropy being a minor factor. The calculated electron-phonon coupling constants are consistent with a picture of moderate- to strong-coupling conventional superconductivity, with large contributions from boron vibrations. We report several calculated material parameters for members of this class of compounds, and compare with some of the experimental data.

KEY WORDS: Borocarbides, superconductor, electronic properties

1. INTRODUCTION

Discovery of superconductivity at temperatures as high as $T_c = 23$ K in a new class of compounds [1,2] immediately suggests the possibility of new high temperature superconductors (HTS). The materials in question are intermetallic borocarbides with the general form RM_2B_2C, where R is a rare earth atom and M is one of the late transition metal elements Ni, Pd, or Pt. The values of T_c are unexpectedly high for materials based on Ni, Pd, and Pt, and both the possibility of magnetic behavior and the layered crystal structures [3] are reminiscent of the cuprate HTS.

We present here several results from self-consistent local-density-based band structure studies and compare with available data. The materials we have studied are YPd_2B_2C ($T_c = 23$ K), $LuNi_2B_2C$ ($T_c = 16.6$ K), YNi_2B_2C ($T_c = 15.5$ K), and $LaNi_2B_2C$ ($T_c = 11$ K). The picture that emerges is of behavior that is distinctly different from the cuprate HTS: the electronic properties are strongly three-dimensional, and the active bands at the Fermi level involve all atoms in the structure. Their behavior is consistent with conventional strong coupling superconductivity, with important contributions to coupling from the boron atoms. The present evidence indicates that, while these are unusually interesting new materials, there is no essential new physics necessary to understand their impressive values of T_c.

[1]Complex Systems Theory Branch, Naval Research Laboratory, Washington, DC 20375

2. CRYSTAL STRUCTURE AND METHODS

The crystal structure of this class of materials was first reported by Siegrist et al. for $LuNi_2B_2C$ [3]. The space group is I4/mmm, with layers of Ni atoms bonded to B atoms above and below in a nearly perfect tetrahedral configuration. These B-Ni_2-B trilayers may be considered to be connected by C atoms bridging the B atoms along the c axis of the crystal, since the B-C distance is indicative of covalent bonding between these atoms. (We return to this interpretation below.) The Lu atoms lie in the plane of C atoms, in fourfold coordination. The crystal structure is determined by the lattice constants **a** and **c** and the z-coordinate (z_B) of the B atom.

Our results are based on well converged, self-consistent, general potential linearized augmented planewave calculations [4]. A local orbital extension was used to treat high lying extended core states and the Lu f states [5]. Further details of the method may be found in Ref. 6.

3. ELECTRONIC STRUCTURE OF $LuNi_2B_2C$

The total [N(E)] and atom-projected densities of states (DOS) are shown in Fig. 1. The most noteworthy aspect is the occurrence of a strong peak in N(E) at the Fermi energy E_F, which contains a majority of Ni d character but also involves contributions from all other atoms. This peak arises from a flat band in a region around the $(\pi/a,\pi/a,0)$ point that, as

0896-1107/95/0800-0425$07.50/0

noted also by Mattheiss [7], does not have any immediate simple interpretation (such as the Cu d - O p antibonding σ^* band that dominates considerations in cuprates). It may be of particular significance that this peak involves a fraction of Ni d states that are split away from the main Ni d complex by more than 1 eV.

In attempting to understand the origin of this peak in N(E), we have carried out a series of calculations with portions of the structure: (1) an isolated Ni monolayer; (2) an isolated B-Ni_2-B trilayer; (3) Ni_2B_2 layers connected by C atoms, i.e. the actual structure without Lu present; (4) the actual structure but with C missing instead of Lu as in (3). Only in case (4) is there a splitting off of Ni d states from the main d complex that is reminiscent of the structure in Fig. 1, and even then the shape of the DOS is rather different. This series of calculations indicates that not only are the B atoms necessary (obviously, since they are closely coordinated with Ni), but that interactions with the Lu d states are instrumental in producing the peak. In $LuNi_2B_2$ the peak is well split off from the main Ni d DOS, but the Fermi level does not lie at the peak until the C atom is included. This calculation indicates that C is an electron donor in this compound.

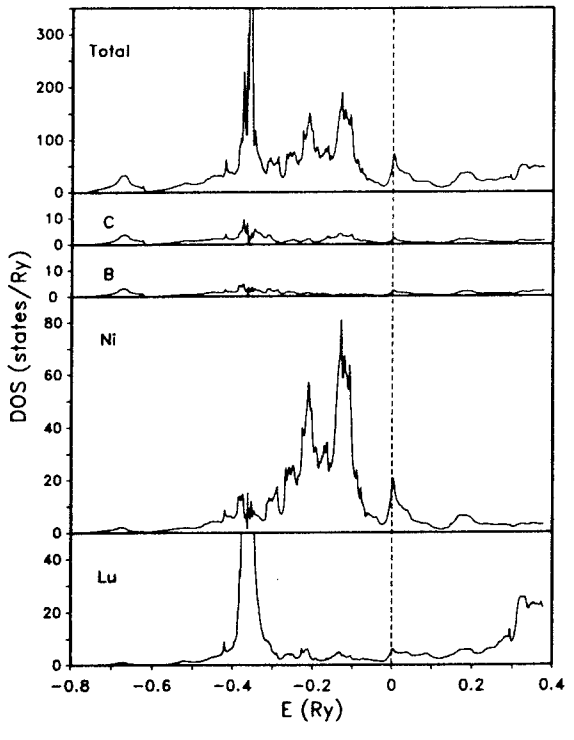

Figure 1. Total (top) and atom-projected densities of states of $LuNi_2B_2C$. The dashed vertical line denotes the Fermi energy. The peak at -0.35 Ry is due to Lu 5f states.

The calculated density of states $N(E_F)$ is 4.80 states/eV-cell. Since this value is 60% of the (very large) value for paramagnetic Ni which is unstable to ferromagnetism, and much of it arises from Ni d character, there is a real possibility of magnetic instability. We have performed self-consistent fixed spin moment calculations that establish that there is no magnetic instability. The Stoner enhancement of the spin susceptibility $\chi/\chi_o \approx 1.3 \pm 0.2$ indicates that correlation effects should not be large.

From the band structure, shown in Ref. 4, it is evident that the electronic properties will be strongly three dimensional rather than quasi-two dimensional as might have been expected from the crystal structure. Specifically, there are two distinct pieces of Fermi surface perpendicular to the Γ-Z (z axis) line, and the mean k_z dispersion is similar to that in the k_x-k_y plane. Calculation of the r.m.s. Fermi velocities bear this out: $v_{F,x} = v_{F,y} = 2.1 \times 10^7$ cm/s, and $v_{F,z}$ is equal to $v_{F,x}$ to within 2%.

The variation of v_k from its r.m.s. value may be important. Of the three bands that cross E_F, the lowest and highest (which contribute 79% and 1% to $N(E_F)$ respectively) have $v_{F,z}/v_{F,x} = 0.75$-0.80. For the middle band (20% of $N(E_F)$) the z component is the largest: $v_{F,z}/v_{F,x} = 2.25$. This variation in the anisotropy may lead to variation in the energy gap over the Fermi surface, which is known to enhance T_c. [8]

In the clean limit (mean free path much greater than the coherence length), which these materials appear to satisfy, the field penetration depth Λ is given in terms of the Drude plasma frequency Ω_p by $\Lambda = c/\Omega_p$. For $LuNi_2B_2C$ we obtain Ω_p = 5.1 eV, Λ = 390 Å. Takagi et al. [9] have used critical field data to infer Λ = 710 Å. These two distinct estimates establish the order of magnitude of Λ as ~ 500 Å.

4. $LaNi_2B_2C$, YNi_2B_2C, AND YPd_2B_2C

To establish the trends we have studied $LaNi_2B_2C$, YNi_2B_2C, and YPd_2B_2C, which have both lower and higher values of T_c, 11 K, 15.5 K, and 23 K respectively. The characteristics of $LaNi_2B_2C$ have been presented elsewhere.[10] The DOS is rather similar to that of $LuNi_2B_2C$, but the peak in N(E) near E_F is broader and the maximum lies 0.5 eV above E_F. The value of $N(E_F)$ is only 52% of that of $LuNi_2B_2C$, accounting at least qualitatively for the lower T_c.

Our calculated photoemission spectrum for YNi_2B_2C has been compared with data.[11] The strong Fermi edge, the occurrence of a shoulder just below E_F and a strong peak at ~1.7 eV binding energy are

similar to the data, but this peak binding energy is overestimated by 0.25 eV, suggesting some band narrowing by electronic interactions.

Since we are not aware of any determination for YPd_2B_2C of the internal coordinate z_B giving the B atom position, we have determined it by energy minimization, obtaining $z_B=0.3640$. This corresponds to a B-C bond length of 1.470 Å, almost identical to the value (1.466 Å) in $LuNi_2B_2C$, and close to the values for two samples of YNi_2B_2C (1.476 Å, 1.486 Å) reported by Chakoumakos and Paranthaman [12]. Along with the high frequency of the B-C stretching mode (see below), this regularity suggests that the B-C distance may be one of the most rigid in this structure.

In YPd_2B_2C the flat band that gives rise to the peak very near E_F in $LuNi_2B_2C$ lies 0.35 eV above E_F. This band is a combination of strong Pd (resp. Ni) d character, with B p and Y (resp. Lu) d character, and a small amount of C character. It would be simplest to be able to account for the variation in T_c in terms of the value of $N(E_F)$; indeed $LuNi_2B_2C$ and $LaPt_2B_2C$ follow the correct behavior. However, we calculate YPd_2B_2C to have $N(E_F)=3.57$ states/eV-cell, 25% smaller than for $LuNi_2B_2C$, whereas T_c is larger.

One possibility for reconciling this result is that the borocarbides are not stoichiometric, so our calculations for stoichiometric compounds are not directly applicable. If the materials are very near stoichiometry, then a change in the character of the electron-phonon coupling or a substantial change in the important phonon frequencies is required to account for $T_c=23$ K in YPd_2B_2C.

5. BORON VIBRATIONS

By calculating the total energy while varying the internal coordinate z_B of the B atom, we predict the equilibrium position of the B atom and its vibrational frequency. The energy surface $E(z_B)$ and the force on the B atom $F(z_B)$ are shown in Fig. 2. The predicted position is within 0.025 Å of that obtained from x-ray data [3]. The displacement corresponds precisely to an A_{1g} Raman-active eigenmode of the lattice, with calculated frequency of 848 cm^{-1}.

The rms displacement for the B atom in this mode is $u_{rms}=0.043$ Å. Anharmonicity (lack of symmetry of the energy curve, non-linearity of the force) is visible on this scale in Fig. 2; however, it is primarily cubic anharmonicity and does not have a great effect on the frequency (the calculated harmonic frequency is ~9 cm^{-1} higher). Given that this displacement corresponds directly to the stretching of the B-C bonds

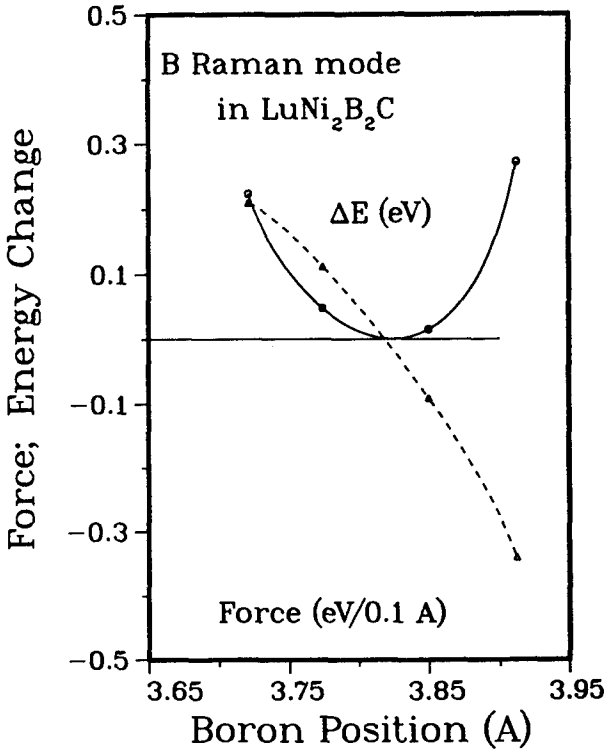

Figure 2. The crystal energy (solid curve) and the calculated force on the boron atom (dashed curve) versus the B height. The lines are simply spline curves through the calculated values. The anharmonicity is visible as non-parabolic (resp. non-linear) variation. The anharmonicity is primarily cubic and lowers the frequency by only 1% from the harmonic value.

(and bending of B-Ni bonds, of course), and the B-C separation is typical of covalent bonding, this rather high frequency is not unexpected.

Hadjiev et al. [13] have recently reported the identification by Raman scattering of the four A_{1g} modes in YNi_2B_2C, which is isostructural with $LuNi_2B_2C$ and should be expected to have a very similar B vibrational frequency. They report $\omega=832$ cm^{-1} for the highest mode, within 2% of our calculated value.

6. ELECTRON-PHONON COUPLING

The large value of $N(E_F)$ and an isotropic electronic structure, corresponding to good three-dimensional screening, suggests that a rigid-atom picture of electron-phonon coupling should be realistic. We have applied the Gaspari-Gyorffy [14] ("rigid muffin-tin") model to $LuNi_2B_2C$; some details have been presented elsewhere.[4] The contribution of each atom (j) to the coupling is given by $\varsigma_j=\eta_j/M_j$, where η is a mean squared electron-ion scattering matrix

element at the Fermi surface, and M is the mass. The contributions ς_j are about 20%, 50%, and 30% of the total value of $(31.3\ meV)^2$ for Ni, B, and C, respectively, indicating the light atoms contribute 80% of the electron-phonon coupling.

This conclusion has been supported by two more developments. Lawrie and Franck [15] have reported a strong isotope dependence of T_c for YM_2B_2C for both M=Ni and M=Pd, $\alpha_B=0.27\pm0.1$, reflecting strong coupling of B vibrations to the carriers. Mattheiss, Siegrist, and Cava [16] have noted the strong dependence of the position of a Ni-B-C sp band in $LuNi_2B_2C$ upon the B position z_B, which translates into strong coupling of the B atom. The movement of this band influences the position of E_F with respect to the flat band, thereby introducing B coupling with the high DOS peak.

7. $La_3Ni_2B_2N_3$, A RELATED SUPERCONDUCTOR

The discovery of superconductivity at 12 K in $La_3Ni_2B_2N_3$ [17], which has the same BNi_2B trilayers but separated by three LaN layers, suggests a much more anisotropic (or possibly quasi-2D) material. Since the internal coordinates were not reported in the original report [17], they were determined by energy minimization. Our predictions [18] differ substantially from analysis of electron diffraction data.[19] Our calculations [18] support a three dimensional picture of conduction in this compound. The r.m.s Fermi velocities are $v_{F,x}=2.92\times10^7$ cm/s, $v_{F,z}=1.48\times10^7$ cm/s, i.e. a 2:1 ratio. Of the four bands that cross E_F, two have large Fermi surface areas perpendicular to the c axis, so the resulting electronic structure is not in any sense two dimensional. The DOS peak near E_F is similar to the borocarbides, and $N(E_F)$ = 4.2 states/eV-cell; comparing with $LuNi_2B_2C$ (above) leads to the conclusion that their relative values of T_c can be rationalized in terms of $N(E_F)$ alone. This boronitride material seems to very similar to the borocarbides.

8. SUMMARY

The evidence at this time indicates that this new class of metals gives rise to conventional high DOS, strongly phonon-coupled superconductivity rather than a novel type. The materials themselves are novel, however, and it would not have been possible to guess that they would be impressive superconductors based on their composition and crystal structure alone. Deciding if these materials can be completely understood in terms of conventional theory requires carrying out a careful comparision of experimental data with calculated characteristics. This process is well underway, and some of the early results have been reported here.

ACKNOWLEDGEMENTS

We thank the authors of Refs. 12, 13, and 15 for preprints of their results prior to publication. This work was supported by the Office of Naval Research. Computations were performed at the DoD CEWES Computing Center and the Arctic Region Supercomputer Center.

REFERENCES

1. R. Nagarajan, C. Mazumdar, Z. Hossain, S. K. Dhar, K. V. Gopalakrishnan, L. C. Gupta, C. Godart, B. D. Padalia, and R. Vijayaraghavan, Phys. Rev. Lett. 72, 274 (1994).
2. R. J. Cava, H. Takagi, B. Batlogg, H. W. Zandbergen, J. J. Krajewski, W. F. Peck, Jr., R. B. van Dover, R. J. Felder, T. Siegrist, K. Mizuhashi, J. O. Lee, H. Eisaki, S. A. Carter, and S. Uchida, Nature 367, 146 (1994); ibid., 367, 252 (1994).
3. T. Siegrist, H. W. Zandbergen, R. J. Cava, J. J. Krajewski, and W. F. Peck, Jr., Nature 367, 254 (1994).
4. W.E. Pickett and D. J. Singh, Phys. Rev. Lett. 72, 3702 (1994).
5. D. Singh, Phys. Rev. B 43, 6388 (1991).
6. D.J. Singh, Planewaves Pseudopotentials and the LAPW Method, (Kluwer Academic, Boston, 1994) and references therein.
7. L. F. Mattheiss, Phys. Rev. B49, 13279 (1994).
8. W. H. Butler and P. B. Allen, in Superconductivity in d- and f-band Metals, ed. D. H. Douglass (Plenum, New York, 1976).
9. H. Takagi, R. J. Cava, H. Eisaki, J. O. Lee, K. Mizuhashi, B. Batlogg, S. Uchida, J. J. Krajewski, and W. F. Peck, Jr., Physica C 228, 389 (1994).
10. D. J. Singh, Phys. Rev. B50, 6486 (1994).
11. M. S. Golden, M. Knupfer, M. Kielwein, M. Buchgeister, J. Fink, D. Teehan, W. E. Pickett, and D. J. Singh, Europhys. Lett. 28, 369 (1994).
12. B. C. Chakoumakos and M. Paranthaman, Physica C (in press).
13. V. G. Hadjiev, L. N. Bozukov, and M. G. Baychev, Phys. Rev. B50, 16726 (1994).
14. G. D. Gaspari and B. L. Gyorffy, Phys. Rev. Lett. 29, 801 (1972).
15. D. D. Lawrie and J. P. Franck, Physica C (in press).
16. L. F. Mattheiss, T. Siegrist, and R. J. Cava, Solid State Commun. 91, 587 (1994).
17. R. J. Cava, H. W. Zanbergen, B. Batlogg, H. Eisaki, H. Takagi, J. J. Krajewski, W. F. Peck Jr., E. M. Gyorgy, and S. Uchida, nature 372, 245 (1994).
18. D. J. Singh and W. E. Pickett (preprint).
19. H. W. Zandbergen, J. Jansen, R. J. Cava, J. J. Krajewski, and W. F. Beck Jr., Nature 372, 759 (1994).

Journal of Superconductivity, Vol. 8, No. 4, 1995

Electron-Phonon Locking and Superconductivity

Yasutami Takada[1]

Received 5 January 1995

The electron-phonon vertex part Λ is investigated as a function of real frequencies in a narrow-band electron system coupled with local phonons. Even though the bare electron-phonon coupling is not very strong, Λ is found to diverge at some characteristic frequencies $\tilde{\omega}_\ell$. The divergence induces the vanishment of the electron Green's function at $\tilde{\omega}_\ell$. This phenomenon can be interpreted as the locking of an electron by such local phonons. By including this effect in the theory of superconductivity, we suggest an anomalous behavior in the tunneling spectroscopy.

KEY WORDS: Vertex corrections; strong coupling; locking effect; tunneling.

1. INTRODUCTION

The intramolecular high-frequency ($\sim$ 0.2eV) phonon modes are believed to bring about superconductivity with T_c in the range 20-30K in the alkali-metal-doped C_{60} [1]. This belief is based upon the crude estimates of T_c in the conventional Migdal-Eliashberg (ME) theory for superconductivity [2] in which all the vertex corrections to the electron-phonon coupling are neglected. In the fullerene, however, the neglect of those corrections cannot be justified, because its conduction electrons have the Fermi energy ϵ_F of only 0.2eV which is comparable with the energy ω_0 of phonons in question. Thus, in order to confirm the mechanism of superconductivity in this material, we need to make a further development of theories for superconductivity, in particular, for the vertex function Λ.

Basically, $\hbar/\epsilon_F$ represents the average time for stay of an electron at a molecular site at which the electron exerts a force on the ions in the molecule to produce local phonons. If the time is very small compared to $\hbar/\omega_0$ which gives a time scale for the motions of ions, the electron does not feel any reactions from the actual displacement of the ions. This indicates that we need not consider such reactions, or the vertex corrections, in the case of $\epsilon_F \gg \omega_0$, as Migdal pointed out many years ago. However, we must include those reactions for the case of ϵ_F comparable to or smaller than ω_0. In a recent paper [3], a theory was presented to evaluate T_c with those corrections up to infinite order. An enhancement of T_c due to the effect was discussed in the paper, but no clear physical picture was given about a qualitative difference between theories with and without vertex corrections. In this paper, we shall discuss Λ along with the electronic self-energy as a function of real frequencies ω so as to suggest a hint to establish experimentally the importance of this function in an electron-phonon system.

2. EXACT RESULTS IN THE ANTIADIABATIC LIMIT

We shall deal with a system of electrons hopping around in a crystal composed of molecular units, each of which provides an intramolecular high-energy optic phonon coupled strongly to the electrons. We assume that both the energy of the phonon ω_0 and the electron-phonon coupling constant g are independent of wave vectors. Employing ω_0 as units for energies, we can write the Hamiltonian of the system as

$$H = \sum_{\mathbf{k}\sigma} (\epsilon_{\mathbf{k}} - \mu)\, c^\dagger_{\mathbf{k}\sigma} c_{\mathbf{k}\sigma} + U \sum_i n_{i\uparrow} n_{i\downarrow} + \sum_i a^\dagger_i a_i + \sqrt{\alpha} \sum_{i\sigma} n_{i\sigma} \left(a_i + a^\dagger_i \right), \quad (1)$$

with $n_{i\sigma} = c^\dagger_{i\sigma} c_{i\sigma}$, where $c_{i\sigma}$ denotes the annihilation operator of an electron with spin σ at i site, $c_{\mathbf{k}\sigma}$ is its Fourier transform, $\epsilon_{\mathbf{k}}$ is the single-electron energy, μ

[1]Institute for Solid State Physics, University of Tokyo, 7-22-1 Roppongi, Minato-ku, Tokyo 106, Japan.

0896-1107/95/0800-0429$07.50/0

is the chemical potential, and U is the intramolecular Coulomb repulsion between electrons. The non-dimensional electron-phonon coupling constant α is related to g through $\alpha \equiv g^2/2M\omega_0^3$ with the reduced mass of ions M.

Let us consider the antiadiabatic case for the time being. By antiadiabatic we mean that the band width W determined by $\epsilon_{\mathbf{k}}$ is negligibly small compared to ω_0. In this limit, the problem is reduced to that in one molecular site and it can be solved exactly by the canonical transformation due to Lang and Firsov [4]. We note that all the quantities such as the retarded electron Green's function G^R depend only on the frequency variable ω in this case. The result for $G^R(\omega)$ is given by

$$G^R(\omega) = \int_{-\infty}^{\infty} d\omega' \frac{A(\omega')}{\omega + i\eta - \omega'}, \tag{2}$$

with an infinitesimally small positive quantity η and the spectral function $A(\omega)$, obtained as

$$\begin{aligned} A(\omega) \;=\; & e^{-\alpha} \sum_{\ell=0}^{\infty} \frac{\alpha^\ell}{\ell!} \left[f_0(\mu+\alpha)\delta(\omega - \ell + \mu + \alpha) \right. \\ & + f_1(\mu+\alpha)\delta(\omega - \ell + \mu - U + 3\alpha) \\ & + f_1(\mu+\alpha)\delta(\omega + \ell + \mu + \alpha) \\ & \left. + f_2(\mu+\alpha)\delta(\omega + \ell + \mu - U + 3\alpha) \right], \end{aligned} \tag{3}$$

where f_n represents the probability of occupation by n electrons, given as

$$f_0(\omega) = \left[1 + 2e^{\frac{\omega}{T}} + e^{\frac{2\omega - U + 2\alpha}{T}} \right]^{-1}, \tag{4}$$

$$f_1(\omega) = e^{\frac{\omega}{T}} \; f_0(\omega), \tag{5}$$

and

$$f_2(\omega) = e^{\frac{2\omega - U + 2\alpha}{T}} \; f_0(\omega), \tag{6}$$

at the temperature T. We can determine μ by specifying the electron number per spin and site, $\langle n \rangle$.

We have examined $A(\omega)$ in various cases of α, U, and $\langle n \rangle$. As anticipated from the outset, the cases of $U < 2\alpha$ and $U > 2\alpha$ correspond, respectively, to the charge- and spin-density-wave states and thus the delta-function peak in $A(\omega)$ does not come to the Fermi level, $\omega = 0$. This implies that we cannot expect metallic behaviors, not to mention superconductivity, even if we include the hopping effect through $\epsilon_{\mathbf{k}}$ to make the width of the density-of-states finite. Thus in this paper, we confine ourselves to the case of $U = 2\alpha$. With this choice, the effect of the Coulomb repulsion does not appear explicitly, but it plays an important role in keeping the system away from the charge- and spin-density-wave states.

At half-fillig, i.e., $\langle n \rangle = 1/2$, μ is determined to be $-\alpha$ and the electronic self-energy $\Sigma^R(\omega)$ is obtained as

$$\Sigma^R(\omega) \equiv \omega \left[1 - Z^R(\omega) \right] = \omega \left[1 - \frac{e^\alpha}{\gamma(\omega + i\eta)} \right], \tag{7}$$

with the renormalization function $Z^R(\omega)$ and a function $\gamma(\omega)$, defined by

$$\gamma(\omega) = 1 + \sum_{\ell=1}^{\infty} \frac{\alpha^\ell}{\ell!} \frac{\omega^2}{\omega^2 - \ell^2} \; . \tag{8}$$

We find that $\Sigma^R(\omega)$ or equivalently $Z^R(\omega)$ diverges at the zeros of $\gamma(\omega)$ which will be denoted by $\tilde{\omega}_\ell$. The electron-phonon vertex function $\Lambda(\omega, \omega')$ is obtained as

$$\Lambda(\omega, \omega') = \frac{\omega Z^R(\omega) - \omega' Z^R(\omega')}{\omega - \omega'}, \tag{9}$$

for $\omega \neq \omega'$. For $\omega = \omega'$, Λ is given in a similar but a little different form as obtained through the derivative of the self-energy with respect to μ. Equation (9) indicates clearly that Λ also diverges at $\tilde{\omega}_\ell$. We note that $\tilde{\omega}_\ell$ behaves as

$$\tilde{\omega}_\ell \approx \ell - \frac{\alpha^\ell}{2\,(\ell-1)!}, \tag{10}$$

with $\ell = 1, 2, 3, \cdots$ for small α, but $\tilde{\omega}_\ell$ approaches $(\ell - 1)$ quickly with the increase of α.

Physically, $\Lambda(\omega, \omega')$ describes the effective coupling of an electron with local phonons for the process of the initial electron state with frequency ω scattered into the state with frequency ω'. The divergence in Λ implies that a complete locking of an electron by phonons occurs. Due to this locking, the electron loses its original properties completely, as suggested by the zero lifetime which can be deduced from the divergence at $\omega = \tilde{\omega}_\ell$ in $\mathrm{Im}\Sigma^R(\omega)$. However, this effect is not easy to observe experimentally, because this does not correspond to the divergence in $G^R(\omega)$ but to the zeros of $G^R(\omega)$.

3. SUPERCONDUCTIVITY IN NARROW-BAND SYSTEMS

Inclusion of the hopping effect by $\epsilon_{\mathbf{k}}$ is absolutely necessary to discuss superconductivity, but the Lang-Firsov transformation does not provide exact solutions in this case. Thus the merit to adopt this method is lost. In addition, the method has a demerit that it cannot make a direct connection to the conventional strong-coupling theory for superconductivity. In view of this situation, we shall employ the gauge-invariant self-consistent (GISC) method in order to discuss the electron-phonon locking effect and its implications to superconductivity in the case of a finite bandwidth W. As for GISC, we shall give the following comments in order: Basically, GISC is a theory to extend ME by the inclusion of Λ. Its first version was presented in Ref. [3] and quite recently a firm basis of the method has been constructed [5] as an extension of the Baym-Kadanoff's conserving approximations [6]. The check of GISC in the antiadiabatic limit has also been done [7]. This check suggests that we need a modification of the original GISC by using the derivative of the self-energy with respect to μ for $\Lambda(\omega,\omega)$ to obtain the exact results. At the same time, it shows that even if $\Lambda(\omega,\omega)$ is evaluated by the limit of $\omega' \to \omega$ in Eq. (9) as prescribed in Ref. [8], we obtain qualitatively correct results for both Σ and Λ. Therefore, GISC in the version of Ref. [8] seems to be good enough to discuss qualitative features of the locking effect. Due to the limited space alloted to this paper, we shall not reiterate the formulation of GISC given in Ref. [8], but we employ it to calculate $Z^R(\omega)$ in both normal and superconducting states and the superconducting gap function $\Delta^R(\omega)$ at $T \approx 0$.

In Fig. 1, we show $Z^R(\omega)$ in the normal state with and without the vertex corrections for the case of the half-filling in the square density-of-states with $W = \omega_0$ and the conventional electron-phonon coupling constant $\lambda = 2$. Note that the so-called Eliashberg function $\alpha^2F(\Omega)$ is assumed to be

$$\alpha^2F(\Omega) = \lambda\frac{\omega_0}{2}\delta(\Omega - \omega_0), \tag{11}$$

and λ is related to α in Eq. (1) through $\lambda = 2\omega_0\alpha/W$. In ME, $\mathrm{Re}Z^R(\omega)$ diverges logarithmically, reflecting the step-function feature at the edge of the density-of-states, but in GISC, $Z^R(\omega)$ behaves in a quite different way: Both $\mathrm{Re}Z^R(\omega)$ and $\mathrm{Im}Z^R(\omega)$ diverge at the locking energy $\tilde{\omega}_\ell$ which is a little smaller than $\ell\omega_0$, as has been suggested by the exact results in Sec. 2. ME fails to account for this behavior, because Λ is always taken to be unity in the approximation.

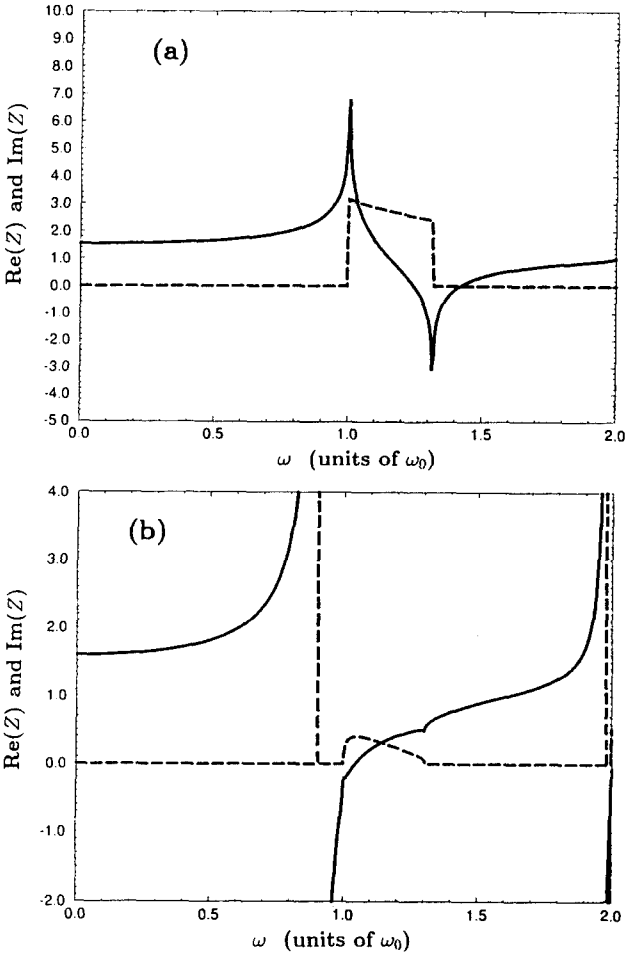

Fig. 1. Renormalization function in the normal state as a function of ω in units of the Einstein phonon energy ω_0 (a) without and (b) with the vertex corrections. The solid and dashed curves correspond, respectively, to ReZ and ImZ. The case of $\lambda = 2$ and the half-filling in the square density-of states with $W = \omega_0$ is considered.

Similarly, we can discuss the superconducting state. Quantitatively, we cannot find a large discrepancy between ME and GISC in the present version for such quantities as T_c. For example, k_BT_c is obtained as $0.125\omega_0$ in ME and $0.164\omega_0$ in GISC for the case treated in Fig. 1. The ratio of the gap at $T = 0$ to k_BT_c, $2\Delta_0/k_BT_c$, is given by 4.96 in ME and 5.58 in GISC. However, the qualitative feature of $Z^R(\omega)$ and $\Delta^R(\omega)$ as a function of ω is quite different. In Fig. 2, $\Delta^R(\omega)$ in GISC is plotted at $T \approx 0$ for the same parameters as employed in Fig. 1. As in $Z^R(\omega)$,

divergence due to the electron-phonon locking effect also appears in $\Delta^R(\omega)$, though the locking energy is shifted to higher energy than that in $Z^R(\omega)$.

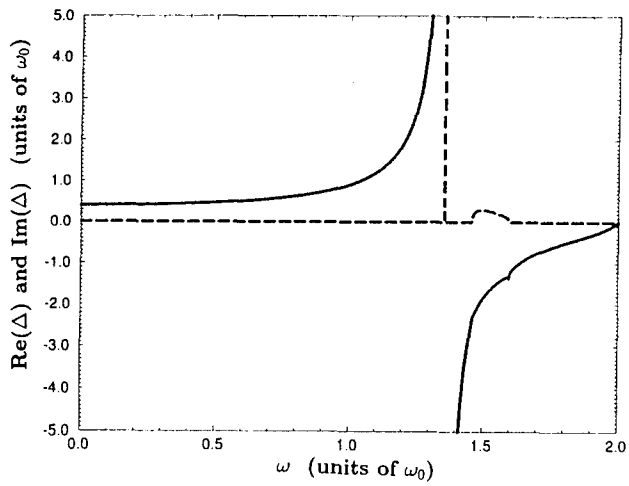

Fig. 2. Gap function at $k_B T = 0.001\omega_0$ as a function of ω in units of the Einstein phonon energy ω_0 in GISC in the version of Ref. [8] for the same situation as in Fig. 1. The solid and dashed curves correspond, respectively, to ReΔ and ImΔ.

Such a divergence in $\Delta^R(\omega)$ may be observed by the tunneling spectroscopy, because the experiment measures essentially the quasi-particle density-of-states, given by

$$\mathrm{Re}\left[\frac{\omega}{\sqrt{\omega^2 - \Delta^R(\omega)^2}}\right] . \qquad (12)$$

In Fig. 3, we show an example of the calculated results for the quantity in Eq. (12) as a function of ω. Note that the vanishment of this quantity for $0 < \omega < \Delta_0$ followed by the inverse square-root divergence is the well-known BCS behavior. The new feature appears for ω around the energy of the electron-phonon locking effect: The quasi-particle density-of-states diverges first and then vanishes completely. This is related to the trapping of electrons by local phonons or the absence of the tunneling current due to the locking at those values of ω.

4. CONCLUSION AND DISCUSSION

We have pointed out the electron-phonon dynamical locking effect due to the divergence in the electron-phonon vertex function in the narrow-band systems. We have also suggested that such an effect may be observed in the tunneling spectroscopy. Since the system treated in this paper is fairly ideal, we may need to consider the effects such as the broadening of the phonon energy, impurities, and so on in actual situations. However, I believe that this effect should be investigated experimentally.

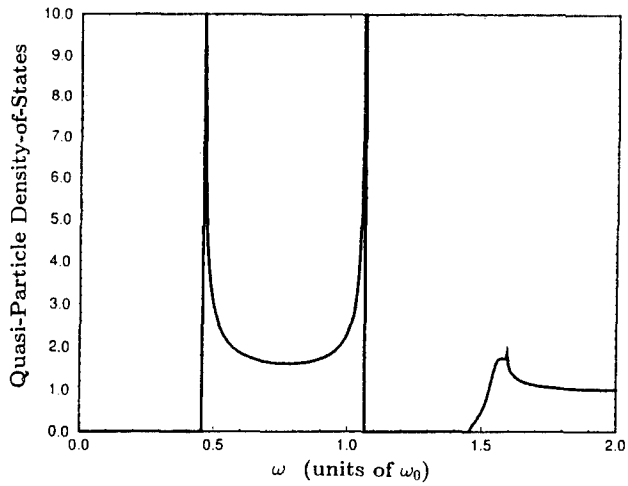

Fig. 3. Quantity defined in Eq. (12) as a function of ω in units of ω_0. This quantity is related to the quasi-particle density-of-states and may be observed directly in the tunneling spectroscopy. We consider the same parameters as those in Figs. 1 and 2.

ACKNOWLEDGMENTS

This work is supported in part by Grant-in-Aid for Scientific Research from Ministry of Education, Science and Culture, Japan.

REFERENCES

1. C. M. Varma, J. Zaanen, and K. Raghavachari, *Science* **245**, 989 (1991); M. Schluter, M. Lannoo, M. Needles, and G. A. Baraff, *Phys. Rev. Lett.* **68**,526 (1992); R. A. Jishi and M. S. Dresselhaus, *Phys. Rev.* B**45**, 2597 (1992).
2. A. B. Migdal, *Sov. Phys.*-JETP **7**, 996 (1958); G. M. Eliashberg, *Sov. Phys.*-JETP **11**, 696 (1960).
3. Y. Takada, *J. Phys. Chem. Solids* **54**, 1779 (1993).
4. I. G. Lang and Yu. A. Firsov, *Sov. Phys.*-JETP **16**, 1301 (1963).
5. Y. Takada, submitted to *Phys. Rev.* B.
6. G. Baym and L. P. Kadanoff, *Phys. Rev.* **124**, 287 (1961); G. Baym, *Phys. Rev.* **127**, 1391 (1962).
7. T. Higuchi and Y. Takada, submitted to *Phys. Rev.* B.
8. Y. Takada, in *Condensed Matter Theories*, Vol. 10, M. Casas, M. de Llano, J. Navarro, A. Polls, eds. (Nova, New York, 1995).

Journal of Superconductivity, Vol. 8, No. 4, 1995

Electron-Phonon Interaction and its Manifestation in High-Temperature Superconductors

E. G. Maksimov[1]

Received 31 January 1995

Different types of band structure approaches for a description of electrons in systems with strong correlations are discussed. It is shown that all methods considered give different electron energy dispersions and Fermi surfaces. The good agreement between measured Fermi surfaces and those calculated by LDA shows that the spatial dispersion of the correlation interaction is not so important in HTSC systems. The same conclusion can be obtained from the optical and photoemission spectra. It is shown that the most important contribution beyond a band structure approach is given by an energy dependence of the electron self-energy. The most likely interaction responsible for this energy dependence is the electron-phonon one. Evidences about this fact are given.

KEY WORDS: Electron-phonon interaction; band structures.

The usually used band structure (BS) approach to electron systems is based on density functional theory (DFT). Hohenberg and Kohn introduced [1] this method and proved that the ground state energy E of an electron system is an unequivocal functional of the electron density $n(r)$ and E has a minimum with respect to variations in $n(r)$

$$\frac{\delta E\{n(r)\}}{\delta n(r)} = 0 \tag{1}$$

Kohn and Sham suggested [2] a technique for a practical treatment of this method. They introduced for the ground state energy an expression of the form

$$E = T_s + \int d^3r n(r) V_{ext}(r) \tag{2}$$

$$+ \int\int d^3r_1 d^3r_2 \frac{n(r_1)n(r_2)}{|r_1 - r_2|} + E_{xc} \tag{3}$$

Here T_s is the kinetic energy of a noninteracting electron gas of density $n(r)$, V_{ext} is the external potential, and E_{ex} is the exchange-correlation energy. They used an eigenfunction description of T_s

$$T_s = -1/2m \int d^3r \sum_j \psi_j^+(r) \nabla^2 \psi_j(r) \tag{4}$$

It allows the Schrodinger-type equation for the eigenfunctions $\psi_j(r)$ to be obtained from the minimum condition (1)

$$\left(-\frac{\nabla^2}{2m} + V_{ext}(r) + V_H(r) + \right. \tag{5}$$

$$\left. V_{xc}(r) - \mu\right)\psi_j(r) = \epsilon_j \psi_j(r) \tag{6}$$

Here μ is the chemical potential, ϵ_j is an energy eigenvalue,

$$V_H(r) = \int \frac{n(r')}{|r - r'|} d^3r'$$

and

$$V_{xc} = \frac{\delta E_{xc}}{\delta n(r)}$$

Additionally Kohn and Sham suggested an approximation for E_{ex} which allows practical calculation to be made. That is the local density approximation (LDA)

$$E_{xc} = \int d^3r n(r) \epsilon_{xc}(n(r)) \tag{7}$$

where ϵ_{xc} is the exchange-correlation energy per particle of an uniform interacting electron gas of density

[1]P.N.Lebedev Physical Institute, Moscow, Russia

0896-1107/95/0800-0433$07.50/0

n. We should remind at this point that ψ_j and ϵ_j are auxiliary quantities which have no physical meaning. We can solve the equations in the Bloch wave functions representation and find the auxiliary excitation spectrum $\epsilon_{k\lambda}$. One can obtain the Fermi surface from the condition

$$\epsilon_{k\lambda} = 0 \tag{8}$$

But we should again emphasize that the interrelation between this Fermi surface and the real metal Fermi surface is unclear.

The DFT approach to BS is not unique. Let us consider another approach going back to the works of Luttinger [3] and Abrikosov [4]. For the following discussion it is convenient to use the one-particle Green functions $G(x,x')$. We define also the self-energy $\Sigma(x,x')$ and its Fourier component

$$G^{-1}(r,r',\omega) = -\frac{\nabla^2}{2m} + V_{ext}(r)$$

$$+\int \frac{n(r')}{|r-r'|} - \Sigma(r,r',\omega)$$

As is well known [4], the operator $G(r,r',\omega)$ cannot be diagonalized in the Bloch wave function representation simultaneously at all ω points. However, this can be done for the operator $G(r,r',0)$, and we can write

$$\left(-\frac{\nabla^2}{2m} + V_{ext}(r) + \int \frac{n(r')}{|r-r'|} - \mu\right)\psi_{k\lambda}(r) \tag{9}$$

$$-\int dr'\Sigma(r,r',0)\psi_{k\lambda}(r') = \tilde{\epsilon}_{k\lambda}\psi_{k\lambda}(r)$$

This equation introduces the new BS excitation spectrum $\tilde{\epsilon}_{k\lambda}$. This spectrum as well as that given by DFT is fictitious and does not describe the real one-particle excitations. But this spectrum has at least two very important properties in comparison with the DFT one. Firstly, the Fermi surface described by the condition

$$\tilde{\epsilon}_{k\lambda} = 0 \tag{10}$$

coincides with the real metal Fermi surface measured, for example, by photoemission. Secondly, the density of the electron states on the Fermi surface can be obtained exactly from this BS as

$$N(0) = 2\sum_{\lambda}\int \frac{dS_F}{v_{k\lambda}}$$

where $v_{k\lambda}$ is the Fermi velocity

$$v_{k\lambda} = \nabla_k\tilde{\epsilon}_{k\lambda}$$

On the other hand,this approach has some serious disadvantages in comparison with the DFT. The first one is the absence of any selfconsistent and closed expression for the self-energy corresponding to the LDA. This value can be calculated only in the framework of a perturbation theory using the functionals proposed in the works [5,6]. The next disadvantage is connected with the nonlocality of the self-energy, which complicates seriously the solution of equation (10) in comparison with the DFT approach with the local operator $V_{xc}(r)$. This may be the main reason why this approach to BS has not been used widely for practical calculations. We can mention only the recent attempt made by Eliashberg [7,8].

Nevertheless such calculations can be done for some model systems. We have made [9] the calculations of both type BS for highly compressed metallic hydrogen. The RPA approximation was used for the self-energy and the potential V_{xc}. It was shown that the two methods different Fermi surfaces even for cubic crystals. As is well known [10] in HTSC systems the Fermi surfaces measured by photoemission coincide well with those calculated by DFT. This can mean that, at least, the spatial dispersion or the nonlocality of the exchange-correlation interaction is not very important in HTSC. Moreover the LDA predictions are not so far from reality also for the electron energy dispersion, as is found in the comparison between the calculated optical spectra [11] and the experimental ones [12,15]. Although the behavior of HTSC materials is considerably well described by DFT at moderate and high energies there are some "anomalies" and an "unconventional" type behavior at low energies.

As was shown [13,14] the main part of all these "anomalies" can be explained by the assumption that the one-particle relaxation rate has linear dependences on T and ω

$$-2\mathrm{Im}\Sigma(\omega) = \frac{1}{\tau(\omega)} = \alpha\pi T + \beta\omega$$

The main problem is now to understand how such behavior can appear in real systems. There are a lot of suggestions for the explanations of this fact including the marginal Fermi liquid,spin-fluctuations, a "nested" Fermi surface etc. It was shown [14] that, indeed, all these mechanisms, as well as the usual

electron-phonon interaction, can explain all "anomalies" in the behavior of the normal state of HTSC. The distinction between different mechanisms can be done only through a detailed quantitative comparison between a number of calculated and measured properties.

For example, the electrical resistivity R at high temperatures can be expressed as

$$R = \frac{8\pi^2 \lambda T}{\omega_{pl}^2}$$

where ω_{pl} is the electron plasma frequency and λ is a suitable constant of coupling (spin-fluctuations,electron-phonon etc.). The ω_{pl} obtained from the band structure calculation [11] and confirmed by the analysis of experimental optical data [12,15] is of order 3 eV. Then from the absolute values of R one can conclude [16] that for HTSC $1 \leq \lambda \leq 2$. It is very unlikely that these high values of λ can be explained by an interaction other than the electron-phonon one.

The next argument is concerning the frequency dependence of the relaxation rate obtained by the optical spectroscopy. As it is well known the one-particle relaxation rate (determined by $-\mathrm{Im}\Sigma(\omega)$) reaches its constant asymptotic value $2\pi\lambda < \omega >$ at energies of the order of the cutoff energy of a phonon spectrum $\omega_c \leq 0.1$ eV. But the optical relaxation rate increases linearly with ω up to energies ω of the order 0.3–0.4 eV. This relaxation rate was determined [17] using the generalized Drude expression for the conductivity

$$\sigma(\omega) = \frac{ne^2}{m(\omega)(1/\tau(\omega)) - i\omega}$$

in term of the energy-dependent mass $m(\omega)$ and relaxation rate $1/\tau(\omega)$. As was shown in our work [18] the value $1/\tau(\omega)$ in this formula cannot be considered as a real relaxation rate because this formula cannot be applied to systems with a strong interaction. We calculated $\sigma(\omega)$ using the Kubo approach. The calculated $\sigma(\omega)$ was fitted by this formula and it was shown that the optically measured value $1/\tau(\omega)$ is nothing but the linear interpolation between the minimal value of the one-particle relaxation rate and its maximal value $\gamma = 2\pi\lambda < \omega > \simeq 0.3 - 0.4$ eV. Moreover,our calculations [14,18,19] using the Eliashberg function, obtained from tunnelling results [20] give a very good agreement with experimental data on the resistivity, optical and EELS spectra of HTSC systems in the normal state.

The same Eliashberg function gives $\lambda = 2$ and $T_c = 125$ K. Moreover, the existence of the large values of the relaxation rate near T_c can explain the smearing of the electron density of states and the lack of the Hebel-Slichter coherence peak in the NMR and optical results. The numerical solution of the Eliashberg equations demonstrate also the non-BSC behavior of a set of superconducting properties near T_c.

ACKNOWLEDGMENTS

We are indebted to International Science Foundation for financial support.
This work was partially supported by ISF and RFFI (No 94-02-04186a) grants.

REFERENCES

1. P.Hohenberg, W. Kohn, *Phys.Rev.*, **B136**, 864 (1964).
2. W. Kohn, L. J. Sham, *Phys. Rev.*, **B10**, 731 (1974).
3. J.M.Luttinger, *Phys.Rev.*, **119**, 1153 (1960).
4 A.A.Abrikosov,*Sov.Phys.JETP*,**16**, 765 (1963).
5. J.M.Luttinger, *et al.*, *Phys. Rev.*, **118**, 1417 (1960).
6 G.Baym, *Phys. Rev.*, **127**, 1391 (1962).
7. G.M.Eliashberg, *Physica*, **A200**, 95 (1993).
8. G.M.Eliashberg,*at al.*,*JETP Lett.*,**59**,441,(1994).
9. E.G.Maksimov, *unpublished.*
10. J.C.Campuzano, *et al.*,*Phys.rev.Lett.*,**64**,2308 (1990).
11. E.G.Maksimov, *et al.*, it Phys.Rev.Lett.,**63**,1870 (1989).
12. B.Bucher, it et al.,*Phys.Rev.*,**B 45**, 3026 (1992).
13. C.M.Varma, *et al.*, *Phys.Rev.Lett.*,**63**,1996 (1989).
14. V.L.Ginzburg,*et al.*,*Physica*,**C** *in press*
15. I.Bozovich, *Phys.Rev.*,**B 42**, 1969 (1990).
16. I.I.Mazin,*et al..Phys.Rev.*,**B42** ,2509 (1992).
17. Z.Shlesinger,*et al. Phys.Rev.Lett.*,**65**.801 (1990) .
18. S.V.Sulga *et al.*, Physica,**C178**.266 (1991.
19. O.V.Dolgov *et al.*, Solid State Comm.,**89**,827 (1994).
20. S.I.Vedeneev *et al.*,*Phys.Rev.*,**B49**,9823 (1994)

Journal of Superconductivity, Vol. 8, No. 4, 1995

Gap States in HTSC by Infrared Spectroscopy

T. Timusk[1], D.N. Basov[1], C.C. Homes[2], A.V. Puchkov[1], and M. Reedyk[3]

Received 5 January 1995

Recent infrared reflectance spectroscopy on high quality crystals of a number of HTSC systems shows that *all* have finite conductivity in the frequency region of the superconducting gap. Results on untwinned YBCO from a number of laboratories show that this absorption is not due to experimental problems or sample-to-sample variations. Other materials also show absorption features in the gap region in the form of peaks. We discuss these results in terms of recent ideas of the effect of impurities in d-wave superconductors.

KEY WORDS: *Superconductivity, gap, infrared, d-wave*

1. INTRODUCTION

The observation of the superconducting gap by infrared spectroscopy has been a goal from the beginning of the discovery of high temperature superconductivity.[1] For several reason this search has been unsuccessful. First, it appears, from angle resolved photo emission, that the gap, at least in $Bi_2Sr_2CaCu_2O_8$, is highly anisotropic in k-space. The corresponding optical spectrum would not exhibit a sharp onset of conductivity.

Secondly, it is known that the materials are in the clean limit, and from momentum selection rules, an onset of absorption at the gap frequency is not possible. In this limit, absorption starts at twice the gap frequency, plus the frequency of the relevant excitations responsible for transport scattering. Thus given the combination of a d-wave density of states and a smoothly rising excitation spectrum any sharp feature corresponding to the gap will be washed out. Recent interest has focussed on breaking down the momentum selection rules using defects, introduced either by doping,[2] or radiation damage.[3,4]

Surprisingly, the effect of defects on the optical absorption spectrum in the gap region does not produce dirty-limit behaviour as seen in conventional superconductors – an onset of absorption at 2Δ. Instead, a new low frequency, Drude-like, absorption appears in the superconducting state, taking spectral weight away from the superconducting condensate. The total low frequency spectral weight remains constant[3,4] and equal to the Drude spectral weight in the normal state.

In this review we will cover some recent work on the ab-plane conductivity in the cuprates. There have been substantial improvements in the technology of crystal growth[5,6] as well as optical spectroscopy of smaller and smaller crystals.[7]

2. RESULTS

2.1 a-axis Conductivity of $YBa_2Cu_3O_{7-\delta}$

$YBa_2Cu_3O_{7-\delta}$ is the most studied of the cuprates but it is important to study detwinned crystals since the optical properties are quite anisotropic.[8] Much of the variability in the properties of $YBa_2Cu_3O_{7-\delta}$ seems to stem from the quality of the chains which tend to incorporate aluminum and gold from the crucibles used for growth.[9] The a-direction properties do not depend as much on currents carried in the chains and material variability is much reduced. This is illustrated in Fig. 1.

[1] Department of Physics, McMaster University, Hamilton ON Canada, L8S 4M1

[2] Department of Physics, Simon Fraser University, Burnaby BC Canada, V5A 1S6

[2] Department of Physics, Brock University, St Catherines ON Canada, L2S 3A1

0896-1107/95/0800-0437$07.50/0

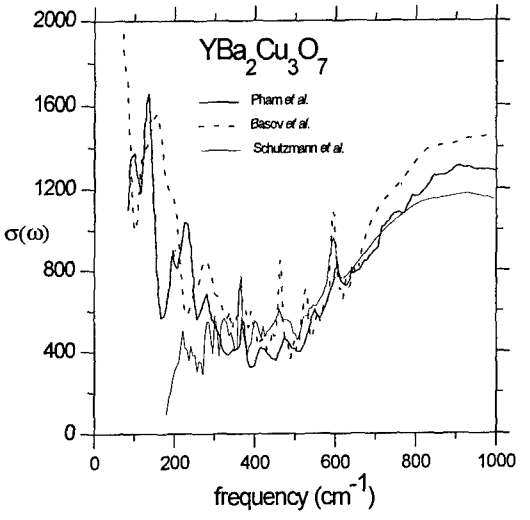

Fig 1. The a-axis optical conductivity of $YBa_2Cu_3O_{6.95}$ from three groups. There is overall agreement to the value of the conductivity for crystals from different sources. Note the absence of a true gap and a fairly constant conductivity of 350 $(\Omega cm)^{-1}$ at the minimum.

Fig. 1 shows the a-axis optical conductivity with light polarized normal to the chains. Curves from three laboratories are shown. The heavy line is a spectrum from Pham *et al.*[10] measured by direct absorption and therefore having perhaps the highest absolute accuracy. The dashed curve is a recent measurement by Basov *et al.* on crystals grown in zirconia crucibles with highly conducting chains. In contrast, the light solid curve, measured by Scützmann *et al.*[11] is on crystals with fragmented chains that show effects of localization. Two things are clear from these data: there is good overall agreement between the measurements over a large range of frequency on crystals from a wide range of sources. A fourth data set, by the Florida group, using crystals from the Illinois group, not shown here, is in excellent agreement with these.[9]

The spectra are characterized by a broad minimum centered at 400 cm^{-1} where the conductivity reaches a value of 400 $\Omega^{-1}cm^{-1}$. At lower frequencies the conductivity rises again and if extrapolated to zero frequency reaches a value of about 2000 $\Omega^{-1}cm^{-1}$. This is approximately half of the residual conductivity seen in samples from the same source by microwave techniques, 4500 $\Omega^{-1}cm^{-1}$.[12]

2.2 Conductivity of $Tl_2Ba_2CuO_{6+\delta}$.

The $Tl_2Ba_2CuO_{6+\delta}$ material has a single copper-oxygen plane and a T_c close to 90 K at optimal doping. Its T_c can be reduced to zero by oxygen annealing. At optimal doping, it shows a linear resistivity variation with temperature, typical of most high T_c materials, changing towards a T^2 in the over doped region. We report here preliminary results of the optical conductivity of this material.[13]

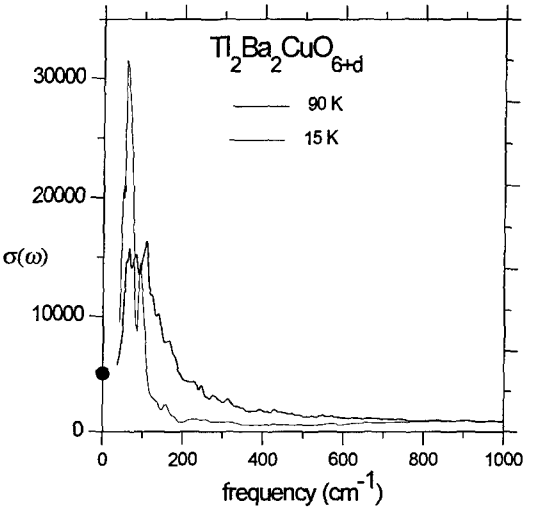

Fig 2. The the optical conductivity of $Tl_2Ba_2CuO_{6+\delta}$ The thick line is the 90 K curve just above the superconducting transition of 88 K and the thin line the low temperature spectrum. The spectrum is dominated by a large peak. a pseudogap develops at 70 cm^{-1} already in the normal state.

Figure 2. shows the ab plane conductivity of a crystal of optimally doped $Tl_2Ba_2CuO_{6+\delta}$ with $T_c = 88$ K. Two temperatures are shown, 90 K just above the superconducting transition, and 15 K in the superconducting state. The conductivity is unusual for a metal since, instead of a Drude absorption the spectrum consists of a peak at approximately 100 cm^{-1}. In the superconducting state this peak sharpens and moves to lower frequency.

The normal state dc conductivity is metallic (linear with a positive temperature coefficient) whereas the optical conductivity shows a low-lying peak rising from the dc value (shown as a black point at zero frequency). A positive *frequency* coefficient of conductivity is usually associated with localization and

is then accompanied by a *negative* temperature coefficient of resistivity. The superconducting state conductivity is also anomalous. First, there is no sign of an energy gap, but the pseudogap visible in the normal state deepens in the superconducting state. The onset frequency of this gap is 70 cm^{-1}.

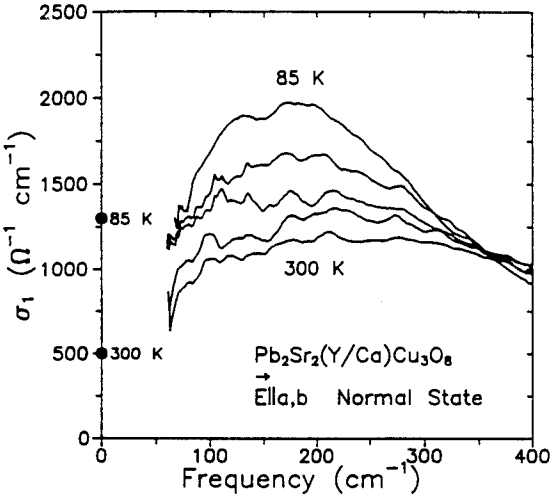

Fig 3. The the optical conductivity of $Pb_2Sr_2(Y/Ca)Cu_3O_{8+\delta}$. The 85 K curve is in the normal state. As superconductivity develops a pseudogap develops around 70 cm^{-1}. There is no sign of a superconducting gap only a pseudogap which is already present in the normal state.

A careful analysis of the spectral weight, using the conductivity sum rule, shows that the region from 0 to 600 cm^{-1} supplies all the spectral weight for the superconducting condensate. The London penetration depth, calculated from this missing spectral weight, is 2400 ± 200 Å. The condensate density, per copper plane, is similar to the a-axis value of $YBa_2Cu_3O_{7-\delta}$ which is 1600 Å[9] ($2400/\sqrt{2} = 1700$ Å).

2.3 Conductivity of $Pb_2Sr_2(Y/Ca)Cu_3O_{8+\delta}$

The third material we want to discuss here is $Pb_2Sr_2(Y/Ca)Cu_3O_{8+\delta}$. Structurally it shares elements with $YBa_2Cu_3O_{7-\delta}$ and $Bi_2Sr_2CaCu_2O_8$. There is a copper oxide bi-layer, and like the former, it has a third single copper layer midway between the bilayers. By varying the Ca/Y ratio, a T_c close to 90 K can be obtained.[14,15,16]

Fig. 3 shows the optical conductivity of $Pb_2Sr_2(Y/Ca)Cu_3O_{8+\delta}$with T_c = 80 K at a series of temperatures. A broad peak can be seen, centered around 200 cm^{-1} in the normal state, moving to 80 cm^{-1} in the superconducting state. The peak is similar in appearance to the peak in $Tl_2Ba_2CuO_{6+\delta}$but has much less spectral weight associated with it. Again, there is no sign of a superconducting gap and the spectral weight for the condensate appears to originate from a wide frequency range to account for the relatively large condensate density, measured by dc techniques such as magnetization[17] where a penetration depth of 2575 Å is obtained, and μSR where a similar value is found.[18]

1. DISCUSSION

In what follows we would like to focus on a common element in in the spectra of these three materials – finite conductivity in the region of the spectrum where a conventional superconductor is expected to be gapped. Before discussing possible sources for this conductivity we address the question of the reality of this conductivity, since it is claimed by one group at least, that the a-axis conductivity in $YBa_2Cu_3O_{7-\delta}$ is gapped.[8,19] The current consensus is however that there is a non-zero *minimum* conductivity and that the conductivity *rises* towards lower frequencies. There is general agreement on the value of the minimum conductivity (400 ± 50 $\Omega^{-1}cm^{-1}$) and since the bolometric experiment of the Maryland group is intrinsically an order of magnitude more sensitive than any reflectance data, we must accept this value as being a fundamental characteristic of the fully doped material.

More important than a non-zero minimum value is the general rise of conductivity toward lower frequencies. Very strong minima in conductivity are caused by coupling to LO phonons[20] and for example in $YBa_2Cu_4O_8$ there is a minimum in the conductivity at 400 cm^{-1} where the conductivity value is only 200 $\Omega^{-1}cm^{-1}$.[9] Similar strong minima have been seen in $Tl_2Ba_2CaCu_2O_8$.[21] Nevertheless, all materials investigated have a background conductivity away from the minima that ranges from 250 to 1000 $\Omega^{-1}cm^{-1}$, ref. 1, fig. 56, summarizes some of the early data.

One explanation that has been used to account for this residual conductivity has been in terms of defects or disorder. The difficulty with this explanation is the fact that the background absorption shows relatively little sample-to-sample variation. For ex-

ample the ab plane dc resistivity of single crystals of $YBa_2Cu_3O_{7-\delta}$ varies by more than a factor of two from laboratory to laboratory whereas, as we see in Fig. 1, the variation in the background conductivity is quite small.

A potential solution to the problem is provided by a recent suggestion of Lee[22] in terms of the limiting conductivity for a d-wave superconductor in the presence of resonance scattering defects, predicted to be $\sigma_{00} = \omega_p^2/\pi\Delta_0$. Taking the a-axis value $\omega_p = 10000$ cm^{-1}[9] we find the limiting conductivity to be $\approx 2300\ \Omega^{-1}$cm^{-1}, which is in rough agreement with the low frequency limit of the optical conductivity. Furthermore the conductivity is predicted to be *independent* of defect concentration. This process would account for the magnitude of the observed conductivity as well as the lack of sample-to-sample variation.

The conductivity of the other two materials, $Tl_2Ba_2CuO_{6+\delta}$and $Pb_2Sr_2(Y/Ca)Cu_3O_{8+\delta}$cannot be explained by this process since the observed peak is already present in the normal state and only grows in sharpness as superconductivity is established. Nevertheless localization may be responsible for these structures as well. Both materials have wide transitions and the doping process involves oxygen vacancies.[23] Anther process that is capable of producing a low temperature peak is the development of spin density wave correlations.[24]

REFERENCES

1. A review of the background to this paper is found in D.B. Tanner and T. Timusk, *Physical Properties of High-Temperature Superconductors, vol III* D.M. Ginsberg, editor, (World Scientific, Singapore, 1992) p. 363.
2. M.J. Sumner, J-T. Kim, and T.R. Lemberger, *Phys. Rev. B* **47** 12248 (1993).
3. T. Strach, thesis, McMaster University, 1992
4. D.N. Basov, A.V. Puchkov, R.A. Hughes, T. Starch, J. Preston, T. Timusk, D.A. Bonn, R. Liang and W.N. Hardy, *Phys. Rev. B* **49** 12165 (1994).
5. T.A. Friedmann, M.W. Rabin, J. Giapintzakis, J.P. Rice, and D.M. Ginsberg, Phys. Rev. B **42** 6217 (1990).
6. R. Liang, P. Dosanjh, D.A. Bonn, D.J. Baar, J.F. Carolan, and W.N. Hardy, Physica C **195** 51 (1992).
7. C.C. Homes, M.A. Reedyk, D.A. Crandles, and T. Timusk, Applied Optics **32,** 2976, (1993).
8. Z. Schlesinger, R.T. Collins, F. Holtzberg, C. Feild, S.H. Blanton, U. Welp, G.W. Crabtree, Y. Fang, and J.Z. Liu, *Phys. Rev. Lett.* **65** 801 (1990).
9. D.N. Basov, R. Liang, D.A. Bonn, W.N. Hardy, B. Dabrowski, M. Quijada, D.B. Tanner, J.P. Rice, D.M. Ginsberg, and T. Timusk (unpublished).
10. T. Pham, H.D. Drew, S.H. Mosley, and J.Z. Liu, *Phys. Rev. B* **44** 5377 (1991).
11. J. Schützmann, B. Gorshunov, K.F. Renk, J. Münzel, A. Zibold, H.P. Geserich, A. Erb, and G. Müller-Vogt *Phys. Rev. B* **46** 512 (1992).
12. K. Zhang, D.A. Bonn, S. Kamal, R. Liang, D.J. Baar, W.N. Hardy, D. Basov, and T. Timusk, *Phys. Rev. Lett.* **73** 2484 (1994).
13. A.V. Puchkov, T. Timusk, S. Doyle, and A.M. Hermann, (unpublished).
14. R.J. Cava *et al.* Nature **336** 211 (1988).
15. M. Reedyk, Thesis, McMaster University (1992).
16. J.S. Xue, Thesis, McMaster University (1992).
17. M.A. Reedyk, C.V. Stager, T. Timusk, J.S. Xue, and J.E. Greedan, *Phys. Rev. B* **44** 4539 (1994).
18. J.H. Brewer (private communication)
19. L.D. Rotter, Z. Schlesinger, R.T. Collins, F. Holtzberg, C. Feild, U. Welp, G.W. Crabtree, J.Z. Liu, Y. Fang, K.G. Vabdervoort, and S. Flesher, *Phys. Rev. Lett.* **67** 2741 (1991).
20. M. Reedyk and T. Timusk, *Phys. Rev. Lett.* **69** 2705 (1992).
21. C.M. Foster, K.F. Voss, T.W. Hagler, D. Mihailović, A.J. Heeger, M.M. Eddy, W.L. Olsen, and E.J. Smith, *Solid State Comm.* **76** 651 (1990).
22. P.A. Lee *Phys. Rev. Lett.* **71** 1887 (1993).
23. J.S. Xue, M. Reedyk, J.E. Greedan, T. Timusk, and N. Tanaka, *J. of Solid State Chemistry,* **102** 492 (1993)
24. D.A. Bonn, J.D. Garrett, and T. Timusk, *Phys. Rev. Lett.* **61** 1305 (1988).

Journal of Superconductivity, Vol. 8, No. 4, 1995

Energy Spectrum in the High T_c Oxides

V.Z. Kresin,[1] S.A. Wolf,[2] S.D. Adrian,[3] M.E. Reeves,[2,3] and Yu.N. Ovchinnikov[4]

Received 31 January 1995

The energy gap structure of the cuprates depends strongly on levels of doping. The stoichiometric compound $YBa_2Cu_3O_7$ displays a peculiar two-gap structure. Oxygen depletion is accompanied by the transition to the gapless state, and this is manifested in various transport, electromagnetic, etc. properties of the material. The temperature dependence of the penetration depth correlates with oxygen content and is characterized by various power laws in an oxygen depleted sample. In other cuprates, overdoping leads to gaplessness and a peculiar dependence of H_{c2}.

KEY WORDS: Gaplessness; magnetic impurities; penetration depth; H_{c2}.

1. INTRODUCTION

This paper is concerned with the energy spectrum of the cuprates. It will focus on the $YBa_2Cu_3O_{7-\delta}$ compound, because this is the most studied high T_c material, and it turns out that its energy spectrum is greatly affected by the oxygen content. This paper will also discuss the energy spectrum in the overdoped region of other cuprates.

2. STOICHIOMETRIC COMPOUND AND TWO GAP STRUCTURE.

A two-gap spectrum in the high T_c oxides has already been treated theoretically by us [1]. The $YBa_2Cu_3O_{7-\delta}$ compound contains a CuO quasi-one dimensional chain structure in addition to the CuO planes. For the compound that is fully oxygenated the chain structure is particularly well developed, that is, the chain sites are fully occupied and well ordered. The chains provide doping for the CuO planes, but in addition, and this is particularly important for our model, they form an independent conducting subsystem. As a result, the superconducting state of the material displays a two-gap structure. Namely, each of the subsystems is characterized by its own energy gap. Let us denote by α and β the plane and chain subsystems, so that ϵ_α and ϵ_β are the corresponding energy gaps.

To begin, we give an explicit definition of the two-gap spectrum. This means that the density of states has two peaks which can be determined spectroscopically [2]. In the present model, two distinct subsystems, the planes (α) and the chains (β), are coupled by charge transfer. Because of the charge transfer, the system is characterized by a single value of T_c (in the absence of charge transfer there would be two different transition temperatures: T_c^α and T_c^β).

The superconducting state in the CuO plane is caused by the same intrinsic mechanism in all the cuprates. We think that this mechanism is phonon exchange [3], but at the moment this is not essential. As for the chain subsystem, the pairing is induced by two channels, an inelastic channel and an intrinsic proximity effect [1]. The word "intrinsic" stresses the fact that, unlike the usual proximity effect observed in thin-film sandwich structure, we are dealing

[1]Lawrence Berkeley Laboratory, University of California, Berkeley, CA 94720.

[2]Naval Research Laboratory, Washington, DC 20375-5000.

[3]George Washington University, Washington, DC 20052.

[4]Landau Institute for Theoretical Physics, Moscow, Russia 11733.

with a phenomenon occuring on the scale of unit cell. Nevertheless, the physics of the phenomenon is similar and represents the tunneling of the Cooper pair $\alpha \leftrightarrow \beta$ [4]. Note that, unlike the BCS model, in the two-gap analysis there is not any universal relation between the values of the energy gaps and T_c [5].

For the planes, $2\epsilon_\alpha(0)$ is equal to approximately $5T_c$. The smaller gap, on the other hand, is very sensitive to the oxygen content and for $\delta = 0$ is approximately equal to $1.25T_c$. There are two sets of Cooper pairs and correspondingly, two different coherence lengths ξ_α and ξ_β. The coherence lengths are $\xi_\alpha = 15\mathring{A}$ (planes) and $\xi_\beta = 25\mathring{A}$ (chains) [1].

The order parameters and the corresponding renormalization functions, $Z_\alpha(i\omega_n)$ and $Z_\beta(i\omega_n)$, are satisfied by the equations [1]:

$$\Delta_i(i\omega_n)Z_i(i\omega_n) = \lambda_i\pi T\sum_{n'=-\infty}^{\infty} D_{nn'}\frac{\Delta_i(i\omega_{n'})}{K^i_{n'}} + + \lambda_{ik}\pi T\sum_{n'=-\infty}^{\infty} D_{nn'}\frac{\Delta_k(i\omega_{n'})}{K^k_{n'}} + + \Gamma_{ik}\frac{\Delta_k(i\omega_n)}{K^k_n} \quad (1)$$

$$Z_i(i\omega_n) = \left[1+\frac{\lambda_i\pi T}{\omega_n}\sum_{n'=-\infty}^{\infty} D_{nn'}\frac{\omega_{n'}}{K^i_{n'}} + + \frac{\lambda_{ik}\pi T}{\omega_n}\sum_{n'=-\infty}^{\infty} D_{nn'}\frac{\omega_{n'}}{K^k_{n'}} + + \Gamma_{ik}\frac{1}{K^k_{n'}}\right] \quad (2)$$

Here $K^i_n = [\omega_n^2 + \Delta_i^2(i\omega_n)]^{\frac{1}{2}}$ $(i = \alpha, \beta)$, $\Gamma_{\alpha\beta}$ and $\Gamma_{\beta\alpha}$ describe the intrinsic proximity effect, λ_α is the in-plane coupling constant describing the pairing in the CuO plane, $\lambda_{\alpha\beta}$ and $\lambda_{\beta\alpha}$ are the off diagonal coupling constants, $\lambda_\beta = 0$, $D_{nn'} = \tilde{\Omega}^2/[\tilde{\Omega}^2 + (\omega_n - \omega_{n'})^2]$ is the phonon Green's function, and $\tilde{\Omega}$ is the characteristic phonon frequency. These equations describe the pairing state in the absence of magnetic impurity scattering.

Oxygen depletion leads to the formation of local magnetic moments in the chain layer. The removal of oxygen greatly affects the electronic energy states of the chains. Instead of a well-developed chain structure, we have a set of broken chains with Cu atoms at the end. These Cu atoms form local magnetic states, similar to surface states. These magnetic moments act as strong pairbreakers in the chain band, and the presence of the magnetic impurities leads to the formation of the gapless state. The presence of such magnetic moments is manifested in heat capacity data [6], in the appearance of tunneling zero bias anomalies, and in NMR data. In order to study the effect of magnetic impurities, the term $\Gamma_M(K^\beta_{n'})^{-1}$ should be added to the rhs of Eq. (2) for $i = \beta$.

The concept of gapless superconductivity was introduced in Ref. 7 (see also the reviews in [8]). One should note that the gapless state is still a superconducting state. The absence of the gap leads to a power law, rather than exponential dependences of the electronic heat capacity, surface impedance, penetration depth, etc., but nevertheless, the material still exhibits the Meissner effect and zero resistance.

For the cuprates, we are dealing with an unusual case of gapless superconductivity, namely at some value of the impurity concentration the energy gap becomes equal to zero, whereas the shift in T_c, unlike the usual case, is relatively small. The critical concentration n, which corresponds to the appearance of the gapless state can be calculated by use of the method developed for the usual proximity system. For $\delta = 0.1$, that is for $YBa_2Cu_3O_{6.9}$ compound, we are dealing with the gapless state. It corresponds to the criterion $\hbar/\tau_S \simeq \epsilon_\beta$, or $l^c \simeq \xi_\beta$ where $l^c \simeq v_f\tau_c^m$ is the mean free path for magnetic scattering.

It is essential that, although the magnetic moments are introduced in the chain sites only, the energy gaps become equal to zero in both subsystems. Namely, as a consequence of the charge transfer, both densities of states $N_\alpha(w)$ and $N_\beta(w)$ are not equal to zero up to $\omega = 0$. Note also, that even when the gaps are equal to zero, the density of states $N_\alpha(w)$ displays a peak at $\omega = \epsilon_\alpha$, and this peak can be observed experimentally, e.g., by tunneling measurements. The gapless regime is very narrow in the conventional isotropic case [9], namely $n_{cr} = 0.91n'$, n' corresponds to $T_c = 0$. The presence of different subsystems, such as planes and chains, leads to a different picture (see above), and the gapless region becomes much wider [9].

3. PENETRATION DEPTH

The model described here can be used to evaluate the temperature dependences of the penetration depth $\lambda(T)$ [10]. At present, this problem has attracted much interest. Some authors [11,12] have observed exponential dependences for Nd-based cuprates and for fully oxygenated YBCO films. According to others [13,14], $\Delta\lambda \propto T$, whereas a quadratic dependence has also been reported [12,15,16]. The approach developed by us [1] can explain all data [11-16] in a unified way. The dependence $\Delta\lambda(T)$ indeed can vary and is very sensitive to oxygen content. The screening is provided by both subsystems, and the temperature dependence of the penetration depth in the London case $\xi \ll \lambda$ is described by the equation:

$$\frac{\lambda(T)}{\lambda(0)} = \frac{[Q_\alpha(T) + Q_\beta(T)]^{-\frac{1}{2}}}{[Q_\alpha(0) + Q_\beta(0)]^{-\frac{1}{2}}} \qquad (3)$$

The kernels Q_α and Q_β are equal to:

$$Q_\alpha(T) = \rho\pi T \sum_{\omega_n=0}^{\infty} \frac{1}{Z_\alpha(i\omega_n)} \frac{\Delta_\alpha^2(i\omega_n)}{[\omega_n^2 + \Delta_\alpha^2(i\omega_n)]^{\frac{3}{2}}}$$

$$Q_\beta(T) = \pi T \sum_{\omega_n=0}^{\infty} \frac{1}{Z_\beta(i\omega_n)} \frac{\Delta_\beta^2(i\omega_n)}{\left[\omega_n^2 + \Delta_\beta^2(i\omega_n)\right]^{\frac{3}{2}}}$$

The quantity ρ is equal to $\nu_\alpha m_\beta/\nu_\beta m_\alpha$ (ν is the density of states).

First of all, we would like to formulate a qualitative result, namely, that the temperature dependence is different for various concentrations of the impurities. Therefore, for YBCO the functional dependence $\Delta\lambda(T)$ is different for various oxygen contents. If Γ_M=0, then an exponential dependence is obtained for $\Delta\lambda(T)$ as $T \to 0$. An increase in Γ_M, that is, an increase in magnetic impurities, leads to a modification of this dependence. A weaker exponential dependence is observed for small values of Γ_M corresponding to a smaller energy gap. For $\Gamma_M = 90K(\delta \approx .1)$ a linear dependence is obtained. For even larger values of Γ_M, the calculated dependence becomes quadratic.

The value of the parameter Γ_M is directly related to the oxygen content, which allows one to compare our calculations with the experimental data [11-16]. The value ($\Gamma_M = 0$) corresponds to the stoichometric composition, and the dependence of $\Delta\lambda(T)$ is exponential as $T \to 0$. The energy spectrum has a two-gap structure, and $\Delta\lambda(T)$ is dominated by the smaller gap, so that $\Delta\lambda(T) \propto \exp(-\epsilon_\beta/T)$ Such exponential dependence, indeed, has been observed [12] for a fully oxygenated YBCO thin film. Oxygen depletion leads initially to a decrease in the energy gap and, correspondingly, to a weaker exponential dependence. The value ($\Gamma_M = 90K$) corresponds to the transition to the gapless state [1], and the dependence $\Delta\lambda(T)$ is not exponential, but is described by a power law. According to our calculations, the dependence is actually linear. For greater oxygen depletion, the calculated curves exhibit a quadratic tendency. Such quadratic dependence has also been seen [15] with the data more closely matching calculated curves with $\Gamma_M > 90K$. This is consistent with the depressed critical temperatures of the samples used in Ref. 15.

According to our analysis, the linear dependence in Ref. 13 is characteristic of an oxygen depleted sample, which seems at odds with the high T_c of the crystals. This can be understood in light of recent work by Skelton *et al.* [18] who found that some single crystals of YBCO become highly oxygen deficient at the surface while maintaining the stoichiometry in the bulk.

Our approach allows us to describe, in a unified way, the experimental penetration depth data in YBCO, which display different temperature dependences. According to our theory, these differences are sample dependent and correlate with the oxygen content. The oxygen depletion leads to the transformation: $\Delta\lambda_1(T) \to \Delta\lambda_2(T) \to \Delta\lambda_3(T) \to \Delta\lambda_4(T)$ where $\Delta\lambda_1(T) \propto \exp(-\epsilon_\beta/T)$, $\Delta\lambda_2(T) \propto \exp(-\epsilon'_\beta/T)$ ($\epsilon'_\beta < \epsilon_\beta$), $\Delta\lambda_3(T) \propto T$, and $\Delta\lambda_4(T) \propto T^2$.

4. OVERDOPED SYSTEMS

Let us discuss some properties of the overdoped systems such as $Tl_2Ba_2CuO_6$ and $Bi_2Sr_2CuO_6$ [19]. These systems also display a gapless spectrum. The presence of magnetic impurities leads to a larger depression in T_c, for example the shift T_c=85K $\to$ T_c=14K for $Tl_2Ba_2CuO_6$. We think that this depression is mainly due to the presence of magnetic impurities located on the O(4) site. This is supported by heat capacity data [20a], and the measurements [20b]. According to [21], the presence of magnetic impurities allows us to explain the unusual behavior of $H_{c2}(T)$, namely, negative curvature, and a very large

value of $H_{c2}(0)$ relative to the conventional picture.

Note also that the heat capacity measurements [20a] reveal Shottky anomalies (indicating magnetic states) for the samples that are not overdoped. This means that T_c in these materials is already depressed. A similar conclusion follows from [6]. Therefore, the doping process is accompanied by the appearance of magnetic moments, that is, by a factor depressing T_c. If it is possible to increase the carrier concentration by using a different method, one could increase T_c above 85K. This is consistent with a strong positive pressure dependence of T_c [22]. By applying pressure to the crystal, the effective carrier concentration is increased without introducing magnetic pair-breakers.

5. CONCLUSIONS

The main results of the paper can be summarized as follows:

1. The presence of various structural low-dimensional units (planes, chains), along with short coherence length lead to a unique opportunity to observe a two-gap spectrum. The spectroscopy of the stoichoimetric YBCO compound (microwave properties, tunneling, etc.) is determined by the smaller energy gap.
2. The chains are characterized by the induced superconductivity which is due to the charge transfer, e.g. to the intrinsic proximity effect.
3. Oxygen depletion leads to a peculiar gapless state which is characterized by the absence of the energy gap without a noticeable shift in T_c.
4. The gapless state is manifested in the change in the temperature dependence of the penetration depth. This dependence is correlated with oxygen content, allowing all experimental data to be explained from a unified point of view.
5. The presence of magnetic impurities for the overdoped cuprates makes a great impact on the temperature dependence of H_{c2}.

ACKNOWLEDGEMENTS

The research of VZK is supported by the US Office of Naval Research under Contract No. N00014-94-F0006, and the research of MER is supported under Contract No. N00014-94-1-G027.

REFERENCES

1. V.Kresin and S..Wolf, a)*Phys.Rev.* **B41**, 4278 (1990); b) *Physica* **C169**, 476 (1990); c)*Phys. Rev.* **B46**, 6458 (1992).
2. J. Geerk et al., Z. Phys. B **73**, 329 (1988).
3. M.Reeves et al., *Phys. Rev.* **B47**, 6065 (1993).
4. W. McMillan, *Phys. Rev.* **175**, 537 (1968).
5. H.Suhl et al., *Phys. Rev. Lett.* **3**, 552 (1959); B.Geilikman et al., *Sov. Phys.-Solid State* **9**, 642 (1967); V.Kresin, *J. Low Temp. Phys.* **11**, (1973) 519.
7. A.Abrikosov and L.Gor'kov, *Sov. Phys.-JETP* **12**, 1243 (1961).
8. K.Maki, in *Superconductivity*, ed. R. Parks, (Marcel Dekker, NY 1969) p.1035; P.De Gennes, *Superconductivity of Metals and Alloys*, (W. Benjamin, NY 1966), Ch. VIII.
9. V.Kresin and S.Wolf, *Phys. Rev.* B **51**, 1229 (1995).
10. S.D. Adrian et al. Phys. Rev. B **51**, 6800 (1995).
11. S.Anlage et al., *Phys. Rev.* **B44**, 9764 (1991).
12. N.Klein et al., *Phys. Rev. Lett.* **71**, 3355 (1993).
13. W. Hardy et al., *Phys. Rev. Lett.* **70**, 3999 (1993).
14. Jian Mao et al., **51**, Phys. Rev. B, 3316 (1995).
15. M.Beasley, *Physica* **C209**, 43 (1993).
16. Zhengxiang Ma et al., *Phys. Rev. Lett.* **71**, 781 (1993).
17. A. Abrikosov and I. Khalatnikov, *Adv. Phys.* **8**, 45 (1959).
18. E.Skelton et al., *Science* **263**, 1416 (1994).
19. A. Mackenzie et al., Phys. Rev. Lett. **71**, 1938 (1993); M. Osofsky et al., Phys. Rev. Lett. **71**, 2315 (1993).
20. a) J. Wade et al., J. of Supercon. **7**, 261 (1994); b) C. Niedermayer et al., J. of Supercon. **7**, 165 (1994); c) M. Teplov et al., this issue.
21. Yu. Ovchinnikov and V. Kresin, this issue.
22. C.C. Kim et al.,Phys. Rev. B **50**, 13778 (1994).

Journal of Superconductivity, Vol. 8, No. 4, 1995

Heat Conduction in $Ba_{1-x}K_xBiO_3$

Ctirad Uher,[1] Frank Tsui,[1] Baoxing Chen,[1] and P. D. Han[2]

Received 31 January 1995

We have investigated heat conduction of single crystal $Ba_{1-x}K_xBiO_3$ in the temperature range of 2 - 300 K and in a magnetic field of up to 6 Tesla. Temperature dependence of thermal conductivity $\kappa(T)$ reveals the participation of both electrons and phonons with their relative contributions that depend critically on the potassium doping concentration. Crystals underdoped with potassium (samples with higher T_c) exhibit a strong suppression of κ and a glass-like temperature dependence. In contrast, those with a higher potassium content (lower T_c) show an increase as temperature decreases with a peak near 23 K. Field dependence of $\kappa(H)$ is also very sensitive to the level of potassium doping. Crystals exhibiting a large phonon contribution show an initial drop in $\kappa(H)$ at low fields followed by a minimum and then a slow rise to saturation as the field increases. The initial drop is due to the additional phonon scattering by magnetic vortices as the sample enters a mixed state. The high field behavior of $\kappa(H)$, arising from a continuous break-up of Cooper pairs, exhibits scaling which suggests the presence of an unconventional superconducting gap structure in this material.

KEY WORDS: High-T_c superconductors; thermal conductivity; magnetization.

1. INTRODUCTION

The discovery of superconductivity in $Ba_{1-x}K_xBiO_3$ (BKBO) [1,2] and its unique physical properties have stimulated considerable interest. Unlike the copper-oxide layered perovskite superconductors, BKBO is cubic and copperless, contains no magnetic ions, and exhibits a large isotope effect [3]. These and other features suggest that electron-phonon coupling is the relevant mechanism for superconductivity in this compound. Owing to its moderately long coherence length, low microwave loss, and good tunneling characteristics, BKBO is also attracting interest for technological superconductor applications.

One of the less fortunate aspects of BKBO is the presence of mixed phases and a tendency for an inhomogeneous distribution of potassium [4], both of which contribute to a rather high electrical resistivity. This results in considerable difficulties when attempting to determine the essential galvanomagnetic transport parameters. Thermal transport, on the other hand, avoids these problems, and it probes directly the behavior of carriers and phonons in both the normal and the superconducting states [5,6]. A few years back we have reported on the thermopower and thermal conductivity of polycrystalline BKBO [7]. In this paper we report on our recent studies made on high quality single crystals. We show that the thermal conductivity is rather sensitive to the potassium doping concentration, and we provide first results on the magnetic field dependent heat conduction of BKBO crystals.

2. EXPERIMENTAL

Measurements were made on single crystals prepared by a three-electrode, top-seeded growth method [8]. This method facilitates the growth of relatively large crystals with T_c of up to 32 K and sharp superconducting transitions. It provides a possibility to control potassium content by imposing an overpotential. The samples used in this study were typically 1 to 2 mm long and about 1 mm across. We describe results on two samples: sample A with T_c = 18 K, and sample B with a lower potassium content (underdoped) and T_c = 30 K.

Magnetization measurements were carried out using a commercial SQUID magnetometer in order to determine the T_c, the width of the transition, and the magnetic irreversibility. We focused our measurements on two types of sweeps: zero-field-cooled (ZFC) and field-cooled (FC) sweeps at a fixed field (Fig. 1a), and field dependent

[1]Department of Physics, University of Michigan, Ann Arbor, Michigan 48109-1120.
[2]Department of Materials Science and Engineering, University of Illinois at Urbana-Champaign, Urbana, Illinois 61801.

0896-1107/95/0800-0445$07.50/0

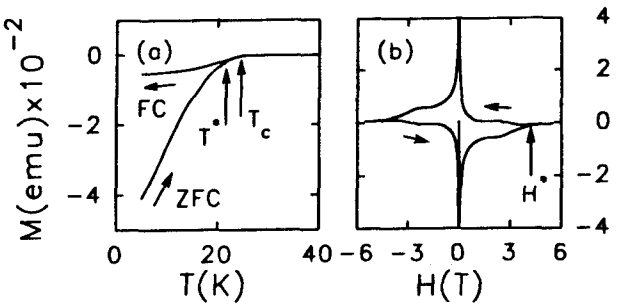

Fig. 1. Typical magnetic hysteresis loops for sample B. (a) Temperature dependent hysteresis curve between zero-field-cooled (ZFC) and field-cooled (FC) magnetizations at 3 Tesla. Arrows indicate T^* and T_c, respectively. (b) Field dependent hysteresis at 20 K. The irreversibility field H^* is indicated by the arrow.

hysteresis at a fixed temperature (Fig. 1b). The irreversibility field H^* and temperature T^* are determined from the points of divergence in the hysteretic traces, as indicated in Fig. 1.

Thermal conductivity was measured by a steady-state technique with the aid of a miniature resistive heater and two pairs of differential chromel-constantan thermocouples. The thermocouples were calibrated to account for small changes in their electromotive force in a magnetic field. Fields of up to 6 Tesla were supplied by a superconducting split-coil magnet, and were directed perpendicular to the heat current.

3. RESULTS

3.1. Magnetization

Our magnetization measurements were designed to probe flux pinning behavior by investigating the magnetic irreversibility and the associated critical parameters, H^* and T^*. The temperature dependent magnetization exhibits Meissner effect below T_c, as shown in Fig. 1a. The irreversibility temperature T^* coincides with T_c at zero field, and it decreases as field increases; the irreversibility field H^*, on the other hand, increases correspondingly with decreasing temperature. Below T_c, the measured H^* is much smaller than the upper critical field H_{c2} (see Fig. 1b). The width of the magnetic hysteresis loop (e.g. Fig. 1), to a good approximation, is directly proportional to the critical current [9].

Fig. 2 traces the irreversibility of sample B. The observed behavior exhibits scaling in the form

$$H^* \sim (1 - T^*/T_c)^3. \quad (1)$$

The exponent of 3 has been observed in $Ba_2Sr_2CaCu_2O_8$ [10], but not in sample A nor other BKBO [11,12] nor in $YBa_2Cu_3O_7$ [10], where an exponent of 3/2 is reported. It has been shown [10,13] that the flux pinning energy and its temperature and field dependences determine the scaling exponent. When flux lines are rigid corresponding to a large pinning energy and collective pinning effects, an exponent of 3 is expected; when flux bundles are weakly correlated, one expects a smaller pinning energy and an exponent of 3/2. The observed exponent for sample B reveals the presence of a high defect concentration arising from potassium underdoping, which leads to stronger pinning effects. More insights on the effects of potassium doping, particularly its influence on the superconducting transition, are obtained from thermal conductivity measurements described below.

3.2. Thermal Conductivity

The temperature dependences of $\kappa(T)$ for samples A and B are shown in Fig. 3. They represent various scattering processes that involve different length scales in these samples. The underdoped sample B exhibits a strong suppression of thermal conductivity compared with sample A, more than a factor of 10 at low temperatures. This is attributed to a reduction in phonon mean free path in underdoped samples due to defects. The estimated phonon mean free path for sample B at 25 K is about 10 Å using data from specific heat measurements [14], and it is expected to be even shorter at higher temperatures. This length scale corresponds to a defect density of nearly one per unit cell. The apparent high defect density may arise from statistical fluctuations of dopant concentration from one unit cell to another in underdoped samples. The high temperature behavior of sample B exhibits a slow increase with temperature (Fig. 3) similar to that of the polycrystalline samples [7]. The behavior is consistent with the short mean free path, and thus a glass-like temperature dependence [15]. It is not that unusual to see glassy behavior in crystalline

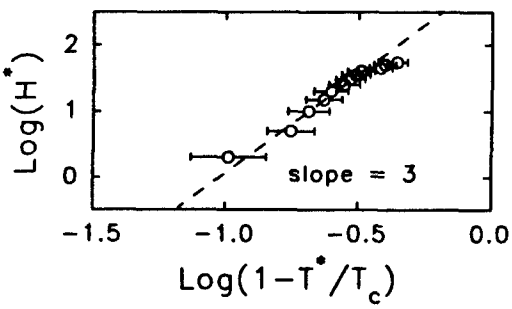

Fig. 2. Log-log plot of irreversibility field H^* versus the reduced irreversibility temperature $(1 - T^*/T_c)$ for sample B. $T_c = 30$ K.

materials; other examples do exist [16,17]. The behavior for sample A, on the other hand, exhibits a decrease as temperature increases which indicates a strong phonon conductivity dominated by Umklapp processes [15]. This is consistent with a low defect density and the crystalline nature of the sample.

As temperature decreases, the rise in heat conduction of sample A slows down; then it rises to a distinct peak around 23 K, before it drops at lower temperatures. Sample B exhibits no such peak, but it also displays a similar decrease at low temperatures. The peak observed in sample A evidently arises from the transition between the high temperature phonon dominated conduction and the low temperature drop due to phonon scattering by imperfections [15]. We believe that the peak is not directly related to the onset of superconductivity, because it occurs well above T_c. As mentioned above, the grain boundaries and scattering centers in these samples arise from the inevitable statistical fluctuations of K doping concentration. We have ruled out the participation of the electronic thermal conduction at this temperature because most electrons are condensed into Cooper pairs. It is also unlikely that a strong suppression of quasiparticle scattering [18] plays any role here, according to the field dependent results discussed below.

More evidence on a large phonon thermal conductivity of sample A is obtained from the field dependent behavior shown in Fig. 4a. For increasing field, κ drops initially at low field and, after reaching a 'dip' at H_d, it slowly rises to saturation. The initial rise in $1/\kappa$ (Fig. 4a, inset) is due to additional phonon scattering by magnetic vortices as the sample enters a mixed state. It cannot be attributed to electron scattering by vortices because the electron mean free path is less than 10 Å, as indicated by results from our measurements and those of others [3,12]. For a 'dilute' system of vortices, the additional phonon scattering is approximately laH/Φ_0 [19] with l the phonon mean free path, a the diameter of the vortex line, Φ_0 the flux quantum, and H the magnetic field. The phonon thermal resistivity $1/\kappa_{ph}(H)$ in this limit is, therefore, linear with H.

The linear dependence fits the observation rather well (see inset in Fig. 4a) with a slope that depends on the product of l and a. At higher fields the strong interaction between vortices leads to the formation of a flux lattice, and consequently phonon scattering by vortices diminishes; thus κ_{ph} no longer drops at H_d. This happens when the penetration depth λ is comparable to the separation of flux lines, so while λ increases with increasing temperature H_d decreases.

The slow rise of κ above H_d arises from increasing electronic contribution due to the continuous break-up of Cooper pairs. This enables us to estimate the electronic contribution κ_e from the size of the total increase in $\kappa(H)$. For instance, at 4.6 K, κ_e is less than 1/5 of the total κ in the normal state. From this we estimate the phonon contribution and the phonon mean free path l using the published specific heat data [14]; at 4.6 K l is ~ 4000 Å. The large mean free path makes the initial drop in $\kappa(H)$ possible because, if l is shorter than the average distance between vortices, κ_{ph} would not be affected by them. Note that the vortex spacing of 4000 Å corresponds to a field strength of about 100 G. The observed large drop at low fields further supports the notion that the phonon contribution dominates the zero field heat conduction.

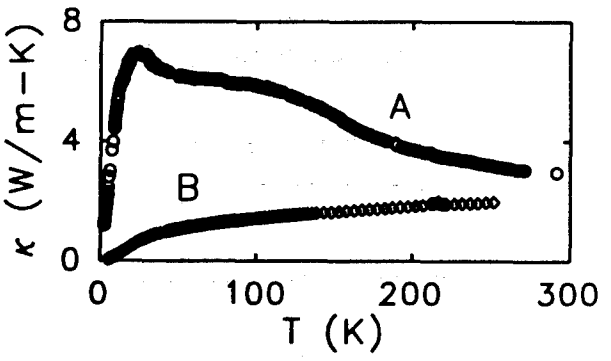

Fig. 3. Temperature dependence of the thermal conductivity for sample A (open circles) and sample B (open diamonds).

In sample B the higher defect concentration leads to a shorter phonon mean free path (~ 100 Å at 4.6 K), hence a smaller phonon contribution to the thermal conductivity. This in turn results in a smaller or no phonon dip in $\kappa(H)$ at low fields. Although the electronic thermal conductivity of sample B is actually comparable to that of sample A, the observed large rise in $\kappa(H)$ for sample B at high fields indicates that its electronic part represents a greater fraction of the conductivity than that in sample A.

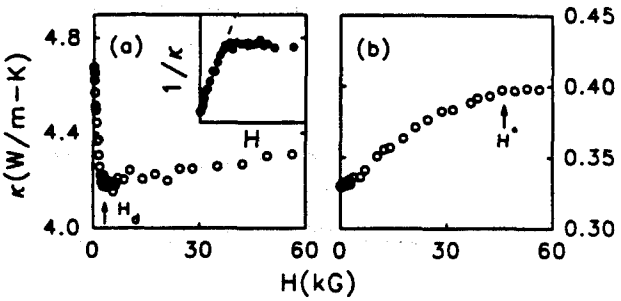

Fig. 4. Field dependent thermal conductivity (a) for sample A at 9.2 K and (b) for sample B at 15.2 K. Inset of (a) shows the corresponding thermal resistivity which exhibits linear behavior at low fields (dashed line). Arrows indicate H_d in (a) and H^* in (b). Note that the two temperatures in (a) and (b) correspond roughly to the same T/T_c value (~ 0.5).

At higher fields, the measured thermal conductivity saturates at a critical field H^*, which is far below H_{c2} (> 5.5 Tesla just below $0.8T_c$, see Section 3.1) obtained from magnetization measurements. The behavior below H^* exhibits scaling in the form

$$\kappa(H^*) - \kappa(H) \sim (H^* - H)^{3/2}, \quad (2)$$

as shown in Fig. 5 for sample B. Eq. (2) corresponds approximately to the electronic thermal conductivity in the superconducting state, κ_{es}. The 3/2-power law differs from the linear behavior of the conventional dirty type-II superconductors [20] given by

$$\kappa(H_{c2}) - \kappa(H) \sim (H_{c2} - H). \quad (3)$$

The observed functional dependence on field suggests the presence of an unusual gap structure in BKBO. In a separate publication [21] we derive self consistently the effective gap from the observed field dependence [Eq. (2)] using a BCS-like treatment [22]. The resulting effective gap in BKBO is given by [21]

$$\varepsilon(H) \sim (H^* - H)^{1/2}, \quad (4)$$

with H^* the field at which the effective gap vanishes. The measured H^* coincides with magnetic irreversibility field obtained from magnetization measurements (Section 3.1). The latter field signals the onset of supercurrent. It is reasonable to conclude that both fields are the same, and that they also determine the onset of the unconventional superconducting gap given by Eq. (4).

The mean-field-like superconducting gap, indicated by the exponent of 1/2 [Eq. (4)], appears to exist in all BKBO crystals we have studied. However, its effects on thermal conductivity are more pronounced in potassium underdoped samples with higher T_c, because the phonon contribution is suppressed by the higher defect concentration, as discussed above. The presence of a robust gap

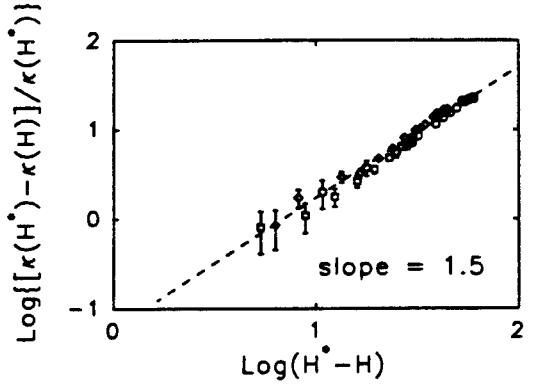

Fig. 5. Scaling behavior of thermal conductivity of sample B at three different temperatures: 12.4 K (circles), 15.2 K (diamonds), and 19.8 K (squares). The respective H^* for the three temperatures are 3, 4.5, and 6 Tesla. The dashed line corresponds to a slope of 1.5.

with a relatively high critical field H^* suggests that the electron-phonon interactions in BKBO are quite strong. While potassium concentration affects directly the thermal conductivity of BKBO through phonon mean free path, it does not appear to influence the form and strength of the gap.

4. CONCLUSION

We have studied the magnetic irreversibility and thermal conductivity of BKBO crystals in a wide range of temperatures and fields. The different roles of electrons and phonons on thermal conduction are examined. Our results reveal that both thermal conductivity and superconducting transition can be tuned by potassium doping concentration, and that the statistical fluctuation of the K concentration determines the phonon mean free path and the character of flux pinning. The observed scaling behavior for the high field thermal conductivity indicates the presence of an unconventional and mean-field-like gap structure in BKBO. The gap and the related phenomena reveal insight into the fundamental processes that cause the superconductivity in BKBO.

ACKNOWLEDGMENTS

The research was supported in part by ONR grant No. N00014-92-J-1335. FT thanks Herman and Margaret Sokol for fellowship support.

REFERENCES

1. L. F. Mattheiss, E. M. Gyorgy and D. W. Johnson, *Phys. Rev. B* **37**, 3745 (1988).
2. R. J. Cava, *et al.*, *Nature* **332**, 814 (1988).
3. B. Batlogg, *et al.*, *Phys. Rev. Lett.* **61**, 1670 (1988).
4. E. S. Hellman and E. H. Hartford, *Phys. Rev. B* **47**, 11346 (1993).
5. C. Uher, *J. Supercond.* **3**, 337 (1990).
6. C. Uher, in *Physical Properties of High Temperature Superconductors III*, edited by D. M. Ginsberg, (World Scientific, Singapore, 1992), p. 159.
7. S. D. Peacor, *et al.*, Phys. Rev. B **42**, 2684 (1990).
8. P. D. Han, L. Chang and D. A. Payne, *J. Crystal Growth* **128**, 798 (1993).
9. C. P. Bean, *Phys. Rev. Lett.* **8**, 250 (1962); *Rev. Mod. Phys.* **36**, 31 (1964).
10. C. C. Almasan, *et al.*, *Phys. Rev. Lett.* **69**, 3812 (1992).
11. Y. Y. Xue, *et al.*, *Physica C* **194**, 194 (1992).
12. B. Chen, F. Tsui and C. Uher, unpublished.
13. J. C. Garland, C. C. Almasan, and M B. Maple, *Physica C* **191**, 158 (1992).
14. G. K. Panova, *et al.*, *JETP* **76**, 302 (1993).
15. R. Berman, *Thermal Conduction in Solids*, (Clarendon Press, Oxford, 1976).
16. P. B. Allen, *et al.*, *Phys. Rev. B* **49**, 9073 (1994).
17. D. G. Cahill and R. O. Pohl, *Phys. Rev. B* **35**, 4067 (1987).
18. R. C. Yu, *et al.*, *Phys. Rev. Lett.* **69**, 1431 (1992).
19. J. Lowell and J. B. Sousa, *J. Low Temp. Phys.* **3**, 65 (1970).
20. D. Saint-James, G. Sarma and E. J. Thomas, *Type II Superconductivity*, (Pergamon Press, Oxford, 1969).
21. B. Chen, *et al.*, *Phys. Rev. B*, submitted.
22. J. Bardeen, G. Rickayzen and T. L. Tewordt, *Phys. Rev.* **113**, 982 (1959).

Journal of Superconductivity, Vol. 8, No. 4, 1995

The Field Dependence of the Thermal Conductivity: Evidence for Nodes in the Gap

M. B. Salamon[1], Fang Yu[1], and V. N. Kopylov[2]

Received February 1, 1995

The increased thermal conductivity below T_c in $YBa_2Cu_3O_{7-x}$ (YBCO) is shown to agree with the microwave electrical conductivity, affirming that increase is due to quasiparticle conduction. The field dependence, particularly in the conducting plane permits us to separate phonon and quasiparticle contributions for both YBCO and $T\ell_2Ba_2CuO_6$ single crystals.

KEY WORDS: thermal conductivity; Andreev reflection; vortex lines; mixed phase

A characteristic feature of the cuprate superconductors is the appearance of a maximum in the thermal conductivity $\kappa(T)$ in the vicinity of $0.5T_c$. The position and relative magnitude of the peak is very sensitive to sample purity and quality, reaching a value more than double the normal state thermal conductivity in untwinned single crystals of $YBa_2Cu_3O_{7-x}$. An early, and very natural, explanation for this effect was based on the well known BRT calculation for conventional superconductors, in which the opening of the superconducting gap provides a "low pass" filter for phonons, permitting the thermal conductivity to reach the value it would achieve in the absence of electron-phonon coupling [1]. However, as has been discussed elsewhere in the literature [2], there are reasons to doubt this scenario. Insulating phases of these materials, whether effected by oxygen content or doping, do not achieve thermal conductivities as large as the observed peak values [3], suggesting that processes other than scattering from electrons limit the phonon mean free path [4]. Further, the thermal conductivity peak is suppressed by magnetic fields [1] in the range $H_{c1} \ll H \ll H_{c2}$ and by certain impurities such as Zn [5]. In this paper we will focus on the field dependence and on the compatibility of the thermal conductivity peak and the quasiparticle electrical conductivity observed in microwave measurements. We will also show that fields applied in the ab plane, for which the vortices are coreless or nearly so, reduce the thermal conductivity at low temperatures and induce a four-fold variation of thermal conductivity as the field is rotated in the plane.

In conventional superconductors, the opening of the superconducting gap rapidly decreases the density of thermally excited quasiparticles (qp's), causing the electronic thermal conductivity to decrease. There is no "coherence peak" observed, such as occurs in the electrical conductivity. In the cuprates, however, microwave measurements show that the electrical conductivity of quasiparticles in the superconducting state increases gradually, without a coherence peak, reaching a maximum at approximately the same temperature as the maximum in $\kappa(T)$ [6]. It has been argued that inelastic electron-electron scattering processes dominate the normal state electrical conductivity, and that these are rapidly suppressed in the superconducting state. The concomitant increase in the mean-free path overcomes the decreasing quasiparticle density, leading to the observed maximum. If this scenario is correct, then the quasiparticle lifetime below T_c will be dominated by elastic processes, and we should expect the Wiedemann-Franz law

$$\kappa^{qp}(T) = TL_o\sigma_1(T) \qquad (1)$$

to hold, where $\kappa^{qp}(T)$ is the quasiparticle contribution to the thermal conductivity, $\sigma_1(T)$, the normal-fluid electrical conductivity, and $L_o = 2.45 \times 10^{-8}$ WΩ/m K, the Lorenz number. Quite recently [7], the electrical conductivity has been measured on high quality untwinned samples of $YBa_2Cu_3O_{7-x}$ with microwave

[1]Department of Physics and Science and Technology Center for Superconductivity, University of Illinois, Urbana, IL 61801

[2]Institute for Solid State Physics, Chernogolovka, Russia

0896-1107/95/0800-0449$07.50/0

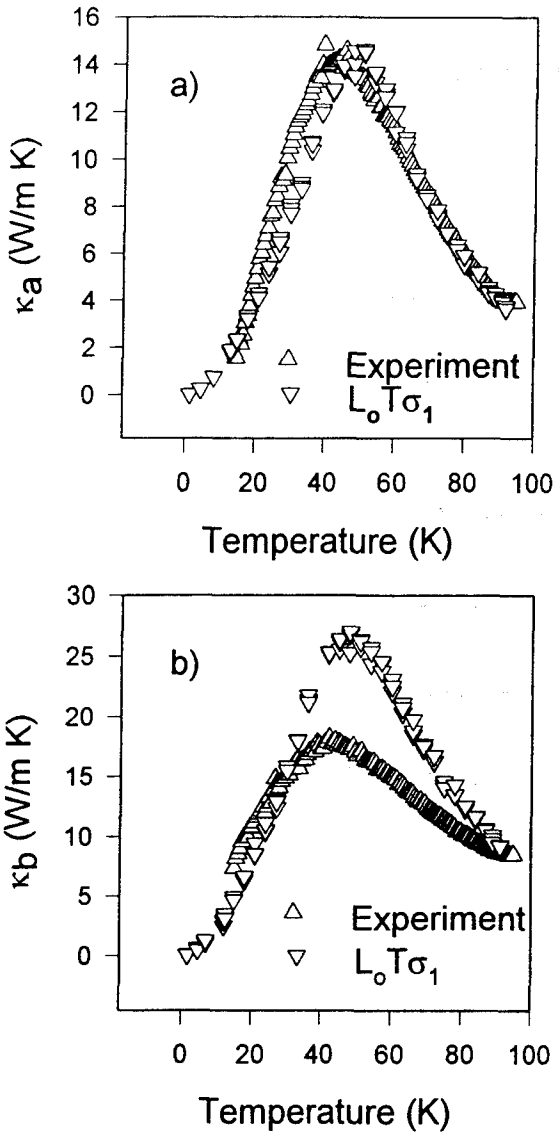

Fig. 1. a) Triangles: the measured a-axis thermal conductivity after subtraction of the phonon contribution. Nablas: the thermal conductivity determined from the microwave electrical conductivity (Ref. 7) via the Wiedemann-Franz law. b) The same along the b-axis.

currents directed along both a- and b-axes. In Fig. 1a, we plot the microwave conductivity, converted to thermal conductivity via Eq. (1) along with previously published data for the a-axis thermal conductivity on comparable samples. These data use the same phonon background subtraction as previously, and its inadequacies contribute to the difference between the two data sets at low temperatures; otherwise, the agreement is excellent. However, as Fig. 1b illustrates, the two data sets are significantly different along the b-axis, which includes the chain contributions. The differences may be experimental artifacts: the microwave analysis involves division by the cube of the penetration depth in the relevant directions, and small errors could therefore lead to large differences in the two directions. In extracting the qp thermal conductivity, the same phonon contribution was subtracted from both data sets, but is likely to be different for a- and b-directions. Possibly the effect is real and reflects a smaller Lorenz number in the b-direction, as would result, for example, if scattering in the chains were strongly inelastic.

The field dependence of the thermal conductivity peak in $YBa_2Cu_3O_{7-x}$ has been studied by a number of authors, and has yet to find an explanation within a scenario in which phonon thermal conductivity dominates [1]. The reason is that phonons are attenuated by the normal electrons within vortex cores, and these represent a negligible volume fraction at fields at which the thermal conductivity peak has been suppressed to the normal state value. It is widely known in conventional type-II superconductors [8], and in heavy fermion systems [9] that vortices are highly effective in scattering quasiparticles, reducing the mean-free path to essentially the vortex spacing. The dramatic increase in quasiparticle mean free path (estimated to be as large as 1 μm) to which we have attributed the existence of the peak, makes the peak susceptible to any process that shortens the mean-free path. Fig. 2 shows the field dependence observed in a single crystal sample of $T\ell_2Ba_2CuO_x$. We have shown elsewhere [10] that these data can be fit to a simple expression of the form

$$\kappa(H,T) = \kappa_{ph}(T) + \frac{\kappa_{qp}(0,T)}{1 + H/H_o}. \qquad (2)$$

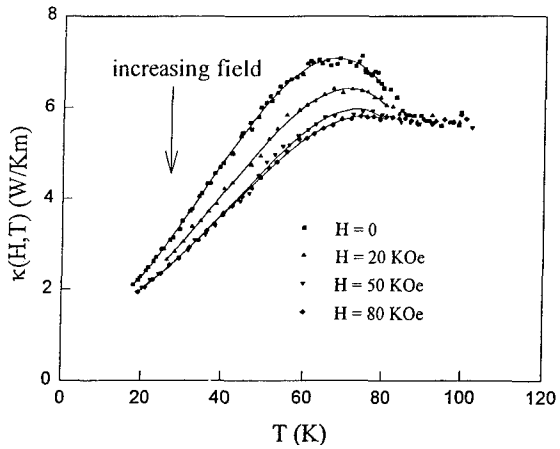

Fig. 2. The field dependence of the thermal conductivity of a single crystal sample of $Tl_2Ba_2CuO_6$ with the field along the c-axis. (Ref. 10)

Here the characteristic field is $H_o \simeq \Phi_o/\ell\xi$, where ℓ is the quasiparticle mean free path in the normal state extrapolated to temperature T and ξ is the coherence length at that temperature. This is smaller than the corresponding expression for phonon attenuation by vortices by a factor $\xi/\ell_m \simeq 10^{-2}$, where ℓ_m is the phonon mean free path in the Meissner phase. At the fields used in the experiments, $H/H_{c2} \leq 0.1$, the phonon effect is negligible. A separation of phonon and quasiparticle contributions through the use of Eq.(2) demonstrates a monotonic decrease in κ_{ph} and with the peak entirely due to κ_{qp} [10]. Similar fits can be made to data in the literature for YBCO, but there are too few data points available with which to effect a similar separation.

In the original discussion of the field dependence of the qp thermal conductivity, Vinen suggested scattering of quasielectrons into quasiholes as a mechanism for the effect [8]. This is a form of Andreev scattering in which the spatial variation of the superfluid velocity, rather than that of the gap is responsible. [11] The energy of a thermal excited quasiparticle, in the presence of superfluid flow may be written in the laboratory frame of reference as

$$E_p^{lab} = E^s_{p-mv_s(r)} + p \cdot v_s, \qquad (3)$$

where the qp energy in the superfluid frame is

$$E_p^s = \sqrt{(p^2/2m^* - \mu)^2 + \Delta^2}, \qquad (4)$$

and Δ is the gap, which may be momentum dependent. The constancy of the laboratory-frame quasiparticle energy requires the superfluid-frame energy to decrease (or increase) as the quasiparticle enters the flow field around a vortex. At the point $E_p^s = |\Delta|$, the quasiparticle is converted to a quasihole, reversing its motion in the superfluid frame and halting its contribution to the thermal current. [12] Fig. 3 sketches the contributions to the energy of a quasiparticle whose trajectory would cause it to pass within ξ of the vortex core. This Andreev-scattering process was first described by Ferrell in a different context [11].

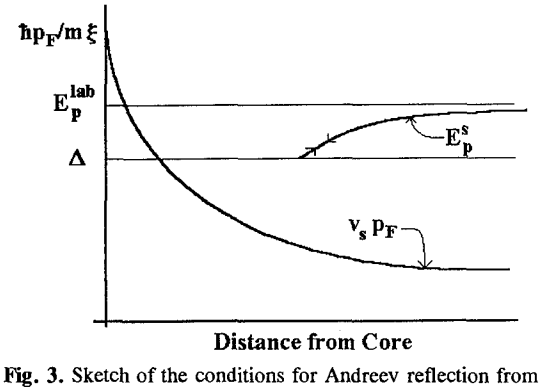

Fig. 3. Sketch of the conditions for Andreev reflection from vortex screening currents. As the quasiparticle approaches the edge of the vortex, its energy in the superfluid frame reaches the gap, at which point it is Andreev reflected back along its incoming trajectory.

Even for YBCO, the least anisotropic of the cuprate superconductors, the coherence length in the c-axis direction is estimated to be smaller than the unit cell dimensions. Under such circumstances, we expect the vortices that form when magnetic fields are applied normal the c-axis to be, to a large extent, coreless. Nonetheless, such fields reduce the thermal conductivity. The same processes to which we attribute quasiparticle scattering for c-axis vortices will occur for vortices in the plane. In this case, however, the screening currents are normal to the field and flow in opposite senses on successive CuO biplanes. Andreev reflection can therefore not occur if the quasiparticle momentum is parallel to the field. This directionality provides a test for the existence of nodal lines in the gap function.

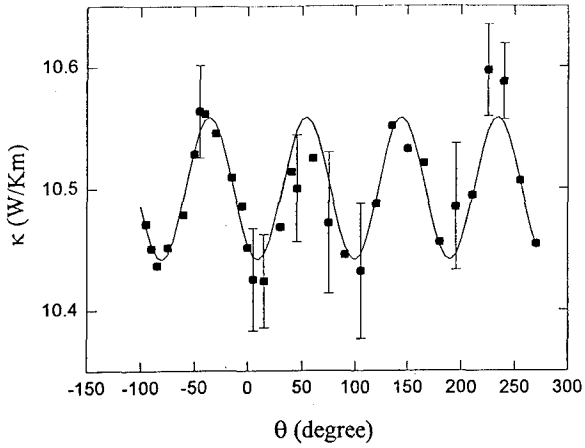

Fig. 4. Thermal conductivity along the a-axis of an untwinned sample of $YBa_2Cu_3O_{7-x}$ at 10 K. A field of 1.5 T is applied perpendicular to the c-axis. The field makes an angle θ relative to the a-axis.

At low temperatures, 10 K here, those quasiparticles that can be thermally excited will have crystal momenta (and, we assume, group velocities) primarily in the directions of the nodes. Fig. 4 shows the thermal conductivity of an untwinned single crystal of $YBa_2Cu_3O_{7-x}$ versus the angle θ of the in-plane applied field. The temperature gradient is applied along the a-axis of the crystal and θ is measured relative to it. The thermal conductivity is quite obviously four-fold; the solid line is a fit to $\sin[4(\theta-\delta)]$, with δ a misalignment angle. Clearly, κ is larger when the field angle is an

odd multiple of 45° than it is when along the principal crystal axes. Such behavior can only occur if there are nodes in the gap, or at least minima « k_B(10 K), in the vicinity of $|k_x| = |k_y|$; when the field is aligned with a nodal direction, those quasiparticles are not Andreev reflected, and the thermal resistance is lower. Elsewhere [12] we have reported the results of a model calculation that treats Andreev reflection and that uses either a $d_{x^2-y^2}$ or an extended s-wave (two node) gap function. Both functions give a qualitative account of the effect. However, the extended s-wave gap requires that the mean-free path in the presence of vortices be less than the mean separation of vortex lines, which seems implausible. The d-wave picture, on the other hand, requires a mean-free path greater than the vortex spacing, and seems to give a better quantitative account of the effect.

In conclusion, we have shown that the increase in thermal conductivity observed in cuprates is to a large extent, perhaps even exclusively, the consequence of a rapid increase in quasiparticle mean free path, completely consistent with observations of the normal-fluid electrical conductivity. We have identified the mechanism by which vortex lines sharply reduce the mean-free path at low fields, and have exploited it to demonstrate clearly the existence of nodes in the superconducting gap. The data, at this juncture, cannot distinguish between a d-wave and an extended s-wave gap function.

ACKNOWLEDGEMENTS

This work was supported in part by National Science Foundation (Grant No. DMR91-20000) through the Science and Technology Center for Superconductivity. We are grateful for the essential input of Professor A.J. Leggett, and to N.N. Kolesnikov, W.C. Lee, and D.M. Ginsberg, who provided excellent samples for this study.

REFERENCES

1. C. Uher, in *Physical Properties of High Temperature Superconductors III*, ed. by D.M. Ginsberg (World Scientific, Singapore, 1992) Ch. 3.
2. R.C. Yu, M.B. Salamon, J.P. Lu, and W.C. Lee, Phys. Rev. Lett. **69**, 1431 (1992); J. Cohn, et al. *ibid.***71**, 1657 (1993); R.C. Yu, et al. *ibid.* **71**, 1658 (1993).
3. J. L. Cohn, (this volume).
4. P.B. Allen, X. Du, L. Mihaly, and L. Forro, Phys. Rev. B **49**, 9073 (1994).
5. S.T. Ting, P. Pernambuco-Wise, and J.E. Crow. Phys. Rev. B **50**, 6375 (1994).
6. D.A. Bonn, P. Dosanjh, R. Liang and W.N. Hardy, Phys. Rev. Lett. **68**, 2390 (1992).
7. K. Zhang, D.A. Bonn, S. Kamal, R. Liang, D.J. Barr, W.N. Hardy, D. Basov, and T. Timusk, Phys. Rev. Lett. **73**, 2484 (1994).
8. W.F. Vinen, E.M. Forgan, C.E. Gough, and M.J. Hood, Physica **55**, 94 (1971).
9. K. Behnia, et al. J. Low Temp. Phys. **84**, 261 (1991).
10. F. Yu, V.N. Kopylov, M.B. Salamon, N.N. Kolesnikov, M.A. Hubbard, and W.C. Lee, (preprint, 1994).
11. R. A. Ferrell, Phys. Rev. Lett. **68**, 2524 (1992).
12. F. Yu, M.B. Salamon, A.J. Leggett, W.C. Lee, and D.M. Ginsberg, (preprint, 1995).

Journal of Superconductivity, Vol. 8, No. 4, 1995

Thermal Conductivity of Zn, Pr and Tb doped YBCO Single Crystals: Theory and Experiment

P. F. Henning[1], G. Cao[2], J. E. Crow[2], W.O. Putikka[2], and P. J. Hirschfeld[3]

The thermal conductivity K(T) vs temperature has been measured for (Y,Pr)$Ba_2Cu_3O_7$, (Y,Tb)$Ba_2Cu_3O_7$ and $YBa_2(Cu,Zn)_3O_7$ single crystals from $10 \le T \le 280$K. For $YBa_2Cu_3O_7$ (YBCO), a strong enhancement in K(T) is observed for $T \le T_c$ with a peak in K(T) at approximately $T \approx T_c/2$ with a sharp change in slope of K(T) at T_c. These results are similar to those reported previously. For the selectively doped YBCO, the peak in K(T) is shifted to lower temperatures and occurs at $T \approx 20$K independent of T_c and the impurity concentration. In addition, the sharp change in slope of K(T) at T_c is not apparent for the doped crystals. These results are discussed along with a theoretical model for electronic conduction including both impurity and inelastic scattering from spin fluctuations.

Key Words: Doping; Thermal Conductivity

Thermal conductivity K(T) is one of the few DC transport properties which provides information on the quasiparticle density and lifetime within both the normal and superconducting states. For this reason, thermal conductivity studies of the high T_c superconductors have been the focus of considerable attention [1,2] and these studies have revealed many interesting features which seem to be common to most of the high T_c cupric based superconductors. In particular, the salient features are (i) a strong sensitivity to composition, (ii) a sharp rise in K(T) below T_c with a peak in the vicinity of $T_c/2$ and (iii) a nearly quadratic temperature dependence of K(T) as T approaches 0.

The second feature, i.e., the large enhancement of K(T) below T_c followed by a peak and drop in K(T) as T approaches 0, has attracted most of the recent attention and is a common feature previously reported for conventional strong coupling superconductors, e.g., lead and lead alloys. Attempts to explain this feature have centered around both electronic and phononic mechanisms [1,2]. In this paper, we present new data from measurements of the of K(T) from $10 \le T \le 280$K for selectively doped $YBa_2Cu_3O_7$ (YBCO) single crystals along with a theoretical discussion of the T- and impurity concentration dependence of K(T) within the superconducting state using a model based on electronic conductivity with both impurity and inelastic scattering from spin fluctuations.

Single crystals of YBCO doped with Pr, Tb or Zn were grown using standard flux growth methods. Characterizations of single crystals are described elsewhere [4]. The thermal conductivity was measured using a standard steady state method.

$Y_{1-x}Pr_xBa_2Cu_3O_7$ (YPBCO) [3], $Y_{1-x}Tb_xBa_2Cu_3O_7$ (YTBCO) [4] and $YBa_2(Cu_{1-x}Zn_x)_3O_7$ (YBCZO) [3] were selected because the impurities interact with the carriers within the CuO_2-planes in different but complementary ways. Zn^{2+} with its filled d-orbitals and spin zero primarily substitutes for the Cu-ions within the CuO_2 planes and causes a precipitous drop in T_c with T_c approaching 0 for $x_{crit} \approx 0.10$. Whereas, Pr^{3+} substitutes for the Y-ions which is located between the CuO_2 planes but, unlike most of the other rare earth ions, hybridizes with the oxygen p-holes depressing T_c to 0 with $x_{crit} \approx 0.55$. However, Tb, which also substitutes for the Y-ions and hybridizes with the carriers in the CuO_2 planes, does not cause a shift in T_c [4].

Shown in Fig. 1 is K(T) normalized to $K(T_c)$ vs. T for an as-grown YBCO and the same crystal after it was given a high pressure oxygen anneal. Both crystals have a sharp normal-superconducting transition in the vicinity of 92K and

[1] Department of Physics, Florida State University, Tallahassee, FL 32306
[2] National High Magnetic Field Laboratory, Florida State University Tallahassee, FL 32306-4005
[3] Physics Department, University of Florida, Gainesville, FL 32611

0896-1107/95/0800-0453$07.50/0

K(T) for both crystals displays a sharp change in slope of K(T) at T_c along with a peak which shifts to lower temperatures and is enhanced with increasing oxygen concentration. This data is typical of previously published results for YBCO and several other high T_c superconductors with the exception that the peak in K(T) is typically larger for the YBCO systems than for other Cu-based high T_c systems [1]. Primarily, two models, one based on phononic conduction with electron and other scattering and the second based on electronic conduction with electron scattering, have been proposed to explain this data and both models can be fit to published data with reasonable parameters. If there is a modest electron-phonon interaction and the primary thermal carriers are phonons then a peak can be explained within the Bardeen, Rickayzen and Tewordt (BRT) theory [1] due to an increase in the phonon mean free path driven by a decrease in electron scattering as the pairs condense into the superconducting ground state. Within this model and as T continues to decrease, K(T) eventually decreases due to the decrease in phonon density along with the dominance of other scattering mechanisms. An alternative model for the electronic thermal conductivity will be presented later in this paper. It is likely that an explanation of the data on both pure and doped samples will require a combination of both theories.

Shown in Fig. 2a is K(T) for $Y_{1-x}Pr_xBa_2Cu_3O_7$ for x=0.15 and x=0.35 vs. T along with K(T) vs. T for $YBa_2(Cu_{1-x}Zn_x)_3O_7$ for x=0.03 in Fig. 2b. Also shown by the arrows in Fig. 2 are T_c for these three samples as determined from both transport and susceptibility measurements. First, it should be noted that the sharp break in the slope of K(T) at T_c is not evident for any of the doped samples shown. This feature is better seen in Fig. 3 where K(T) normalized to K(T_c) vs. T/T_c for YBCO and YPBCO with x=0.15 is shown on an expanded temperature scale. The BRT model, without modification of parameters to account for possible impurity broadening of the superconducting gap, predicts a pronounced change in the slope of K(T) at T_c as T_c is depressed. This prediction is not evident in the data presented here. In addition, the peak in K(T) for all samples shown in Fig. 2 occurs in the vicinity of 20K independent of T_c(x), the type of impurity and the concentration of impurities. The apparent x-independence of the temperature where the peak in K(T) occurs is also inconsistent with predictions from either the BRT theory or the electronic conduction model

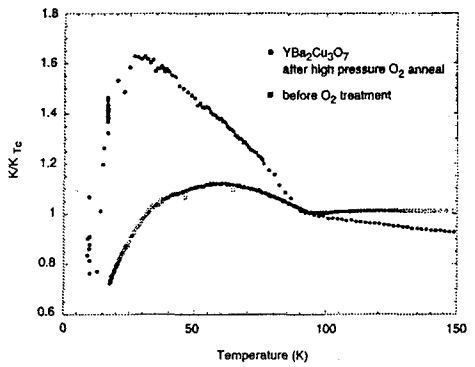

Figure 1 : K (T) normalized to K (Tc) vs. T for on gs-grown crystal (A) and the same crystal O2 annealed.

to be presented,each taken seperately. The K(T) behavior reported here for Zn and Pr doped YBCO is very similar to that reported for the electronic doped high T_c superconductor, $(Nd,Ce)_2CuO_{4-y}$ [5] where the peak in K(T) was attributed to normal K(T) behavior without any evidence of superconductivity on K(T). These features, i.e., the shifting of the peak in K(T) to T≈ 20K and the depression in the change in slope of K(T) at T_c do not occur in YTBCO with x =0.30 and thus these differences driven by Zn and Pr doping reflect dramatic changes in the quasiparticle excitations leading to the features reported for pure YBCO.

Shown in Fig. 4 is K(T) vs. T for YPBCO for x = 0.60 and 1.00. Both of these crystals are non-superconducting and have a very high, semiconducting-like T-dependent resistivity. The important features to be noted are (i) the broad peak in the high temperature portion of K(T) which was not evident in YBCO or the superconducting YPBCO and YBCZO crystals and (ii) the peak in K(T) developing in the vicinity of T ≈ 20K, the same temperature where the peak is seen in the other doped but superconducting YBCO, see Fig. 2. This result coupled with the concentration independence of this peak leads us to believe that

the K(T) behavior shown in Fig. 2 is not due to superconductivity and is not a reflection of the mechanisms leading to the peak reported for pure YBCO.

In view of these striking observations, it is clear that the Pr and Zn doped YBCO indeed differ markedly from the pure YBCO, indicating dramatic changes in the quasiparticle excitations. Thus, without modification of parameters to account for the scattering due to impurities, it would be difficult for any models, such as purely phonon

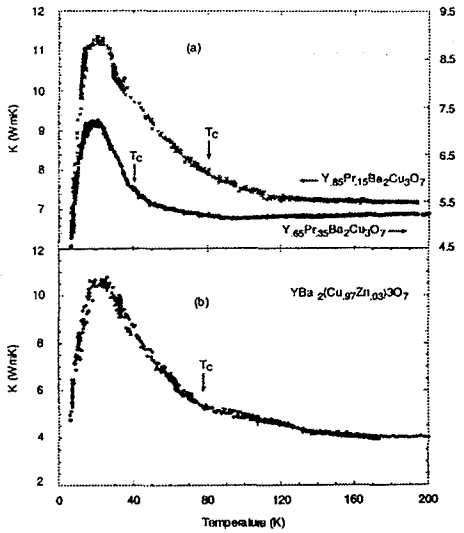

Figure 2: K (T) for (a) PBCO with x=0.15, 0.35 and (b) YBCZ with x=0.03.

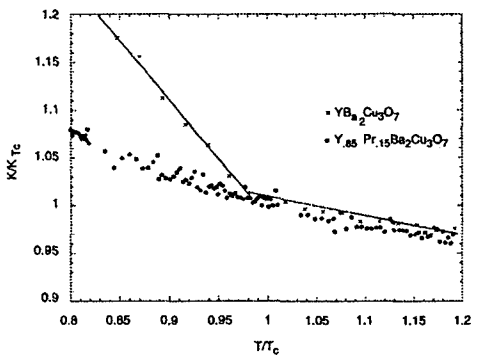

Figure 3: K (T)/K (Tc) for YBCO and YPBCO with x=0.15 near Tc.

or electron models, to predict the behavior shown here. As an attempt to understand thermal conductivity in high T_c systems in general, and the impurity doped YBCO in particular, we present here an alternative model which has been successful in describing many of the features of the electronic conductivity in the superconducting state [6,7]. The discussion is focused on the electronic part of the thermal conductivity.

In this model, we assume the existence of a d_{x2-y2} pair state of the form $\Delta_k = \Delta_o \cos 2\varphi$ over a circular 2D Fermi surface. Quasiparticles excited above this ground state are scattered with total rate $1/\tau = 1/\tau_{imp} + 1/\tau_\varphi$, where $1/\tau_{imp}$ is the relaxation rate due to potential scatterers (impurities), and $1/\tau_\varphi$ describes the rate of scattering by inelastic processes (spin fluctuations). Details are given in Refs. 6, 7.

This model is capable of describing several aspects of recent microwave studies on pure and Zn-doped YBCO single crystals. As an example, we reproduce in Fig. 5 the

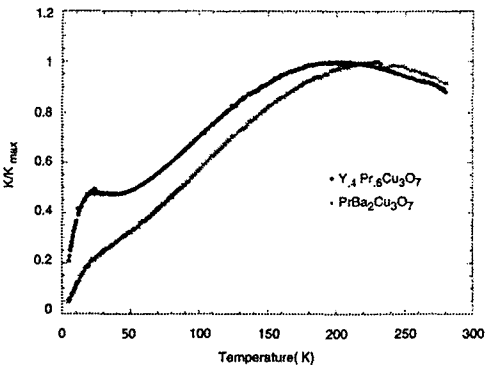

Figure 4: K (T) max vs. T for YPBCO with x=0.6 and 1.

electronic conductivity $\sigma_1(\omega,T)$ calculated within the model [6] compared to the data of Ref. 10 on an untwinned YBCO single crystal. In particular, the height and position of the conductivity peak thought to characterize good samples are well described by the theory. This is true at higher frequencies and impurity concentrations as well, although the low-temperature linear-T variation of the electrical conductivity is not correctly predicted by the theory [6].

It is interesting to compare the predictions of the same model for the electronic thermal conductivity. A similar peak is to be expected for both quantities, since such a peak inevitably results from the competition

between a scattering rate which collapses below T_c but saturates at low temperatures, and a density of charge carriers which decreases (linearly in the d-wave case) with the temperature for $T<<T_c$. Salamon et al. [11] have in fact reported measurements on high purity YBCO crystals exhibiting a scaling of $\sigma_1(T)$ and $K(T)/T$ in the superconducting state similar to the Wiedemann-Franz scaling expected for normal metals, suggesting that the thermal conductivity in such samples is primarily electronic.

We evaluate K_{el} using a Kubo formula for the heat-current response similar to the original treatment for an s-wave superconductor [12]. The generalization to unconventional states has been discussed previously by several groups [8,9,13,14]. In Fig. 6, we plot $K_{el}(T)$ for two values of the normal state impurity scattering rate $1/\tau_{imp,N}$ (the

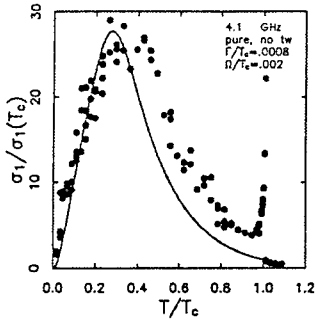

Figure 5: $\sigma/\sigma_1(T_c)$ vs. T/T_c

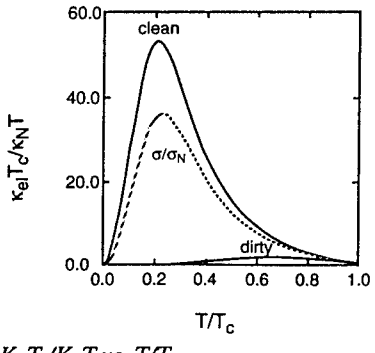

Figure 6: $K_{el}T_c/K_NT$ vs. T/T_c

Hubbard model parameters entering the inelastic rate have been fixed by fits to normal state quantities, and are thus not regarded as adjustable). While the size and position of the peak in the "clean" example ($1/\tau_{imp,N}T_c=0.0016$) is roughly consistent with measurements on nominally pure YBCO crystals, including those reported here, we observe that the effect of increasing the impurity concentration within the theory is to cut off the collapse of the inelastic scattering rate. This leads to a shift in the peak to higher reduced temperatures T/Tc. The model's predictions for clean limit transport properties shown in the figure are sufficient to understand the peak in K(T) in the pure YBCO samples, as well as the observed approximated Wiedemann-Franz scaling of K(T)/T with σ (T) [11].Since the high temperature peak in $K_{el}(T)$ predicted in the "dirty" case is not observed, however, it appears that $K_{ph}(T)$ dominates K_{el} in the doped samples over the entire temperature range. The 20K peak in the non-superconducting YPBCO samples further suggests that this behavior of $K_{ph}(T)$ is only weakly influenced by pair correlations.

References

[1] C. Uher, in *Physical Properties of High Temperature Superonductors.*, D. M. Ginsberg, Ed. (World Scientific, Singapore, 1992), Vol. 3, p. 159 and reference within.
[3] J.T. Market, et al., in Physical Properties of High Temperature Superconductors, D.M. Ginsberg, Ed., (World Scientific, Singpore, New Jersey, London, Hong Kong), Vol. 1
[2] R. C. Yu, et. al., Phys. Rev. Lett. **69**, 1431 (1992).
[4] G. Cao, et. al., J. Appl. Phys. **75**, 6329 (1994) and G. Cao, et. al., (preprint)
[5] J. L. Cohn, et. al., Phys. Rev. **B46**, 12053 (1992)
[6]P.J. Hirschfeld, W.O. Putikka, and D. Scalapino, Phy. Rev. Lett. 71, 3705 (1993); P.J. Hirschfeld, W. O. Putikka, and D. Scalapino, Phys. Rev. B 50, 10250 994); also see E.W. Statt and A. Griffin, Phys. Rev. B **48**, 619 (1993).
[7] S.M. Quinlan et al., Phys. Rev. B **49**, 1470 (1994).
[8] P.J. Hirschfeld et al., Sol. St. Commun. **59**, 111 (1986).
[9] S. Schmitt-Rink et al., Phys. Rev. Lett. **57**, 2575 (1986).
[10] K. Zhang et al., Phys. Rev. Lett. **73**, 2484 (1994).
[11] M. Salamon et al, this conference.
[12]V. Ambegaokar and A. Griffin, Phys. Rev. **137**, A1151 (1965).
[13] B. Arfi et al., Phys. Rev. B **38**, 8959 (1989).
[14] H. Monien et al., Sol. St. Commun. **61**, 581

Journal of Superconductivity, Vol. 8, No. 4, 1995

Anomalous Phonon Damping in Insulating Cuprates

Joshua L. Cohn[1]

Received 31 January, 1995

Measurements of the in-plane (κ_{ab}) and out-of-plane (κ_c) thermal conductivity for insulating cuprate crystals are discussed along with new measurements for $YBa_2Cu_3O_6$ and $PrBa_2Cu_3O_6$, where both κ_{ab} and κ_c are twice the magnitude previously reported for this material. An unusual temperature (T) dependence of κ_{ab} in cuprates with apical oxygen indicates the onset of strong phonon damping for T < 200-250K. Along with dielectric and elastic anomalies reported in this regime, the data suggest the occurrence of a structural phase transition, involving rotations of the CuO polyhedra about an in-plane axis. The role of such local distortions in the thermal transport of superconducting compounds and the superconducting-state enhancement of κ_{ab} are discussed.

KEY WORDS: Cuprates; heat conductivity; phonon scattering; apical oxygen; structural phase transition.

1. INTRODUCTION

Experimental efforts over the past several years have revealed systematic behaviors of the in-plane transport coefficients in the cuprates as functions of temperature and doping. The experimental record for in-plane thermal conductivity, κ_{ab} [1], is considerably less complete. Even in superconducting $YBa_2Cu_3O_{6+x}$, by far the most widely studied material, the temperature dependence of κ_{ab} in the normal state of high-quality crystals shows substantial variability and doping-dependent studies are rare. The enhancement of κ_{ab} in the superconducting state has attracted considerable attention [2-6] for what it may imply about the quasiparticle spectrum, but the absence of any direct means by which to separate electron and phonon contributions to the heat flow makes interpretations of this phenomenon inconclusive.

Measurements of κ_{ab} in insulating cuprates [6,7] should help to place limits on the phonon contribution and phonon scattering mechanisms relevant to superconducting compositions. Here we present measurements of insulating $YBa_2Cu_3O_{6+x}$ (YBCO6+x) and $PrBa_2Cu_3O_{6+x}$ (PBCO6+x) crystals which demonstrate an anomalous decrease in the in-plane thermal conductivity for temperatures below 200K. Comparison of the present results with previous data on other materials suggests that the anomalous behavior is generic to insulating cuprates with apical oxygen, and is associated with local structural distortions of the CuO polyhedra. Light oxygen doping in YBCO (x<0.1) reveals a sensitivity of the phonon damping to basal-plane charge, and provides new insight into the behavior of κ_{ab} in superconducting compounds.

2. EXPERIMENTAL

The crystals were grown by a self-decanting CuO flux method [8] and subsequently annealed in flowing argon or dynamic vacuum at 650C for several days, followed by quenching to room temperature. X-ray diffraction analysis of a YBCO crystal indicated a c-axis lattice constant c=11.8364Å. From a comparison with studies of c vs oxygen content in polycrystals [9,10] we estimate x=0.05. κ_{ab} was measured using a steady-state technique, employing a small heater and 25μm differential chromel-constantan thermocouple. For the out-of-plane measurement (κ_c) the specimen was epoxied between two sapphire chips with a corner exposed, and thermocouple junctions glued to the exposed crystal faces. This technique is similar to that used by Hagen *et al.* [7]. In some cases silver strips were vapor-deposited on the crystal and electrical resistivity and thermopower measured simultaneously with κ_{ab}.

[1] Physics Department, University of Miami, Coral Gables, FL 33124

0896-1107/95/0800-0457$07.50/0

3. DATA AND DISCUSSION

3.1. Survey of κ_{ab} in Insulating Cuprates

Shown in Fig. 1 are κ_{ab} (T) data for YBCO6, PBCO6, Nd_2CuO_4[11] (NCO), La_2CuO_4[12] (LCO), and PBCO7 [13]. NCO exhibits classical dielectric behavior, with a sharp peak at low T and nearly 1/T dependence at high T, both characteristic of phonon-phonon relaxation. Qualitatively similar results have been reported

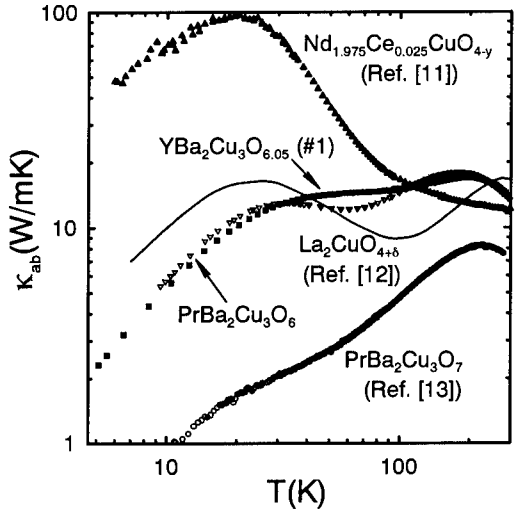

Fig. 1. In-plane thermal conductivity for various cuprate crystals.

for isostructural Pr_2CuO_4 [14]. No anomaly is observed near the expected Néel temperature for this compound (T_N ~260-280K), indicating that at these temperatures the antiferromagnetic ordering has no substantial effect on the heat flow [6].

YBCO6, PBCO6, and LCO have κ_{ab} comparable in magnitude to NCO near room temperature, but at low-T have values an order of magnitude smaller. The temperature dependence is anomalous, with two maxima (at low and high T) and a minimum at 80-100K. PBCO7 shows similar features but κ_{ab} is further suppressed, particularly at low T where the maximum is replaced by a shoulder near 20K. We conclude that an additional phonon damping mechanism operates below T~200-240K in these materials. These new results for YBCO6 and PBCO6, which have T_N~415K [15] and 325K [16], respectively, indicate that the unusual κ_{ab} behavior is unrelated to the onset of antiferromagnetic order. Interestingly, the out-of-plane thermal conductivity (Fig. 2) shows no such anomaly, suggesting that the additional scattering is weaker or absent for c-axis-propagating phonons.

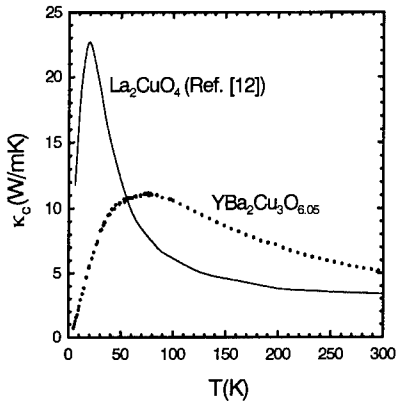

Fig. 2. Out-of-plane thermal conductivity for LCO and YBCO.

It is tempting to correlate this κ_{ab}(T) anomaly with the known structural difference between these materials and those of T′ structure (NCO and PCO). We hypothesize that the damping anomaly is associated with vibrations involving apical oxygen, a point we return to below.

3.2. Oxygen Doping and Hysteresis in YBCO

Further insight into the nature of the damping anomaly is provided by measurements of YBCO crystals which reveal κ_{ab}(T) to be very sensitive to oxygen content and hysteretic. Shown in Fig. 3 are data for three crystals with slightly different oxygen content; the damping is diminished with increasing x, especially at low T where a sharp peak develops. Crystal #1 in the as-prepared state (also shown in Fig. 1) is assigned an oxygen content of 6.05. This sample and a second crystal (#2) were subsequently annealed at 300°C in air for 4H

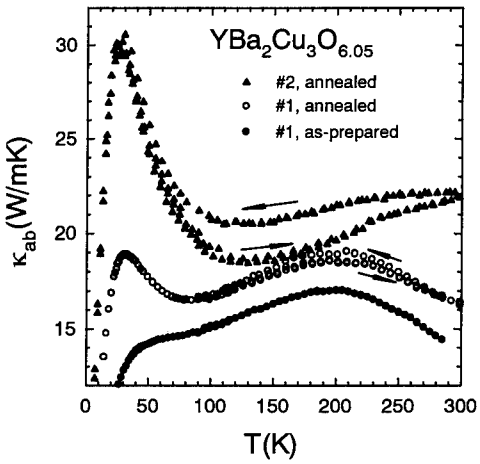

Fig. 3 κ_{ab}(T) for two YBCO crystals showing oxygen sensitivity and hysteresis.

to attach electrical leads for measurements of resistivity and thermopower. These data (Fig. 4) indicate that crystal #2 has a higher oxygen content than crystal #1. Comparison with the thermopower data of Obertelli *et al.* on polycrystals [17] (Fig. 4, lower panel) implies that both of these crystals have x<0.13. The thermal conductivity data suggest that following the anneal, crystal #1 had slightly more oxygen than in the as-prepared state.

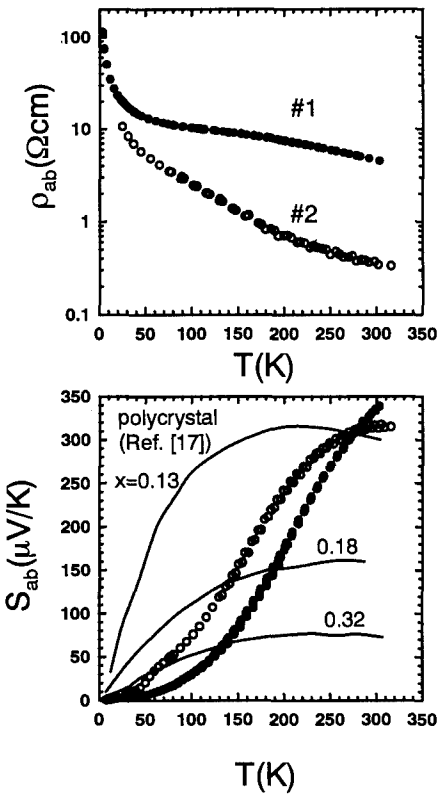

Fig.4 In-plane electrical resistivity and thermopower for the two annealed YBCO crystals.

3.3 Structural Phase Transition

We believe that the anomalous $\kappa_{ab}(T)$ data are best understood as the manifestation of a displacive phase transition (DPT) with onset at T≤ 250K. This hypothesis is supported by studies of the dielectric constant [18] and elastic properties [19] which indicate anomalies for YBCO6 in this temperature range, consistent with a DPT of first order. Similar anomalies have been widely reported near 200K for many superconducting cuprates [20], suggesting that the κ_{ab} behavior is the signature of a more general phenomenon in these materials.

A DPT is also suggested by the striking similarity between the κ_{ab} anomaly observed here and that observed in the thermal conductivity of $SrTiO_3$ at temperatures near its cubic-tetragonal transition at 106K [21]. There the phase transition is a classic soft-mode phenomenon, characterized by rotations of the TiO_6 octahedra about a cube axis.

Rotations of the CuO_6 octahedra about an in-plane axis are associated with the well-known HTT-LTO phase transition in LCO near 500K. There are indications that an instability against further tilts persists in the LTO phase [22]. For YBCO, anomalies in the local structure associated with apical oxygen have been extensively discussed [23], and only quite recently an instability against in-plane tilts of the CuO_5 pyramid has been identified in the average structure [24].

An emerging picture for the various anomalies is that a local structural transition involving in-plane tilts of the CuO polyhedra occurs in domains smaller than 100Å in extent. Presumably the coupling between these distortions and the elastic strain gives rise to temperature dependent acoustic mode velocities and enhanced damping as reflected in the κ_{ab} and elastic anomalies. This interpretation is consistent with the nonobservance of such anomalies in NCO (without apical oxygen) in spite of observations of a soft mode involving rotation of the CuO_4 squares about the c-axis [25].

The coexistence of distorted and undistorted regions within the crystals implies the presence of domain walls. The hysteresis (Fig. 3) may be associated with displacement of these phase interfaces, possibly driven by the motion of oxygen atoms [19] and their local ordering in the basal planes.

3.4 The Superconducting-State Enhancement of κ_{ab}

Our new results for insulating specimens have a direct bearing on interpretations of the normal-state κ_{ab} in superconducting compounds and its enhancement in the superconducting state [13,26]. It has been argued [6,27] that a phononic origin of the superconducting-state enhancement is incompatible with the observation that κ_{ab} in the superconductor exceeds that of the insulator. This argument presumes that the lattice heat conductivity (κ_L) in the insulator and superconductor differ only by the additional phonon-electron scattering in the latter. This argument must be reexamined in light of the anomalous phonon damping reported here for the insulators and its likely importance in superconductors as well. In particu-

lar, the data in Fig. 3 suggest that this damping is weaker in YBCO7. Thus in the absence of phonon-electron scattering, we expect κ_L to be larger in YBCO7 than in YBCO6.

Furthermore, there is clear evidence that the CuO tilts are coupled to the superconductivity [24,28]. An abrupt reduction in tilt amplitude for $T<T_c$ is indicated [24]. According to our proposition that the tilt distortions give rise to substantial phonon damping, their "relaxation" in the superconducting state should enhance κ_L.

Interpretations of the enhancement in the cuprates must address the experimental results summarized in Fig. 5: 1) the maximum in κ_{ab} for fully oxygenated YBCO is substantially larger than in other cuprates, and 2) the enhancement is highly sensitive to chain oxygen for nominally "90K" YBCO. The YBCO compounds are a special case among cuprates because superconductivity can extend to the chain layers via the proximity effect when they are free of disorder [29,30]. Because chain-layer charge couples to the structural anomaly (Fig. 3), it is possible that the relaxation of local distortions occurs exclusively or is enhanced in the superconducting, ordered chain regions. This scenario suggests a contributing role of the local structure in the oxygen dependence of the enhancement.

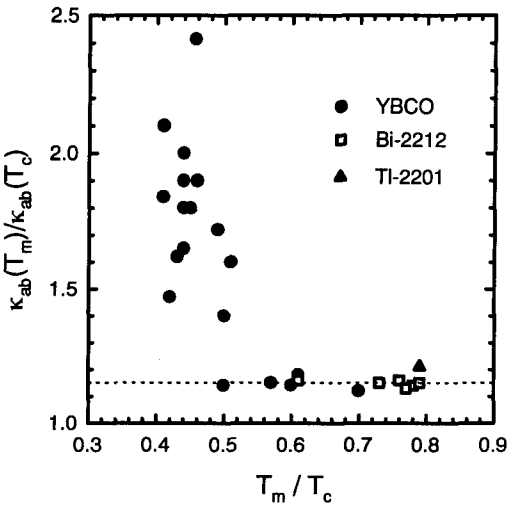

Fig. 5 Maximum values of κ_{ab} (at T_m), normalized to values at T_c, vs normalized temperature for superconducting cuprate crystals from the literature. All YBCO are nominally 90K superconductors. The dashed line represents a relative enhancement of 1.15.

ACKNOWLEDGMENTS

The author is grateful for the efforts of T. A. Vanderah and C. K. Lowe-Ma in the growth and structural characterization of YBCO and PBCO crystals. Thanks also to P. Henning for providing data on PBCO7 prior to publication, and to D. Litvinov for experimental assistance.

REFERENCES

1. For a recent review, see C. Uher in, *Physical Properties of High Temperature Superconductors*, edited by D, M, Ginsberg (World Scientific, Singapore, 1993), Vol. III.
2. J. L. Cohn *et al.*, Phys. Rev. Lett. **71**, 1657 (1993); R. C. Yu, M. B. Salamon, and J. P. Lu, *ibid.*, 1658.
3. A. S. Alexandrov and N. F. Mott, Phys. Rev. Lett. **71**, 1658 (1993).
4. B. W. Statt and A. Griffin, Phys. Rev. B **48**, 619 (1993).
5. C. Uher, Y. Liu, and J. F. Whitaker, J. Supercond. **7**, 323 (1994).
6. P. B. Allen *et al.*, Phys. Rev. B **49**, 9073 (1994).
7. S. J. Hagen, Z. Z. Wang and N.-P. Ong, Phys. Rev. B **40**, 9389 (1989).
8. T. A. Vanderah *et al.* J. Crystal Growth **118**, 385 (1992).
9. M. S. Osofsky *et al.*, Phys. Rev. B **45**, 4916 (1992).
10. M. E. Parks *et al.*, J. Solid St. Chem. **79**, 53 (1989).
11. J. L. Cohn *et al.*, Phys. Rev. B **46**, 12053 (1992).
12. Y. Nakamura *et al.*, Physica **C185-189**, 1409 (1991); the thermal conductivity of this compound was first reported by D. T. Morelli *et al.*, Phys. Rev. B **39**, 804 (1989).
13. P. Henning *et al.*, preceeding paper this volume.
14. A. V. Inyushkin *et al.*, Physica **194-196B**, 479 (1994).
15. J. Rossat-Mignod *et al.*, Physica **169B**, 58 (1991).
16. I. Felner *et al.*, Phys. Rev. B **40**, 6739 (1989).
17. S. D. Obertelli J. R. Cooper, and J. L. Tallon, Phys. Rev. B **46**, 14928 (1992).
18. L. R. Testardi *et al.*, Phys. Rev. B **37**, 2324 (1988).
19. G. Cannelli, R. Cantelli, and F. Cordero, Phys. Rev. B **38**, 7200 (1988); S. De Brion *et al.*, Europhys. Lett. **12**, 281 (1990).
20. Z. Zhao *et al.*, Phys. Rev. B **39**, 721 (1989); Y.-N. Wang *et al.*, Phase Transitions **22**, 9 (1990); H. You, U. Welp, and Y. Fang, Physica **C185-189**, 875 (1991); M. Kund and K. Andres, Physica **C205**, 32 (1993); W. Ting *et al.*, Phys. Rev. B **47**, 12197 (1993); Y. N. Huang *et al.*, Phys. Rev. B **49**, 1320 (1994); T. Fukami *et al.*, Physica **C241**, 336 (1995); J. Sugiyama K. Isawa, and H. Yamauchi, Physica **C242**, 63 (1995).
21. E. F. Steigmeier, Phys. Rev. **168**, 523 (1968).
22. T. R. Thurston *et al.*, Phys. Rev. B **39**, 4327 (1989); M. Braden *et al.*, Z. Phys. B **94**, 29 (1994).
23. B. H. Toby et al., Phys. Rev. Lett. **64**, 2414 (1990); J. Mustre de Leon et al., *ibid.* **65** 1675; M. Arai et al., *ibid.*, **69**, 359 (1992)
24. P. Schweiss *et al.*, Phys. Rev. B **49**, 1387 (1994).
25. N. Pyka *et al.*, Europhys. Lett. **18**, 711 (1992).
26. M. B. Salamon, F. Yu, and V. N. Kopylov, this volume.
27. R. C. Yu *et al.*, Phys. Rev. Lett. **69**, 1431 (1992).
28. C. Meingast *et al.*, Phys. Rev. Lett. **67**, 1634 (1991); M. Barden *et al.*, Phys. Rev. B **47**, 12288 (1993).
29. V. Z. Kresin and S. A. Wolf, Phys. Rev. B **46**, 6458 (1992).
30. J. L. Tallon et al., Phys. Rev. Lett. **74**, 1008 (1995).

Journal of Superconductivity, Vol. 8, No. 4, 1995

Magnetic-Field-Induced Non-Linear Effects of Josephson Coupled Superconductor $Bi_2Sr_2CaCu_2O_{8+\delta}$

Kazuo Kadowaki, Takashi Mochiku, Hiroyuki Takeya and Kazuto Hirata

received 4 January 1995

The dc current-voltage (I-V) relation along the c-axis of single crystalline $Bi_2Sr_2CaCu_2O_{8+\delta}$ has been measured in magnetic fields parallel and perpendicular to the c-axis. In zero field a clear and sharp jump with large hysteresis in the I-V curve was observed, indicative of the dc-Josephson effect. In magnetic field below a characteristic field $B^* \approx 0.4$ T (at T=0 K) parallel to the c-axis the magnetic field suppresses the hysteresis and reduces the critical current I_c drastically, whereas above B^* the I-V curve becomes broad and featureless behavior. The characteristic field scale B^* can be interpreted as an energy scale of the Josephson coupling between superconducting layers in $Bi_2Sr_2CaCu_2O_{8+\delta}$ and is argued with emphasis on the correlation length of pancake vortices in this system.

KEY WORDS: Josephson coupling, layered superconductor, inter-layer coupling

1. INTRODUCTION

There has been a growing interest in the nature of the layered superconductivity with extremely weak coupling between the layers, where the superconducting order parameter is expected to be confined within the layers. This situation results in the modulated order parameter perpendicular to the layers and leads to a highly inhomogeneous superconducting state. In previous studies high T_c superconductors such as $Bi_2Sr_2CaCu_2O_{8+\delta}$ have been considered as a excellent candidate to investigate two dimensionality and the nature of coupling between layers.

The purpose of this paper is to present recent results of our study on the nature of coupling between superconducting layers in high quality single crystalline $Bi_2Sr_2CaCu_2O_{8+\delta}$ by measuring the current-voltage (I-V) relation in magnetic fields both parallel and perpendicular to the superconducting layers. The results show that the I-V curves are highly non-linear with large hysteresis, which was previously interpreted as evidence of the dc-Josephson effect[1,2]. The main characteristic features of the I-V curves observed for the field perpendicular to the layers are similar to that of field parallel to the layers. However, the characteristic field scale B^* is several times larger in the latter case, indicating a higher energy scale for the field parallel to the layer orientation. The magnetic field dependence of the critical current density along the c-axis, J_c^c, decreases exponentially, confirming the Josephson type of coupling between the layers. Because of this fact, J_c^c at high fields diminishes so rapidly with increasing magnetic field that the critical current density along the ab-plane, J_c^{ab}, cannot be supported by J_c^c. This strongly suggests that validity of the brick-wall model[3] for the explanation of high J_c^{ab} in polycrystal materials is clearly disproved and the other model such as the rail-way switch model[4] may be more appropriate.

2. I-V CHARACTERISTICS ALONG c-AXIS IN MAGNETIC FIELDS

The I-V characteristics along the c-axis have been measured at various temperatures between 100 K and 4.2 K in both cases where the magnetic fields are applied parallel to and perpendicular to the superconducting CuO_2 plane. The typical example of the temperature dependence of the I-V curves in zero field is presented in Fig. 1 from just below T_c down to 4.2 K. As the temperature decreases the jump in the voltage with sharp peak which occurs with increasing current at $J_{c\,up}^c$ shifts rapidly toward higher currents. When the

National Research Institute for Metals, 1-2-1, Sengen, Tsukuba, Ibaraki 305, Japan

0896-1107/95/0800-0461$07.50/0

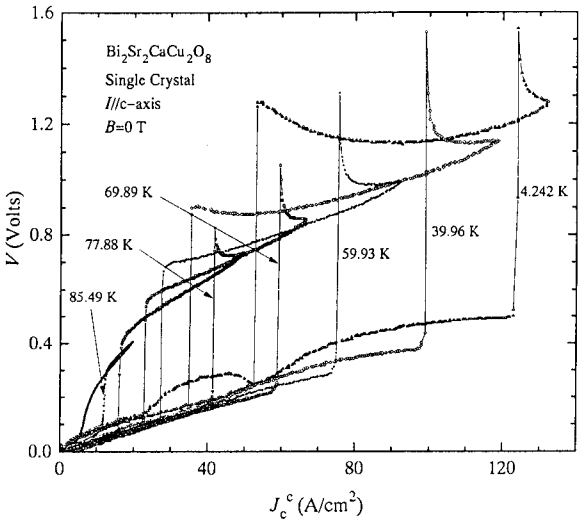

Fig. 1. The zero-field I–V characteristics of the c-axis in single crystalline $Bi_2Sr_2CaCu_2O_{8+\delta}$ at various temperatures.

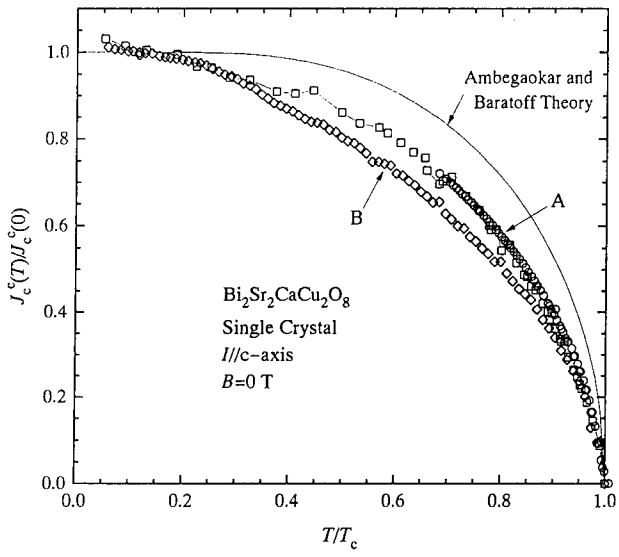

Fig. 2. The normalized J_c^c of single crystalline $Bi_2Sr_2CaCu_2O_{8+\delta}$ in zero field for two samples A and B (see text).

current is reversed at $J>J_{c\,up}^c$ the voltage does not come back the same trace to zero at $J_{c\,up}^c$, but keeps a high level down to a current level close to about 38 % of $J_{c\,up}^c$, which is independent of temperature. At low temperatures below about 50 K, the voltage has a tendency to further increase as J is decreased. This phenomenon is also found to become more pronounced in the measurement in magnetic fields. The dynamic resistance, $r=\partial V/\partial I$, therefore, becomes highly non-linear with respect to the current level and shows even negative at reversed current region below about 50 K. It is noted that the constant bias slope in the I–V curves seen in Fig. 1 and also in all other figures shown below is due to the contact resistance. As is also clearly seen in Fig. 1 the resistivity at a constant temperature above $J_{c\,up}^c$ is also non-linear: it becomes considerably smaller at the higher current level. As a consequence, this non-linear effect of the resistivity has carefully to be taken into account to analyze the resistivity data.

The normalized critical current, $J_{c\,up}^c$, is plotted in Fig. 2 for two independent samples (A and B) as a function of temperature and compared with the conventional theory of Ambegaokar and Baratoff for the Josephson junction with the assumption of $\Delta_1 \gg \Delta_2$. The agreement is not so excellent, probably because the normal state resistivity has both strong temperature and current dependence. It is noted that the sample A seems to be slightly in the over-doped region, while the sample B is approximately at the optimum doped region.

In magnetic fields perpendicular to the superconducting CuO_2 plane, the I–V curves change the character drastically. The change mostly occurs below a characteristic field B^*, where the jump with sharp spike in the I–V curve in zero field rapidly shifts toward lower currents in magnetic fields without losing sharpness of the transition. The example at 78.88 K is shown in Fig. 3. On the contrary to the shift of $J_{c\,up}^c$, the transition of the I–V curve at $J_{c\,down}^c$ (while J is decreasing) does not shift but shows a slight tail (broadening) at the foot of the transition. Therefore, the

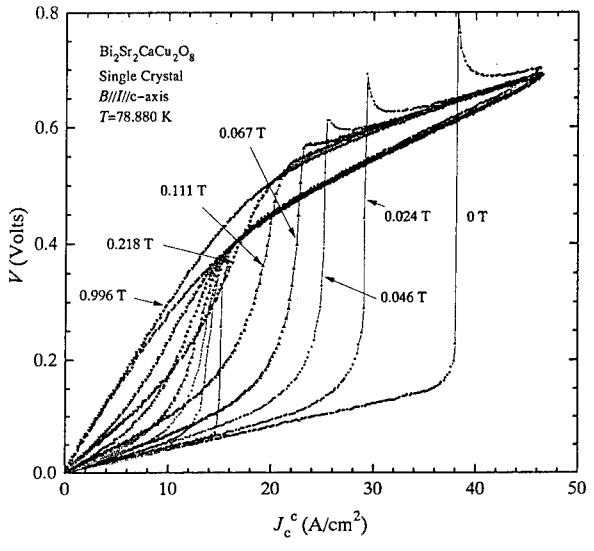

Fig. 3. The I–V characteristics along the c-axis in single crystalline $Bi_2Sr_2CaCu_2O_{8+\delta}$ at 78.88 K at various magnetic fields.

hysteresis in the $I-V$ curve tends to close as the field is increased to B^*. It is noted, however, that the hysteresis with respect to the current does not close completely even at very high fields, probably because the large capacitive coupling in the junction. Above B^* the transition becomes just smeared and the $I-V$ curve asymptotically approaches the normal state $I-V$ curve. In Fig. 3 the resistance, $R=(\partial V/\partial I)_{I\to 0}$, is confirmed to be zero below the irreversibility field of B_{irr}=0.005 T, and it gradually increases as the field is increased. It appears that there is no discontinuity of the resistance R at B^* within the experimental accuracy. This fact as well as no anomaly observed in magnetization curve at B^* indicates that the transition is not sharp phase transition, rather it may be related to some kind of crossover, such as the one from correlated vortex liquid state to uncorrelated vortex liquid state.

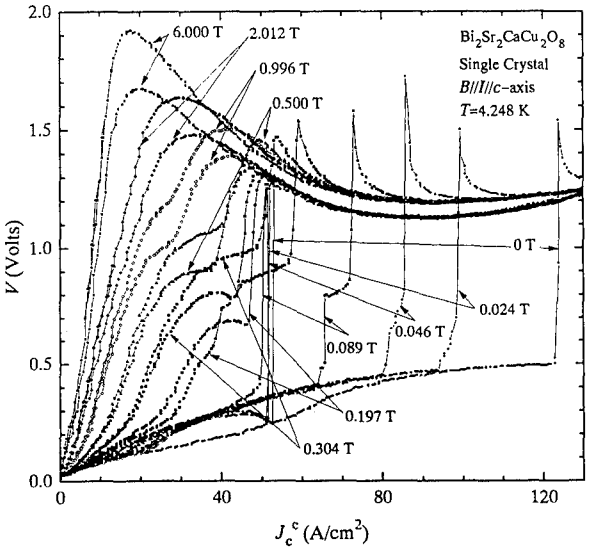

Fig. 4. The $I-V$ characteristics of the c-axis in single crystalline $Bi_2Sr_2CaCu_2O_{8+\delta}$ at 4. 248 K at various magnetic fields.

When the temperature is lowered below about 50 K, the $I-V$ curves begin to show additional features well above B^*. In this region the $I-V$ curve does not have a significant hysteresis but exhibits a broad peak at low current region. This behavior is shown in Fig. 4. Here, the set of $I-V$ curves at various magnetic fields was obtained at 4.248 K. This anomalous peak in the $I-V$ curve can not be interpreted by a conventional Josephson junction model and a new theoretical explanation has to be developed to account for the behavior. At higher current above the peak the dynamic resistance, r, has a significant negative value, which was pointed out above in the case of the zero field $I-V$

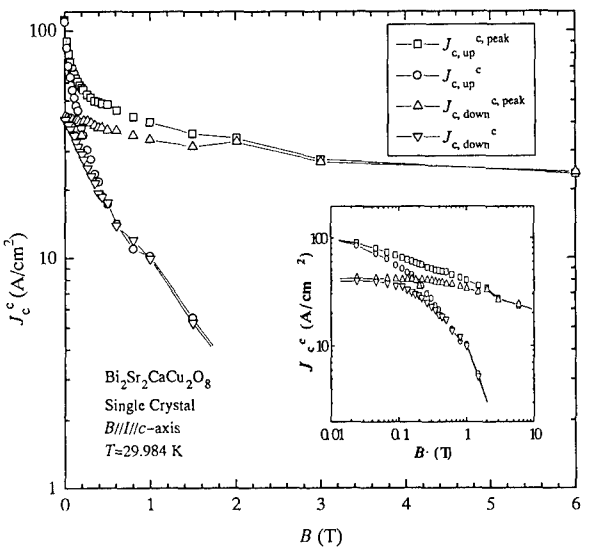

Fig. 5. The c-axis critical current densities of single crystalline $Bi_2Sr_2CaCu_2O_{8+\delta}$ at 29.984 K. The superscript "peak" means the value at the peak of J_c^c.

curves.

Another feature especially seen at low temperatures is the broad foot in the middle range of the field above B^* but below a few Tesla. This behavior is not well reproducible and often consists of several sharp steps similar to the one observed in the low field region. At 4.25 K, B^* is located at about 0.4 T, which is relatively a low filed scale. This is interpreted as the field where the Josephson coupling between adjacent vortex pancakes begins to be destroyed in such a way that the well correlated vortex pancakes perpendicular to the plane are gradually decomposed by magnetic fields and the long range correlations between pancakes can no longer be maintained above B^*. This decoupling precess of adjacent pancakes gradually progresses as the field is increased and results in the weakening of J_c^c at higher fields drastically. This dramatic reduction of J_c^c is presented in Fig. 5. The critical currents $J_{c\,up}^{c}$ and $J_{c\,down}^{c}$ seem to obey exponentially with B. Therefore, at high fields, the supercurrent along the c-axis becomes negligible. This fact clearly disproves the brick-wall model proposed previously by Bulaevskii *et al.*[3] for the explanation of the high critical current density in the melt-textured polycrystalline materials such as practical wires and tapes of this compound. Instead, it seems that the rail-way switch model proposed by Hensel *et al.*[4] seems to be more appropriate in such a compound. Furthermore, the destruction of the Josephson coupling at high fields effectively enhances the two dimensionality, which may enhance further the

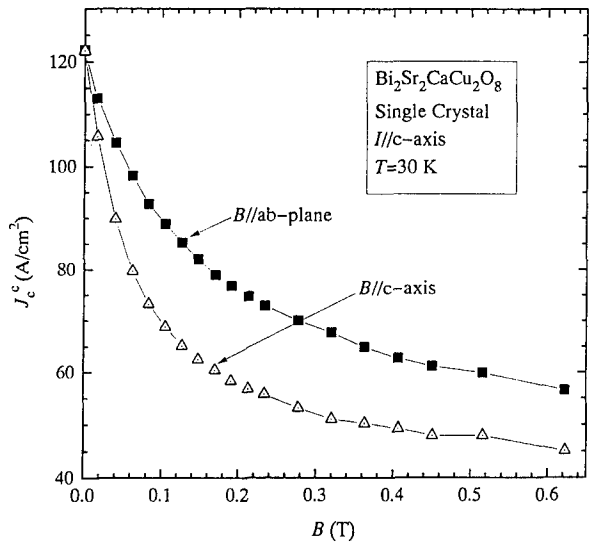

Fig. 6. The anisotropy of J_c^c in single crystalline $Bi_2Sr_2CaCu_2O_{8+\delta}$ with respect to the field parallel and perpendicular directions at 30 K.

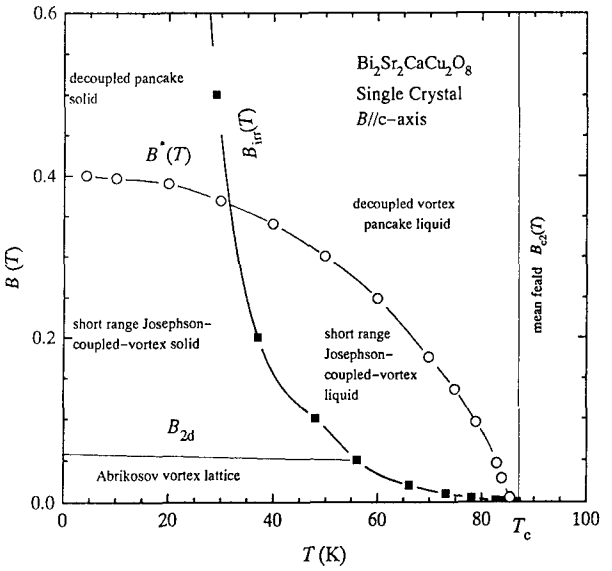

Fig. 7. The phase diagram of the vortex state in single crystalline $Bi_2Sr_2CaCu_2O_{8+\delta}$.

superconducting fluctuation effect even at very low temperatures. This deserves further study of this system at the high field region.

When the magnetic field is applied parallel to the superconducting plane, the main features observed perpendicular to the plane are unchanged, except that the field scale B^* is several times higher for the parallel fields. This is simply caused by the several times higher J_c^c in this field configuration. Although it is expected that for the two cases the vortex state may be entirely different, it is rather surprising that the effect of magnetic field on J_c^c does change only several times: J_c^c is several times higher for the parallel than for the perpendicular configuration. In Fig. 6 an example of the anisotropic field effect of J_c^c is shown at 30 K. Moreover, this is in fact consistent with the relatively small anisotropy of the J_c^{ab} observed in polycrystalline samples with respect to the field direction.

3. THE PHASE DIAGRAM

The phase diagram in the mixed state of $Bi_2Sr_2CaCu_2O_{8+\delta}$ is shown in Fig. 7, where the characteristic field scale $B^*(T)$ is added. Since $B^*(T)$ represents the measure of the Josephson coupling strength between adjacent pancake vortices, the phase regions can be interpreted as described in Fig. 7. In the case of $Bi_2Sr_2CaCu_2O_{8+\delta}$ the irreversibility line represents the superconducting phase transition, which corresponds to the flux-line lattice melting line at low fields and also discriminates the phase from truly superconducting state to normal fluctuation regime. The most important finding in Fig. 7 is the field scale $B^*(T)$, which extends over $B_{irr}(T)$ at high temperature region. Since a sharp feature is observed below $B^*(T)$, a region surrounded by $B_{irr}(T)$ and $B^*(T)$ is interpreted as a short range coupled vortex liquid state. In the high field ($B>B^*(T)$, $B_{irr}(T)$) and high temperature region, the short range correlation is gradually destroyed as temperature and magnetic field are increased. It is noted that this phase is continuously connected the the normal state without phase transition. In the region below $B_{irr}(T)$ and $B^*(T)$ at low temperatures the vortex pancakes are rigid with only slight distortion of the equilibrium configurations: at the lowest field region below B_{2d} existence of the hexagonal vortex lattice is well confirmed by neutron diffraction experiments[5]. In the region between B_{2d} and $B^*(T)$, the vortex lattice is destroyed due to two dimensional collective pinning. It is noted, however, that the strong Josephson coupling between layers still exists. At higher field region above $B^*(T)$ the Josephson coupling is gradually destroyed, resulting in the fatal decrease in J_c^c.

REFERENCES

1. K. Kadowaki and T. Mochiku, Physica B194-196, 2239 (1994).
2. K. Kadowaki, T. Mochiku, H. Takeya, K. Hirata and Y. Saito, Physica C235-240 3275 (1994).
3. L. N. Bulaevskii, J. R. Clem, L. I. Glazman and A. P. Malozemoff, Phys. Rev. B45, 2545 (1992).
4. B. Hensel, J. -C. Grivel, A. Jeremie, A. Perin, A. Pollini and R. Flükiger, Physica C205, 329 (1993).
5. R. Cubitt *et al.*, Nature 365, 407 (1993).

Journal of Superconductivity, Vol. 8, No. 4, 1995

The Penetration Depth of $HgBa_2CuO_{4+\delta}$ with $0.07 \leq \delta \leq 0.35$

Y. Y. Xue[1], Q. Xiong[1,2], Y. Cao[1] and C. W. Chu[1]

The magnetic penetration depth $\lambda(T)$ of three $HgBa_2CuO_{4+\delta}$ samples with $0.16 \leq \delta \leq 0.27$ has been determined from the reversible magnetization. The obtained λ follows a BCS-like correlation of $1/\lambda^2 \propto 1-(T/T_c)^2$ over whole measured temperature range in an underdoped sample with $T_c \sim 90$ K, but deviates significantly from similar fits in an overdoped sample with the same T_c and an optimum doped sample, whose $1/\lambda^2$'s depends on T nearly linearly below $T_c/2$. This asymmetry between the underdoped and overdoped samples suggests that the T-dependence of $1/\lambda^2$ is affected by doping in a complicated way.

KEY WORDS: penetration depth, doping.

The published data on the temperature (T) dependence of $n_s \propto 1/\lambda^2$ below $T_c/2$, which has been taken as a probe for the nodes on the superconducting gap and pairing state, is far from convergent at this stage. The disagreement has been variously attributed to the impurity scattering [1] and sample homogeneity [2]. In addition, μSR data [3] suggest that the T-dependence is also strongly affected by doping, although this interpretation has been challenged on the ground of flux motion and sample quality [4]. To further explore this, the reversible magnetization of three $HgBa_2CuO_{4+\delta}$ samples was measured and the corresponding $1/\lambda^2$ calculated. While our data above $T_c/2$ support the general feature of early μSR data that $1/\lambda^2 \propto 1-(T/T_c)^\alpha$ with $\alpha \sim 2$-3 around the optimum doping level, our results for $1/\lambda^2$ below $T_c/2$ are different in both of the T-dependence and the extrapolated $1/\lambda^2(0)$ for the optimum- and over-doped samples. $1/\lambda^2$ depends on T nearly linearly in these two samples below $T_c/2$, suggesting that the T-dependence is affected by doping in a rather complicated way.

The samples used were ceramic $HgBa_2CuO_{4+\delta}$ annealed under various O_2 partial pressure [5]. One nearly optimally-doped sample B has $T_c \sim 97$ K and $n \sim 0.17$ hole/CuO_2, where n is the carrier concentration deduced from the thermoelectric power at 290 K [5]. The other samples, A and C, have the same T_c of 90 K but different n of 0.12 and 0.21, respectively. Both X-ray and neutron diffraction [6] show less than 5% impurity phases. The field cooling magnetization measured at 5 Oe with a commercial SQUID magnetometer shows a narrow transition width of 1-4 K and a flat (less than 1% variation) plateau at lower temperatures for all the samples, suggesting good sample homogeneity.

The reversible magnetization M(H) was taken as the average magnetization in the field-increasing branch and the field-decreasing branch at fixed temperature to exclude the irreversible contribution, which accounts for ~20-40% of the total magnetization at the lowest T measured. The paramagnetic background was deduced and subtracted using a Curie-Weiss fit above T_C. Two heavily doped samples, one under doped with $T_c < 4.2$ K and one overdoped with $T_c \sim 20$ K were used to verify the background subtraction procedure. The M of our ceramic samples was converted to M of a corresponding single crystal with H//c in the way proposed in Ref. 7.

A modified London correlation of $1/\lambda^2 = 32 \cdot \pi^2 \cdot (dM/d\ln H)/(0.77\phi_o)$ was used to calculate λ [8]. The Hao-Clem model [8] as well as several proposed fluctuation models [9] were used to check this procedure. The agreement is surprisingly good.

Possible non-*s*-wave pairing in cuprates might affect the superconducting condensation energy F_s, therefore, the λ–M correlation. However, the Hao-Clem model, which includes

1. The Texas Center for superconductivity at the University of Houston and the Department of Physics. University of Houston, Houston TX 77204-5932.

2. Department of Physics, University of Arkansas, Fayetteville, Arkansas 72701.

0896-1107/95/0800-0465$07.50/0

F_s, and the London model, which totally ignores F_s, lead to similar λ-M correlation in s-wave superconductors. This may suggest that F_s does not affect our data reduction severely.

The results obtained for $1/\lambda^2$ of the samples are shown in Fig. 1. The data were fitted as $[1/\lambda^2(0)]\cdot[1-(T/T_c)^\alpha]$ above $T_c/2$ with the parameters $1/\lambda^2(0)$ = 27, 34 and 32 μm^{-2} and α = 1.7, 2.6 and 2.0 for samples A, B and C, respectively. Although the fits are rather good for sample A over the whole measured T-range, deviations are obvious below $T_c/2$ for sample B and C. In this low-temperature regime, $1/\lambda^2$ of B and C seems to depend on T almost linearly. An sample similar to B was also measured in a parallel μSR investigation, and the obtained T-dependence was nearly the same [10]. This suggests that the observation is not a measurement related artifact. Similar T-dependence has been observed in a $YBa_2Cu_3O_{6.95}$ crystal [1].

To be more quantitative, the same fitting procedure was also performed below $T_c/2$ with the parameter T_c fixed. The results obtained for α and $\lambda^2(0)$ are shown in Fig. 2 a) and b) respectively. The fitting parameters are nearly the same above and below $T_c/2$ in Sample A. However, both the exponent α and the extrapolated $1/\lambda^2(0)$ differ significantly below and above $T_c/2$ in Samples B and C. In particular, $1/\lambda^2$ depends on T linearly below 40 K for samples B and C (Figures 1 and 2a).

The superfluid density $n_s \propto 1/\lambda^2(0)$ obtained in the fit below $T_c/2$ varies linearly with n as expected. Conversely, the n_s in the fit above $T_c/2$ bends over strangely near n~0.2. This further enhances our confidence that the deviation observed below $T_c/2$ is not an artifact.

In summary, a nearly linear-in-T $1/\lambda^2$ has been observed below 40 K in slightly overdoped $HgBa_2CuO_{4+\delta}$, but not in the underdoped samples with the same T_c. This suggests that this T-dependence may depend on doping in a complicated way.

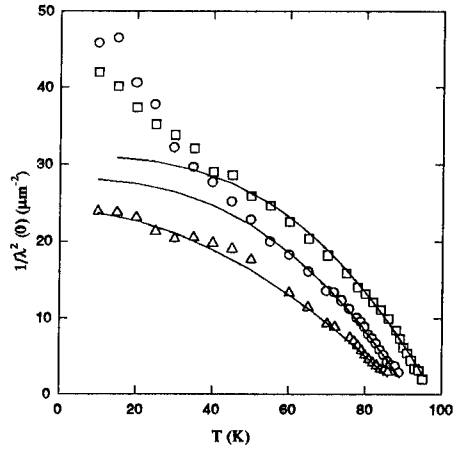

Fig. 1. The deduced $1/\lambda^2$ *vs.* T for Samples A (Δ), B ($\square$) and C ($\circ$). The solid lines are the fits $1/\lambda^2 = [1/\lambda^2(0)]\cdot[1-(T/T_c)^\alpha]$ above $T_c/2$.

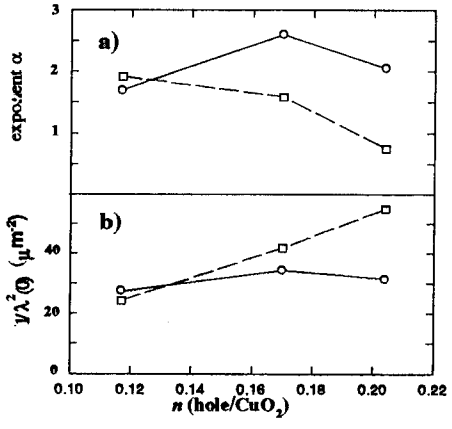

Fig. 2. The parameters a) α and b) $1/\lambda^2(0)$ from the data fitting $\circ$: above $T_c/2$; $\square$: below $T_c/2$.

ACKNOWLEDGMENT

The authors thank Prof. Uemura for μSR data and Drs. Z. Hao, J. H. Xu and J. Clayhold for useful discussions. This work is supported in part by NSF Grant No. DMR 91-22043, USAFOSR Grant No. F49620-93-1-0310by BMDO, the State of Texas through TCSUH and the T. L. L. Temple Foundation.

REFERENCE

1. J.E. Soner *et al.* Phys. Rev. Lett.**72**, 744 (1994).
2. N. Klein *et al.* Phys. Rev. Lett.**71**, 3355 (1993).
3. C. Niedermayer *et al.* Phys. Rev. Lett.**71**. 1764 (1993).
4. For example, D. R. Harshman and A. T. Fioty, Phys. Rev. Lett.**72**, 2501 (1994).
5. Q. Xiong *et al.* Phys. Rev. **B50**, 10346 (1994).
6. Q. Huang *et al.* unpublished.
7. Z. J. Huang *et al.* Physica **C228**, 211 (1994).
8. Z. Hao and J. R. Clem, Phys. Rev. Lett. **67**, 2371 (1991).
9. L. N. Bulaevskii *et al.* Phys. Rev. Lett. **68**, 3773 (1992); Z. Teanovic *et al.* Phys. Rev. Lett. **68**, 3563 (1992).
10. Y. J. Uemura, private communication.

Journal of Superconductivity, Vol. 8, No. 4, 1995

STM Tunneling Spectroscopy on High Tc Superconductors

T. Hasegawa,[1] M. Nantoh,[1] M. Ogino,[1] H. Sugawara,[1] M. Kawasaki,[2] H. Koinuma[2], and K. Kitazawa[1]

Received 31 January 1995

STM tunneling spectroscopy has been performed on the bulk single crystals of BiSrCaCuO (BSCCO) and the epitaxial thin films of YBaCuO (YBCO) at cryogenic temperatures. The STM images and tunneling spectra observed on the (001) surfaces can be classified into three cases; 1) Atomic image is visible. However, the tunneling spectrum shows semiconducting or smeared superconducting gap structures, depending on the tip-sample distance. 2) Clear atomic image can not be obtained. But, the tunneling spectrum shows flat bottom region with quite low zero bias conductance. 3) Tunneling spectra demonstrate gapless behavior, independent of the tip-sample separation. These observations support the quasi-2D electronic picture in which *s*-wave like 2D superconducting layers are coupled with each other through the Josephson effect.

KEY WORDS: STM; superconducting gap; symmetry of order parameter.

I. INTRODUCTION

It is of great importance to clarify the correlation between the normal and superconducting properties of high T_c. superconductors (HTSCs) and their two-dimensional electronic nature associated with the layered crystal structures. High anisotropies in various normal-state transport properties can be understood by modeling the HTSCs as that the conducting CuO_2 layer and other insulating or less conducting layers are alternately stacked and the electron conduction mainly takes place two-dimensionally in the CuO_2 layer. Because of the short coherence, quasi two-dimensional superconducting state is possible. That is, the superconducting order parameter may change from the different layer to another along the *c*-axis.

Recently, the tunneling spectroscopy using scanning tunneling microscopy (STM) has attracted much attentions as a microscopic probe which is capable of measuring the local density of states profiles near the Fermi level [1-8]. Recently, this technique, STS, has been improved to more sophisticated one in which the spectroscopic measurement locations are specified on the STM topographic image simultaneously taken with the tunneling spectra. We have proposed this technique as atomic site tunneling spectroscopy (AST) [6,9]. It has been applied to the layered dichalcogenides, and has shown the local variation of the density of states profiles depending on the atomic site relative to the charge density wave [9].

In this paper, we report on the AST observations on the cleaved surface of $Bi_2Sr_2CaCu_2O_8$ (BSCCO) single crystals and epitaxial thin films of $YBa_2Cu_3O_7$ (YBCO) at 4.2 K. The obtained tunneling data were classified into several cases with respect to the quality of atomic image and the inner gap conductance of superconducing gap structure. These observations were discussed in terms of the quasi two-dimensional electronic nature of HTSCs.

2. EXPERIMENTAL

Cryogenic temperature STM (CSTM) instrument was laboratory constructed. It enables us to perform AST mode operation in which STM image and tunneling spectra were simultaneously taken. The details of our CSTM system were described elsewhere [1].

Single crystals of BSCCO were grown by the floating zone method. The as-grown crystals were

[1]Department of Applied Chemistry, University of Tokyo, Tokyo 113, Japan.
[2]Research Laboratory of Engineering Materials, Tokyo Institute of Technology, Yokohama 227, Japan.

0896-1107/95/0800-0467$07.50/0

further annealed air at 500 °C. The (001) and (110) oriented thin films were prepared by the laser ablation method [7,8].

3. RESULTS AND DISCUSSION

3.1. STM Tunneling Spectroscopy on YBCO (001) and (110) Films

Tunneling spectra observed on YBCO can be classified into three groups, type I, II, and III. The type I spectra observed on the (001) oriented films are characterized by the bias voltage (V_b) dependence, as illustrated in Fig. 1 [7]. In Fig. 1, the set-point current is kept constant, 1 nA. Therefore, lower V_b corresponds to closer tip-sample separation. For higher V_b, the tunneling spectrum shows semiconducting behavior, reflecting that the surface atomic layer is insulating. As V_b decreases, the electron tunneling into inside superconducting layers becomes dominant, and a superconducting gap structure appears. However, it is noted that no clean gap was observed in the type I spectrum.

The type II spectra showing a clean superconducting gap were found on the YBCO (001) films grown at relatively low temperatures [6,7]. Fig. 2 exhibits the typical examples of the type II spectra taken at various measurement locations. The zero bias conductance is as low as 1% of the background, which is one of the lowest value ever reported. Because the tunneling probe in STM has an atomic scale resolution, STM tunneling spectrum gives the local density of states averaged over momentum space [6]. Thus, the clean gap structure in Fig. 2 suggests a finite gap opening in the CuO_2 plane. Obviously, this situation is favored by *s*-wave pairing mechanisms.

The tunneling spectra taken on the YBCO (110) films, classified as the type III data, were shown in Fig. 3 [8]. The type III spectrum demonstrates a superconducting gap structure with high zero bias conductance, independent of the tip-sample separation. By comparing the type II and type III spectra, it is concluded that the CuO chain layer exposed on the (110) surface is responsible to the "gapless" feature in Fig. 3. Thus, the present STM measurements is consistent with the layered electronic model that CuO_2 layers are quasi-2D superconductors with *s*-wave symmetry which induce gapless superconductivity in the CuO chain by the proximity effect [10-12].

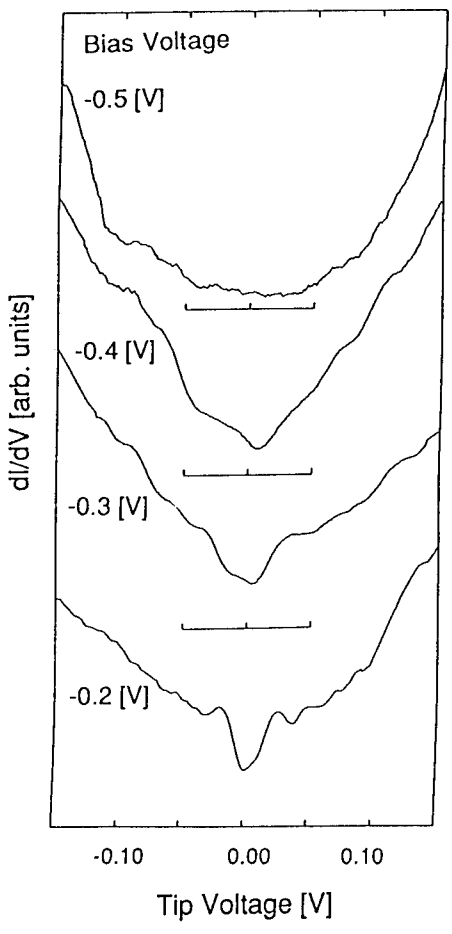

Fig. 1. Bias voltage dependence of tunneling spetra on YBCO (001) film

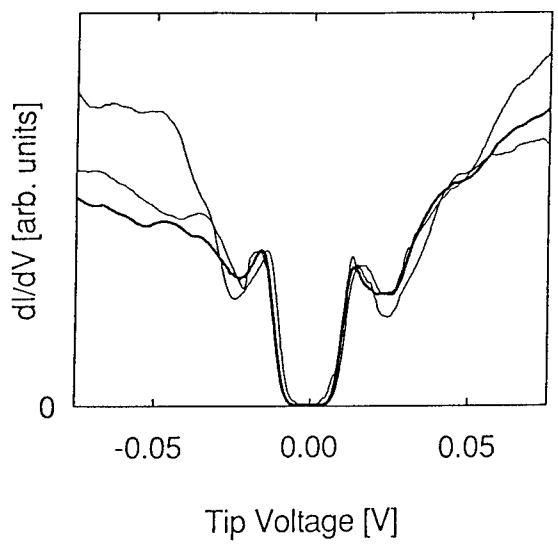

Fig. 2. Tunneling spectra on YBCO (001) film

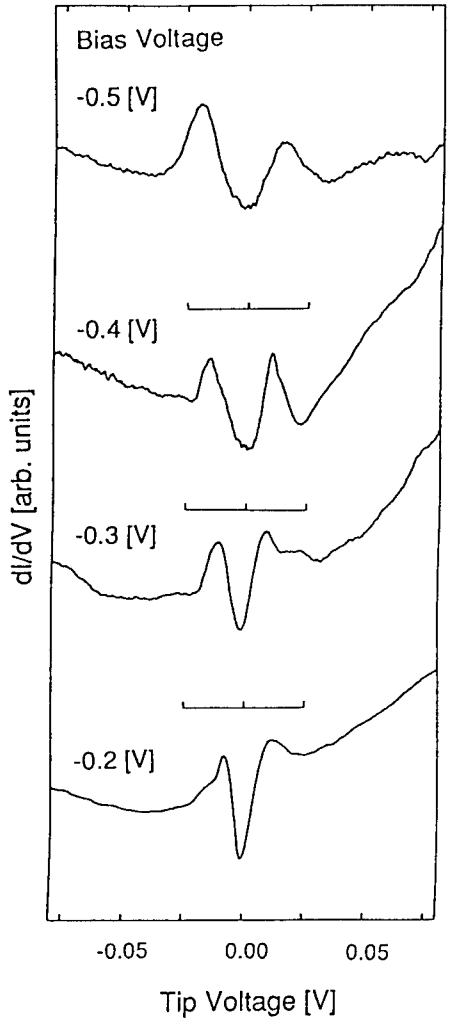

Fig. 3. Bias voltage dependence of tunneling spetra on YBCO (110) film

3.2. STM Tunneling Spectroscopy on the (001) surface of single crystal BSCCO

The type II and type III tunneling spectra were observed on the cleaved (001) surface of BSCCO at 4.2 K, as shown in Fig. 4 and 5, respectively. On atomically flat surfaces where atomic arrangement of Bi can be seen by STM scanning, the type II data were mostly obtained, implying a two dimensional superconductivity in BSCCO as described by the stacking of the essentially insulating $(BiO)_2$ block and superconducting $(CuO_2)_2$. Similar to the YBCO spectra, however, Fig. 4 shows no clean gap structure, and is rather consistent with the *d*-wave superconductivity [3,4].

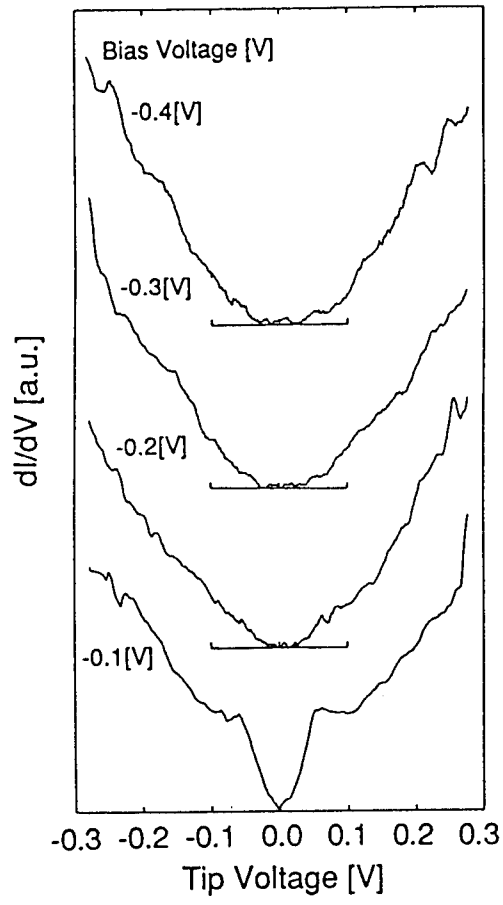

Fig. 4. Bias voltage dependence of tunneling spetra on BSCCO (001) surface

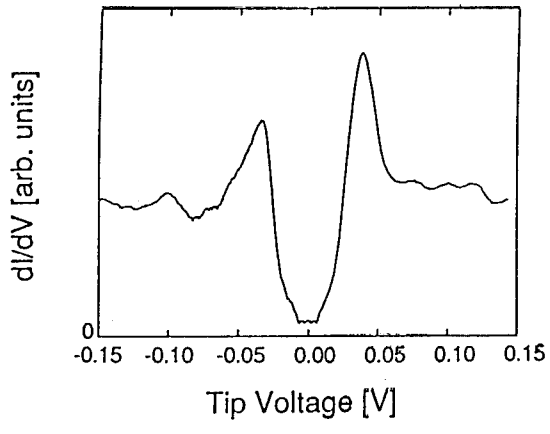

Fig. 5. Tunneling spetrum on BSCCO (001) surface

On the other hand, the type II data was frequently found on the rough surfaces of as-grown samples where no atomic image has not been resolved [1]. We speculate that the type II data was taken on CuO_2 layers partially exposed on the rough surfaces. Our speculation was confirmed by the recent STM tunneling measurement by Murakami *et al.* [5]. From the STM observation, they found a mid-level layer between adjacent BiO layers separated by c/2. The tunneling spectra on the BiO layer is consistent with our type I data in Fig. 4, while those on the mid layer identified as CuO_2 reveal a clean gap structure, which is essentially identical to that in Fig. 5. Therefore, the results of present STM tunneling measurements and Murakami's work leads to the conclusion that the CuO_2 layer has a clean superconducing gap, which supports the *s*-wave paring symmetry, and that the *d*-wave like tunneling spectra reported on BSCCO so far is caused by the surface insulating layer, although its mechanism is not clear at present.

REFERENCES

1. T. Hasegawa, M. Nantoh, and K. Kitazawa, *Jpn. J. Appl. Phys*. **30**, L276 (1991).
2. K. Ichimura and K. Nomura, *J. Phys. Soc. Jpn*. **62**, 3661 (1993).
3. Ch. Renner and Ø. Fisher, *Physica C* **235-240**, 53 (1994).
4. C. Manabe, M. Oda, and M. Ido, *Physica C* **235-240**, 797 (1994).
5. H. Murakami and R. Aoki, *J. Phys. Soc. Jpn.* in press.
6. T. Hasegawa, M. Nantoh, S. Heike, A. Takagi, M. Ogino, M. Kawasaki, H. Koinuma, and K. Kitazawa, *J. Phys. Chem. Solids* **54**, 1351 (1993).
7. M. Nantoh, T. Hasegawa, W. Yamaguchi, A. Takagi, M. Ogino, K. Kitazawa, M. Kawasaki, J. P. Gong, and H. Koinuma, *J. Appl. Phys*. **75**, 5227 (1994).
8. M. Nantoh, T. Hasegawa, W. Yamaguchi, K. Kitazawa, M. Kawasaki, K. Fujito, and H. Koinuma, *Physica C* in press.
9. J.-J. Kim, W. Yamaguchi, T. Hasegawa, and K. Kitazawa, *Phys. Rev. Lett*. **73**, 2103 (1994).
10. M. Tachiki, S. Takahashi, F. Steglich, and H. Adrian, *Z. Phys. B* **80**, 161 (1990).
11. S. H. Liu and R. A. Klemm, *Phys. Rev. Lett*. **73**, 1019 (1994).
12. V. Z. Kresin and S. A. Wolf, *Phys. Rev. B* in press.

Journal of Superconductivity, Vol. 8, No. 4, 1995

Superconductivity and Stoichiometry in the BSCCO-family Materials

Marshall Onellion*

Received 31 January 1995

We report on magnetization, c-axis and ab-plane resistivity, critical current, electroni band structure and superconducting gap properties. Bulk measurements and photoemission data were taken on similar samples.

KEY WORDS: Resistivity; band structure; superconducting gap; symmetry.

I have two purposes in writing this report. One is to provide experimental data that has been reproduced in different laboratories, and so can be viewed as reliable, to serve as the basis for theoretical models. The other is to argue that there is a close connection between changes observed in the superconducting properties (gap size and temperature dependence, critical current, magnetic field dependence) and normal state properties (symmetry of electronic states, topology of Fermi surface, c-axis resistivity).

In our studies, we have found c-axis resistivity data versus oxygen content that are consistent with and extend earlier reports.[1-4] Note that the c-axis resistivity is reduced by a factor of as much as $\times 250$ for overdoped compared to underdoped samples. However, neither we nor our colleagues [1-4] have yet incorporated sufficient oxygen to observe fully metallic ($dR/dT > 0$) behavior for all temperatures down to the superconducting transition temperature (T_c), as has been observed for YBCO-123.[5] The significant point to these measurements is that there is a marked change in the c-axis resistivity, and hence interlayer coupling, with oxygen stoichiometry.

For the same samples for which we measured c-axis resistivity, we also performed angle-resolved photoemission measurements of the normal state.[4] The issue was to determine whether samples that exhibited the change in c-axis resistivity also exhibited any differences in their Fermi surfaces. We have reported elsewhere [6] that there is a finite interlayer coupling between the adjacent CuO_2 planes of the bilayer. We chose Pb-doped BSCCO-2212 samples. By performing careful TEM measurements,[4] we determined that the overdoped and underdoped samples were isostructural in the CuO_2 (ab-)planes. The only structural difference is a change in the periodicity of the superlattice modulation, with the overdoped samples exhibiting a larger period. We found that there is a change of symmetry in the normal state quasiparticle band states as the amount of oxygen is changed. Specifically, the electronic states that comprise the Fermi surface in the $k_x = \pm k_y$ directions exhibited a change in symmetry with oxygen stoichiometry, while the symmetry of the states in the k_x and k_y directions was unaffected by the oxygen stoichiometry. Our results indicate one of two possibilities. One is that the c-axis (interlayer coupling) affects the symmetry of the electronic states. The other possibility is that the electronic states arise due to many-body effects.[7] If the electronic states are interpreted as many-body states,[7] preliminary calculations indicate that interactions beyond the nearest-neighbor must be included to explain the data.[7]

In addition to the symmetry of the normal state electronic states, our data indicate two other important points about the Fermi surface. We find

*Department of Physics, University of Wisconsin, Madison, WI 53706.

0896-1107/95/0800-0471$07.50/0

that there is an extended van Hove singularity,[8] consistent with other reports.[9-11] The extent of the singularity is reduced for overdoped samples.[4] A pocket, absent for underdoped samples, develops around the $(\pi, 0)$ point for overdoped samples,[4,8] consistent with earlier work by C. Olson and colleagues.[12,13] Further, it is noteworthy that P. Aebi and colleagues have used our samples to study the presence and strength of the shadow bands they reported earlier.[14] In their previous work,[14] they reported observing shadow bands only on samples that were particularly flat and well-ordered (to reduce scattering that averages over the Brillouin zone). Using our samples, they find such shadow bands, and find that the shadow bands are weaker, but present, for the overdoped samples (T_c = 75 K) compared to the underdoped samples (T_c = 80 K).[15] These data indicate that both the symmetry of the Fermi surface electronic states, and the topology of the Fermi surface, change with oxygen doping.

Note that we have found results consistent with other investigators for those measurements where consistency is expected. For that reason, our results as to the symmetry and topology of the Fermi surface electronic states appear representative of samples in different laboratories. As an additional check of our samples, we have studied the current versus voltage measurements for supercurrent along the c-axis and applied magnetic field in the ab-plane.[16] The issue is whether the change in c-axis resistivity, and Fermi surface electronic states, both normal state properties, are related to superconducting state properties.

We found that for our samples, the CuO_2 planes are stacked very close to parallel, with an ab-plane misalignment below 0.02 degrees. This allowed us to orient the applied magnetic field parallel to the ab-plane with high accuracy. The results at lower magnetic fields (below 1 Tesla) reproduce earlier work by Kleiner et.al.[17,18] For underdoped samples, the data indicate a S-I-S Josephson junction stacking of planes along the c-axis. For overdoped samples, the critical current density increases between ($\times 100 - \times 1000$) and the stacking is S-N(S')-S. Our results indicate a marked increase in critical current density for overdoped samples, the same samples that exhibit the changes in normal state properties.

However, neither our results [16] nor those of our colleagues, [17,18] conclusively establish whether the c-axis coupling in overdoped samples is Josephson-junction or three dimensional. One new, and pertinent, result is that overdoped samples obey the Kim-Stevens relation,[19] as do three- dimensional superconductors. We found H_{c_2} is already 14 Tesla only 4 K below T_c. [16]

In magnetization studies of cuprate superconductors, much has been made of the "fishtail" behavior,[20-22] a region of applied magnetic field for which the magnetization increases with increasing applied field. Using samples similar to those used in photoemission studies, X.Y. Cai *et al.*[22] reported that the fishtail exists for both underdoped and overdoped samples, although such samples exhibit very different quantitative magnetization response. The data were interpreted as indicating that there are always stronger and weaker superconducting regions. These are the same sample types described above. Consequently, the fact that all samples exhibit the fishtail behavior indicates that all samples exhibit both stronger and weaker superconducting regions.

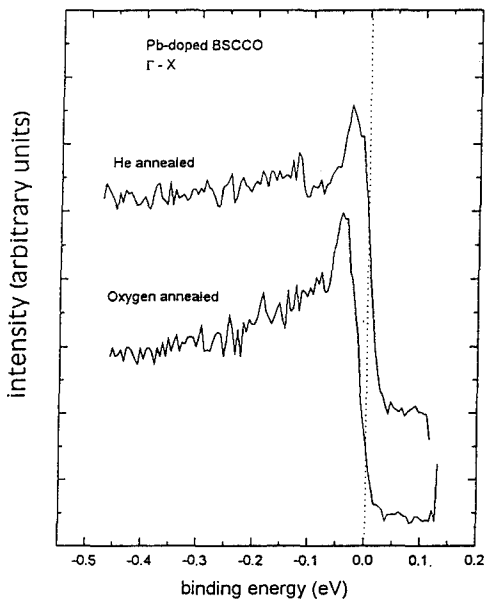

Fig. 1. Photoemission spectra in the normal state along the $k_x = k_y$ direction for He-annealed, Pb-doped sample (gap = 0-2 meV) and oxygen-annealed, overdoped sample (gap = 10-12 meV).[27]

For the same sample types, we also conducted angle-resolved photoemission measurements of the size of the superconducting gap for two high-symmetry directions, k_x (Cu-O-Cu bond axis in real space) and $k_x = k_y$ (Bi-O-Bi bond axis perpendicular to superlattice modulation).[23,24] Figure One illustrates the results. We found that for samples with less oxygen, particularly if underdoped, the gap along $k_x = k_y$ is indistinguishable from zero (2 ± 2 meV), consistent with earlier reports by B.O. Wells and Z.-X. Shen.[25,26] However, for overdoped samples, the data indicate unambiguously that the superconducting gap in the $k_x = k_y$ direction is non-zero.[27] Observing a non-zero gap in the $k_x = k_y$ direction has also been reported earlier by several research groups.[28-31] One significant point is that this study is the first to directly connect the size of the superconducting gap and the bulk critical current and magnetization properties of a cuprate superconductor system.

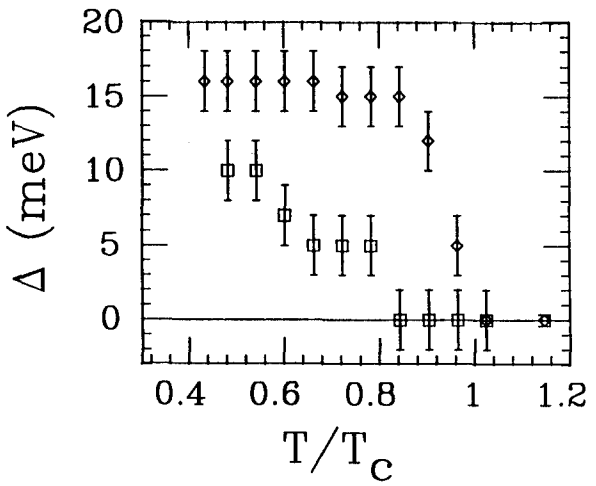

Fig. 2. Superconducting gap (in meV) versus temperature for k_x direction (diamonds) and $k_x = k_y$ direction (squares).[32]

These results can be regarded as solid, because they either reproduce earlier work or have been independently confirmed by other investigators, including other investigators using our samples.[15] The last experimental result that we wish to report is the temperature and momentum-resolved study of the superconducting gap for oxygen overdoped samples.[32] We studied the variation of the superconducting gap with temperature for two Brillouin zone directions, k_x and $k_x = k_y$. Figure Two illustrates the results. We found that the temperature dependence of the superconducting gap along the two symmetry directions is qualitatively different. In particular, the gap along the $k_x = k_y$ direction becomes indistinguishable from zero at $0.82T_c$, while along k_x the gap remains at 90-100% of its value at $0.35T_c$. Some parts of the data in Fig. 2 have been independently confirmed. The rapid, non-BCS, increase of the gap with decreasing temperature in the k_x direction has been confirmed by J.C. Campuzano and colleagues.[33] The non-zero gap in the $k_x = k_y$ direction at lower temperatures has been reported earlier.[28-31]

What inferences can be drawn that are based strictly on data reproduced in different laboratories? I am confident of the following:

- Saying that the symmetry of the order parameter (gap) remains identical for all stoichiometry has been ruled out;[27-29,31-34]
- There is a marked increase in interlayer coupling for overdoped samples, as reflected in bulk measurements [1-4,16-18] and the symmetry of the normal state electronic states;[6]
- The shadow bands reported earlier by P. Aebi et.al. [14] are observed for samples from different laboratories, and exist well into the overdoped regime;[15]
- The gap increases more rapidly for temperatures below T_c than a would a BCS superconductor.[32,33]

In addition, if all the results of of Ref. 32 are confirmed by independent work, these results indicate that, for overdoped samples, just below T_c there may be only d-wave pairing, while at lower temperatures a more complicated pairing interaction exists. However, for underdoped samples, the small value of the gap along the $k_x = k_y$ direction (at $0.35T_c$) indicates that a predominant d-wave pairing extends to lower temperature.

ACKNOWLEDGEMENTS

Various parts of the work reported were performed in collaboration with, above all, my students and postdocs, Jian Ma, Ronald Kelley and Christoph Quitmann, as well as with other colleagues, including Cai Xueyu, Yi Feng, David Larbalestier, Philippe Almeras, Helmut Berger, and Giorgio Margaritondo. Financial support was provided by the U.S. NSF, Ecole Polytechnique Fédérale, Fonds National Suisse de la Recherche Scientifique, and the Deutsche Forschungsgemeinschaft.

REFERENCES

1. C. Kendziora *et al., Phys. Rev. B* **48**, 3531 (1993).
2. D. Mandrus *et al., Phys. Rev. B* **44**, 2418 (1991).
3. F.X. Reiz *et al., IEEE Trans. Appl. Supercon.* **3**, 1190 (1993).
4. Jian Ma *et al., Phys. Rev. B*, in press (1995).
5. L. Forro *et al.*, Phys. Rev. B **46**, 6626 (1992).
6. C. Quitmann *et al.*, submitted to *Phys. Rev. B.*
7. E. Dagotto *et al., Phys. Rev. Lett.* **73**, 728 (1994).
8. Jian Ma *et al., Phys. Rev. B*, in press (Feb. 1, 1995).
9. A. Abrikosov *et al., Physica C* **214**, 73 (1993).
10. K. Gofron *et al., Phys. Rev. Lett.* **73**, 3302 (1994).
11. D. Dessau *et al., Phys. Rev. Lett.* **71**, 2781 (1993).
12. C. Olson *et al., Phys. Rev. B* **42**, 381 (1990).
13. B.O. Wells *et al., Phys. Rev. Lett.* **65**, 3056 (1990).
14. P. Aebi *et al., Phys. Rev. Lett.* **72**, 2757 (1994).
15. P. Aebi *et al*, unpublished.
16. X.Y. Cai *et al*, unpublished.
17. R. Kleiner and P. Mueller, *Phys. Rev. B* **49**, 1327 (1994).
18. R. Kleiner *et al., Phys. Rev. B* **50**, 3942 (1994); R. Kleiner, op. cit., 6919 (1994).
19. R.D. Parks, Ed. *"Superconductivity"*, , Marcel Dekker, NY, 1969, Ch. 19.
20. M. Daeumling *et al., Nature* **346**, 332 (1990).
21. V.N. Kopylov *et al, Physica C* **170**, 291 (1990).
22. X.Y. Cai *et al., Phys. Rev. B* **50**, 16774 (1994).
23. S. Sunshine *et al., Phys. Rev. B* **38**, 893 (1988).
24. M.D. Kirk *et al., Science* **242**, 1673 (1988).
25. B.O. Wells *et al., Phys. Rev. B* **46**, 11830 (1992).
26. Z.-X. Shen *et al., Phys. Rev. Lett.* **70**, 1553 (1993).
27. R.J. Kelley *et al., Phys. Rev. B* **50**, 590 (1994) and unpublished.
28. C. Olson *et al., Science* **245**, 731 (1989); *Solid State Commun.* **76**, 411 (1990).
29. R.J. Kelley *et al., Phys. Rev. Lett.* **71**, 4051 (1993).
30. H. Ding *et al., Phys. Rev. B* **50**, 1333 (1994).
31. H. Ding *et al.*, preprint and private communication.
32. Jian Ma *et al., Science*, in press (1995).
33. J.C. Campuzano, private communication and oral presentation at the 1994 Wisconsin Synchrotron Radiation Center Users Meeting.
34. A. Abrikosov, private communication.

Journal of Superconductivity, Vol. 8, No. 4, 1995

Shadow Bands in Models of Correlated Electrons

Adriana Moreo[1], Stephan Haas[1], and Elbio Dagotto[1]

Received 15 January 1995

A consequence of strong antiferromagnetic correlations in models of high-Tc cuprates is the appearance in photoemission (PES) calculations of considerable more weight above the Fermi momentum $\mathbf{p_F}$ than expected for non-interacting electrons. This effect, qualitatively discussed by Kampf and Schrieffer under the name of "shadow bands", is here quantitatively analyzed in the two dimensional Hubbard and t-J models using Monte Carlo and exact diagonalization techniques in the realistic strong coupling regime.

KEY WORDS: Superconductivity, Hubbard Model, Shadow Bands.

The importance of antiferromagnetic correlations in the normal and superconducting states of the high critical temperature cuprate materials is under much discussion. While recently most of the debate has been concentrated on the symmetry of the superconducting order parameter, studies of the strength of the antiferromagnetic correlation length, ξ_{AF}, in the normal state are still crucial to test these ideas. A key issue is how large ξ_{AF} should be to produce observable effects in experiments for the high-Tc compounds. NMR studies in the normal state of optimally doped $YBa_2Cu_3O_{6.94}$ (YBCO) suggest $\xi_{AF} \sim 2a$ (where a is the lattice spacing). [1] Naively, this correlation seems too small to be of relevance. On the other hand, recent photoemission (PES) experimental results by Aebi et al.[2]in $Bi_2Sr_2CaCu_2O_8$ (Bi2212) with Tc=85K, using sequential angle-scanning data acquisition to obtain PES intensities within a narrow energy window near the Fermi energy E_F, reported evidence of antiferromagnetically induced spectral weight above p_F ($\omega < 0$). This result is compatible with the "shadow bands" scenario of Kampf and Schrieffer.[3] At half-filling, these bands are caused by the enlarged magnetic unit cell of the CuO_2 planes produced by the long range antiferromagnetic order in the ground state. This effective reduction in the size of the Brillouin zone (BZ) has interesting implications for PES experiments.[3] For example, along the diagonal $p_x = p_y = p$, and assuming long-range order, peaks at momenta $\mathbf{p_1} = (p, p)$ and $\mathbf{p_2} = (\pi - p, \pi - p)$ should appear at the same energy location, for any value of p. The PES weight ($\omega < 0$) observed in the region*above* the non-interacting $\mathbf{p_F}$ is induced by strong magnetic correlations.[3]

How does this antiferromagnetically induced PES signal evolve as ξ_{AF} is made finite by the effect of hole doping? There are no quantitative estimations in the literature in a realistic region of parameter space. It is likely that its intensity will smoothly diminish doping away from half-filling. Since in optimally doped Bi2212 the antiferromagnetic correlation length in the CuO_2 planes should be similar to that of optimally doped YBCO (since they should have the same in-plane hole density), then a natural question arises: can a small correlation length ($\sim 2a$) produce observable weight in PES experiments above $\mathbf{p_F}$? On one hand, recent calculations[4] carried out in an antiferromagnetic background have reproduced the flat band features near $\mathbf{p} = (\pi, 0)$ observed in Bi2212 suggesting that a short ξ_{AF} can appreciably influence some experimental quantities. On the other hand, since the actual experimental PES signal is weak, concerns may arise about the interpretation of the data. Thus, a theoretical *quantitative* calculation is needed to compare with experiments, and decide if Aebi et al.'s PES data are compatible with models

[1]Department of Physics, National High Magnetic Field Lab and, Supercomputer Computations Research Institute, Florida State University, Tallahassee, FL 32306, USA

0896-1107/95/0800-0475$07.50/0

of strongly correlated electrons which present PES weight above p_F. Here, this issue is explicitly addressed. PES spectra and spin correlations are calculated for models of correlated electrons expected to describe the CuO_2 planes. Consider first the two dimensional (2D) one band Hubbard model defined by the Hamiltonian

$$H = -t \sum_{<i,j>\sigma} (c^{\dagger}_{i\sigma} c_{j\sigma} + h.c.) + U \sum_{i} n_{i\uparrow} n_{i\downarrow}, \quad (1)$$

in the standard notation. We simulated this model numerically using standard quantum Monte Carlo techniques. In order to extract the dynamical spectral function $A(p,\omega)$ corresponding to the removal or addition of an electron with momentum p to the system, the maximum entropy (ME) technique was used.[6] To analyze the strength of the signal above p_F, we calculated the amount of spectral weight below the chemical potential μ at momenta along the diagonal $p_x = p_y$ in the BZ with respect to the total intensity (adding PES and inverse PES) which for the Hubbard model satisfies the sum rule $\int_{-\infty}^{+\infty} d\omega A(p,\omega) = 1$ at all dopings.

Before describing the computational results, let us clarify when a theoretically calculated PES signal can be labeled as being "observable" in an experiment. PES spectra have large backgrounds, whose origin and shape are a matter of discussion, superimposed on the actual relevant signal. This background depends on the momentum, and also changes from sample to sample with fluctuations as large as 50%. Since the background is convex, the natural requirement for a PES theoretical signal to be observable is that the combination background-signal produces a local maximum (i.e. a peak in the measured intensity).[7] From the data shown in Ref.[5], and the intensity of the signal at the last point where the dispersion is observed i.e. $p = (0.7\pi, 0.7\pi)$, it is believed that a peak with an intensity of roughly about 10% of the largest signal (located at $p = (0.5\pi, 0.5\pi)$) would be at the verge of being detected.[2] This is the criterion followed in the present paper to label a result as "observable".

The choice of coupling is important in our search for PES weight above p_F. For example, we observed that working on an 8×8 cluster, at $U/t = 4$, half-filling and temperature $T = t/4$, the percentage of PES spectral weight at $p = (3\pi/4, 3\pi/4)$, i.e. the next available momentum after $(\pi/2, \pi/2)$ on this cluster, is very small (less than 5% of the total), even though the spin correlations show clear indications of long-range order. Then, the actual value of the local moments is as important as the antiferromagnetic correlation length for the effect we are investigating. Since evidence has been recently given that another feature induced by antiferromagnetism,[7] namely the "hole" pockets, are washed out by temperature effects in QMC simulations at $U/t = 4$, then we consider this coupling to be too small for our purposes. Actually, studies of the optical conductivity have shown that a larger coupling U/t, approximately between 8 and 12, is needed to correctly reproduce the main features observed experimentally.[8] Since at $U/t = 12$ there are serious numerical instabilities in the simulations, then here the analysis was restricted to $U/t = 8$.

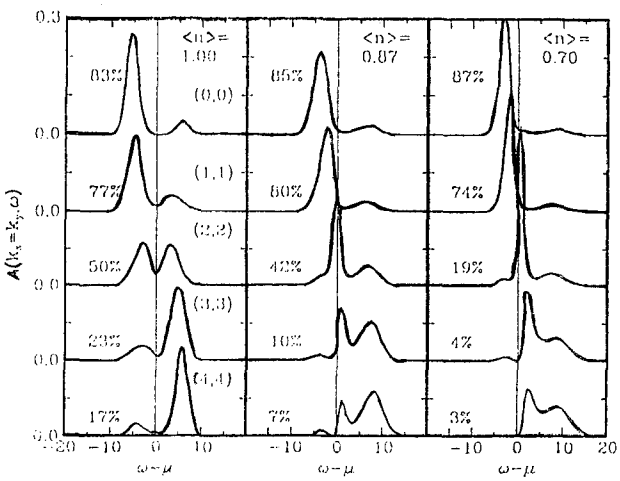

Fig.1. $A(p,\omega)$, evaluated using QMC and ME techniques, for the 2D Hubbard model at $U/t = 8$, $T = t/2$ on an 8×8 cluster, at several densities $\langle n \rangle$. The momentum label varies along the diagonal in the BZ in units of $\pi/4$, and the percentages correspond to the integrated PES part of the spectral weight with respect to the total intensity (=1). The energy is in units of t.

In Fig.1, $A(p,\omega)$ at $T = t/2$ is shown.[9] It isdifficult to reduce T due to sign problems, but nevertheless this temperature allows us to study the PES signal above p_F at different correlation lengths as the density is changed, which is the main purpose of the paper. At half-filling, $\langle n \rangle = 1$, the chemical potential is located in the gap. The percentage of spectral weight is shown for each momentum. A nonzero PES signal above the non-interacting Fermi momentum is clearly visible, and at $p = (3\pi/4, 3\pi/4)$ it carries $\sim 23\%$ of the total weight. This result is very similar if the temperature is reduced to $T = t/4$, thus finite temperature effects are not too severe for this quantity at half-filling. Actually, our results for the intensity of the weight above p_F are in excellent agree-

[2] We thank B. O. Wells (private communication) for this suggestion.

ment with the spin density wave mean-field approximation.[10]Since for a pure spin-1/2 antiferromagnet the weight at $\mathbf{p} = (\pi/4, \pi/4)$ and $\mathbf{p} = (3\pi/4, 3\pi/4)$ should be identical at this density, it is natural to conclude that the finite coupling U/t is responsible for the reduction of the intensity of the PES signal above the naive $\mathbf{p_F}$ at half-filling.

Away from half-filling, at $\langle n \rangle = 0.87$, the amount of weight at $\mathbf{p} = (3\pi/4, 3\pi/4)$ is reduced to $\sim 10\%$, which is still visible in the scale of the plot. The height of the peak, as a percentage of the peak height at $\mathbf{p} = (\pi/2, \pi/2)$ and half-filling is about 15%. Following the criteria described before, the result obtained at $\langle n \rangle = 0.87$ in the Hubbard model is labeled as still "observable" (although it is rather weak). Whether this PES weight corresponds to an actual sharp band dispersing, to a broader feature, or a combination of both, is difficult to address with the ME technique which has low resolution, but nevertheless it is clear that it is induced by antiferromagnetism. At $\langle n \rangle = 0.70$, the signal at $\mathbf{p} = (3\pi/4, 3\pi/4)$ carries a small weight of only 4%, and as the electronic density is reduced further the system smoothly converges to the non-interacting limit. Then, for this particular calculation we tentatively conclude that a doping of 25% holes makes the antiferromagnetically induced weight almost negligible, while at 12% doping the effect is still observable.

To check the sensitivity of our conclusions to the model used, let us also consider the well-known 2D $t-J$ Hamiltonian. This model cannot be studied with Monte Carlo techniques, thus exact diagonalization was used.[9]This algorithm works at T=0, and dynamical information can be obtained in real time. Its restriction to small clusters should not be a major problem in calculations where ξ_{AF} is very small. To increase the momentum resolution along the diagonal in the BZ, we combined the results of the 16 sites cluster (providing momenta $(0,0), (\frac{\pi}{2}, \frac{\pi}{2}), (\pi, \pi)$) and the 18 sites cluster (containing $(\frac{\pi}{3}, \frac{\pi}{3}), (\frac{2\pi}{3}, \frac{2\pi}{3})$).[3] In Fig.2, the PES $A(\mathbf{p}, \omega)$ spectrum is shown for the t-J model.$J/t = 0.4$ was selected as an example, but we checked that the results are similar in the range between $J/t = 0.2$ and $J/t = 0.8$. As expected, at half-filling the largest peak near the chemical potential (quasiparticle) is obtained at $\mathbf{p} = (\frac{\pi}{2}, \frac{\pi}{2})$. Increasing the diagonal momenta away from it, a considerable amount of spectral weight induced by ξ_{AF} is observed. Moving away from half-filling into the subspace of two holes (nominal density $\langle n \rangle \sim 0.88$) the dominant peak remains at $\mathbf{p} = (\frac{\pi}{2}, \frac{\pi}{2})$ within our momentum resolution. At $(\frac{\pi}{3}, \frac{\pi}{3})$ the quasiparticle strength is still large and coherent. On the other hand, at $\mathbf{p} = (\frac{2\pi}{3}, \frac{2\pi}{3})$ the peak seems now broader in the scale used, although its integrated spectral weight remains close to that of $\mathbf{p} = (\frac{\pi}{3}, \frac{\pi}{3})$.

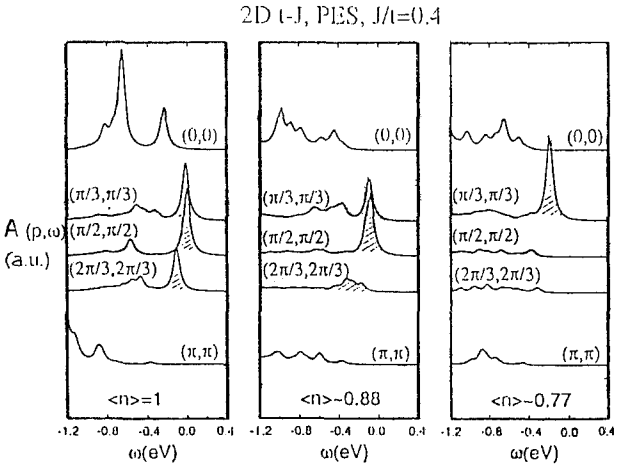

Fig.2.PES $A(\mathbf{p}, \omega)$ evaluated using exact diagonalization techniques for the 2D t-J model, at $J/t = 0.4$ on 4×4 and $\sqrt{18} \times \sqrt{18}$ clusters. We assumed $t = 0.4$eV, and provided a width $\delta = 0.1t$ to the peaks.

The height of the peak at $\mathbf{p} = (2\pi/3, 2\pi/3)$ as a percentage of the largest peak located at $\mathbf{p} = (\pi/2, \pi/2)$ (with or without holes) is 15-20% i.e. within the "observable" region defined before. Finally, at density $\langle n \rangle = 0.77$, the result resembles that of a non-interacting system with a Fermi momentum close to $\mathbf{p} = (\pi/3, \pi/3)$, above which the signal is too weak to be observable in PES experiments. Then, our rough estimations within the t-J model are similar to those of the Hubbard model, i.e. weight above $\mathbf{p_F}$ can still be observed at $\langle n \rangle \sim 0.88$ but no longer at density $\langle n \rangle \sim 0.77$. To make contact with experiments it is necessary to consider the spin correlations[11]. At half-filling, ξ_{AF} is clearly larger than the lattice size. At $\langle n \rangle \sim 0.88$, a crude exponential fit of the spin correlation vs. distance gives $\xi_{AF} \sim 1.5a$ (similar to that of YBCO and Bi2212 at optimal doping), while at $\langle n \rangle \sim 0.77$, ξ_{AF} is less than one lattice spacing. Then, we again arrive to the conclusion that for a real material with $\xi_{AF} \sim 2a$ the antiferromagnetically generated PES weight is weak but may still be observable above the background.

In Fig.3, $A(\mathbf{p}, \omega)$ is shown again at $\langle n \rangle \sim 0.88$ using an expanded energy scale. The dispersion of the sharp peak (I) discussed before in Fig.2, has a bandwidth of order J, while at higher energies a con-

[3] These calculations were carried out on a Cray-90 supercomputer and IBM workstations. The largest Hilbert space handled (i.e. N=18, 5 holes) contains 816816 states, exploiting the translational invariance symmetry. Typically each PES figure contains about 200 poles.

siderable amount of spectral weight is found contributing to the bulk of the valence band (II). Peak (I) is clearly caused by antiferromagnetic correlations and it is in good agreement with the qualitative discussion of Kampf and Schrieffer.[3]ME entropy techniques cannot resolve these two peak structure, and thus exact diagonalization is needed to quantitatively analyze these features.

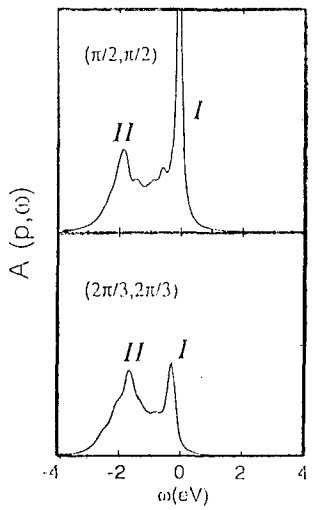

Fig.3.PES $A(p,\omega)$ for the t-J model at $\langle n \rangle \sim 0.88$, J/t=0.4, clusters of 16 and 18 sites, and expanding the energy scale to observe the two peak structure. We use $\delta = 0.25t$.

Summarizing, an analysis of the PES spectra in the 2D Hubbard and t-J models, at several densities and couplings, was reported. If these models reproduce the physics of the high-Tc compounds, then we conclude that antiferromagnetically induced photoemission weight should be observable even for materials with spin correlations lengths of only a couple of lattice spacings, as in Bi2212 at optimal doping. This is *compatible* with the experimental results of Ref.[2]. However, this regime is at the verge of observability. The PES signal above p_F should no longer be visible above the large PES experimental background at slightly larger dopings. To gather further evidence that the weak experimental signal is indeed caused by antiferromagnetism we believe that it is necessary to carry out PES experiments as a function of hole doping. The strength of the signal above p_F should increase as the system moves away from the optimal doping towards half-filling. A possible candidate for such a study is YBCO with a critical temperature of about 60K. Another alternative within the Bi2212 family would be to consider $Bi_2Sr_2Ca_{1-x}Lu_xCu_2O_{8+\delta}$ which seem to be underdoped.[12]

ACKNOWLEDGMENTS

We thank J. R. Schrieffer, P. Monthoux, D. Scalapino, M. Onellion, and A. Nazarenko for conversations, and J. Riera for providing us with programs for the t-J model. E. D. and A. M. are supported by the Office of Naval Research under grant ONR N00014-93-0495. E. D. also thanks the donors of the Petroleum Research Fund administered by the American Chemical Society. We also thank MARTECH (FSU) for support.

REFERENCES

1. T. Imai et al., Phys. Rev. **B 47**, 9158 (1993).
2. P. Aebi et al., Phys. Rev. Lett. **72**, 2757 (1994); J. Osterwalder et al., preprint.
3. A. Kampf and J. R. Schrieffer, Phys. Rev. **B 41**, 6399 (1990); Phys. Rev. **B42**, 7967 (1990).
4. E. Dagotto, A. Nazarenko and M. Boninsegni, Phys. Rev. Lett. **73**, 728 (1994); E. Dagotto, A. Nazarenko and A. Moreo, preprint.
5. B. O. Wells, Z.-X. Shen, A. Matsuura, D. M. King, M. A. Kastner, M. Greven, and R. J. Birgeneau, preprint.
6. R. N. Silver et al., Phys. Rev. **B 41**, 2380 (1990); S. R. White, Phys. Rev. **B 44**, 4670 (1991).
7. A. Moreo and D. Duffy, preprint; R. Eder and Y. Ohta, preprint; S. Trugman, Phys. Rev. Lett. **65**, 500 (1990).
8. E. Dagotto, Rev. Mod. Phys. **66**, 763 (1994).
9. For similar QMC ME results, see N. Bulut, D. J. Scalapino and S. R. White, Phys. Rev. **B 50**, 7215 (1994).
10. E. Dagotto, F. Ortolani and D. Scalapino, Phys. Rev. **B 46**, 3183 (1992); N. Bulut, D. J. Scalapino and S. R. White, Phys. Rev. Lett. **73**, 748 (1994).
11. S. Haas, A. Moreo and E. Dagotto, preprint.
12. Y. Koike et al., Physica C 159, 105 (1989).

Journal of Superconductivity, Vol. 8, No. 4, 1995

Electronic Properties of CuO_2 Planes

Daniel C. Mattis*

Received 31 January, 1995

We study a 3-band model of CuO_2 with"bare bones" interactions: hopping from copper ions to nearest-neighbor oxygens t_{pd} only, a two-body interaction on the copper ions U_{dd} only, and an overlap copper-oxygen parameter λ_{pd}. In the limit $t_{pd} \propto U_{dd}^{1/2} \to \infty$, $t^* = t_{pd}^2/2U_{dd}$ is the unit of energy with $8\lambda_{pd}^2$ as the only parameter of significance. If the two-body interaction is invariant under particle-hole interchange, the low-lying states (energy O(t*)) can be described by conserved particles and can all be classified. They are quite distinct from the high-lying states (energies $O(U_{dd})$). The dynamics of the conserved fermion-like elementary particles are well described by a modified *t-J* model with extended hopping and nearest-neighbor superexchange attraction. This is a scenario known to be favorable to high-temperature superconductivity, but it must be noted that both the hopping range and the exchange are functions of $8\lambda_{pd}^2$. Moreover, if the Hamiltonian is *not* invariant under particle-hole interchange the dynamics becomes much more complex and possibly more inimical to high-temperature superconductivity. This may provide an explanation for the deleterious effect on superconductivity of very small concentrations of certain impurities.

KEY WORDS: Copper oxide; three-band model; *t-J* model.

INTRODUCTION

The low-energy states of a unit cell in a CuO_2 plane consists of a doublet Cu^{2+} ion (2 spin orientations) and two singlet O^{2-} ions (each convertible to a doublet O^{1-}) for a total of 2x3x3 = 18 possibilities. If we allowed high-energy states $Cu^{1+}$and Cu^{3+} as well, that raises the total to 36. Thus the simple "hopping" of an electron (or hole) from one cell to the next involves possibly as many as (½) x 36^2 x 36^2 = $O(10^6)$ matrix elements. Conservation laws and other constraints reduce this number to O(100), but that is still too great for practical purposes. This paper describes a procedure which reduces the effective number of matrix elements to a manageable few, allowing the low-lying states to be described by an extended *t-J* model with some additional embellishments. There are several key concepts contributing to the simplification.

* Department of Physics, University of Utah
Salt Lake City, UT 84112

1. Use of nonorthogonal orbitals allows both the exchange mechanism and the band structure for the motion of composite particles to be computed in lowest-order of perturbation theory.

2. Inclusion of the nonorthogonality parameter λ into the *anticommutation relations* permits the many-body problem to be formulated in the usual way, without incurring the so-called "nonorthogonality catastrophe."

3. Use of an Hamiltonian invariant under particle-hole transformations results in *conserved* quasiparticles, such as the "holes" which are injected into an antiferromagnetic plane and which convert it into a high-temperature superconductor ("HTS"). The numbers seem to indicate that this is an approximate symmetry property for Cu, so that the symmetric interaction Hamiltonian in Eq. (7) below is essentially correct for Cu but not necessarily for substitutional metal impurities. Those which strongly violate this symmetry cause large-scale fluctuations inimical to HTS, so a low concentration of such impurities may suffice to wipe out HTS.

4. The "limit model" procedure (described below) ensures

0896-1107/95/0800-0479$07.50/0

all interesting terms scale with $t^*=t_{pd}^2/2U_{dd}$, our unit of energy, to a fractional accuracy of $O(t_{pd}/U_{dd})$ or $O(t_{pd}/U_{dd})^2$.

NONORTHOGONALITY

Anderson [1] pointed out that the principal contribution to the mechanism of superexchange occurs in leading (second-) order of the orbital overlap parameter and *not* in fourth-order in the hopping parameter. We limit the overlap to the copper orbital with any of its nearest-neighbor oxygens:

$$\lambda_{pd}=\int dr \Phi_p^* \Psi_d \tag{1}$$

As a consequence we find [2] that superexchange is confined to nearest-neighbor interactions, with $J = 16t^*\lambda_{pd}^2$. The principal charge carriers are composite SU_2 states embedded in a background of Zhang-Rice singlets [3]. They are subject to a hard-core on-site repulsion and possess a band-structure:

$$\varepsilon_\lambda(k)\equiv\Omega_\lambda(k)6t^*T(0) \tag{2}$$

where $T(0)$ is just the average of $\Omega_\lambda(k)$ over the *B.Z.*, the latter defined by:

$$\Omega_\lambda(k)\equiv\omega(k)\sqrt{1-\lambda_{pd}^2\omega^2(k)}\ ,\ with$$
$$\omega(k)\equiv 2\sqrt{\sin^2\frac{kx}{2}+\sin^2\frac{ky}{2}} \tag{3}$$

The quantities $T(\mathbf{R})$ are the lattice F.T.'s of $\Omega_\lambda(k)$. The effective hopping matrix element of the charge carriers is given by $t_{eff}(\mathbf{R}_{ij})6t^*T(0)$. An abridged table of T's follows.

TABLE I: A few $T(\mathbf{R})$ as function of overlap

$8\lambda_{pd}^2$ ↓	**R**=(0,0)	**R**=(1,0) or (0,1), etc. (n.-n)	**R**=(1,1) or (-1,1), etc. (n.n.-n.)	**R**=(2,0) or (0,2), etc. (n.n.-n.)
0	1.9162	0.2802	-0.0470	-0.0275
0.3	1.7422	0.2212	-0.0561	-0.0321
0.6	1.5433	0.1496	-0.0705	-0.0394

These, then, are the parameters which enter the effective *t-J* model. What follows is a brief explanation of how they were obtained. We show the dispersion in Fig. 1 below.

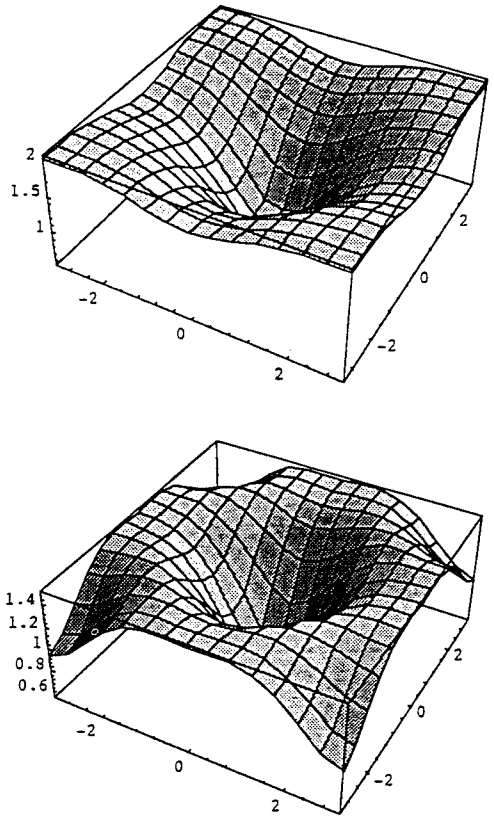

Fig.1. Dispersion of a single "electron" (ε in arbitrary units *vs.* k_x, k_y)
top: for $8\lambda^2=0.5$
bottom: for $8\lambda^2=0.9$

With nearest-neighbor hopping parameter t_{pd} and a 2-body interaction Hamiltonian $H_{2,i}$ centered on the coppers, the starting point is:

$$H=2t_{pd}\sum_{k,\sigma}[c_{k,\sigma}^+(a_{k,\sigma}\cos\frac{k_x}{2}+b_{k,\sigma}\cos\frac{k_y}{2})+H.C.]+\sum_i H_{2,i} \tag{4}$$

where *a* refers to horizontal ligand-oxygen orbital $\Phi_p(x)$,*b* to vertical ligands $\Phi_p(y)$, and *c* to the copper $\Psi_d(x^2-y^2)$ orbital. As these are not mutually orthogonal it is possible to insert an electron in a $p(x)$, and pull it out of one of the 2 neighboring $d(x^2-y^2)$'s with nonzero probability amplitude λ_{pd}. The equivalent statement in second-quantization is simply, $\{a_i,c_j^+\}=\lambda_{pd}$ for i,j nearest-neighbors, in correspondence with Eq.(1). When expressed in terms of the Bloch operators this results in novel anticommutation relations,

$$\{b_{k,\sigma},c^{+}_{k',\sigma'}\} = 2\lambda_{pd}\cos\frac{k_y}{2}\delta_{k,k'}\delta_{\sigma,\sigma'}$$
$$\{a_{k,\sigma},c^{+}_{k',\sigma'}\} = 2\lambda_{pd}\cos\frac{k_x}{2}\delta_{k,k'}\delta_{\sigma,\sigma'} \quad (5)$$

The a and b operators are then expanded in an orthogonal basis of α, β, and c operators. After some algebra, one finds that (4) transforms into:

$$H=t_{pd}\sum_{k,\sigma}\{-[c^{+}_{k,\sigma}(\alpha_{k,\sigma}\omega(k)\sqrt{1-\lambda^2_{pd}\omega^2(k)})+H.C.]$$
$$-2\lambda_{pd}\omega^2(k)c^{+}_{k,\sigma}c_{k,\sigma}\}+\sum_i H_{2,i} \quad (6)$$

The symmetric 2-body interaction Hamiltonian on the i^{th} copper ion is unaffected,

$$H_{2,i}=\frac{1}{2}U_{dd}[(2n_{i,\uparrow}-1)(2n_{i,\downarrow}-1)+1] \quad ; \quad n_{i,\sigma}\equiv c^{+}_{i,\sigma}c_{i,\sigma}. \quad (7)$$

Note the absence of β operators in (6); this implies that a band of localized "β" states is found at 0 energy. As this band is normally fully occupied, together with one electron on the copper we conclude each cell contains at least 3 electrons. For present purposes, we shall denote such a state with 2 electrons on the oxygens and a single electron on the copper as a SU_2 "hole". The energy of an electron on the copper (Cu^{2+}) is 0, in "resonance" with the energy of an electron on an oxygen orbital. In the symmetric model, the energy of Cu^{3+} is set equal to the energy of Cu^{1+}; both are U_{dd}.

Next we decompose the Hamiltonian into the site-diagonal contributions, which include the 2-body forces $H_{2,i}$, and the inter-site contributions. A cell containing 4 electrons can be either in a Zhang-Rice singlet configuration, or in a triplet configuration; the former lies much lower. For present purposes, we shall call this state a singlet or triplet "vacancy". Relative to the "vacancy", a "hole" is positively charged, and a state with 5 electrons is negatively charged. The lowest energy state of a cell with 5 electrons is an SU_2 doublet. (These 5's are essentially the particles which are found to "hop" on background of 4's,and are dynamically subject to an extended t-J model as described above. Some details of the calculation are found in ref. 2.) We shall denote the 5's"electrons" for present purposes. When there is an "electron" at each site the nearest-neighbor antiferromagnetic bonds J produce what is essentially an Heisenberg model of spins 1/2. The hard-core potential makes the fermi statistics irrelevant in the absence of any "vacancies". The electrical conductivity - and , a *fortiori*, superconductivity - depends on the presence of a finite fraction of "vacancies".

The particle-hole symmetry in (7) can be broken in any number of ways, the simplest being by the introduction of a 1-body energy correction $H' \; \Delta e_d(n_{i,\uparrow}+n_{i,\downarrow})$. Note that H' lifts the "resonance" of the d-orbital with the p-orbitals. If Δe_d is a significant fraction of U_{dd} then 2 nearby "vacancies" can scatter into a "hole"-"electron" pair with finite probability amplitude. To the extent that these virtual processes occur, they block configuration-space for "electrons" and act as pair-breakers for Cooper pairs of "electrons" in the superconducting phase. An impurity atom substituting for a copper ion at the i^{th} site would, typically, have a significant magnitude of $|\Delta e_d|$ and would simulate a fixed "vacancy". Combined with a nearby mobile "vacancy" this forms an extended "hole"-"electron" pair complex inimical to the passage of free "electrons". The effective scattering cross-section of such a complex depends on the value of the parameter Δe_d, the amount of deviation from particle-hole symmetry, a property of the particular impurity. As the scattering from such fluctuations could easily exceed the unitarity limit of scattering from those ordinary perturbations which are expressible as fixed potentials, this may provide the explanation of how a negligibly small percentage concentration of substitutional Zn^{2+} suffices to destroy HTS. [4]

CONCLUSION

We have investigated the nature of the quasiparticles in copper oxide planes and find that the most important ones are the complexes we have denoted "electrons","vacancies" and "holes". In addition there are "triplet vacancies". Their role, and that of the high-energy states remains to be clarified. For the "electrons" in the presence of "vacancies", a modified t-J model describes the low-lying dynamics quite satisfactorily. Symmetry-breaking, whether caused by replacing copper with another divalent metal ion, or replacing oxygen by a different ligand, causes spontaneous "electron"-"hole" pair formation in the neighborhood of the impurities, thereby scattering free "electrons" or breaking up all nearby Cooper pairs of such "electrons" in the superconducting phase of the material..

REFERENCES

1. P.W. Anderson, Phys. Rev. **115**, 2 (1959)
2. D.C. Mattis and J.M. Wheatley, "Theory of Superexchange in CuO_2" submitted (Dec. 1994)
3. F.C. Zhang and T.M. Rice, Phys. Rev. **B37**, 3759 (1988)
4. Y. Kitaoka, K. Ishida and K. Asayama, J. Phys. Soc. Jpn. **63**, 2053 (1994) T.R. Chien, Z.Z. Wang and N.P. Ong, Phys. Rev. Lett. **67**, 2088 (1991)

Journal of Superconductivity, Vol. 8, No. 4, 1995

A Simple Theory for the Cuprates: the Antiferromagnetic van Hove Scenario

E. Dagotto[1], A. Nazarenko[1], A. Moreo[1], S. Haas[1], and M. Boninsegni[2]

Received 15 January 1995

A model of weakly interacting hole quasiparticles is proposed to describe the normal state of the high temperature superconductors. The effect of strong correlations is contained in the dispersion of the holes. Many-body effects induce anomalous quasiparticle *flat* bands similar to those observed in recent angle-resolved photoemission experiments. A model of weakly interacting hole quasiparticles is proposed to describe the physics of carriers in the cuprates. The model predicts superconductivity in the $d_{x^2-y^2}$ channel, with a typical $T_c \sim 100K$. The concept of "optimal doping" appears naturally in this model, as well as a large ratio $2\Delta/kT_c \sim 5$.

KEY WORDS: Superconductivity, t-J and Hubbard models, Mechanisms

1. INTRODUCTION

In this paper, it is briefly reviewed a model of hole carriers in an antiferromagnetic background that has been recently introduced by the author and his collaborators under the name of "Antiferromagnetic van Hove" (AFVH) scenario.[1,2]The model explains in a natural way many anomalous properties of the cuprates, and it predicts the presence of d-wave superconductivity as well as the existence of an optimal doping where the critical temperature is maximized. The main assumption is that the normal state of the cuprates can be described by a weakly-interacting dilute gas of hole-quasiparticles.[3] These carriers are strongly dressed by antiferromagnetic spin fluctuations. The influence of antiferromagnetism and strong correlations is contained in the special dispersion relation, $\epsilon(\mathbf{k})$, which is obtained using a numerical method applied to a one band model description of the CuO_2 planes,[1] and the interaction between the quasiparticles is also inspired by the two hole problem in the $t-J$ model. Here, the main points that lead to the AFVH scenario are discussed. The reader is urged to consult the original literature for details.

2. ARPES DATA AND HOLE DISPERSION

Using ARPES techniques it has been recently reported[4,5] that an extended region of flat CuO_2-derived bands very near the Fermi energy exist for Bi2212, Bi2201, Y123 and Y124. Such a universal behavior of the cuprates cannot be explained within band structure calculations which use different effective electronic potentials for each compound. Let us analyze what is the prediction of one band models for ARPES data in the cuprates. The calculation of $\epsilon(\mathbf{k})$ was carried out with the two dimensional $t-J$ model[1] but other models could have been used as long as antiferromagnetic correlations are strong. The $t-J$ model Hamiltonian is defined as

$$H = -t\sum_{\langle ij\rangle}(\tilde{c}^{\dagger}_{i\sigma}\tilde{c}_{j\sigma} + \text{h.c.}) + J\sum_{\langle ij\rangle}(\mathbf{S_i}.\mathbf{S_j} - \frac{1}{4}n_i n_j), \quad (1)$$

where the notation is standard. $\epsilon(\mathbf{k})$ was calculated

[1]Department of Physics, National High Magnetic Field Lab, and Supercomputer Computations Research Institute, Florida State University, Tallahassee, FL 32306, USA

[2]National Center for Supercomputing Applications, University of Illinois, Urbana, IL 61801, USA

0896-1107/95/0800-0483$07.50/0

using a Green Function Monte Carlo (GFMC) method[6] which allows the study of large clusters of 8 × 8, 12 × 12 and 16 × 16 sites minimizing finite size effects. Other techniques (Lanczos method on clusters from 16 to 26 sites and non-crossing diagrammatic approximations), produce results in good agreement with GFMC.[7] In Fig.1a, the numerically evaluated $\epsilon(\mathbf{k})$ is shown for $J/t = 0.4$ along particular directions in the Brillouin zone. The minimum in

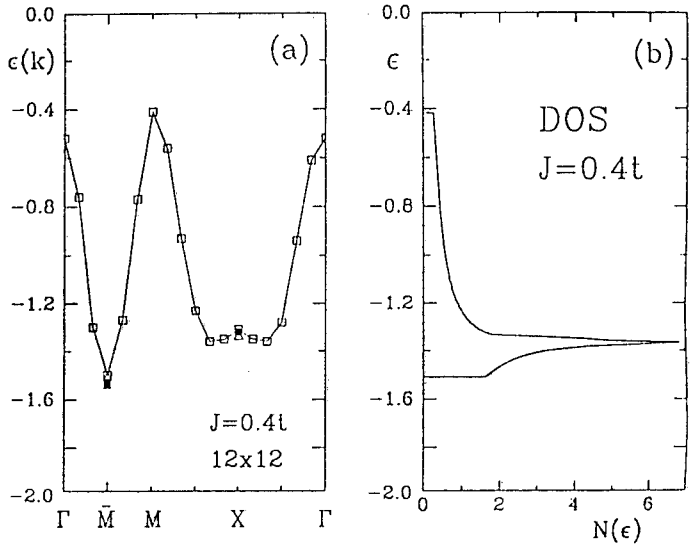

Fig.1.(a) Energy of a hole in the t − J model, $\epsilon(\mathbf{k})$, vs momentum obtained with the GFMC method on a 12 × 12 lattice (open squares) and $J/t = 0.4$ (in units of t). Results for an 8 × 8 cluster (open triangles) and a 16 × 16 cluster (full squares) are shown. (b) Density of states obtained from a fit of the numerical data Fig.1a showing the van-Hove singularity between $\bar{M}$ and X. The unit of energy is t (from Ref.[1]).

the energy is obtained at the $\bar{M}$ point $\mathbf{k} = (\pi/2, \pi/2)$ in agreement with several previous approximate calculations. The main *effective* contribution to $\epsilon(\mathbf{k})$ arises from hole hopping between sites belonging to the same sublattice, to avoid distorting the AF background. The total bandwidth, W, is severely reduced from that of a gas of non-interacting electrons due to the antiferromagnetic correlations (the vertical axis in Fig.1a,b is in units of the hopping t, which is ≈ 0.4eV). Note also that all momenta belonging to the non-interacting 2D Fermi surface $cosk_x + cosk_y = 0$ are very close in energy in the t − J model. In the range $0.3 \leq J/t \leq 0.7$, we found that the energy difference between $(\pi/2, \pi/2)$ and $(0, \pi)$ is approximately 15% to 20% of the total bandwidth. Since $W \sim J$, then important effects are expected at room temperature.[1]This small energy scale produces a Hall coefficient R_H in quantitative agreement with the experimental data for LSCO. For details the reader should consult Ref.[1].

An important detail of Fig.1a is the near flatness of the energy in the vicinity of $\mathbf{k} = (\pi, 0)$. This feature is in good agreement with ARPES results.[4,5] These authors remarked that such a flat region near $(0, \pi)$, $(\pi, 0)$ is observed in several high-Tc compounds and seems a universal property of the hole-doped cuprates. In Ref.[1] and [2] the theoretically observed flat region of Fig.1a was explicitly compared with ARPES experiments finding an excellent agreement. Thus, the flatness of the $\mathbf{k} = (\pi, 0)$ region in the cuprates has a many-body origin, rather than being induced by band effects. Intuitively, it is the presence of saddle-points near X and Y (also noticed in Ref.[3]) which is responsible for the abnormal flatness of the hole dispersion. The presence of the saddle-points produces a density of states DOS with a van-Hove (vH) singularity (Fig.1b). The similarities with the vH scenarios discussed before in the literature are remarkable.[8] In the previous vH ideas the saddle point is generated by band effects, while here *many − body* effects in the CuO_2 planes are crucial, and thus our predictions are universal for all hole-doped cuprates. Even recent experiments by Wells et al.[9] on $Sr_2CuO_2Cl_2$ (half-filling), can be fit well by the inclusion of a hopping amplitude along the diagonals i.e. the $t - t' - J$ model.[10]

3. AF-INDUCED PES SIGNAL

Before continuing with the discussion of the AFVH model for weakly interacting quasiparticles, let us address the presence of antiferromagnetic correlations in the normal state of the cuprates at optimal doping. NMR studies in the normal state of $YBa_2Cu_3O_{6.94}$ (YBCO) suggest an antiferromagnetic correlation length $\xi_{AF} \sim 2a$ (where a is the lattice spacing).[11] Naively, this correlation seems too small to be of relevance. On the other hand, recent photoemission (PES) experimental results by Aebi et al.[12]in $Bi_2Sr_2CaCu_2O_8$ (Bi2212) with Tc=85K, using sequential angle-scanning data acquisition to obtain PES intensities within a narrow energy window near the Fermi energy E_F, reported evidence of antiferromagnetically induced spectral weight above the naive Fermi momentum p_F ($\omega < 0$). This result is compatible with the "shadow bands" scenario of Kampf and Schrieffer[13] which is a consequence of antiferromagnetic correlations in the normal state. At half-filling, these bands above p_F are caused by the enlarged magnetic unit cell of the CuO_2 planes produced by the long range antiferromagnetic order in the ground state. This effective reduction in the

size of the Brillouin zone (BZ) has interesting implications for PES experiments.[13] For example, along the diagonal $p_x = p_y = p$, and assuming long-range order, peaks at momenta p_1=(p, p) and $p_2 = (\pi - p, \pi - p)$ should appear at the same energy location, for any value of p. The PES weight ($\omega < 0$) observed in the region *above* the non-interacting p_F is induced by strong magnetic correlations.[13] How important is this antiferromagnetically generated PES weight at finite density? Only recently aQuantum Monte Carlo and Exact Diagonalization calculation in the proper regime of strong coupling has been discussed.[14]. At density $\langle n \rangle = 0.88$ and coupling $J/t = 0.4$, the AF correlation is of only two lattice spacings as in optimal YBCO. Nevertheless a sharp peak was observed in Ref.[14] near the chemical potential (located at zero energy) even for momenta $(2\pi/3, 2\pi/3)$ i.e. above the naive Fermi momentum. This peak is correlated with AF and dissappears with further increasing of the density. But at $\langle n \rangle = 0.88$ it is still observable, giving more support to the interpretation of Aebi et al.'s data[12]and to theoretical scenarios based on AF.[13,15,2] In short, an antiferromagnetic correlation of two lattice spacings can produce observable results in PES experiments for the cuprates.

4. d-WAVE SUPERCONDUCTIVITY

Let us now introduce interactions among the quasiparticles. We will follow ideas based on antiferromagnetism to produce the pairing attraction needed for superconductivity. However, there is an important distinction with respect to previous "AF-oriented" literature[15]: the DOS of the quasiparticles has a large peak that induces in a natural way the existence of an optimal doping i.e. a density at which the critical temperature is maximized. Previous AF scenarios in the literature do not explain easily the presence of an optimal doping in the cuprates.

Consider the rigid band approximation for the hole dispersion i.e. we assume that the DOS does not change much with doping near half-filling (numerical results supporting this scenario will be published soon). To build up a model for the cuprates we construct the interaction between the quasiparticles based on the two dimensional t − J model, where it is well-known that an effective attractive force exists in an antiferromagnet leading to the bound state of two holes in the d-wave channel.[7]As shown numerically in many studies, the dominant effective attraction is between nearest-neighbors sites. Thus, the model we will use in our studies is

$$H = -\sum_{p,\alpha} \epsilon_p c^{\dagger}_{p\alpha} c_{p\alpha} - |V| \sum_{(ij)} n_i n_j, \quad (2)$$

where $c_{p\alpha}$ is an operator that destroys a quasiparticle with momentum p in sublattice $\alpha = A, B$; n_i is the number operator at site i; $|V| = 0.6J$ (which can be deduced from the t − J model as discussed in Ref.[2]), and ϵ_p is the dispersion evaluated in Ref.[1]. Since in the original t-J language quasiparticles with spin-up(down) move in sublattice A(B), the interaction term can also be written as a spin-spin interaction. This Hamiltonian has been constructed based on strong AF correlations, and it has a vH singularity in the noninteracting DOS, thus we will refer to it as the "antiferromagnetic-van Hove" (AFVH) model.

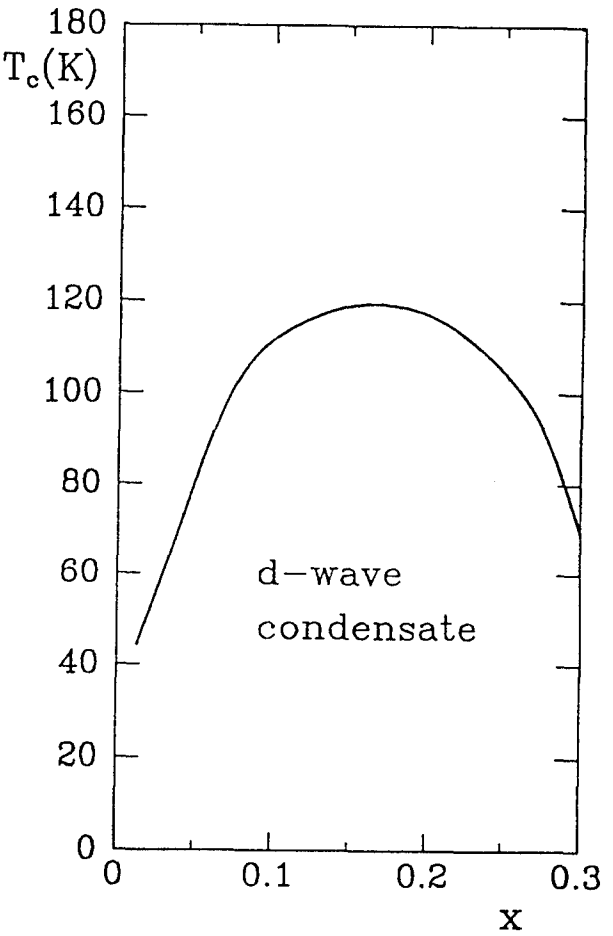

Fig.2.Critical temperature T_c of the AFVH model as a function of hole density x (= 1 − ⟨n⟩) (using the BCS gap equation). The superconducting state is d-wave.

We studied the AFVH model with the standard BCS formalism. Since $|V|/W \sim 0.3$, where W is the bandwidth of the quasiparticles, the gap equation

should produce a reliable estimation of Tc since we are effectively exploring the "weak" coupling regime of the AFVH model. Solving the gap equation on 200 × 200 grids, we observed that the free energy is minimized using a $d_{x^2-y^2}$ order parameter. In Fig.2, T_c against the hole density is shown. Two features need to be remarked: i) an optimal doping exists at which T_c is maximized which is a direct consequence of the large peak in the DOS of the quasiparticles. Note that such a peak would have an important effect even in theories where the hole interaction is phonon mediated rather than spin-wave mediated. In other words, one of the main concepts introduced in Ref.[1] and [2], i.e. a van Hove singularity generated by antiferromagnetism, is not restricted to models where superconductivity is produced by an electronic mechanism; ii) the optimal doping (15%) and optimal $T_c \sim 100$K are in good agreement with the cuprates phenomenology. Although in the AFVH model the natural scale of the problem is J $\sim$ 1000K, since the ratio between coupling and bandwidth is small, T_c is further reduced in the weak coupling BCS formalism to about 100K. Note that this quantitative agreement with experiments is obtained without the need of ad-hoc fitting parameters.

The ratio $R(T) = 2\Delta_{max}(T)/kT_c$ can be calculated from the gap equation, (for a d-wave condensate, $\Delta_{max}(T)$ is defined as the maximum value of the gap). At $T = 0$, the AFVH model predicts $R(0) = 5.2$ while recent tunneling experiments[16] give 6.2.Other experiments have reported a smaller value for R(0). For example, ARPES data by Ma et al.[17] obtained $R(0) = 4.6$, while an average over the pre-1992 literature[18]suggested $R(0) = 5 \pm 1$ supporting the results of the AFVH model. We have also verified that an important feature of previous vH scenarios[8] also exists in our model, i.e. a quasiparticle lifetime linear with frequency at the optimal doping.[2] The stability of the van Hove scenario with respect to perturbations, like a small amount of disorder, has been addressed explicitly in Ref.[2] The conclusion is that the number of states in the vicinity of the vH singularity is of the order of the total number of states in the full band, and thus the influence of disorder on the DOS is mild.

Many calculations are in preparation. In particular, the Hall coefficient at finite temperature, specific heat, thermopower coefficient, the possibility of a nonzero isotope effect in the AFVH scenario, and the phenomenology of the d-wave superconducting model defined in Eq.(2) will be addressed soon.

ACKNOWLEDGMENTS

Discussions with J. C. Campuzano, D. W. Hess, M. Horbach, R. Laughlin, J. Ma, R. S. Markiewicz, M. Onellion, J. Osterwalder, J. Riera, Z.-X. Shen, S. Trugman, and B. O. Wells are gratefully acknowledged. E.D. and A.M. are supported by the ONR under N00014-93-0495, and the donors of the PRF administered by the ACS. A.N. is supported by NHMFL and S.H. is supported by SCRI.

REFERENCES

1. E. Dagotto, A. Nazarenko and M. Boninsegni, Phys. Rev. Lett. **73**, 728 (1994).
2. E. Dagotto, A. Nazarenko, and A. Moreo, Phys. Rev. Lett. **74**, 310 (1995).
3. In this respect our approach is similar to that of S. Trugman, Phys. Rev. Lett. **65**, 500 (1990); Phys. Rev. B **37**, 1597 (1988).
4. D. S. Dessau et al., Phys. Rev. Lett. **71**, 2781 (1993); K. J. Gofron et al., J. Phys. Chem. Solids **54**, 1193 (1993); Z.-X. Shen and D. S. Dessau, preprint (1994); J. Ma, et al., preprint.
5. A. A. Abrikosov, J. C. Campuzano, and K. Gofron, Physica **C 214**, 73 (1993).
6. M. Boninsegni, Phys. Lett. **A 188**, 330 (1994); M. Boninsegni and E. Manousakis, Phys. Rev. B **46**, 560 (1992).
7. For a comprehensive review of this issue, see E. Dagotto, Rev. Mod. Phys. **66**, 763 (1994).
8. C. C. Tsuei et al., Phys. Rev. Lett. **65**, 2724 (1990); R. S. Markiewicz, J. Phys. Condens. Matt. **2**, 6223 (1990); D. M. Newns, et al., Phys. Rev. B **43**, 3075 (1991).
9. B.O. Wells, et al., Phys. Rev. Lett. **00**, 00 (1994).
10. A. Nazarenko, K. Vos, S. Haas, E. Dagotto, and R. Gooding, preprint (1994).
11. T. Imai et al., Phys. Rev. **B 47**, 9158 (1993).
12. P. Aebi et al., Phys. Rev. Lett. **72**, 2757 (1994).
13. A. Kampf and J. R. Schrieffer, Phys. Rev. **B 41**, 6399 (1990); Phys. Rev. **B42**, 7967 (1990).
14. S. Haas, A. Moreo and E. Dagotto, NHMFL preprint. See also R. Putz et al., preprint.
15. N. E. Bickers, D. J. Scalapino, and S. R. White, Phys. Rev. Lett. **62**, 961 (1989); E. Dagotto, J. Riera and A. P. Young, Phys. Rev. **B 42**, 2347 (1990); P. Monthoux and D. Pines, Phys. Rev. Lett. **69**, 961 (1992); E. Dagotto and J. Riera, Phys. Rev. Lett. **70**, 682 (1993).
16. S. I. Vedeneev et al., Phys. Rev. **B 49**, 9823 (1994).
17. Jian Ma et al., Madison preprint, May 1994.
18. B. Batlogg, Springer Series, Vol. 106, Eds.: S. Maekawa and M. Sato, page 219 (1992).

Journal of Superconductivity, Vol. 8, No. 4, 1995

Symmetry Tests Using the Half-Integer Flux Quantum Effect in Cuprate Superconducting Rings

J.R. Kirtley[1], C.C. Tsuei[1], J.Z. Sun[1], C.C. Chi[2], Lock See Yu-Jahnes[1], A. Gupta[1], M. Rupp[1], and M.B. Ketchen[1]

Received 4 January 1995

The presence or absence of the half-integer flux quantum effect in controlled orientation tricrystal grain boundary rings is a general test of the phase of the superconducting order parameter. One such test proves that this effect is symmetry dependent, and that the order parameter in $YBa_2Cu_3O_{7-\delta}$ has lobes and nodes consistent with d-wave symmetry. Our measurements show that the flux in the 1/2 integer ground state is quantized to $\Phi_0/2$ within $\pm$ 3%. This puts limits on the imaginary component of the superconducting order parameter in $YBa_2Cu_3O_{7-\delta}$.

KEY WORDS: Symmetry; tricrystal; half-integer; flux-quanta.

Possibly the single most controversial topic in solid-state physics at present is the mechanism for high-T_c superconductivity. Of special interest is the question of whether the interaction that forms Cooper pairs in the high-T_c superconductors is mediated by phonons or by spin-fluctuations. Although there is a great deal of controversy over how to distinguish between these two possibilities, one test is nearly universally agreed upon: If the superconducting order parameter does not have d-wave ($k_x^2 - k_y^2$) symmetry, then the pairing mechanism probably does not involve spin-fluctuations[1].

A distinctive feature of an order parameter with d-wave symmetry is that it switches sign on rotation by 90 degrees relative to the crystalline axes. Almost a decade ago Geshkenbein et al.[2] predicted that such a sign change in unconventional superconductors could result in flux quantization with half the conventional value. The basic argument is simple: Consider a superconducting ring with one Josephson weak link arranged such that in the absence of a supercurrent there is a sign change of the superconducting order parameter across the weak link. A ring with an odd number of such sign changes, or π shifts in phase, is called a π-ring. A π-shift costs Josephson coupling energy, and if the inductive energy associated with circulating supercurrent is less than this energy ($2\pi LI_c >> \Phi_0$, where L is the ring inductance and $\Phi_0 = h/2e = 20.7G - \mu m^2$ is the flux quantum), it is energetically favorable for a spontaneous magnetization of $\Phi_0/2$ to appear in the ring. The flux threading the ring causes a phase change of π to develop around the ring, which adds to the π change at the interface for a total change of 2π, making the order parameter single valued. There is a ladder of allowed flux states in such a ring with values $(N + 1/2)\Phi_0$, where N is an integer.

There have been a number of reports of indirect evidence for such spontaneous magnetization, either from the magnetic properties of granular high-T_c films[3],[4], or from measurements of SQUIDs with special geometries[5], [6]. Recently we reported the first direct observation of half-integer quantization, in tricrystal grain-boundary junction thin-film rings of $YBa_2Cu_3O_{7-\delta}$[7], using a scanning SQUID microscope. This observation strongly supports d-wave pairing, since d-wave pairing provides a natural mechanism for π phase shifts.

[1]IBM Thomas J. Watson Research Center, P.O. Box 218, Yorktown Heights, NY 10598.
[2] Materials Science Center and Department of Physics, National Tsing-Hua University, Taiwan, R.O.C.

However, there have been at least two symmetry independent mechanisms, spin-flip scattering by magnetic impurities at the tunnel barrier[8], and indirect tunneling through a localized state (correlation effects) [9] suggested to cause π-phase shifts at the junction interfaces, resulting in the 1/2 integer flux quantum effect in our 3-junction rings. We have designed and built 2 samples with slightly different crystalline and grain boundary angles, chosen so that one 3-junction ring should show the 1/2 integer flux quantum effect, while the other should not, if $YBa_2Cu_3O_{7-\delta}$ is a d-wave superconductor. The results are as predicted for a d-wave superconductor, confirming that this effect is symmetry dependent. In principle, symmetry test experiments with the standard 2-junction SQUID geometry [5],[6],[10] should also provide a distinction between d-wave symmetry and symmetry independent mechanisms- in favor of d-wave. However, these experiments are controversial because of their complex geometries[11].

Figure 1 shows the design parameters for the two samples. The rings are photolithographically patterned, ion milled films 1200 Å thick, 10 μm wide, with 24 μm inside diameter, of epitaxially grown $YBa_2Cu_3O_{7-\delta}$ on the substrate. The substrate is $SrTiO_3$ cut, reoriented, polished, and fused in such a way that three pieces with different crystalline orientations meet at a point. The $YBa_2Cu_3O_{7-\delta}$ grows epitaxially and with axes aligned along the underlying $SrTiO_3$. The polar plots in Figure 1 show the orientations of an assumed d-wave superconducting order parameter aligned with the crystalline a and b axes. Junctions result each time a ring crosses a grain boundary. The strength of the Josephson coupling across each grain boundary is proportional to the product of the components of the order parameter projected onto the normal to the interface. The 3-junction ring in the π-ring geometry has an odd number of sign changes of the normal component of the order parameter across the grain boundaries, and the 3-junction ring in the 0-ring geometry has an even number of sign changes, independent of the sign chosen to align along, e.g. the (100) axis for any of the sections of the ring. Therefore, while the 0-junction rings and 2-junction rings should show integer flux quantization, only the 3-junction ring in the π-ring geometry should show the 1/2 integer quantum effect if it is due to nodes in the superconducting order parameter, but both 3-junction rings should show the effect if it is due to a symmetry-independent mechanism. Sample characterization has been described elsewhere[7]. The only difference between sample fabrication and measurement of the two samples was the tricrystal substrate geometry. In particular, both samples had $I_cL \sim 100\Phi_0$ for all of the rings with junctions.

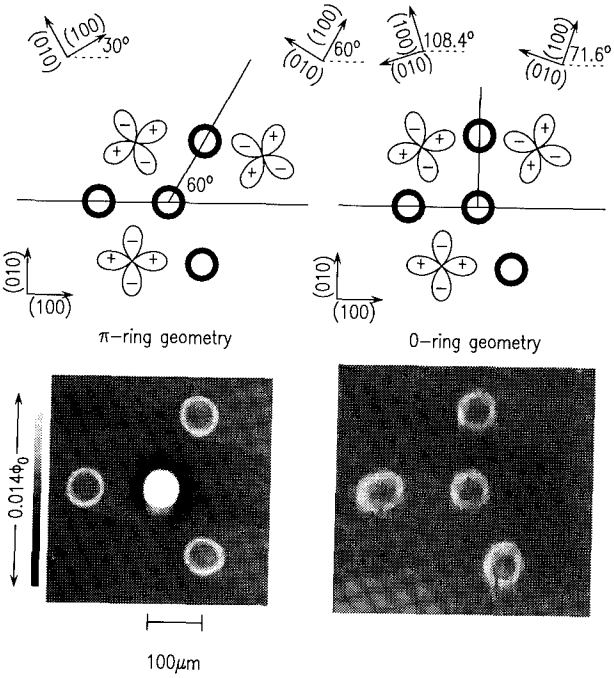

Fig. 1. The upper section shows the sample geometries for the two tricrystal ring samples described in this paper. The lower section shows scanning SQUID microscope images of these samples. The 3-junction ring in the π-ring geometry has $\Phi_0/2$ flux spontaneously generated in it. All of the other rings have no flux in them.

The lower section of Figure 1 compares scanning Superconducting Quantum Interference Device (SQUID) microscope [12],[13], [14], [15] images from a $YBa_2Cu_3O_{7-\delta}$ tricrystal ring sample with the π-ring geometry (a) (a different sample but identical geometry as in Reference [7]) and the 0-ring geometry (b), cooled to the measuring temperature of 4.2K in fields less than 2 mGauss. These images were taken by mechanically scanning the 10 micron diameter pickup loop of a SQUID relative to the sample. The end of the SQUID substrate was pol-

ished to a sharp point about 10 microns from the center of the pickup loop. The images were taken with the SQUID substrate oriented about 20 degrees from parallel to and in direct contact with the sample, so that the loop sampled primarily the normal component of the magnetic field about 3 microns above the sample surface. The images in Figure 1 were taken in zero field. The false color table in this image spans a range of 0.014 Φ_0 change in flux through the sensor SQUID. The mutual inductance between a ring and the pickup loop centered above a ring is $\sim$ 2.4 pH, and the self-inductance of the rings is about 100 pH, so that $\Phi_0/2$ flux in the ring couples about $0.012\Phi_0$ into the sensor loop: The flux threading through the center 3-junction ring in the π-ring geometry sample (a) is very close to $\Phi_0/2$, while the others have very close to 0 flux. The rings with no flux trapped in them are visible because of slight changes in the inductance of the SQUID pickup loop when it passes over the superconducting material in the rings. Images taken with these samples cooled in different fields showed that the 3-junction π-ring always had $(N+1/2)\ \Phi_0$ (N an integer) flux in it, while the 3-junction 0-ring always had $N\Phi_0$, ruling out symmetry-independent mechanisms for the 1/2 integer flux quantization.

We calibrated the SQUID signal resulting from flux trapped in our rings in three ways, all of which agreed within 10%. First, direct calculation as described above, gave very good agreement both for the absoluted magnitude, and the detailed shape, of the images observed, assuming $\Phi_0/2$ flux was trapped in the 3-junction ring in the π-ring geometry. Second, the sensor response was measured when single flux quanta were driven into the rings by applying a large magnetic field[7]. We describe a third method, which we term "field titration"[16], here. Figure 2 shows a scanning SQUID microscope image of one of our π-ring samples, cooled rapidly through the superconducting transition in a field of about 15mG. The dynamics of the cooling process must be very complex, but somehow the sample has arrived at a state where the central 3-junction ring has $3\Phi_0/2$ flux trapped in it, the upper right and left hand 2-junction rings have $2\Phi_0$ flux, and the lower 0-junction ring has $3\Phi_0$ flux.

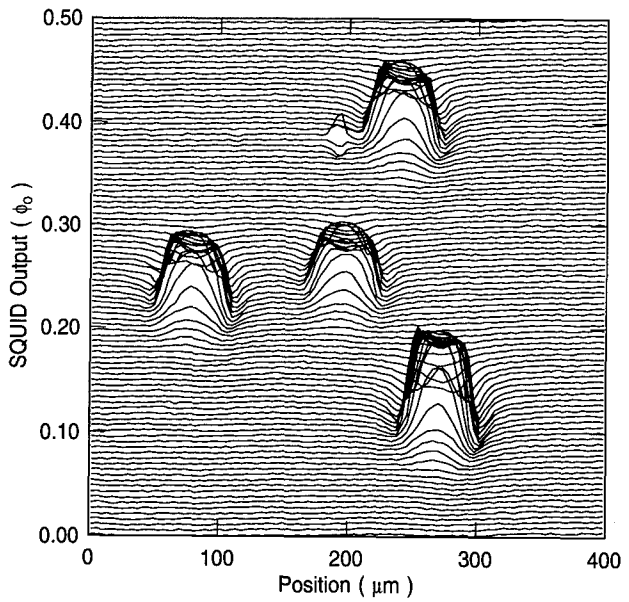

Fig. 2. Scanning SQUID microscope image of the π-ring tricrystal sample. Here the center 3-junction ring has 3/2 flux quanta in it, the left and top 2-junction rings have 2 flux quanta, and the bottom 0-junction ring has 3 flux quanta in it.

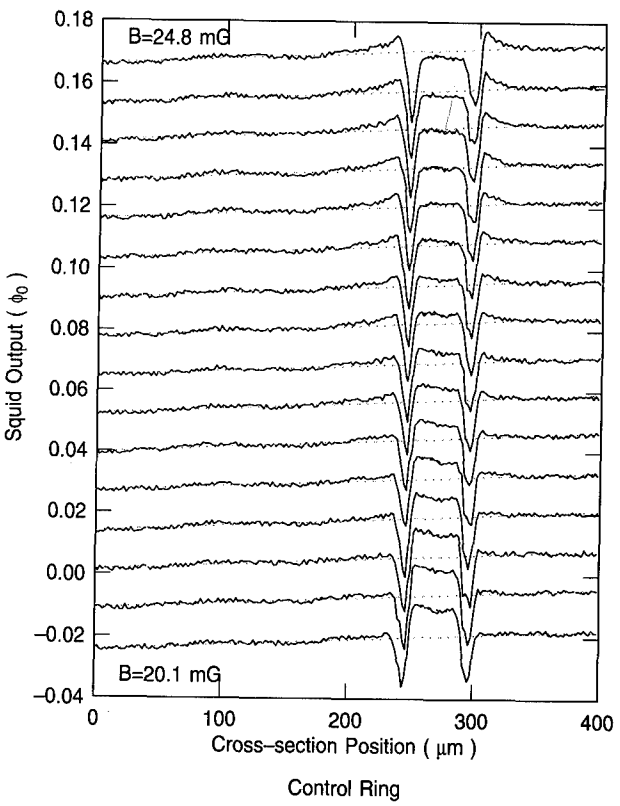

Fig. 3. Scanning SQUID microscope cross sections through the 0-junction ring, for a series of evenly spaced applied external magnetic fields.

Figure 3 shows the results when the SQUID pickup loop is scanned over the control ring while the applied magnetic field is changed from 20.1mG to 24.8mG in even steps. At a field of 23.8mG, the field inside and outside the ring is the same. Taking the effective area of the ring to be the geometric mean area $A = \pi r_i r_o = 2564\mu m^2$, where r_i, r_o are the inner and outer radii of the rings respectively, the flux through it is $\Phi = BA = 61\ G\text{-}\mu m^2 = 2.95\ \Phi_0$. Figure 4 shows a plot of the difference in the SQUID output signal as a function of applied magnetic field, obtained by fitting the data inside and outside the rings to straight lines, for all of the rings in the π-ring sample. The x-axis intercepts for the two 2-junction rings differ by 1.5%, which we attribute to slight lithographic differences in the two rings. If we assume that the 0-junction and 2-junction rings have exactly 3 and 2 flux quanta in them respectively, then the effective area for the rings is $2572 \pm 53\mu m^2$, in good agreement with the geometric mean area of $2564\mu m^2$:. Such measurements with all of the rings in their lowest flux state show that the 3-junction ring in the π-ring geometry has $\Phi = 0.490 \pm 0.015\Phi_0$ trapped in it. Further, the difference in flux between any of the other rings in either the π-ring or the 0-ring geometries is $|\Delta\Phi| < 0.01\Phi_0$. Our calculations indicate that any e.g. s-wave component to a presumed s+id superconducting order parameter would alter the flux quantization condition away from exactly $\Phi_0/2$ by roughly the fractional portion that is s-wave. We therefore conclude that the superconducting order parameter in $YBa_2Cu_3O_{7-\delta}$ has lobes and nodes consistent with d-wave symmetry and put experimental limits of about 4% on any out of phase s-wave component.

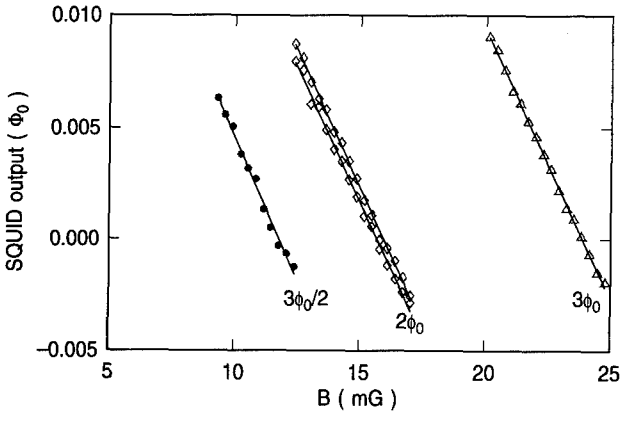

Fig. 4. Difference in sensor flux for the sensor positioned at the center of the ring vs outside the ring, for all of the rings. These measurements give a value of $0.490 \pm 0.015\Phi_0$ flux enclosed in the 3-junction π-ring sample in the lowest flux state.

Experiments on niobium rings with the same size, shape, and I_cL products as our $YBa_2Cu_3O_{7-\delta}$ rings, always show the conventional integer flux quantization. Recently we have repeated these experiments with $HgBa_2CaCu_2O_6$ tricrystal rings: They also show 1/2 integer flux quantization in the 3-junction ring in the π-ring geometry. This result is significant because $HgBa_2CaCu_2O_6$ does not have CuO chains or twins, and has tetragonal rather than orthorhombic symmetry. An experimental geometry designed to distinguish between d-wave ($\Delta(k) \sim \cos(2\theta)$) and extended s-wave ($\Delta(k) \sim \cos(4\theta)$) favors d-wave pairing. We will report on these results in detail elsewhere.

Partial financial support from the Max Planck Research Prize (CCT) from Germany is gratefully acknowledged. The scanning SQUID microscope used in this study was developed under the auspices of the Consortium for Superconducting Electronics.

REFERENCES

1. D.J. Scalapino, Physics Reports, in press.
2. V.B. Geshkenbein, A.I. Larkin, and A. Barone, Phys. Rev. B**36**,235(1987).
3. W. Braunisch et al., Phys. Rev. Lett. **68**,1908 (1992).
4. Manfred Sigrist and T.M. Rice, J. Phys. Soc. Japan, **61**,4283(1992).
5. D.A. Wollman, D.J. van Harlingen, W.C. Lee, D.M. Ginsberg, and A.J. Leggett, Phys. Rev. Lett. **71**,2134(1993).
6. D.A. Brawner, and H.R. Ott, Phys. Rev. B **50**,6530(1994).
7. C.C. Tsuei, et al. Phys. Rev. Lett. **73**,593(1994).
8. L.N. Bulaevski, V.V. Kuzii, and A.A. Sobyanin, JETP Lett. **25**,290(1977).
9. B.I. Spivak, and S. Kivelson, Phys. Rev. B **43**,3740(1991).
10. A. Mathai, et al. submitted to Phys. Rev. Lett..
11. R.A. Klemm, Phys. Rev. Lett. **73**,1871(1994).
12 F.P. Rogers, " A Device for Experimental Observation of Flux Vortices Trapped in Superconducting Thin Films", MIT, Boston, MA, Master's dissertation, 1983
13. L.N. Vu, M.S. Wistrom, and D.J. van Harlingen, Appl. Phys. Lett. **63**,1693(1993).
14. R.C. Black et al. Appl. Phys. Lett.**62**,2128(1993).
15. J.R. Kirtley et al. submitted to Applied Physics Letters.
16. J.R. Kirtley et al. Nature in press.

Journal of Superconductivity, Vol. 8, No. 4, 1995

Experimental determination of the symmetry of the order parameter in YBCO

A. Mathai, Y. Gim, R. C. Black, A. Amar and F. C. Wellstood

Received 31 January 1995

At present, the symmetry of the order parameter in the high temperature superconductor YBCO is quite controversial. Recent experiments using SQUIDs and Josephson junctions appear to support competing theories, with some experiments supporting a $d_{x^2-y^2}$ pairing symmetry for the order parameter and others a s-wave pairing symmetry. We note that a number of factors such as trapped flux, magnetic field gradients and SQUID asymmetries could lead such measurements astray. We use a Scanning SQUID Microscope and a time-reversal invariance test to resolve these experimental problems. We find the order parameter in YBCO has a time-reversal invariant $d_{x^2-y^2}$ symmetric component. We estimate the amplitude of any *imaginary* s-wave symmetric component to be less than 4% and any *real* s-wave component to be less than 82%.

KEY WORDS: Superconductivity; pairing symmetry, YBCO, SQUID

1. INTRODUCTION

The symmetry of the order parameter in $YBa_2Cu_3O_7$ (YBCO) has been the subject of much controversy [1]. Some novel theories of high temperature superconductivity predict a $d_{x^2-y^2}$ spatial pairing symmetry for the order parameter [2] while a competing model, the interlayer coupling model, predicts an anisotropic s-wave pairing symmetry [3]. Experimentally, some work using SQUIDs and Josephson junctions has supported a $d_{x^2-y^2}$ pairing symmetry in YBCO [4-11] while others have not [12,13].

Unfortunately, most SQUID and junction experiments are susceptible to systematic errors due to, for example, trapped flux, magnetic field gradients or SQUID asymmetries. We resolve these experimental problems by using a Scanning SQUID Microscope to both image and measure the screening response of sample SQUIDs.

2. THE EXPERIMENT

2.1. Basic Idea

Consider the type 'a-b' YBCO-Ag-PbIn SQUID shown in Fig. 1(a) [4]. PbIn is a conventional low-T_c superconductor and is s-wave symmetric. If YBCO has a $d_{x^2-y^2}$ pairing symmetry, the wavefunction has four lobes with adjacent lobes having opposite phase. In zero magnetic field, this produces an intrinsic phase shift, $\delta_d=\pi$, for pairs moving along the a-axis with respect to pairs moving along the b-axis. If YBCO is s-wave symmetric, there is no such phase shift, i.e $\delta_d=0$.

As in a simple superconducting loop, a SQUID tries to maintain the total flux in its loop at a constant value by generating a screening current, J, that opposes any externally applied flux. The magnitude of the screening current is limited by the critical current, I_0, of the SQUID. A plot of screening current vs. applied flux thus produces a series of almost parallel lines separated horizontally from one another by about 1 flux quantum

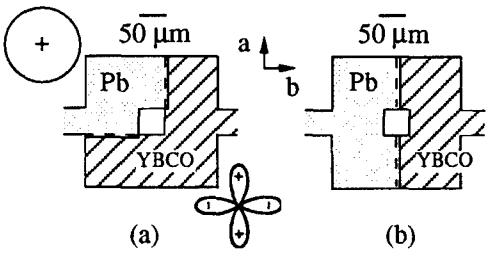

Fig. 1. (a) Schematic of type a-b sample SQUID, dashed lines show location of YBCO-Ag-PbIn edge junctions, (b) type a-a SQUID.

Center for Superconductivity Research, Department of Physics, University of Maryland, College Park, MD 20742.

0896-1107/95/0800-0491$07.50/0

Φ_0=h/2e. Fig. 2(a) shows the s-wave case. The overall envelope is due to the magnetic field dependence of the junction critical currents. For the d-wave case, the lines are shifted along the flux axis by 1/2 Φ_0, due to the intrinsic phase shift of π, as shown in Fig. 2(b).

2.2. Time-reversal symmetry

This 1/2 Φ_0 shift has a profound effect on the time-reversal properties of the J-Φ data. Reversing time is equivalent to reversing the directions of all currents and magnetic fields [see Fig. 2(c)]. Mathematically, the equations for a SQUID are time-reversal invariant only if $\delta_d=n\pi$; n=0,±1, ±2,..... In these cases if (J,Φ) is a solution, (-J,-Φ) is also a solution [10]. This mapping, (J,Φ) → (-J,-Φ), is an inversion about the origin, (J,Φ)=(0,0), and only one point in this plot, the origin, maps onto itself. In the s-wave case, where a screening line goes through the origin, we extend this to saying that the entire line going through (0,0) maps onto itself.

The invariant point (J,Φ)=(0,0) is a solution in the s-wave case but not in the d-wave case. Thus, the presence or absence of a point (or state) that time-reversal maps onto itself will tell us if YBCO is s-wave or d-wave. The absence of time-reversal symmetry would indicate a complex symmetry [14,15] or the presence of stray fields which do not time-reverse.

As a control for the experiment, we have fabricated a type 'a-a' YBCO-Ag-PbIn SQUID with the geometry shown in Fig. 1(b). There is no intrinsic phase shift in this type of SQUID, so that δ_d=0 regardless of the pairing symmetry of YBCO.

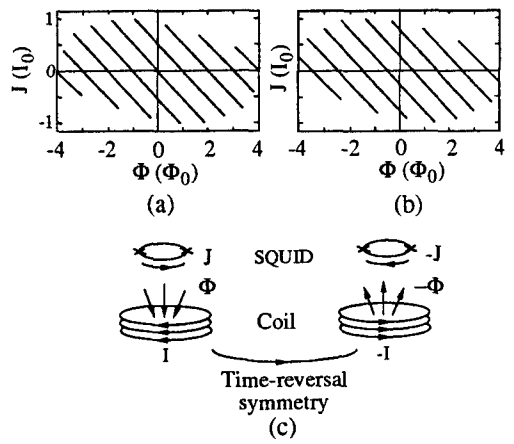

Fig. 2. (a) Schematic of J(Φ) for δ_d=0 case, (b) Schematic of J(Φ) for δ_d=π case, (c) Time-reversal symmetry.

2.3. Experimental arrangements

The sensor in our Scanning SQUID Microscope [10] is a low-T_c Nb-PbIn SQUID. Fabrication details of the sample have been given elsewhere [10]. We fabricate six YBCO-Ag-PbIn SQUIDs on a $LaAlO_3$ substrate, three of the a-b type and three of the a-a type (see Fig. 1). The critical currents range from 90 μA to 270 μA, which correspond to $\beta=2LI_0/\Phi_0$ ranging from 7 to 21, where L is the SQUID inductance and I_0 is the average critical current of the junctions in zero magnetic field. We will discuss in detail results from one pair of a-a and a-b SQUIDs with β values of 8 and 21, respectively.

3. SCREENING DATA

To rule out any false signatures of d-wave superconductivity from trapped flux, we first take a magnetic scan of the sample. We eliminate any detected trapped flux by heating the sample above the T_c of YBCO and then cooling down. We then position the sensor over the center of one of the sample SQUIDs and measure the fields produced by current flowing around the SQUID loop, J, vs. the applied flux, Φ.

Figure 3 shows J-Φ data from the a-b SQUID, with no bias current applied to the SQUID. The data is taken by ramping the applied field back and forth with varying amplitude to sample the endpoints many times and fill in the SQUID states. To check for time-reversal invariance, we need to reverse all the fields applied to the sample: this includes any fields caused by the sensor. The data in Fig. 3(a) is taken with all the currents in the sensor flowing in one direction ('positive'). We turn down the applied field to zero at the end of the data taking and note which line the SQUID is on [open circle in Fig. 3(a)]. We then turn down the currents to the sensor, reverse the leads and restart the measurement. The first data point of this 'negative' data set is labelled with a closed circle and the rest with dots in Fig. 3(b). We see that the time-reversal is very good, i.e., flipping the 'positive' data about the J and Φ axes produces a plot which is nearly identical to the 'negative' data set. This is shown in Fig. 3(b) where we show the time-reversed 'positive' data as lines.

The absence of a state that time-reverses onto itself would confirm that $\delta_d=\pi$. Since the magnetic field changes involved in reversing the leads are small, the number of flux quanta in the SQUID should be

unchanged. Thus the states labelled by the open circle in Fig. 3(a) and the closed circle in Fig. 3(b) are really the same state n, i.e. have the same flux, $n\Phi_0$, in the SQUID loop. Under time-reversal for the a-b SQUID, we see that the state n marked with the closed circle in Fig 3(b) [or by open circle in fig 3(a)] time-reverses onto the state next to it, -n (marked with open square). *There is no state in between that maps onto itself and thus there is no n=0 state.*

To provide a quantitative analysis of the time-reversal, we fit the envelope of the 'positive' data to the envelope of the 'negative' data and then measure the deviations of the states from a perfect fit. For the data in Figures 3(a) and 3(b), we find $\delta_d=(1.02\pm0.08)\pi$.

As a check on the experiment, Figures 3(c) and 3(d) show similar sets of J-Φ data for the a-a SQUID. The state marked with the closed circle maps into a state 6 Φ_0 away. Thus there is a state exactly mid-way, marked with arrows, that time-reverses onto itself. This is the n=0 state. Further analysis reveals that $\delta_d=(-0.01\pm0.04)\pi$. In all, we have measured six SQUIDs. For the three a-a SQUIDs, there is always a state that maps onto itself. For the three a-b SQUIDs, there is no such state. Our best estimate for the shift in the three a-b SQUIDs is $\delta_d=(0.98\pm0.05)\pi$ [10].

4. SCREENING DATA WITH BIAS CURRENT

We have also taken J-Φ data while sending a dc current, I_{bias}, into the sample SQUIDs. As we increase I_{bias}, the maximum amplitude of the screening current decreases. If we increase I_{bias} until the SQUID goes into the finite voltage state, we can also make resistance measurements of the SQUIDs as a function of the applied field.

Some of the prior experimental evidence for $d_{x^2-y^2}$ pairing in YBCO has been derived from resistance measurements of SQUIDs and involves a linear extrapolation of the resistance data to the superconducting state of the SQUID [4,7]. To check the validity of such an extrapolation we also make resistance measurements for different values of I_{bias}. We then take 'positive' J-Φ data for lower values of I_{bias}

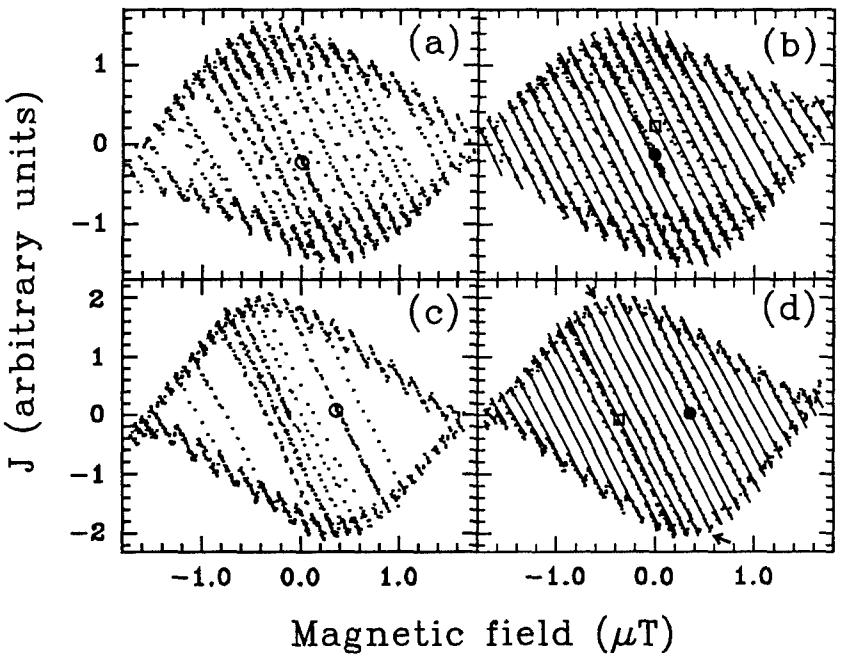

Fig. 3. (a) Dots are measured J vs. magnetic field for an a-b SQUID with positive sensor bias. Open circle shows ending SQUID state n for positive data. (b) Dots are measured J vs. magnetic field for the same SQUID with negative sensor bias. Closed circle shows starting SQUID state n for negative data. Lines are fits to time-reversed positive data (open square marks the time-reversed ending state, -n). We see that the closed circle and the open square lie on adjacent states. This shows that n=-1/2 and there is no state that time-reverses onto itself. (c) Corresponding data for an a-a SQUID with positive sensor bias. (d) Dots show data for an a-a SQUID with negative sensor bias and lines are fits to the time-reversed positive data. We see that the closed circle (state n) and the open square (state -n) have six states in between them. So there is a state exactly in between that time-reverses onto itself (marked with arrows) and n=3.

all the way down to zero bias.

In Fig. 4, we show such data for another a-b SQUID. For this SQUID, I_0=130μA (β≈10) [10]. We show the resistance data as a plot of I_{bias} vs. the flux at the resistance minima. We also present the J-Φ data as a plot of I_{bias} vs. the flux at the mid-points of the SQUID states. The dashed lines join the data points and are a guide to the eye. As we see, the plot bends. This is due to the critical current asymmetry of the two junctions of the sample SQUID: as we increase I_{bias}, the current divides unequally in the two arms of the SQUID and so couples flux into the SQUID loop. This shows that a linear extrapolation from the finite voltage state is invalid.

4. POSSIBLE COMPONENTS OF SYMMETRY

We can use our results to put upper bounds on any real or imaginary s-wave symmetric components of the order parameter. For our analysis, we use wavefunctions that are two-dimensional. In k-space we write the angular part of the $d_{x^2-y^2}$ component and that of any isotropic s-wave symmetric component respectively, as

$$\psi_d(\phi) = \cos 2\phi/\sqrt{\pi}, \qquad \psi_s(\phi) = 1/\sqrt{2\pi} \qquad (1)$$

Here, φ is the polar angle.

If an *imaginary* isotropic s-wave symmetric component is present, then the order parameter is

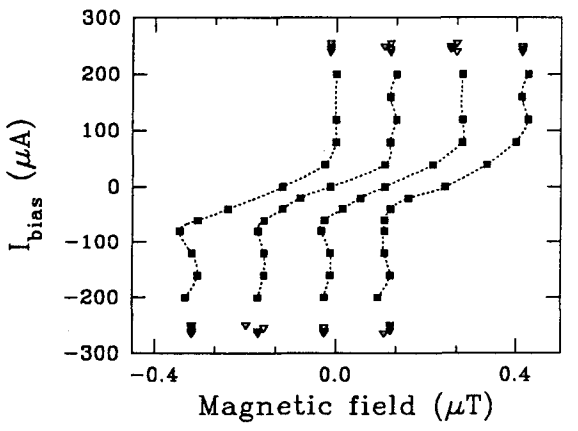

Fig. 4. Open triangles show resistance data as a plot of I_{bias} of a-b SQUID vs. the flux at the resistance minima. Closed squares show J-Φ data as a plot of the I_{bias} vs. the flux at the mid-points of the SQUID states. Dashed lines join the data points and are a guide to the eye. The bend in the plot is due to the critical current asymmetry of the SQUID.

$$\psi = a\psi_d + ib\psi_s, \qquad \text{where, } a^2+b^2=1 \qquad (3)$$

Solving for b and using our best estimate of δ_d=0.98π gives b ≤0.04.

Now suppose the order parameter has a real isotropic s-wave symmetric component, c. Noting that, experimentally, we find a sign reversal for φ=0 and setting ψ slightly less than zero yields an *upper* bound c<0.82.

5. CONCLUSIONS

In conclusion, we have used a scanning SQUID microscope to find that the pairing symmetry in YBCO has a time-reversal invariant $d_{x^2-y^2}$ symmetric component. We find that any *real* isotropic s-wave component must have an amplitude of less than 82%, and that any *imaginary* isotropic s-wave component must have an amplitude of less than 4%.

ACKNOWLEDGMENTS

We thank T. Venkatesan, I. Takeuchi, S. Mao and C. Doughty for assistance with sample fabrication. We also acknowledge discussions with D. Scalapino, V. Emery and S. Anlage.

REFERENCES

1. See for example: B. G. Levi, *Physics Today*, **5** 17, (1993).
2. N. E. Bickers, D. J. Scalapino and S. R. White, *Phys. Rev. Lett.* **62**, 961, (1989); P. Monthoux, A. V. Balatsky and D. Pines, *Phys. Rev. B*, **46**, 14803 (1992).
3. S. Chakravarty, A. Sudbo, P. W. Anderson, and S. Strong, *Science* **261**, 337, (1993).
4. D. A. Wollman, D. J. Van Harlingen, W. C. Lee, D. M. Ginsburg, and A. J. Leggett, *Phys. Rev. Lett.* **71**, 2134, (1993).
5. D. A. Wollman, D. J. Van Harlingen, J. Gianpintzakis, and D. M. Ginsburg, unpublished.
6. I. Iguchi and Z. Wen, *Phys. Rev. B* **49**, 12388, (1994).
7. D. A. Brawner and H. R. Ott, *Phys. Rev. B* **50**, 6530, (1994).
8. C. C. Tsuei, J. R. Kirtley, C. C. Chi, Lock See Yu-Jahnes, A. Gupta, T. Shaw, J. Z. Sun and M. B. Ketchen, *Phys. Rev. Lett.* **73**, 593, (1994).
9. J. Miller Jr., Q. Y. Ying, Z. G. Zou, N. Q. Fan, J. H. Xu, M. F. Davis and J. C. Wolfe, unpublished.
10. A. Mathai, Y. Gim, R. C. Black, A. Amar and F. C. Wellstood, unpublished.
11. J. Kirtley, C. C. Tsuei, J. Z. Sun, C. C. Chi, Lock See Yu-Jahnes, A. Gupta, M. Rupp and M. B. Ketchen, unpublished.
12. A. G. Sun, D. A. Gajewski, M. B. Maple and R. C. Dynes, *Phys. Rev. Lett.* **72**, 2267, (1994).
13. P. Chaudhari and S.-Y Lin, *Phys. Rev. Lett.* **72**, 1084, (1994).
14. G. Kotliar, *Phys. Rev. B* **37**, 3664, (1988).
15. D. S. Rokhsar, *Phys. Rev. Lett.* **70**, 493, (1993); R. B. Laughlin, unpublished.

Journal of Superconductivity, Vol. 8, No. 4, 1995

Raman Scattering Investigation of the Superconducting Gap Anisotropy In $La_{2-x}Sr_xCuO_4$

J. C. Irwin,[1] X. K. Chen,[1] H. J. Trodahl,[2] T. Kimura[3] and K. Kishio[3]

Received 5 January 1995

The low energy electronic Raman continua of a $La_{1.83}Sr_{0.17}CuO_4$ single crystal have been obtained in several different scattering geometries, and for temperatures above and below Tc. Based upon the polarization dependence of the spectra obtained for $T \leq Tc$ it is concluded that the superconducting gap is anisotropic with nodes located near the $(\pm 1,\pm 1)$ directions in reciprocal space and maxima close to the k_x and k_y axes. The results are compared to spectra obtained from other high-Tc compounds and the possible compatibility of the results with particular gap functions is discussed.

KEY WORDS: Raman Scattering high-temperature superconductor, superconducting gap

1. INTRODUCTION

The nature of the pairing mechanism in high-temperature superconductors is a problem that continues to attract a great deal of interest. In particular many experiments have been carried out recently in an attempt to identify the symmetry of the pairing state since it is believed that this information will provide important constraints that will assist in the identification of the actual pairing mechanism. For example several investigations have been stimulated by the apparent success of a model[1,2] in which pairing was induced by the exchange of antiferromagnetic spin fluctuations, and the prediction that if this model was correct, the pairing state would necessarily have d-wave type symmetry. A number of experiments[3-10] on the bilayer, higher-T_c materials $YBa_2Cu_3O_y$(Y123) and $Bi_2Sr_2CaCu_2O_8$ (Bi2212) have provided support for the existence of an anisotropic nodal (s-wave or d-wave) gap in these materials. The situation appears to be somewhat different however in materials having a single CuO_2 layer in the unit cell. Mason et al[11] have carried out inelastic neutron scattering and specific heat measurements on $La_{2-x}Sr_xCuO_4$(La214(x)) and did not identify any features that could be associated with an anisotropic gap. Results obtained from tunneling measurements[12] carried out on the single layer compound $HgBa_2CuO_y$ suggested the existence of an isotropic s-wave gap and microwave surface impedance measurements[13] on $Nd_{1.85}Ce_{0.15}CuO_4$ were in accord with a single BCS s-wave gap picture. Given that there have been relatively few experiments carried out on the single layer compounds and furthermore that the results obtained from these experiments suggest a picture of the gap that is at variance with that obtained from many experiments on the bilayer materials, further investigations of the gap in materials such as La214 are clearly suggested.

In this paper we will describe some results obtained from inelastic light scattering studies of the low energy Raman continua in La214. The spectra obtained from superconducting La214 are qualitatively similar[14] to those obtained from the double layer compounds Bi2212[6,7] and Y123[5,8] and the energies associated with the characteristic features in the spectra scale approximately with the critical temperatures of the different compounds. In contrast to previous reports[11-13] on single layer cuprate superconductors the present results suggest that the superconducting gap ($\Delta(\mathbf{k})$) in La214 is anisotropic with nodes located near the $(\pm 1,\pm 1)$ directions in reciprocal space. We did not obtain any definitive evidence for the subsidiary gap maxima observed in recent photoemission experiments[10] on Bi2212.

[1]Physics Department, Simon Fraser University, Burnaby, British Columbia, Canada V5A 1S6.

[2]Physics Department, Victoria University of Wellington, P. O. Box 600, Wellington, New Zealand.

[3]Department of Applied Chemistry, University of Tokyo, Tokyo 113, Japan.

0896-1107/95/0800-0495$07.50/0

2. RAMAN SCATTERING

A typical feature in the Raman spectra of superconductors is a low energy continuum[15,16] that arises from scattering from electronic excitations on the Fermi surface. As the sample is cooled below T_c, the frequency distribution of the electronic continua changes to reflect the opening of the superconducting gap, and thus the spectra can provide direct information on the nature of the gap. In the high-T_c superconductors the optical penetration depth λ is much greater than the coherence length ξ and the relevant wavevector transfer is $q \approx \lambda^{-1}$. Klein and Dierker[16] developed a theory to describe the scattering from superconductors in this small q limit and obtained for the photon scattering cross section[16]

$$\frac{d^2R}{d\omega d\Omega} = \frac{4N(0)r_0^2}{\omega}\left\langle \frac{|\gamma(\mathbf{k})|^2|\Delta(\mathbf{k})|^2}{(\omega^2 - 4|\Delta(\mathbf{k})|^2)^{1/2}} \right\rangle \qquad (1)$$

where N(0) is the density of states for one spin, r_0 is the Thomson radius and <...> denotes an average over the Fermi surface with the restriction that $\omega > 2|\Delta(\mathbf{k})|$. In the non-resonant limit $\gamma(\mathbf{k})$ is given by

$$\gamma(\mathbf{k}) = \frac{m}{\hbar^2}\mathbf{e}^i \bullet \frac{1}{m^*} \bullet \mathbf{e}^s = \frac{m}{\hbar^2} e_i^i \frac{\partial^2 E(\mathbf{k})}{\partial k_i \partial k_j} e_j^s \qquad (2)$$

where m^* is the effective mass tensor , $\mathbf{e}^i$ and $\mathbf{e}^s$ are the polarization vectors of the incident and scattered light and $E(\mathbf{k})$ is the dispersion relation of the conduction band. From equation (2) it is evident that choosing a particular scattering geometry is equivalent to choosing a particular component of the effective mass tensor. The different components of the effective mass tensor can in turn have quite different **k**-dependences, particularly for anisotropic materials, and hence one can in principle probe the superconducting gap on different parts of the Fermi surface(FS).

In the present case our experiments will be carried out in a quasi-backscattering geometry with the wavevectors of the incident and scattered light approximately parallel to the z-axis (which is taken perpendicular to the CuO_2 planes of the La214 crystal). The Raman spectra are then measured in the $z(xx)\bar{z}$, $z(x'x')\bar{z}$, $z(xy)\bar{z}$, and $z(x'y')\bar{z}$ scattering geometries where the letters inside the brackets refer to the directions of the polarization vectors of the incident and scattered light. Here the x and y axes are parallel to the Cu-O bonds and the x' and y' axes are rotated by 45 degrees with respect to x and y. Considered within the D_{4h} tetragonal point group the (xy) geometry provides coupling to excitations with B_{2g} symmetry, the (x'y') geometry to B_{1g} excitations and (xx)[x'x'] to A_{1g} and B_{1g} [B_{2g}] excitations.

To illustrate the different **k**-dependences of the Raman tensor components we have calculated the x'y' and xy components (Fig. 1) using a second nearest neighbour tight binding model[9] to determine $E(\mathbf{k})$ and the FS. The model parameters ($s = -0.3t$ and $\mu = -1.16t$) were chosen to yield a FS (Fig. 1) similar to that used by previous workers[17].

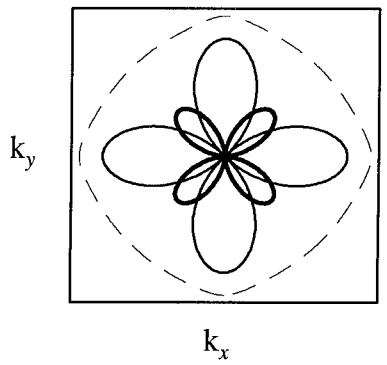

Fig. 1. A plot of the absolute value of value of $x'y'(B_{1g})$ component (thin solid lines) and the $xy(B_{2g})$ component (thick solid lines) of the reciprocal effective mass tensor evaluated on the Fermi surface, depicted by the dashed line (centered at π, π).

As is evident from Fig. 1 the B_{1g} component of the Raman vertex ($\gamma_{x'y'}$) transforms as $k_x^2 - k_y^2$. in the two-dimensional reciprocal space associated with the CuO_2 planes. Thus $\gamma_{x'y'}$ vanishes along the $(\pm 1, \pm 1)$ directions and has maxima along the $(\pm 1, 0)$ and $(0, \pm 1)$ axes in reciprocal space. The inverse is true for the B_{2g} component of the Raman tensor, as is evident from Fig. 1 and hence the xy and x'y' components of the Raman tensor sample different, but complimentary, regions of the FS. This property can be exploited to obtain information on the variation of the gap $\Delta(\mathbf{k})$ over the FS. Thus, as an example, if one has a gap with d-wave (B_{1g}) symmetry, the B_{1g} continuum obtained from equation (1) should be peaked at $2|\Delta_{max}|$ since both $\gamma_{x'y'}$ and $\Delta(\mathbf{k})$ have their maxima along the axes. The B_{2g} continuum, however should be peaked at a lower frequency since γ_{xy} is zero along k_x and k_y where $\Delta(\mathbf{k})$ has its maximum.

3. RESULTS AND DISCUSSION

The La214(0.17) sample[18] used in this work was a single crystal with a critical temperature of 37K. The surfaces of the crystal were polished using diamond paste and etched[19] in a Bromine-ethanol solution. The incident laser power was kept less than $10W/cm^2$ to minimize local heating of the sample. The temperatures quoted in the remainder of this paper refer[14] to the temperature in the excited region of the sample which was about 11K higher than the ambient temperature.

The Raman spectra obtained in the various scattering geometries are shown in Fig. 2 and the x'y' and xy spectra calculated using (1) and (2) and a simple d-wave gap are shown in Fig. 3(a). It is clear from Fig. 2 that when the temperature is reduced from 40K(just above T_c) to 15K ($<T_c$) there is a superconductivity induced redistribution of the electronic continua in all geometries that results in a depletion at low frequencies, and the appearance of a broad maximum which occurs at about $200cm^{-1}$ in the x'y'(B_{1g}) continuum and at about $130cm^{-1}$ in the xy(B_{2g}) spectrum This behaviour is similar to that observed in Bi2212 and in Y123 in that below T_c the continua become depleted at low energies and a broad peak, whose central frequency depends on scattering geometry, appears in the spectra. For a conventional BCS-type superconductor with an isotropic s-wave gap one would expect this depletion to be approximately complete below the characteristic BCS energy of $2\Delta = 3.5kT_c$. In La214 however, as in other hole-doped cuprates, the intensity in the scattered spectra (Fig. 2) remains finite at energies well below this value and there is some scattering even for frequencies approaching zero. This observation can be taken to imply that the magnitude of the superconducting gap varies over the FS. Furthermore, in La214, as in Bi2212[6,7] and Y123[20-22] , the peak frequency in the x'y'(B_{1g}) spectrum occurs at an energy that is about 1.6 times the frequency of the peaks observed in the x'x'(A_{1g}+ B_{2g}) and xy(B_{2g}) spectra. This suggests that the peak frequency in the x'y' spectra should be taken as a measure of the maximum gap energy, $2\Delta_{max}$,, This suggestion is supported by the fact that the peak frequencies in the x'y' continua of La214, Bi2212[6,7] and Y123[5,20,21] appear to scale with the critical temperature according to the relation $2\Delta_{max} \cong 8\ kT_c$. Given the **k**-dependence of the x'y' component of the Raman tensor (Fig. 1) these observations further suggest that the gap assumes its maximum value along the k_x and k_y axes. From Fig. 2 one can also note that the scattered intensity in the x'x' and xy spectra appears to extrapolate

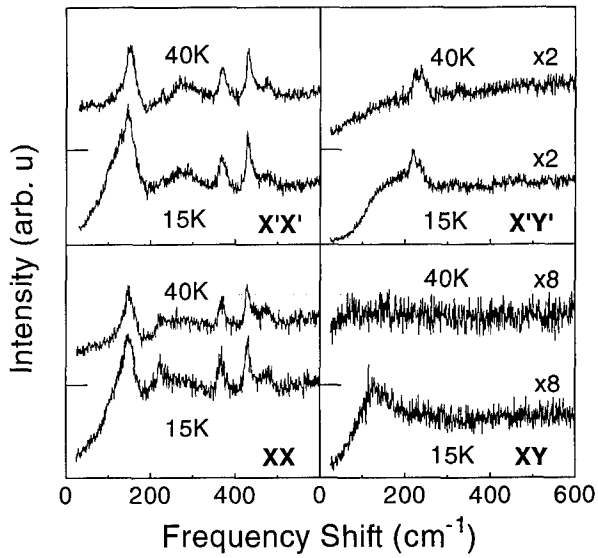

Fig. 2. Raman spectra of $La_{1.83}Sr_{0.17}CuO_4$ obtained at 40 K and 15 K in the x'y'(B_{1g}), xy(B_{2g}), x'x'(A_{1g}+B_{1g}) and xx(A_{1g}+B_{1g}) scattering geometries.

linearly to zero at zero frequency with a relatively steep slope while the x'y' spectrum is much more strongly depleted at low frequencies. This observation can be taken as evidence[14] that the nodes of the gap are situated near the x' and y' axes. It should also be noted that the ratio of the frequency of the peak in the xy spectrum to the frequency of the $2\Delta_{max}$ peak in the x'y' spectrum is about 0.6 in both the measured and calculated(See Fig. 3) spectra. Approximately the same value is obtained[7] for this ratio in Bi2212.

From the above it is concluded that the superconducting gap in La214 is anisotropic and the variation with direction in **k**-space is similar to that observed in Bi2212 and Y123. One must thus conclude that this anisotropy is intrinsic to a single Cu-O layer and does not arise from interactions between adjacent Cu-O layers as might have been inferred from measurements[11,12] on other single layer compounds.

Recently, high resolution photoemission experiments were carried out[10] on Bi2212. These experiments revealed the presence of an anisotropic gap $\Delta(\mathbf{k})$ with maxima along $(\pm 1,0)$ and $(0,\pm 1)$ in agreement with previous photoemission results[9] and with the Raman results[6-8,14] in several cuprates. They also found nodes in the gap which occurred along directions in **k**-space that were displaced with respect to the x',y' axes. Subsidiary gap maxima (Δ_{sub}) that occurred between each pair of nodes were found to occur approximately along the $(\pm 1,\pm 1)$ directions in the

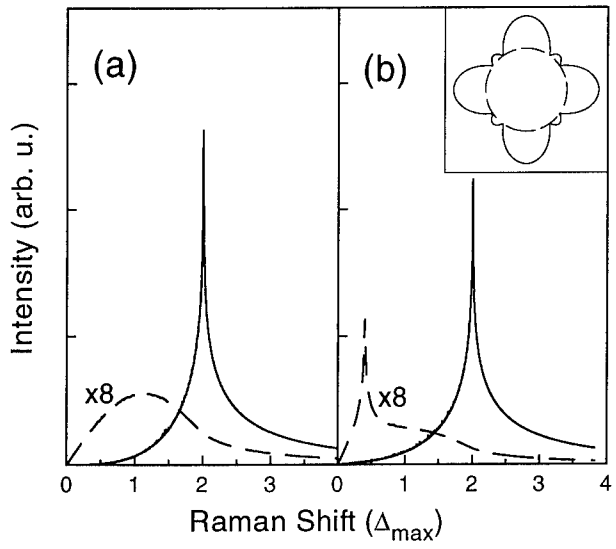

Fig. 3. Calculated Raman spectra using (1). (a) for a d-wave gap $\Delta(\mathbf{k})=\Delta_0(\cos k_x a - \cos k_y a)$. (b) for a gap given by (3) shown in the insert.

Brillouin zone. It is interesting to speculate on how such features might affect the observed Raman spectra. To simulate a gap with subsidiary maxima Δ_{sub} having a magnitude similar to the value obtained from the photoemission experiments (that is $\Delta_{sub} \approx 0.20\Delta_{max}$) we have used a gap with the form

$$\Delta(\theta) = \Delta_0\{\cos(k_o \cos 2\theta) - \cos(k_o \sin 2\theta)\} + C \qquad (3)$$

where $\theta = \sin^{-1}(k_y / k_0)$, $k_0 = \sqrt{k_x^2 + k_y^2}$ and C is a constant. The resulting gap is shown in the insert of Fig. 3(b). The Raman spectra were then calculated using equations (1) and (2) and the FS used to derive the results shown in Fig. 1. The calculated spectra are shown in Fig. 3(b). It is clear that the x'y'(B_{1g}) spectrum is essentially the same for both gaps and thus no evidence of the subsidiary maxima would be expected in this geometry. The xy (B_{2g}) spectrum on the other hand has distinct features that arise because of the presence of a finite gap along the x' and y' directions. Such features have not been observed in any of the spectra obtained to date from the superconducting cuprates. It should be noted, however, that it is possible that such spectral features could be partially washed out if the magnitudes of the subsidiary gap maxima were different in different quadrants of the Brillouin zone, as is in fact indicated by the results in ref. [10]. Even in this case however some structure should appear in the low energy B_{2g} spectra. If however, the doping in the crystal was spatially inhomogeneous this could lead to changes in the spectra that would appear only as an increase in the slope at low frequencies and a reduction in the peak frequency of the B_{2g} spectrum and this would be difficult to detect.

ACKNOWLEDGMENT

The financial support of the Natural Sciences and Engineering Research Council of Canada is gratefully acknowledged.

REFERENCES

1. P. Monthoux, A. Balatsky and D. Pines, *Phys. Rev. Lett.* **67**, 3448 (1991); *Phys. Rev.* **B46,** 14803 (1992).
2. N. E. Bickers, D. J. Scalapino and S. R. White, *Phys. Rev. Lett.* **62**, 961 (1989).
3. D. A. Wollman, D. J. van Harlingen, W. C. Lee, D. M. Ginsberg and A.J. Leggett, *Phys. Rev. Lett.* **71,** 2134 (1993).
4. W. N. Hardy, D. A. Bonn, D. C. Morgan, R. Liang and K. Zhang, *Phys. Rev. Lett.* **70**, 3999 (1993); D. A. Bonn et al., *Phys. Rev.* **B47,** 11314 (1993).
5. S. L. Cooper et al., *Phys. Rev.* **B38**, 11934 (1988); S. L. Cooper and M. V. Klein, *Comments Condensed Matter Phys.* **15,** 99 (1990).
6. T. Staufer, R. Nemetschek, R. Hackl, P. Muller and H. Veith, *Phys. Rev. Lett.* **68,** 1069 (1992).
7. T. P. Devereaux et al., *Phys. Rev. Lett.* **72**, 396 (1994).
8. X. K. Chen , J. C. Irwin, R. Liang and W. N. Hardy, *J. of Supercond.* **7**, 435 (1994); *Physica* **C227**, 113 (1994).
9. Z. X. Shen et al., *Phys. Rev. Lett.* **70**, 1553 (1993).
10. H. Ding et al., *Preprint, submitted to Phys. Rev Lett.*
11. T. E. Mason, G. Aeppli, S. M. Hayden, A. P. Ramirez and H. A. Mook, *Phys. Rev. Lett.* **71,** 919 (1993) .
12. J. Chen, J. F. Zasadzinski, K. E. Gray, J. L. Wagner, and D. G. Hinks, *Phys. Rev.* **B49**, 3683 (1994).
13. M. Anlage, D. H. Wu, J. Mao, X. X. Xi, T. Venkatesan, J. L. Peng and R. L. Greene, *Phys. Rev.* **B50**, 523 (1994).
14. X. K. Chen, J. C. Irwin, H. J. Trodahl, T. Kimura and K. Kishio, *Phys. Rev. Lett.* **73,** 3290 (1994).
15. S. B. Dierker, M. V. Klein, G. W. Webb and Z. Fisk, *Phys. Rev. Lett.* **50**, 853 (1983); R. Hackl, R. Kaiser and S. Schicktanz, *J. Phys.* **C16**, 1729 (1983).
16. M. V. Klein and S. B. Dierker, *Phys. Rev.* **B29,** 4976 (1984).
17. W. E. Pickett, *Rev. of Modern Physics* **61**, 433 (1989).
18. T. Kimura, K. Kishio, T. Kobayashi, Y. Nakayama, N. Motohira, K. Kitazawa and K. Yamafuji, *Physica* **C192**, 247 (1992).
19. D. J. Werder, G. H. Chen, M. Gurvitch, B. Miller, L. F. Schneemeyer and J. F. Waszczak, *Physica* **C160**, 411 (1989).
20. X. K. Chen, E Altendorf, J.C. Irwin, R. Liang and W. N. Hardy, *Phys. Rev.* **B48**, 10530 (1993).
21. X. K. Chen and J. C. Irwin, *to appear in Physica C*(Proc. of M^2HTSC IV)
22. R. Hackl, W. Glaser, P. Muller, D. Einzel and K. Andres, *Phys. Rev.***B38**, 7133 (1988).

Journal of Superconductivity, Vol. 8, No. 4, 1995

What Does Instrinsic Josephson Coupling Say about the Pairing Symmetry in the Cuprates?

R. J. Radtke,* C. N. Lau,† and K. Levin†

Received 5 January 1995

Measurements of the c-axis properties of the cuprate superconductors show anomalous behavior in both normal and superconducting states. In particular, there is strong evidence that pairs of CuO_2 planes in neighboring unit cells act as Josephson junctions below the critical temperature T_c. We present a theory based on incoherent transport along the c-axis which naturally reproduces the anisotropic normal-state resistivity and the superconducting-state Josephson coupling. Applying this theory to $YBa_2Cu_3O_{7-\delta}$ (YBCO), we make quantitative predictions for the strength and temperature dependence of the Josephson coupling as well as the variation of T_c with disorder. Beyond the expected low-temperature behavior, the Josephson critical current does not make a clean separation between s- and d-wave superconductors, but the disorder-induced T_c variation does. Further experimental and theoretical work along these lines may therefore help determine the order parameter symmetry in the cuprates.

KEY WORDS: c-axis, Josephson coupling, order-parameter symmetry, T_c suppression

The recent availability of high-quality single crystals of the cuprate superconductors allows precise characterization of both the usual in-plane (ab-axis) and the less-studied out-of-plane (c-axis) properties. These data show several unusual features in both the normal- and superconducting-state [1]. In this paper, we will examine some of these measurements and present a theory which seems to be able to describe them. The fundamental postulate of this theory is that the charge transport between the CuO_2 planes is incoherent, as opposed to the coherent transport assumed in the conventional Bloch-Boltzmann picture. With the assumption of incoherent transport, we can make sense of the normal-state resistivity data and make quantitative predictions about the nature and strength of the Josephson coupling between the CuO_2 planes. We also consider the influence of intra- and inter-planar non-magnetic disorder on the critical temperature T_c. Comparing our results with experiment may yield information on the order parameter symmetry in these systems.

*Department of Physics, University of Maryland, College Park, Maryland 20742.

†Department of Physics and the James Franck Institute, The University of Chicago, Chicago, Illinois 60637

We begin by examining the normal-state resistivity in the ab (ρ_{ab}) and c (ρ_c) directions. The typical temperature dependence of these quantities are illustrated in the insets to Fig. 1. The data shown were obtained from Veal *et al.* [2], but the qualitative features we will discuss are seen in all the cuprate superconductors. One is immediately struck by the anisotropy of the resistivities: $\rho_c/\rho_{ab} \approx 10^1$ - 10^5 depending on the material, its doping, and the temperature T. Another important feature is that the superconducting transition appears in both ρ_{ab} and ρ_c at the same temperature. From these two observations, we can conclude that the interlayer coupling is weak but that the superconductivity is nonetheless three dimensional. Additionally, looking at the T dependence of the resistivities reveals that $\rho_c \propto \rho_{ab}$ at optimal doping but $\rho_c \propto 1/\rho_{ab}$ away from this stoichiometry. Within the context of Bloch-Boltzmann transport theory, the resistivities at optimal doping can be interpreted as charge transport in the presence of a strongly anisotropic effective mass. However, the T dependence of the underdoped compounds finds no such simple explanation, and this fact leads us to consider alternatives to the conventional theory.

0896-1107/95/0800-0499$07.50/0

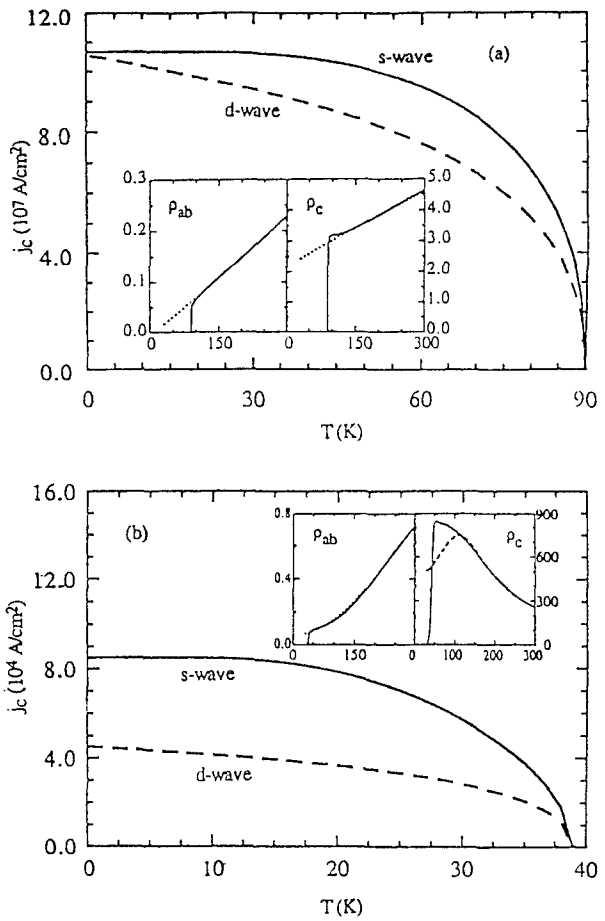

Fig. 1. Predicted Josephson critical current $j_c(T)$ as a function of temperature T for (a) $YBa_2Cu_3O_{6.93}$ and (b) $YBa_2Cu_3O_{6.42}$ assuming s-wave (solid line) and d-wave (dashed line) pairing (see text). Insets: Normal-state resistivity along the c-axis ρ_c and in the ab-plane ρ_{ab} in mΩ cm as a function of temperature in K for experimental data (solid line) [2] and the fit to the Rojo-Levin model (dashed line) [7]. The discrepancy near T_c in ρ_c is presumably a fluctuation effect.

In constructing this alternative theory, we are also guided by the experimental fact that the cuprates behave like a stack of SIS Josephson junctions along the c-axis in the superconducting state. Kleiner *et al.* obtain this surprising result by studying several single-crystal samples of BSCCO and TBCCO [3]. They observe strongly hysteretic c-axis current-voltage characteristics, suggesting the presence of a series of large-capacitance SIS Josephson junctions. Moreover, the critical current as a function of the in-plane magnetic field shows the Fraunhofer-like pattern which would be produced by a Josephson junction of width 15 Å. Finally, the samples emit microwave radiation at frequencies consistent with the ac Josephson effect for a large number of SIS junctions. Taken together, these measurements provide strong evidence that these materials can be viewed as a stack of Josephson junctions with one junction per unit cell.

We see that both normal- and superconducting-state c-axis properties are very different from the properties of conventional superconducting materials. We are therefore led to consider an unconventional theory to describe them. The basis of the conventional picture is that the periodicity of the crystal potential results in the formation of Bloch waves over the entire sample which allows the coherent propagation of quasiparticles. In the cuprates, weak interlayer coupling in the presence of strong elastic and inelastic scattering may prevent the formation of Bloch waves along the c-axis over more than a few unit cells, resulting in incoherent quasiparticle transport. Working under the assumption that the c-axis transport is incoherent, we will develop a theory which explains the observed anomalies and which can also shed light on the question of the order parameter symmetry in these systems.

We first approximate the complicated structure of the cuprates with multiple CuO_2 planes per unit cell by treating these planes as a tightly-coupled "layer." This layer is assumed to be a two-dimensional Fermi liquid. Interlayer coupling is introduced through a direct hopping, similar to that in tight-binding models, and an assisted hopping, which can be either elastic (e.g., by disorder) or inelastic (e.g., by phonons). We impose the constraint of incoherence on this model by restricting all our calculations to second order in the interlayer hopping amplitudes. Many authors have pursed theories along these lines [4, 5, 6, 7], but our viewpoint most closely resembles that of Rojo and Levin [7].

This theory provides a natural explanation for the T dependence of ρ_{ab} and ρ_c. At optimal stoichiometry, we expect the layers to be strongly coupled and nearly coherent, implying that the direct hopping dominates the transport, and so $\rho_c \propto \rho_{ab}$ as in the conventional picture. Off optimal stoichiometry, the direct interlayer coupling weakens relative to the assisted processes, and the material becomes increasingly incoherent. While this change does not strongly affect ρ_{ab}, ρ_c is now dominated by assisted hopping, the inelastic component of which freezes out at low T. Thus, as T decreases, the interlayer hopping amplitude is reduced and ρ_c increases as observed experimentally. These qualitative arguments

can be made quantitative by fitting this model to the observed resistivities, as demonstrated in the insets to Fig. 1 [8].

The theory also immediately implies interlayer Josephson coupling. Moreover, the total c-axis Josephson critical current can be computed from the sum of the critical currents due to direct and assisted hopping and depends on the pairing symmetry. In general, the critical current from assisted hopping has the usual Ambegaokar-Baratoff form [9]. However, the direct hopping leads to an unusual critical current: the zero-temperature value is proportional to the square of the direct interlayer hopping amplitude rather than to the T = 0 gap, and the critical current falls like the square root of the reduced temperature near T_c instead of linearly [8]. The pairing symmetry also enters into this calculation in a fundamental way. For an s-wave superconductor, both assisted and direct hoppings contribute and are nearly temperature-independent at low T. For a d-wave superconductor, the assisted processes do not contribute and the direct hopping produces the canonical linear-in-T critical current at low T. Therefore, measurements of the temperature dependence of the critical current can probe the order parameter symmetry. To facilitate the comparison of theory and experiment, Fig. 1 shows the expected strength and T dependence of the c-axis critical current for YBCO using fits to the normal-state resistivity to fix the model parameters [8].

Currently, there exist several measurements of the c-axis critical currents to which we can compare our theory. Kleiner *et al.* have measured the critical current in BSCCO directly and found Ambegaokar-Baratoff behavior [3]. Within our model, we can interpret this result in terms of an s-wave order parameter with purely assisted hopping between the layers. Indirect measurements of the critical current come from electrodynamical measurements of the penetration depth, which is related to the Josephson critical current in a model of our type [10]. Results of this kind on LSCO from Shibauchi *et al.* exhibit the Ambegaokar-Baratoff temperature dependence, again supporting s-wave superconductivity and pure assisted interlayer hopping [11]. The situation in YBCO is less clear, however. Some data show an SNS-like temperature dependence which is incompatible with our model [12] while other data have the form expected within our theory. Until reproducible data are obtained, it is premature to draw any conclusions about YBCO.

Another implication of the theory is the response of the critical temperature to disorder. For an s-wave superconductor, Anderson's theorem states that small concentrations of non-magnetic disorder should not affect the superconducting properties [13]. d-wave superconductors, on the other hand, should show a pronounced suppression of T_c when non-magnetic disorder is introduced [14, 15]. The disorder can be located either within or between the layers, but both types of disorder contribute to $\rho_{ab}(T = 0)$). By generalizing the Abrikosov-Gor'kov (AG) theory of impurity scattering, we can express the critical temperature as a function of the (measurable) $\rho_{ab}(T = 0)$ once the T_c of the pure material and the in-plane plasma frequency are known [15]. By looking at the response of the superconductor to the controlled introduction of non-magnetic disorder, we should therefore be able to distinguish between different order parameter symmetries.

Experiments to test this idea can introduce disorder in two ways: irradiation or doping. Low-dose irradiation creates local disruptions in the crystalline order but should leave the plasma frequency unchanged, and so the T_c suppression should follow the familiar AG form [Fig. 2(a)]. Two groups have completed controlled irradiation experiments on YBCO [16, 17], but the measurements agree with neither the isotropic s-wave nor the d-wave predictions for isotropic disorder scattering. The observed behavior *is* consistent with either an anisotropic s-wave order parameter or a d-wave order parameter in the presence of anisotropic disorder scattering, but still seems to exclude isotropic s-wave pairing [17]. One important question in these experiments is whether the induced disorder is magnetic or not; although neither group has directly answered this question, the relative insensitivity to the T_c to the disorder argues against its being magnetic.

Doping introduces scattering centers and also modifies the number of charge carriers within the layers, making the plasma frequency a function of dopant concentration. If we take this variation into account within the generalized AG theory and make the gross simplification that the pairing interaction is independent of doping, we can estimate the magnitude of the T_c suppression [Fig. 2(b)]. In this case, large d-wave T_c's can exist despite large residual resistivities. Within our theory, the persistence of the superconductivity at large $\rho_{ab}(0)$ is due to a large pure T_c and a small plasma frequency, implying that the approach to the insulator makes the supercon-

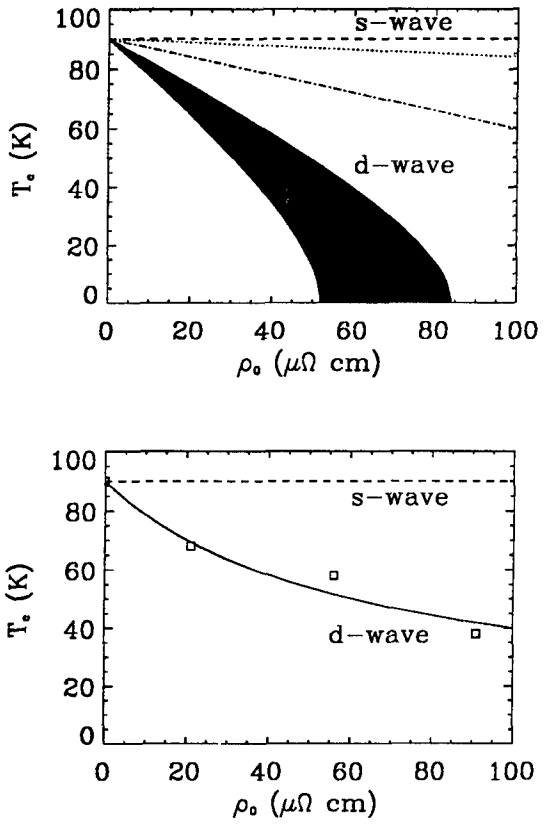

Fig. 2. Non-magnetic-disorder-induced suppression of T_c in YBCO. (a) For irradiation-induced non-magnetic disorder, $\omega_{ab}^2 \approx$ constant, so the T_c for a d-wave order parameter is given by the generalized Abrikosov-Gor'kov theory (shaded area) and for an s-wave order parameter is constant (dashed line) [15]. Experimental results from Sun *et al.* [16] and Giapintzakis *et al.* [17] are shown as dotted and dot-dashed lines, respectively. (b) For doping-induced disorder, $\omega_{ab}^2 \propto$ hole doping, so the prediction for T_c in a d-wave superconductor is modified from that in (a) (solid line), although the s-wave prediction is unchanged for small doping (dashed line). Open boxes: Data extracted from the measurements of Veal *et al.* [2].

ductor more tolerant of disorder. Under the assumption that the vacancies in the CuO chains induced by de-oxygenation are non-magnetic, we can use the data of Veal *et al.* [2] to compare to this theory. These data are shown in Fig. 2(b) and agree strikingly well with the d-wave predictions. However, since these predictions are based on the assumption that the pairing interaction is independent of doping, the quantitative agreement with experiment must be viewed with caution.

To summarize, the idea of incoherent interlayer coupling can account for the measured normal-state resistivity and the Josephson-like superconducting properties along the c-axis. Moreover, this theory makes concrete predictions for the c-axis critical current and the disorder-induced suppression of T_c, which depend on the relative importance of direct and assisted interlayer hopping and on order-parameter symmetry. Further experimental and theoretical work can therefore provide an acid test for this theory and hopefully shed some light on the important question of the pairing symmetry in the cuprates.

ACKNOWLEDGEMENTS

The authors would like to thank B. W. Veal for providing us with the resistivity data for YBCO. This work was supported by the National Science Foundation (DMR 91-20000) through the Science and Technology Center for Superconductivity and DMR-MRL-8819860 (RJR).

REFERENCES

1. For a review, see S. L. Cooper and K. E. Gray, in *Physical Properties of High-Temperature Superconductors IV*, D. M. Ginsberg, ed. (World Scientific, Singapore, 1994).
2. B. W. Veal, A. P. Paulikas and P. Kostic, unpublished.
3. R. Kleiner, F. Steinmeyer, G. Kunkel, and P. Müller, *Phys. Rev. Lett.* **68**, 2394 (1992); R. Kleiner and P. Müller, *Phys. Rev. B* **49**, 1327 (1994).
4. N. Kumar and A. M. Jayannavar, *Phys. Rev. B* **45**, 5001 (1992).
5. A. J. Leggett, *Braz. J. Phys.* **22**, 129 (1992).
6. M. J. Graf, D. Rainer, and J. A. Sauls, *Phys. Rev. B* **47**, 12089 (1993) and unpublished.
7. A. G. Rojo and K. Levin, *Phys. Rev. B* **48**, 16861 (1993).
8. R. J. Radtke, Ph.D. Thesis, The University of Chicago, Chicago, Illinois, 1994; R. J. Radtke, C. N. Lau, and K. Levin, unpublished.
9. V. Ambegaokar and A. Baratoff, *Phys. Rev. Lett.* **10**, 486 (1963); *ibid.* **11**, 104 (1963).
10. L. N. Bulaevskii, *Sov. Phys.-JETP* **37**, 1133 (1973); J. R. Clem, *Physica (Amsterdam)* **162-164C**, 1137 (1989).
11. T. Shibauchi, H. Kitano, K. Uchinokura, A. Maeda, T. Kimura, and K. Kishio, *Phys. Rev. Lett.* **72**, 2263 (1994).
12. Jian Mao, D. J. Wu, J. L. Peng, R. L. Greene, and S. M. Anlage, *Phys. Rev. B*, in press.
13. P. W. Anderson, *J. Phys. Chem. Solids* **11**, 26 (1959).
14. A. J. Millis, S. Sachdev, and C. M. Varma, *Phys. Rev. B* **37**, 4975 (1988).
15. R. J. Radtke, K. Levin, H.-B. Schüttler, and M. R. Norman, *Phys. Rev. B* **48**, 653 (1993).
16. A. G. Sun, L. M. Paulius, D. A. Gajewski, and M. B. Maple, *Phys. Rev. B* **50**, 3266 (1994).
17. J. Giapintzakis, D. M. Ginsberg, M. A. Kirk, and S. Ockers, unpublished.

Journal of Superconductivity, Vol. 8, No. 4, 1995

A Scenario to the Anomalous Hall Effect in the Mixed State of Superconductors

Ping Ao[1]

Received 4 January 1995

We argue that the motion of vacancies in a pinned vortex lattice may dominate the contribution to the Hall effect in an appropriate parameter regime for a superconductor. Based on this consideration a model is constructed to explain the anomalous Hall effect without any modification of the basic vortex dynamic equation. Quantitative predictions are obtained. Present model can be directly tested by an observation of the vacancy motion.

KEY WORDS: Hall effect; vortex dynamics; type II superconductors.

It is generally believed that the motion of vortices in a superconductor is responsible for the apparence of resistance. Indeed, there is a well and successful account of dissipative phenomena in superconductors based on this idea[1]. However, the ubiquitous occurrence of the anomalous Hall effect in the mixed state of both conventional and oxide superconductors, the sign change of the Hall resistance below the superconducting transition temperature, seems to be inexplainable by standard models for vortex dynamics in superconductors[2]. The purpose of the present paper is to show that it is nevertheless possible to understand the anomalous Hall effect without either a modification of vortex dynamics or assuming two types of carriers(or more complicated electronic band structures). The essential idea in the present model is the domination of the vacancy motion in a pinned vortex lattice under a suitable condition. Contrast to previous ones in this model both the strong interaction between vortices, which leads to the many-body correlation effect, and the strong pinning effect are crucial. In the following we present the arguments leading to the model, and discuss its predictions and experimental verifications. For simplicity, we will consider an isotropic s-pairing superconductor with one type of charge carriers in two dimension. In this situation vortices(or straight vortex lines) can be viewed as point particles.

[1]Department of Theoretical Physics, Umeå University, S-901 87, Umeå, SWEDEN

We begin with the discussion of vortex dynamics. The equation of motion for a vortex generally takes the form of the Langevin equation similar to that of a charged particle in the presence of a magnetic field:

$$m_v\ddot{\mathbf{r}} = q_v\frac{\rho_s}{2}hd\,(\mathbf{v}_s - \dot{\mathbf{r}})\times\hat{z} - \eta\dot{\mathbf{r}} + \mathbf{F}_{pin} + \mathbf{f}\,, \quad (1)$$

with an effective mass m_v, a pinning force $\mathbf{F}_{pin}$, a vortex viscosity η, and a fluctuating force $\mathbf{f}$. The viscosity is related to the fluctuating force by the usual fluctuation-dissipation theorem. In Eq.(1) $q_v = \pm 1$ describes the vorticity, h is the Planck constant, ρ_s the superfluid electron number density at temperature T, d the thickness of the superconductor film, and $\hat{z}$ the unit vector in z-direction. Normal current is assumed to be zero and a uniform temperature in the whole film is also assumed in Eq.(1). The term associated with the superconducting electron velocity $\mathbf{v}_s$ and the vortex velocity $\dot{\mathbf{r}}$ at the right side of Eq.(1) is the so-called Magnus force. It has been shown that under the general properties of a superconductor it must take such a form[3]. Closely related but different phenomenological equations for vortices have been discussed in the literature[4]. Eq.(1) is the starting point in recent studies of vortex tunneling in superconductors[5].

We first consider the measured electric field generated by a steady motion of vortices and the resulting Hall effect. In a steady state, if there is no pinning force, i.e. $\mathbf{F}_{pin} = 0$, from Eq.(1) the velocity of the vortices is

$$\dot{\mathbf{r}} = \frac{(\rho_s dh/2)^2}{\eta^2 + (\rho_s dh/2)^2}\,\mathbf{v}_s + q_v \frac{(\rho_s dh/2)\eta}{\eta^2 + (\rho_s dh/2)^2}\,\mathbf{v}_s \times \hat{z}\ . \tag{2}$$

According to the Josephson relation, the motion of vortices produces phase slippages, therefore generates an electrochemical potential difference in a superconductor, which is the reaction force to the superconducting electrons due to the vortex velocity part of the Magnus force in Eq.(1). This potential difference corresponds to the measured electric field $\mathbf{E}$. For a vortex density n with an average velocity $\dot{\mathbf{r}} = \mathbf{v}_l$, we have

$$\mathbf{E} = -q_v \frac{h}{2e}\, n\, \mathbf{v}_l \times \hat{z}\ . \tag{3}$$

If the density of moving vortices is equal to the vortex density induced by the applied perpendicular magnetic field $\mathbf{B} = B\hat{z}$, $n = |B|/\Phi_0$ with $\Phi_0 = hc/2|e|$ the flux quantum of Cooper pairs, we have the usual expression

$$\mathbf{E} = -\frac{1}{c}\mathbf{v}_l \times \mathbf{B}\ . \tag{4}$$

Therefore, in the steady state and in the absence of pinning, all vortices move with the same velocity and we have the longitudinal resistivity ρ_{xx} as

$$\rho_{xx} = \frac{E_x}{J} = \frac{q_v}{ec}\,\frac{(dh/2)\eta}{\eta^2 + (\rho_s dh/2)^2}\,B$$

$$= \frac{\Phi_0}{c^2}\,\frac{\eta d}{\eta^2 + (\rho_s dh/2)^2}\,|B|\ , \tag{5}$$

and the transversal(Hall) resistivity ρ_{yx} as

$$\rho_{yx} = \frac{E_y}{J} = \frac{1}{ec}\,\frac{(dh/2)^2\rho_s}{\eta^2 + (\rho_s dh/2)^2}\,B$$

$$= q_v \frac{\Phi_0}{c^2}\,\frac{\rho_s d^2 h/2}{\eta^2 + (\rho_s dh/2)^2}\,|B|\ . \tag{6}$$

Here the current density $\mathbf{J} = e\rho_s \mathbf{v}_s$ is along x-direction. The relation between vorticity q_v, the charge sign of carriers, and the direction of the magnetic field is $q_v e/|e| = B/|B|$. It is clear that from Eq.(6) the Hall effect in the superconducting state has the same sign as that of the normal state. This, and also those similar conclusions based on the classical models for the vortex dynamics in superconductors, are in apparent contradiction with many experimental observations[2], the so-called anomalous Hall effect.

There is a serious problem related to the many-body correlation between vortices and the pinning effect in the using of the above simple minded result, Eq.(6), for real superconducting materials. The many-body correlation due to the strong and long range interaction between vortices gives arise to the Abrikosov lattice in the mixed state of a superconductor. However, even after the consideration of the strong many-body effect, if there were no pinning for vortices, the whole vortex lattice would move together under the influence of an externally applied current in the same manner as that of independent vortices. Hence one would get the same sign of the Hall effect in both superconducting and normal states. This will be changed in the presence of pinnings. If we introduce some strong pinning centers into the film and consider the edge pinning, the vortex lattice will be pinned down. In such a situation the motion of the vortex lattice is made possible by various kinds of thermal fluctuations. We will argue below that at low temperatures the dominant contribution to the motion is due to vacancies. We will advance our argument in the following way. First we will show that the creations and motions of vacancies and interstitials are energetically favored over vortices hopping into and out of pinning centers as well as other motions. Then we will argue that vacancies are even more favourable than interstitials.

For two vortices separated by a distance r, which is less than the effective magnetic screening length $\lambda_\perp = \lambda_L^2/d (d < \lambda_L,\ \lambda_\perp = \lambda_L$ if $d > \lambda_L)$ but greater than ξ_0, the interaction potential is[6]

$$V_l(r) = 2\left(\frac{\Phi_0}{4\pi\lambda_L}\right)^2 d\,\ln\frac{r}{\xi_0} = 2\frac{h^2\rho_s}{8\pi m^*} d\,\ln\frac{r}{\xi_0}$$

$$\equiv 2\epsilon_0 \ln\frac{r}{\xi_0}\ . \tag{7}$$

Here $\lambda_L^2 = m^* c^2/8\pi\rho_s e^2$ is the London penetration depth, m^* the effective mass of a Cooper pair, and ξ_0 the coherence length of the superconductor. The energy scale ϵ_0 sets both the scale for the strength of vortex interaction and the scale for the strength of a strong pinning center. The interaction potential between a dislocation pair separated by a distance larger than the lattice constant a_0 is given by[7]

$$V_d(r) = \frac{1}{2\sqrt{3}\pi}\epsilon_0 \ln\frac{r}{a_0} \equiv 2\epsilon \ln\frac{r}{a_0}\ . \tag{8}$$

The energy scale ϵ for the dislocation interaction here is about 20 times smaller than ϵ_0 for the vortex interaction and pinning centers. It is therefore energetically much more favorable to have dislocation pairs in the lattice. Hence for temperature $T << \epsilon_0$ we can ignore the contribution from the vortices hopping out of pinning centers(and also the creation of vortex-antivortex

pairs). The vortex lattice is then effectively pinned at such temperatures. The precise calculation of the vacancy ϵ_v and interstitial energy ϵ_i is difficult, because the detailed information on the scale of lattice constant is needed. However, because vacancies and interstitials can be viewed as the smallest dislocation pairs[8], we immediately have the estimated energy scale for ϵ_v as, by putting $r \sim 2a_0$ in Eq.(8),

$$\epsilon_v \sim 2\epsilon = \frac{1}{2\sqrt{3}\pi}\left(\frac{\Phi_0}{4\pi\lambda_L}\right)^2 d\,. \tag{9}$$

There might be a weak dependence on the magnetic field through the vortex lattice constant, which is neglected here. It is clear from the above analysis that vacancies and interstitials have the lowest excitation energy scale.

Now let us compare the creation energy of a vacancy and that of an interstitial. At low magnetic fields the vacancy formation energy is lower than that of interstitials, because of the strong short range and repulsive nature of the interaction between vortices. This has been shown theoretically[9]. Therefore vacancies will dominate over interstitials at low temperatures and low fields, which has been observed experimentally[10]. Similar phenomenon has also been observed in other crystalline structures[8]. At high magnetic fields the vortex interaction becomes of long range comparing with the vortex lattice constant. The short range behavior which determines the formation energy difference between vacancies and interstitials becomes relatively unimportant. Although one expects a zero formation energy difference for an infinite range interaction, vacancies may still have a lower formation energy for a finite range interaction. This is based on the plausible expectation that the formation energy difference between vacancies and interstitials increases monotonically to zero with the interaction range. We will not be surprised if the anomalous Hall effect is more pronounced at lower magnetic fields.

We examine its experimental consequencies if the vacancy motion dominates. Effectively, the motion of a vacancy in the pinned vortex lattice behaves as an antivortex, that is, with a vorticity $-q_v$ under the action of an applied supercurrent. This leads us to our main conclusion that at low enough temperatures the sign of the Hall resistance is different from its sign in the normal state. Quantitatively, the motion of vacancies is governed by an equation of the same form as Eq.(1), and can be viewed as independent particles moving in the periodic potential formed by the vortex lattice and a random potential due to the residue effect of pinnings. The potential height of the periodic potential as well as that of the random potential is presumably the order of ϵ_v. Assuming the vacancy density n_v in a steady state, following the same procedure as from Eq.(1) to Eqs.(5-6), the longitudinal resistivity is then

$$\rho_{xx} = \frac{h}{2e^2}\,\frac{\eta_{eff}\,\rho_s dh/2}{\eta_{eff}^2 + (\rho_s dh/2)^2}\,\frac{n_v}{\rho_s}\,, \tag{10}$$

and the Hall resistivity

$$\rho_{yx} = -q_v\frac{h}{2e^2}\,\frac{(\rho_s dh/2)^2}{\eta_{eff}^2 + (\rho_s dh/2)^2}\,\frac{n_v}{\rho_s}\,. \tag{11}$$

It is evident that the sign for ρ_{yx} in Eq.(11) is opposite to that in Eq.(6). Here η_{eff} is the effective vacancy viscosity, related to the vacancy diffusion constant in the periodic potential due to the vortex lattice by the Einstein relation between the diffusion constant and the mobility. We expect that $\eta_{eff} = \eta_0\, e^{a\,\epsilon_v/K_BT}$ with a a numerical factor of order unity at low temperatures. In the low temperature limit, superfluid electron number density ρ_s approaches a constant, vacancy density $n_v = n_0\, e^{-b\,\epsilon_v/k_BT}$ may be exponentially small($b = 1$ for the thermally activated vacancies, and $b = 0$ for the pinning center induced vacancies), and the effective vacancy viscosity η_{eff} can be exponentially large. In this limit both longitudinal and Hall resistances vanish exponentially, and we obtain a scaling relation between the Hall and longitudinal resistivities as

$$\rho_{yx} = A\,\rho_{xx}^{\nu}\,, \tag{12}$$

with $A = -q_v(\rho_s dh/2\eta_0)^{b/(a+b)}(2e^2\rho_s/hn_0)^{a/(a+b)}$ and the power $\nu = (2a+b)/(a+b)$ varies between 1 and 2 depending on the detail of a sample which determines the numerical factors a and b. It is interesting to note that the present range of ν covers the values obtained previously by completely different approaches[11]. We also note that if the vortex (vacancy) tunneling process[5] is allowed, there will be a finite Hall resistance at zero temperature.

The linear film thickness d dependence of the vacancy formation energy ϵ_v, Eq.(9), can also be tested experimentally. We expect this linear dependence to hold for thin enough films. For a thick film a vortex line will bend in the z-direction, and the straight line assumption in reaching Eq.(9) is no longer valid. This suggests a critical thickness d_c such that Eq.(9) is valid for $d < d_c$ and ϵ_v will be saturated for $d > d_c$. This critical thickness may reflect the many-body correlation along the direction of the magnetic field and is likely a sensitive function of both the magnetic field and the temperature.

Now we discuss the qualitative features of the model. In the above picture, we need the vortex lattice to define vacancies, and a sufficiently strong pinnings to prevent the slidding of vortex lattice in order to obtain a maximum contribution of vacancies. However, there is no need for a whole lattice structure. Sufficiently large local structures, like lattice domains, will be enough to define vacancies. Therefore one may even have vacancy like excitations in a vortex liquid state, where large local orderings exist. Whether or not this is also true for a vortex glass state depending on its randomness. On the other hand, if the pinning is too strong, for example, the pinning center density is much larger than the vortex density, vortices will be individually pinned down and the local lattice structure required for the formations of vacancies and interstitials will be lost. Therefore we only expect to see the anomalous Hall effect in a suitable range of pinnings and magnetic fields, that is, for $B_l < |B| < B_u$ with the lower and upper critical fields determined by pinnings.

As shown by Eqs.(7-9) a large London penetration depth reduces down all the relevant energy scales, and energetically it is more favorable to observe the anomalous Hall effect. This may explain the experimental observation that it is difficult to observe the anomalous Hall effect in a clean conventional superconductor, but easy in a dirty superconductor as well as in a high temperature superconductor where the London penetration depth is large[2]. At this point, we wish to point out the important difference between the pinning centers for vortices and the mean free path of electrons: The vortex dynamics is sensitive to pinning, not to the mean free path. There is no obvious relationship between them.

If the temperature is increased towards the superconducting transition temperature, all energy scales become small, and so does the difference between ϵ_v and ϵ_i. Other contributions, such as those of quasiparticles, the slidding of vortex lattice, and vortices hopping out of pinning centers, become dominant. Those contributions have a different sign for the Hall resistance, but the same sign for the longitudinal resistance as vacancies. Therefore one expects a sign change in the Hall resistance below the transition temperature.

It is important to check whether or not the present model can also explain experiments concerning vortex motion other than the Hall and longitudinal resistivity experiments. We will mention here the Nernst effect. Under the driving of a temperature gradient the force felt by a vacancy is opposite of the force felt by an interstitial or a vortex in direction but equal in magnitude. Then the Nernst effect due to vacancies has the same sign as that of vortices or interstitials. Therefore our model gives that in the anomalous Hall effect regime there is no sign change for the Nernst effect, and furthermore, the Nernst effect is more pronounced because of the large contribution due to both vacancies and interstitials. This is in agreement with the experimental observations[12].

In conclusion, a model based on the motion of vacancies in a pinned lattice is proposed to explain the anomalous Hall effect. No modification of the basic vortex dynamics equation is needed. Quantitatively it leads to an exponential tail and the scaling relation at low temperatures, and no sign change for the Nernst effect. For thin enough films the activation energy in the low temperature limit has a linear film thickness dependence. Present model provides a framework to understand relevant experiments, and further experiments are needed to test it. The most direct way might be the observation of the vacancy motion.

ACKNOWLEDGEMENTS

Valuable discussions with David Thouless and Andrei Shelankov, in particular their sharp remarks, as well as the correspondences on experimental aspects of the problem from John Graybeal and Chris Lobb, are gratefully acknowledged.

REFERENCES

1. *Superconductivity*, Vol. II, edited by R.D. Parks (Marcel Dekker, New York, 1969).
2. See, for example, S.J. Hagen *et al.*, Phys. Rev. **B47**, 1064 (1993), for both experimental and theoretical overviews.
3. P. Ao and D.J. Thouless, Phys. Rev. Lett. **70**, 2158 (1993); D.J. Thouless, P. Ao, and Q. Niu, Physica **A200**, 42 (1993); P. Ao, Q. Niu, and D.J. Thouless, Physica **B194-196**, 1453 (1994).
4. J. Bardeen and M.J. Stephen, Phys. Rev. **140**, A1197 (1965); P. Nozières and W.F. Vinen, Phil. Mag. **14**, 667 (1966).
5. P. Ao and D.J. Thouless, Phys. Rev. Lett. **72**, 132 (1994); M.J. Stephen, *ibid*, 1534 (1994).
6. P.G. de Gennes, *Superconductivity of Metals and Alloys* (Addison-Wesley, Reading, 1966).
7. E.H. Brandt, Phys. Rev. **B34**, 6514 (1986).
8. J. Friedel, *Dislocations*(Addison-Wesley, Reading, 1964).
9. E.H. Brandt, Phys. Stat. Sol. **36**, 371 (1969); D.C. Hill, D.D. Morrison, and R.M. Rose, J. Appl. Phys. **40**, 5160 (1969).
10. H. Träuble and U. Essmann, Phys. Status Solidi **18**, 813 (1966); I.V. Grigor'eva, Sov. Phys. JETP **69**, 194 (1989).
11. A.T. Dorsey and M.P.A. Fisher, Phys. Rev. Lett. **68**, 694 (1992); V.M. Vinokur *et al.*, *ibid* **71**, 1242 (1993).
12. S.J. Hagen *et al.*, Phys. Rev. **B42**, 6777 (1990); H.-C. Ri *et al.*, *ibid* **B50**, 3312 (1994).

Journal of Superconductivity, Vol. 8, No. 4, 1995

Cation and Anion Disorder in $HgBa_2Ca_{n-1}Cu_nO_{2n+2+\delta}$

Massimo Marezio,[1,2] Edgar T. Alexandre,[1] Pierre Bordet,[1] Jean-Jacques Capponi,[1] Catherine Chaillout,[1] Evgueni M. Kopnin,[1] Sergio M. Loureiro,[1] Paolo G. Radaelli,[3] and Gustaaf Van Tendeloo[4]

January 5, 1995

Cu and C substitution for Hg in Hg-based cuprate superconductors is discussed. The large Hg Debye-Waller factor usually obtained from refinements based on diffraction data should be interpreted as an indication of carbon substitution for the Hg cations. This assumption is corroborated by HREM, powder x-ray anomalous dispersion, and powder neutron diffraction investigations.

KEY WORDS: Mercury superconductors; cation disorder.

Samples of compounds belonging to the $HgBa_2Ca_{n-1}Cu_nO_{2n+2+x}$ series were found to exhibit record-high superconducting transition temperatures [1, 2]. The structures of these compounds are very similar to those of the other layered cuprates in which oxygen-deficient perovskite blocks alternate with oxygen-deficient NaCl blocks. For example, they contain the following layer sequence:

$$(HgO_\delta)(BaO)(CuO_2)\{(Ca)(CuO_2)\}_{n-1}(BaO)(HgO_\delta)$$

Fig. 1 shows the structural arrangements of the members with $n = 1$ and $n = 3$. The specific, structural features of these compounds can be summarized as follows: i) The CuO_2 layers exhibit very small buckling; ii) Because of the tetragonal symmetry, the a parameters are almost exactly twice the Cu-O in-plane distances and depend on the copper valence; iii) The Cu-O apical distances are anomalously large (2.8 Å) as compared to the corresponding distances in similar compounds, for example, in superconducting $YBa_2Cu_3O_7$ the Cu-O apical distance is 2.28 Å; iv) The Hg cations are surrounded by two close oxygen atoms, belonging to the BaO layers above and below, forming a dumbbell along the c axis; v) The oxygen sites of the Hg layers, namely those forming the NaCl layers of the charge reservoir, are partially occupied and the maximum occupancy factor vary from one member to the next. The doping mechanism inducing superconductivity is strictly linked to these oxygen atoms.

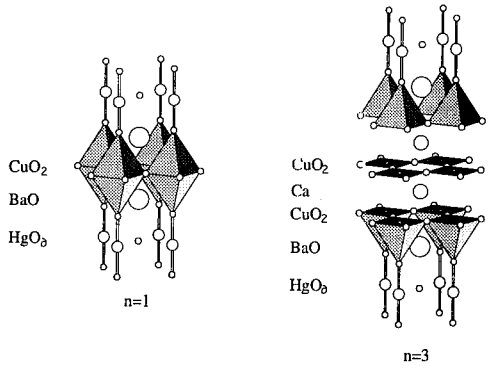

Fig. 1. Schematic structural arrangement for $HgBa_2CuO_{4+\delta}$ and $HgBa_2Ca_2Cu_3O_{8+\delta}$

Most of the structural data for these compounds have been obtained either by powder neutron diffraction techniques or by high resolution electron microscopy. All the structural refinements based on neutron data analyzed by the Rietveld method have yielded anomalously large Debye Waller factor for the Hg cations. In diffraction experiments this may be the result of static or dynamic displacive disorder or of partial substitution by another cation with smaller scattering power. In the very first structural refinement of the first member of the series, $HgBa_2CuO_{4+\delta}$ or Hg-1201, carried out by Wagner et al. [3] the large Debye-Waller factor of Hg was interpreted as an indication that some of the Hg cations were replaced by Cu. The subsequent refinement including the disorder between Hg and Cu indicated that 7% of the Hg cations were replaced by Cu. These authors also found that additional

1 Laboratoire de Cristallographie CNRS, BP 166, 38042 Grenoble cedex 09, France
2 AT&T Bell Laboratory, 600 Mountain Ave., Murray Hill, NJ 07974, USA
3 Institut Laue-Langevin, BP 156, 38042 Grenoble cedex 09, France
4 EMAT, University of Antwerp (RUCA), Groenenborglaan 171, B-2020 Antwerp, Belgium

0896-1107/95/0800-0507$07.50/0

oxygen atoms were located near the edge of the Hg mesh at (0.5,0,0.043). This site and that in the middle of the mesh at (0.5,0.5,0) would not be occupied simultaneously, but the former would be around the Cu and the latter around the Hg cations. The distribution of the additional oxygen would be such that each Cu would have a square co-ordination. This model was corroborated by the heat-treatment experiments carried out by Wagner et al. [3]. When the oxidized sample with T_c = 95 K was reduced in Ar at 500°C for 24 hours, T_c decreased to 59 K. The structural refinement of this sample showed that the occupancy factor of the oxygen at (0.5,0.5,0) dropped practically to 0, while that at (0.5,0,0.043) remained unchanged. The 59 K superconducting sample and its structure seem to indicate that in Hg-1201 there are two doping mechanisms, one related to the oxygen in the middle of the mesh and the other to the oxygen on the middle of the edge. The local stoichiometry and structure around the Cu cations substituting for the Hg ones correspond to the hypothetical compound $CuBa_2CuO_{4+x}$ (x depending on the number of oxygen on the chain copper). This would be the first member of the homologous series $CuBa_2Y_{n-1}Cu_nO_{2n+2+x}$, of which $YBa_2Cu_3O_7$ written as $CuBa_2Y_{n-1}Cu_nO_{2n+2+x}$ is the second member. The superconductivity at 59 K observed in the reduced sample of reference [3] could be due to domains of $CuBa_2CuO_{4+x}$ composition. Chmaissem et al. [4] who refined the structure of the original sample of Hg-1201 prepared by Putilin et al. [1] also found an anomalously large Debye-Waller factor for Hg, but no additional oxygen was found to exist on the edge of the Hg mesh. This feature is essential to make the substitution plausible. If the Cu cations were in the dumbbell co-ordination they would be necessarily in the +1 valence state, and this is not likely when oxidized precursors are used to prepare the samples.

To study the existence of the $Hg_{1-x}Cu_xBa_2CuO_{4+\delta}$ solid solution, samples with x = 0.00, 0.05, 0.10, 0.15, 0.20, 0.25, and 0.50, were synthesized using high pressure and high temperature technique [5]. Only the sample with x = 0 was found to be monophase by powder x-ray diffraction and depending upon the heat treatment was either non-superconducting or had a T_c = 50 K. The lattice parameters showed that these samples were overdoped. All the other samples with $x \neq 0$ contain impurities, whose nature and relative quantities depend upon x and the compound used as extra Cu source. The structure of the sample with x = 0 and exhibiting T_c = 50 K was refined by synchrotron x-ray powder diffraction data [6]. The preparation of this sample and its thermal history are reported in detail in reference [5]. The data collection was carried out at the beam line X7A of the NSLS, Brookhaven. A Si111 monochromator and a scintillation counter together with the capillary (0.3mm) geometry were used. In order to enhance the contribution of the Cu cations substituting for Hg, the pattern was collected at two different wavelengths, one at λ = 1.0504 Å far from the Cu K edge and the other very close to it at 1.3725 Å. In the pattern at the short wavelength only a very weak reflection due to an unknown impurity was detected. Its relative intensity indicates that the sample was better than 99% pure. Because of absorption this reflection was not visible in the pattern corresponding to the wavelength close to the edge. Simultaneous structural refinements on both sets of data were carried out by using the GSAS program. The final parameters are given in Table 1. The occupancy factor of the Hg site clearly indicates that the substitution of Hg by Cu is nil within our experimental errors. Note that the Debye-Waller factor for Hg is still appreciably higher than that of Ba. The δ value of 0.12(2) and that of T_c (50 K) confirmed that this sample of Hg-1201 is overdoped.

Table 1: Structural parameters from simultaneous refinements of synchrotron x-ray diffraction data at λ_1=1.0504 and λ_2=1.3725 Å

a=b		3.87320(2)	O1	x=z	0.5
c=		9.48088(8)		y	0.0
Hg/Cu	x=y	0.0		U_{iso}	0.0016(1)
	z	0.0	O2	x=y	0.0
	n(Hg)	1.01(3)		z	0.2068(7)
	n(Cu)	-0.09(6)		U_{11}=U_{22}	0.037(3)
	U_{11}=U_{22}	0.0165(4)		U_{33}	0.002(4)
	U_{33}	0.0166(7)	O3	x=y	0.5
Ba	x=y	0.5		z	0.0
	z	0.29520(6)		n	0.12(2)
	U_{iso}	0.0075(3)		U_{iso}	0.001
Cu	x=y	0.0			
	z	0.5		R_{wp}	5.49%
	U_{iso}	0.0018(5)		R_{exp}	3.01%

It is clear that the x-ray and neutron powder data results are contradictory. There are two possible explanations for this discrepancy: 1) one of the two results is incorrect; 2) the two samples are fundamentally different. Actually, they were prepared by completely different techniques. The one of reference [3] was prepared in a sealed tube and heat treated for 8 hours at 845°C, the present sample was prepared in a belt-type high-pressure apparatus. One crucial experiment would be to obtained anomalous x-ray diffraction data on the sample of reference [3].

Recently, compounds in the system Ba-Ca-Cu-O, which were referred to as copper-cuprates, were synthesized by high pressure and high temperature techniques [7, 8] and found to have high superconducting transition temperatures ($\approx$ 120 K). It was shown by HREM that these compounds contain C and their formula should be very similar to

$(Cu_{1-x}C_x)Ba_2Ca_{n-1}Cu_nO_y$, in which the single layer sandwiched between two BaO layers, contains ordered Cu and C cations [9]. It is possible that the same substitution occurs for the Hg cuprates, namely some of the Hg are replaced by C. An ordered occupation of Hg and C was found by HREM in some crystallites of a $(Hg,C)Ba_2Sr_2Cu_2O_x$ sample [10]. The structure of this phase derives from that of Hg-1201 in which Ba and Sr occupy the Ba sites of $HgBa_2CuO_{4+\delta}$ and Hg and C those of Hg. The carbon cations are surrounded by three oxygen atoms arranged as a triangle. Two of these oxygen are located in the two (BaO) layers above and below while the third lies in the same layer as C. Such co-ordination was found to exist in the structure of $Sr_2CuO_2CO_3$ [11,12] which contains the layer sequence $(CuO_2)(SrO)(CO)(SrO)$.

A structural refinement of an overdoped non superconducting Hg-1201 sample, based on neutron diffraction data, has been recently carried out [13]. The refinement including the atoms corresponding to the $HgBa_2CuO_{4+\delta}$ formula yielded the usual high Debye-Waller factor for Hg (B=1.37 Å). The value of δ (0.21(3)) together with the fact that no superconductivity was detected proved that the sample was indeed overdoped. Attempts to find additional oxygen in the middle of the edge of the Hg layer which would be a signature for the presence of Cu on the Hg sites resulted in a slightly negative occupancy factor for this position. Because of the possibility of C replacing Hg in this type of compounds, refinements of models containing carbonate groups were carried out. The two models which gave reasonable agreement between observed and calculated intensities and more importantly were not rejected during the refinement process are shown in Fig. 2. In the first, the C atoms were placed at (0,0,z), two of the three co-ordinating oxygen atoms at (x,x,0) and (-x,-x,0) and the third, belonging to one of the adjacent (BaO) layer, at (0,0,z'). In this configuration oxygen vacancies may be created on the other adjacent (BaO) layer, as shown in Fig. 2. In the second configuration the C atoms are located in (x,x,0), with one of the co-ordinated oxygen atoms at (1/2,1/2,0) and the other two, belonging to the (BaO) layers, at (0,0,z) and (0,0,-z). Unfortunately, the refinements did not allow one to choose between the two models. It should be pointed out that the first configuration allows the possibility of a second doping mechanism based on the extra oxygen brought in by the carbonate group. This could be partly compensated by vacancies on the BaO layer as shown in Fig. 2. The additional doping mechanisms would explain the superconductivity at 59 K for the reduced sample reported in reference [3]. On the other hand, the second configuration can reconcile a systematic difference, commonly obtained for the Hg cuprate samples, between the δ values determined by diffraction techniques and that deduced from iodometric titration. For example, for the present compound the δ value deduced from the latter technique is 0.13(2) as compared to 0.21(2) determined by neutron diffraction. The latter is larger than the former because the diffraction technique determines the occupation factor of the oxygen site at (1/2,1/2,0) without discriminating whether these oxygen atoms are bonded to Hg or C. Iodometric titration determines the amount of Cu^{3+}, therefore, the concentration of the doping oxygen. The difference between the values of δ represents the concentration of the C atoms. The structural refinement yielded an occupancy factor for the C atoms equal to 0.084(12), which agrees surprisingly well with the difference between 0.21(2) and 0.13(2).

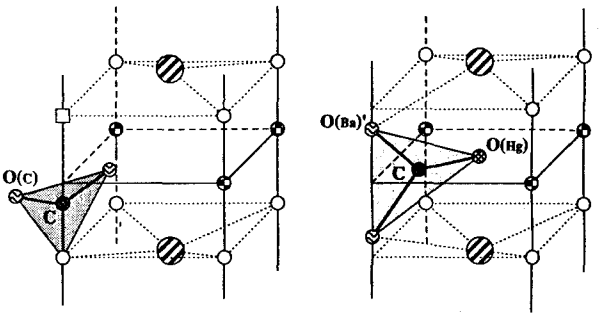

Fig. 2. Model of the carbonate defects with C atom shifted along the c axis (on the left) and with the C atom on the Hg layer (on the right).

To prove that carbonate groups may be incorporated into the structures of the Hg cuprates, Kopnin et al. [14] have synthesized samples of Hg-1223 and Hg-1234 by using precursors obtained by the decomposition of BaO_2, $CaCO_3$ and CuO. The samples were found to exhibit much lower T_c's (64 K for 1223 phase, and no superconductivity for the 1234 phase) than the corresponding Hg-based samples prepared by different precursors and this even after heat treatments in oxygen flow. The lattice parameters measured by conventional x-ray powder diffraction of the 1223 phase were found to be a=3.8653(5)Å, c=15.671(4)Å. These values differ largely from the parameters of a sample prepared by a nitrate precursor (a=3.8532(6) Å, c=15.818(2) Å) [15]. Note that the c parameter of the sample prepared from

carbonates is smaller than that of the sample prepared from nitrates. The incorporation of carbonate groups induces a decrease of the c parameter because the C-O distances are much shorter than the Hg-O ones. The variation of the lattice parameters cannot be attributed to different oxygen contents, because a variation of δ would change both parameters in the same direction. The structural refinement of the 1223 phase carried out by using synchrotron X-ray powder data revealed a large deficiency of the Hg site. The occupancy factor for this site was found to be 0.69(1). This may be explained by the replacement of some of the Hg cations by C.

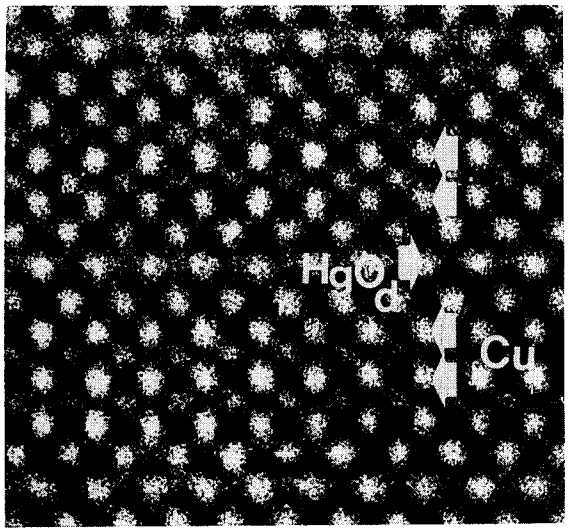

Fig. 3. High resolution image along [010] of the 1223 phase, showing the individual cation columns as bright dots.

Electron diffraction and high resolution electron microscopy for the 1223 sample reveal the perfect 1223 structure, with no traces of superstructure or imperfections. In the image of Fig. 3 all cations are revealed as bright dots and the HgO_δ layer can be easily identified as the more diffuse one; this follows by comparison with computer simulated images. Within this layer, however, we do see variations in the intensities of the different bright dots. These variations can be quantified by densitomer traces along the HgO_δ layer as well as along the neighboring CuO_2 layer. The results are shown in Fig. 4 where the intensity of different bright dots along a single HgO_δ row and labelled from 1 to 34 are shown. A clear, somewhat periodic, variation in the intensity is observed, whereas, almost no variation was detected for a CuO_2 row. This indicates a variation in the occupation of the Hg positions. If these variations were not random, but periodic, they would give rise to weak superstructure reflections visible in the diffraction patterns. Measurements of the local composition by EDX reveal indeed a deficiency of Hg (70-80%) with respect to the other elements, but not excess of Cu. All these observations seem to indicate that some of the Hg cations are replaced by carbon.

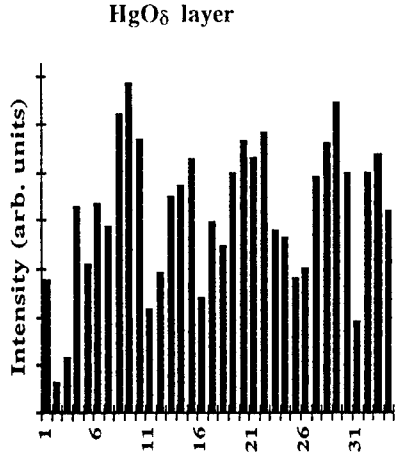

Fig. 4. Intensity measurements of individual dots along a HgO_δ row of Fig. 3.

REFERENCES

1. S.N. Putilin, E.V. Antipov, O. Chmaissem & M. Marezio, *Nature* **362** 226 (1993).
2. A. Schilling, M. Cantoni, J.D. Guo & H.R. Ott, *Nature* **363** 56 (1993).
3. J.L. Wagner, P.G. Radaelli, D.G. Hinks, J.D. Jorgensen, J.F. Mitchell, B. Drabowski, G.S. Knapp & M.A. Beno, *Physica C* **210** 447 (1993).
4. O. Chmaissem, Q. Huang, S.N. Putilin, M. Marezio, & A. Santoro, *Physica C* **212** 259 (1993).
5. E.T. Alexandre, S.M. Loureiro, E.V. Antipov, P. Bordet, S. de Brion, J.J. Capponi, & M. Marezio, *Physica C*, submitted.
6. P.G. Radaelli, to be published.
7. M. Alario-Franco, C. Chaillout, J.J. Capponi, B. Souletie, & J.L. Tholence, *Physica C* **222** 52 (1994).
8. X.-J. Wu, S. Adachi, C.-Q. Jin, H. Yamauchi, & S. Tanaka, *Physica C* **223** 243 (1994).
9. T. Kawashima, Y. Matsui & E. Takayama-Muromachi, *Physica C* **224** 69 (1994).
10. M. Uehara, S. Sahoda, H. Nakata, J. Akimitsu & Y. Matsui, *Physica C* **222** 27 (1994).
11. D.V. Fomichev, A.L. Kharlanov, E.V. Antipov & L.M. Kovba, *Superconductivity: Physics, Chemistry & Technique,* **3** p. 126 (1990) (English translation).
12. Y. Miyazaki, H. Yamane, T. Kajitani, T. Oku, K. Hiraga, Y. Morii, K. Fuchizaki, S. Funahashi & T. Hirai, *Physica C* **191** 434 (1992).
13. S.M. Loureiro, E.T. Alexandre, E.V. Antipov, J.J.Capponi, S. de Brion, B. Souletie, J.L. Tholence, M.Marezio, Q. Huang, & A. Santoro, *Physica C* accepted 1995
14. E.M. Kopnin, E.V. Antipov, J.J. Capponi, P. Bordet, C. Chaillout, S. De Brion, M. Marezio, A.P. Bobbylev and G. Van Tendeloo, *Physica C* submitted.
15. E.V. Antipov, S.M. Loureiro, C. Chaillout, J.J. Capponi, P. Bordet, J.L. Tholence, S.N. Putilin , and M. Marezio, *Physica C* **215**, 1 (1993).

Journal of Superconductivity, Vol. 8, No. 4, 1995

Superconductivity Above 100 K in Compounds Containing Hg

M. S. Osofsky,[1] W. L. Lechter,[1] L. E. Toth,[1] E. F. Skelton,[1] A. R. Drews,[1]

C. C. Kim,[1,2] B. Das,[1] S. B. Qadri,[1] A. W. Webb,[1] and R. J. Soulen, Jr.[1]

The results of studies of new Hg based cuprate superconductors are reported. Several members of a new family of $(Hg,Tl)(Ba,Sr)Ca_{n-2}Cu_nO_x$ high temperature superconductors have been synthesized. These compounds, which are analogs to the Hg-Ba-Ca- and Tl-Ba-Ca- layered cuprates, are multi-phased and have superconducting transition temperatures above 100 K. Incorporation of Hg appears to stabilize several of the Tl-compounds, including a double layer Tl/Sr system, in a manner similar to the role that Pb plays in the Tl/Sr- and Bi/Sr-systems. It has been suggested that recent reports of resistive T_c's above 200 K in Hg based samples are due to the presence of free Hg. Magnetization measurements of such a sample confirm this hypothesis.

KEY WORDS: superconductivity, cuprate, Hg, Tl.

1. INTRODUCTION

Recent reports of new Hg based high temperature superconductors (HTS) has rejuvenated the search for ever higher superconducting transition temperatures (T_c). While there have been reports of large drops in sample resistance above 200 K, the highest known confirmed T_c at ambient pressure occurs in the $HgBa_2Ca_{n-1}Cu_nO_y$ [1,2] system. The next highest set of transition temperatures exists in the TlBaCaCuO layered cuprate family [3,4]. Attempts to increase T_c in these compounds by doping has not succeeded: Substituting Sr for Ba significantly reduces T_c in the Tl system [5] and apparently has a similar effect in the Hg system. Recently, there was a report of a Hg/Tl intergrowth forming a unit cell wherein a 1201/Hg was combined with a 2201/Tl [6] with a T_c about half that of either end member. Hur et al. [7] reported the synthesis of a (HgTl)BaCaSrCuO compound with a single Hg/Tl layer and T_c values of 128-132 K. Bryntse [8] reported a $(Hg,Tl)_2Ba_2CaCu_2O_y$ material with a T_c of 100 K, and Sun et al [9] reported a T_c as high as 140 K in $(Hg,Tl)Ba_2Ca_2Cu_3O_y$.

We initiated a systematic effort to synthesize mixed Hg and Tl cuprate compounds with the hope of producing several new intergrowth structures with high superconductive transition temperatures. We used a hot isostatic press (HIP) [5,10] to prepare samples since it was successful in synthesizing compounds difficult to fabricate by other means. In addition to offering the element of safety, this technique allows the operator to select a broader range of reaction temperatures and pressures than are normally accessible in conventional processing. More recently we showed that HTS Hg compounds could also be fabricated by the HIP [11] process where the externally applied pressure served to contain the high Hg pressures developed during the reaction. We also demonstrated that bulk devices such as shields and test bars could be fabricated directly in a HIP. In addition, for several samples we used a tetrahedral press to achieve even higher pressures and temperatures during synthesis.

In this report, we describe our success in synthesizing compounds with nominal compositions corresponding to the intergrowth formulas $Tl_{1(or\ 2)}Hg(Ba(Sr))_4Ca_{2n}Cu_{2+2n}O_x$. For n=0, this formula corresponds to a layer sequence of TlO-TlO-(Ba,Sr)O-CuO_2-(Ba,Sr)O-HgO-(Ba,Sr)O-CuO_2-(Ba,Sr)O-TlO-TlO-(Ba,Sr)O-CuO_2-(Ba,Sr)O-HgO-(Ba,Sr)O-CuO_2-(Ba,Sr)O. Martin et al. [6] have synthesized the n=0 Ba compound has a tetragonal unit cell with a=3.86 Å and c=42.2 Å.

We also report on the results of the superconducting properties of a $HgBa_2CuO_y$ sample

[1] Naval Research Laboratory, Washington D. C. 20375-5000
[2] present address: University of Illinois, Chicago, IL 60607

0896-1107/95/0800-0511$07.50/0

with a large resistance drop at 240 K. These results strongly suggest that such "transitions" are not due to superconductivity but to the freezing of free Hg in the sample.

2. SAMPLE PREPARATION

Precursors of the Ba, Sr, Ca, and Cu oxides were prepared and mixed with HgO and Tl_2O_3. These mixed powders were placed in a pouch of gold foil, which was then sealed inside a thin-walled stainless steel container under vacuum. Most of the samples were processed at 850°C and 160 MPa for 30 minutes after which time the power to the furnace was shut off. Several samples were made at 900°C and 210 MPa for three hours. Details of the sample preparation are presented elsewhere [12].

After processing and removal from the stainless steel container, the gold foil was peeled off the sample. No evidence for a reaction between the stainless steel and gold, or between the gold and the sample was found. We were also successful in synthesizing these compounds at much higher pressures (~ 6 GPa) and at higher temperatures in a tetrahedral press, the details of those efforts will be reported elsewhere [13].

3. COMPOSITIONAL ANALYSIS

Due to the volatility of Hg and the fact that many of the T_c values of the (Hg,Tl) compounds are comparable to those found for the pure Tl compounds, we carried out a study to determine the extent to which the Hg was actually incorporated into the superconducting material [12]. Imaging in the SEM clearly revealed small amounts of unreacted masses, which corroborated optical observations of polished samples in polarized light. EDS analysis of grains for chemical composition showed clear evidence for incorporation of Hg. To determine the homogeneity of the Hg and Tl, an x-ray dot map was made of a region containing several large grains. No variation of Hg or Tl composition was visible within the grains. Earlier EDS analyses of Tl/Hg/Sr samples also showed that the Tl and Hg were uniformly distributed [5]. Grains of Ca- or Ba-cuprates were also found.

Samples were also sent to a commercial laboratory for ICP analyses. These results showed that the Hg and Tl content of the reacted bulk samples was very nearly equal to that of the nominal composition of the starting material [14], indicating that very little Hg could have escaped from the sample. Furthermore, examination of the gold and stainless steel containment pouches by x-ray fluorescence showed no evidence of Hg contamination.

4. X-RAY STRUCTURAL ANALYSIS

Standard polycrystalline x-ray diffraction methods were used to identify the crystal structures of the phases present in each of the samples [12]. The measured spectra were compared to those of the known structures. Interpretation of the data is complicated by the fact that none of our synthesis efforts yielded a single phase product. The x-ray patterns for what are believed to be the dominant phases were analyzed and the *a*- and *c* axis parameters were determined. Most of the patterns could be interpreted as originating from samples containing a mixture of two or more of the known Tl-structures, "2212", "2223", and "2234". All diffraction patterns showed *a*-axes of about 3.8 Å, which is approximately the same value for all the known Hg- and Tl-compounds. The *c*-axis parameters, though, were inconsistent with the nominal chemistry of intergrowth structures, phase separated end-members of Tl and Hg compounds, or Tl compounds alone. The last case was considered as a likely consequence in the event of loss of all the Hg.

For most samples the spectrum was matched with a known structure which was expected from the nominal composition. In other cases, the spectra best matched a structure that was inconsistent with the nominal composition. These inconsistent results may be explained by phase separation, intergrowths with disordered stackings of Hg and Tl like unit cells, or substitution of Hg into sites within a Tl-superconductor structure.

5. SUPERCONDUCTING PROPERTIES

The superconducting transition temperatures were determined from plots of the resistance versus temperature, R(T), using four-probe ac resistance measurements. All of the (Hg/Tl) layered cuprates were found to be superconducting. The samples containing Ba always had T_c values above 100 K, which were invariably higher than their Sr analogs. Fig. 1 shows the R(T) plot for several samples of $HgTl_2Ba_4Ca_4Cu_6O_x$ which were the best results to date for this system. The best sample had an onset at 132 K and R=0 at 127 K and was made in the tet press [13].

The dc magnetic moment, m(T), of the samples was also measured as a function of temperature using a Quantum Design™ MPMS SQUID system.

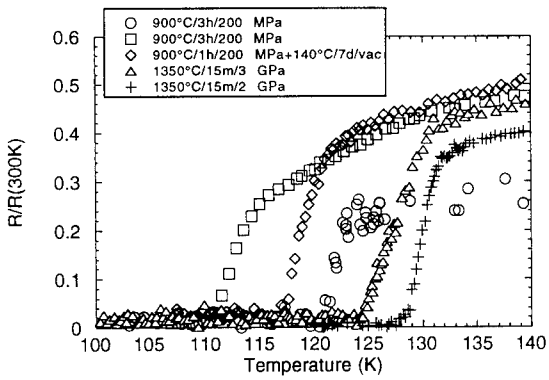

Fig. 1:. Resistance (normalized to the room temperature resistance) versus temperature for the samples of $HgTl_2Ba_4Ca_4Cu_6O_x$ with the highest transition temperatures.

The moments of small pieces of the samples were recorded in a magnetic field of 10 Oe in both field-cooled and zero-field-cooled situations. An example of the behavior seen is shown in Fig. 2 for a sample of $HgTl_2Ba_4Ca_4Cu_6O_x$. As in the R(T) measurements, more than one transition was observed. These temperatures are not identified with a particular phenomenon such as an onset temperature or a temperature where full diamagnetism occurs because these features are not uniquely defined by the measurements. There is reasonably good agreement between the onset temperature determined from the R(T) curves and the temperature at which diamagnetism first appears. Correlations between any other transitions identified by R(T) or χ(T) are not clear-cut.

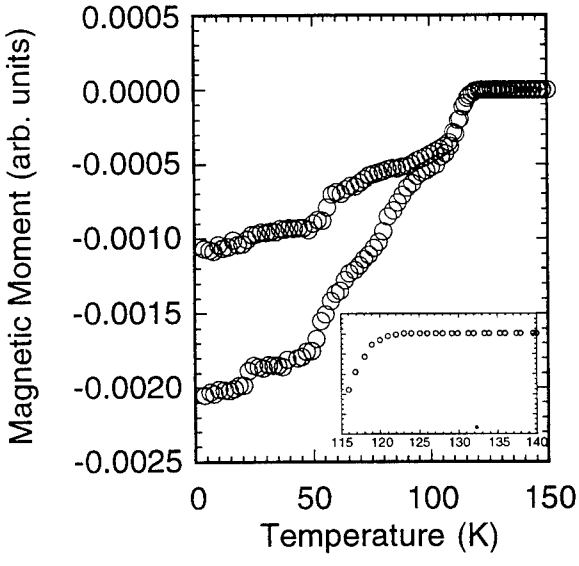

Fig. 2 Magnetic moment for a sample of $HgTl_2Ba_4Ca_4Cu_6O_x$ versus temperature. A magnetic field of 10 Oe was applied to obtain the field-cooled trace (upper) and zero-field-cooled trace (lower). Inset: expanded temperature display near the onset of superconductivity.

6. DISCUSSION

We have synthesized several Hg/Ba and Tl/Ba (calcium) cuprates with T_c values between those for the Hg/Ba- and Tl/Ba-compounds. This observation applies for both the single and double layer Tl cuprates. While we do not have conclusive evidence for the formation of the higher order intergrowth structures of Hg/Tl compounds, EDS clearly shows that the superconducting materials contain both Tl and Hg.

For Hg/Tl/Sr compositions, superconductivity was found in crystal structures corresponding to both single and double Tl-O layers [12]. When the predominant structure was 1212, corresponding to a 1:1 ratio of Hg and Tl, the T_c at R=0 was either 40 K, or nearly 100 K. It is probable that the higher transitions are for a 1223 like structure. Higher T_c values were also observed in samples with double Tl-O layers, 2212, with R=0 at 70 to 80 K and onsets greater than 100 K. Without the addition of Hg, double layers of Tl-O are not found in Tl/Sr cuprates. In fact, without the addition of some stabilizing element such as Pb or Hg, Tl/Sr cuprates are difficult to form. T_c values in the (Tl,Hg)Sr compounds are not as high as found in the Tl/Pb/Sr cuprates; Tl/Pb/Sr 1223 has an onset of 125 K [15], whereas the highest transition observed for Tl/Hg/Sr is 114 K. These high onset temperatures (>100 K) indicate that Hg/Tl/Sr cuprates are potentially interesting and useful materials.

7. POSSIBLE HIGHER T_C'S?

Recently there have been several reports of large resistance drops, even to R=0, in Hg based samples. Since the resistance of elemental Hg drops significantly at its melting temperature of ≈240 K [16] it has been suggested that the resistance anomalies observed in the HTS are due to free Hg which has accumulated at grain boundaries.

Fig. 3 is a plot of the resistivity vs. temperature for a sample of $HgBa_2CuO_y$ made in the tetrahedral press showing a significant drop in resistivity at

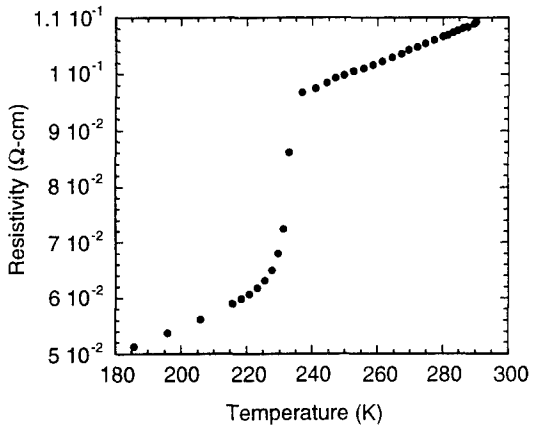

Fig. 3. Resistance as a function of temperature for a $HgBa_2CuO_y$ sample showing a large resistance drop at 240 K.

approximately 240 K. Magnetization measurements made on this sample (Fig. 4) display no hint of a diamagnetic transition at high temperature. At 237 K there is what appears to be a drop in the moment but we attribute that to measurement noise. At around 60 K

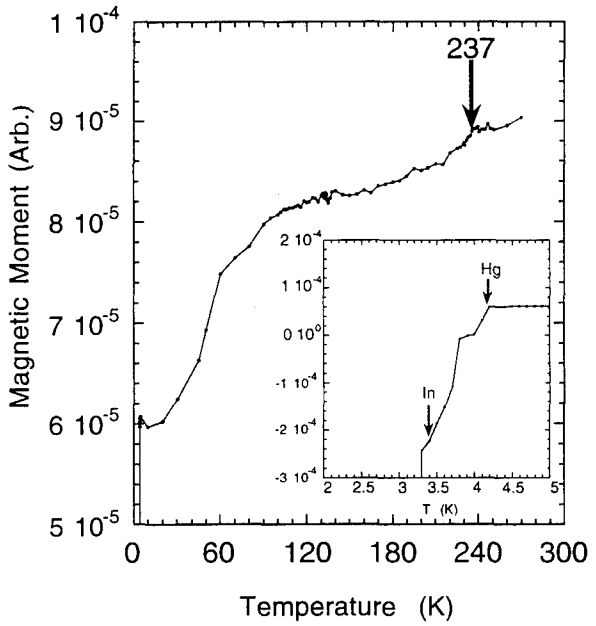

Fig. 4. Magnetization for the sample in Fig. 3 from room temperature down to 4.2K. Inset:: Magnification of the curve below 5 K.

there appears to be an onset of diamagnetism although the moment never drops below zero.

The inset of Fig. 4 is a magnification of the plot for temperatures below 5 K. Arrows indicate the transition temperatures of Hg and In (since In solder was used for the resistance measurements). These results strongly suggest that the large resistive anomalies are, indeed, due to elemental Hg which has been freed during sample processing. Thus, researchers looking for very high temperature T_C's in the Hg based HTS should include magnetization measurements below 5 K as a regular practice in verifying suspicious resistive anomalies at much higher temperatures.

ACKNOWLEDGMENTS

We thank Ken Killian for his help in all aspects of running the HIP. We also acknowledge the financial support of the Naval Research Laboratory, the Office of Naval Research and the Advanced Research Projects Agency. One of us (ARD) acknowledges the support of the National Research Council for its support through a post-doctoral fellowship. We all thank D. U. Gubser for his continuing interest in this project.

REFERENCES

1. S. N. Putilin, E. V. Antipov, O. Chmaissem and M. Marezio, *Nature* **362** , 226 (1993).
2. A. Schilling, M. Cantoni, J.-D. Guo and H. R. Ott, *Nature* **363** , 56 (1993).
3. Z. Z. Sheng and A. M. Hermann, *Nature* **332**, 138 (1988)
4. Cf. K. Yvon and M. Francois, Z. Phys. B **76**, 413 (1989)
5. W. L. Lechter, M. S. Osofsky, R. J. Soulen, Jr., V. M. LeTourneau, E. F. Skelton, S. B. Qadri, W. T. Elam, H. A. Hoff, R. A. Hein, L. Humphreys, C. Skowronek, A. K. Singh, J. V. Gilfrich, L. E. Toth and S. A. Wolf, *Solid State Communications* **68** , 519 (1988); H. A. Hoff, W. L. Lechter, and L. E. Toth, *J. Scanning Microscopy* **13**, 265 (1991).
6. C. Martin, M. Huve, G. Van Tendeloo, A. Maignan, C. Michel, M. Hervieu, and B. Raveau, *Physica C* **212** , 274 (1993).
7. N. H. Hur, N. H. Kim, K. W. Lee, Y. K. Park and J. C. Park, Mat. Res. Bull., **29**, 959 (1994).
8. I. Bryntse, to be published in *Physica C.*
9. G. F. Sun, K. W. Wong, B. R. Xu, T. Xin, and D. F. Lu, preprint
10. W. L. Lechter, M. S. Osofsky, E. F. Skelton and L.E. Toth, United States Patent No. 5,120,704 (1992).
11. W. Lechter, L. Toth, M. Osofsky, J. Schwartz, J. Kessler, and C. Wolfers, submitted to *Physica C.*
12. W. L. Lechter, M. S. Osofsky, L. E. Toth, E. F. Skelton, A. R. Drews, C. C. Kim, B. Das, S. B. Qadri, A. W. Webb, and R. J. Soulen, Jr., Physica C, in press.
13. Complete details of samples prepared in the tetrahedral press will be given in a separate paper.
14. Galbraith Laboratories, Inc., Knoxville, TN.
15. M. A. Subramanian, C. C. Torardi, J. Gopalakrishnan, P. L. Gai, J. C. Calabrese, T. R. Askew, R. B. Flippen and A. W. Sleight, *Science* **242**, 249 (1988).
16. J. Dewar and J. A. Fleming, Proc. Roy. Soc. 76 (1896).

Journal of Superconductivity, Vol. 8, No. 4, 1995

SINGLE CRYSTALS of Hg-12(n-1)n and INFINITE LAYER-$CaCuO_2$ OBTAINED at GAS PRESSURE P=10kbar

J.Karpinski[1], K.Conder[1], H.Schwer[1], J.Löhle[1], L.Lesne[1,2], C.Rossel[2], A.Morawski[3], A.Paszewin[3], T.Lada[3]

Received 31 January 1995

Single crystals of $Hg_{1-x}Pb_xBa_2Ca_{n-1}Cu_nO_{2n+2+\delta}$ (x=0, 0.2, 0.5; n=2,3,4,5) and infinite layer $CaCuO_2$ compounds have been grown using a high gas pressure. Resistivity measurements have been performed in fields up to 10 T. The $Hg_{0.8}Pb_{0.2}$-1234 single crystals of a size up to 0.5x0.5 mm^2 have a T_c onset of 130 K. Single crystals of $CaCuO_2$ of a size up to 2x1 mm^2 have a T_c onset between 70 and 100 K. X-ray structural refinements have been performed on the $CaCuO_2$ and HgPb-12(n-1)n single crystals.

KEY WORDS: Single crystals, high pressure synthesis, structure, HgBaCaCuO, $CaCuO_2$.

1.INTRODUCTION

There are two families of superconducting compounds which are especially interesting: the family of HgBaCaCuO [1,2] which recently attracts much interest due to the highest critical temperature, $T_c=135$ K, and the infinite-layer $(CaA)CuO_2$ (where A-alkaline-earth metal) compounds, which have the simplest crystallographic structure displaying superconductivity.

One of the main difficulties with the synthesis of HgBaCaCuO is a low thermal stability of the mercury compounds. HgO, used for the preparation of HgBaCaCuO compounds decomposes at ambient pressure at about 400°C. At this temperature kinetics of the formation of HgBaCaCuO is very slow. In order to prevent decomposition of HgO and evaporation of Hg before the reaction takes place Hg12(n-1)n compounds have usually been synthesized in quartz glass ampoules at ambient or slightly increased pressure, or at high pressure in a belt type apparatus. In the first case, dependent on a free volume of the ampoule, a part of HgO decomposes creating relatively high pressure of Hg, HgO, and O_2 vapours of more than 10 bars leading sometimes to explosion of the ampoules. Due to difficulties with the control of Hg partial pressure it is very difficult to obtain stoichiometric samples.

[1]Laboratorium für Festkörperphysik ETH 8093-Zürich, Switzerland.
[2]IBM Research Division 8803 Rüschlikon, Switzerland.
[3]High Pressure Research Center "Unipress" Polish Academy of Science 01142 Warsaw, Poland.

Therefore, high pressure techniques with a solid-medium, usually pyrophylite, have been frequently applied.

In the case of the infinite layer-$CaCuO_2$ the reason for using the high pressure technique was different: the superconducting phase is metastable at ambient pressure and a pressure of 50 kbar has been reported to be necessary to stabilize the phase in a solid-medium pressure systems. The solid-medium pressure technique has many disadvantages: The sample is limited up to ~0.5 cm^3. The pressure and temperature distributions are not homogeneous and the partial oxygen pressure is difficult to control, resulting in undefined preparation conditions. Single crystal growth is impossible as well. There is also a great probability of introducing impurities from the pressure medium. These disadvantages disappear in a gas pressure system. An Ar gas atmosphere with a defined partial oxygen pressure leaves free space for a single-crystal growth. A temperature gradient in a multizone furnace is relatively easy to control. A maximum sample volume can be several cm^2. Using such a system we have synthesized Hg12(n-1)n and infinite layer-$CaCuO_2$ single and polycrystalline samples.

2. CRYSTAL GROWTH OF HgPb-12(n-1)n

In order to succesfully perform a synthesis of a compound it is desirable to have basic thermodynamic data like vapor pressures of gaseous components as a function of a temperature and melting points. Although

0896-1107/95/0800-0515$07.50/0

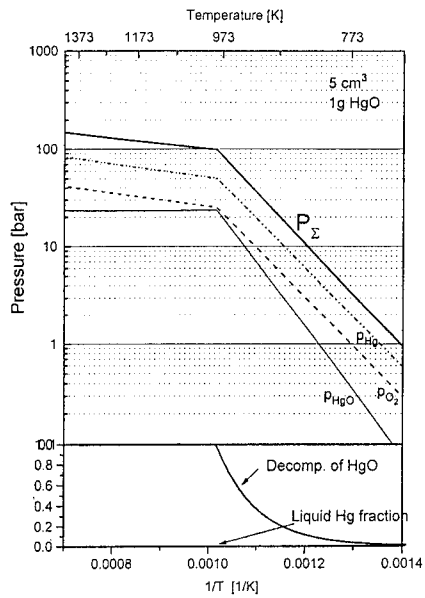

a)

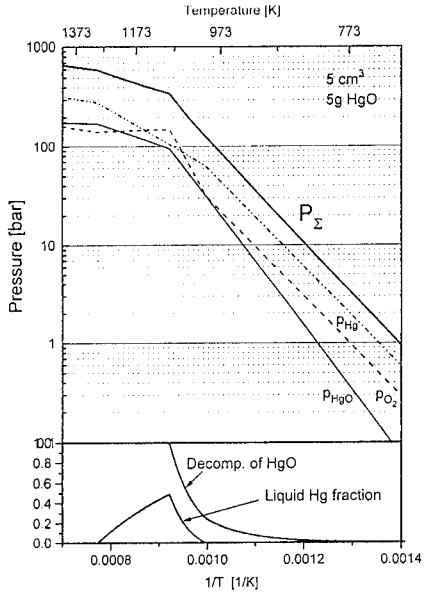

b)

Fig.1 Partial and total pressures created in a closed crucible of a volume 5 cm^3 by a decomposition of: 1g HgO; a), 5g HgO; b). In the lower part of the figure one can see fraction of decomposed solid HgO and appearance of liquid Hg in a certain temperature range.

many papers appeared on the synthesis of these compounds, there is no information in the literature concerning thermodynamics of this system.

Using existing data we have calculated partial pressures in closed crucibles by a decomposition of HgO only. As one can see in Fig.1, dependent on the free volume of the crucible and the amount of the material, these pressures can reach several hundreds bars at the synthesis temperature. By a variation of the relation between the free space and the mass of the sample one can control partial pressures of the components. As we observed in our crystal growth experiments, an increase of the partial pressures by lowering of the volume leads to the synthesis of the compounds with higher n.

Hg-12(n-1)n compounds melt peritectically, but at ambient pressure they decompose before melting and the volatile components evaporate. Our goal was to prevent decomposition by an encapsulation of the sample with a high hydrostatic inert gas pressure until the peritectic temperature is reached. Due to the high density of Ar gas at this pressure the evaporation of Hg is strongly supressed. Additionally, application of a flux with a lower melting point allows growth of single crystals below the peritectic decomposition temperature. As a flux PbO or $BaCuO_2$-CuO mixture have been used. The crystallization temperature was $1020° < T < 1070°C$. All experiments have been performed at Ar pressure 10 kbar. Two crucible materials have been applied: alumina and yttria. Crystal growth in the alumina crucible leads to a strong doping with Al and mixed (HgAl)BaCaCuO have been obtained. In yttria crucibles we have crystallized HgPb-1234 and HgPb-1245 pure phase crystals as well as HgPb-1212 strongly doped with Y. The details of the crystal growth procedure have been published in a separate paper [3,4].

Figure 2 shows a HgPb-1234 single crystal with characteristic growth steps. T_c values derived from the onset of the superconducting transition measured by DC SQUID technique on single crystals with various n = 2-5 are shown in Fig.3 in comparison with the literature data for ceramic samples [5]. There is a relatively good agreement for n =4, for n=5 the T_c is higher, however for n = 2 and 3 the T_c is much lower (for n=2 due to strong substitution of Y for Ca).

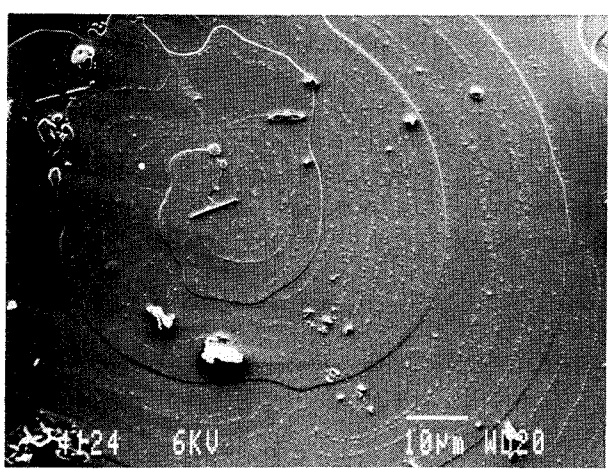

Fig.2. Single crystal of HgPb-1234 phase with characteristic spiral-like growth steps.

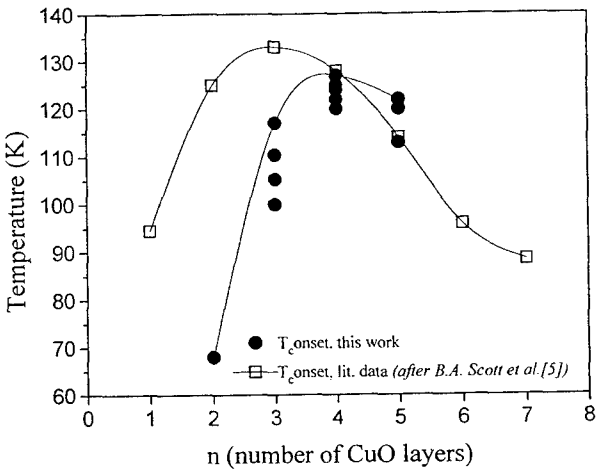

Fig. 3. T_c values of single crystals with various n in comparison with the literature data for ceramic samples.

The composition of our crystals determined by microprobe measurements were for n=4: $Hg_{0.8}Pb_{0.2}Ba_2Ca_3Cu_4O_{10+x}$, n = 5 : $Hg_{0.5}Pb_{0.5}Ba_2Ca_4Cu_5O_{12+x}$, n = 2 : $Hg_{0.5}Pb_{0.5}Ba_2Ca_{0.5}Y_{0.5}Cu_2O_{6+x}$. Unexpectedly in the same batch we found some crystals of 1245 and 1212 phase, but only 1212 contains large amount of Y. It seems, that the solubility of Y is larger in 1212 than in 1234 or 1245 crystals.

3. TRANSPORT MEASUREMENTS.

The in-plane resistance was measured on $Hg_{0.8}Pb_{0.2}Ca_2Ba_3Cu_4O_{10+x}$ single crystal by the van derPauw method. The crystal was contacted at the edges in such a way that the current flows along the ab-plane and the magnetic field was applied parallel to the c-axis. The resistivity as a function of temperature is shown in the Fig.4. The crystal has an onset of T_c=130 K. The shape of $\varrho(T)$ is not linear, as in other optimally doped superconductors, but has a downward curvature which is typical for underdoped cuprates. The linearity is reached at temperatures above 300 K. Similar results have been recently published on Hg-1223 crystals [6,7]. Although, according to the authors of ref. [7] these are multiphase crystals framed by a majority lattice of Hg1223.

4. CRYSTAL GROWTH OF INFINITE LAYER-$CaCuO_2$.

The infinite layer compound-$CaCuO_2$, consists of a stack of CuO_2 planes separated by Ca atoms. It has the simplest crystallographic structure, superconducting cuprate and is the best candidate for study of the origin

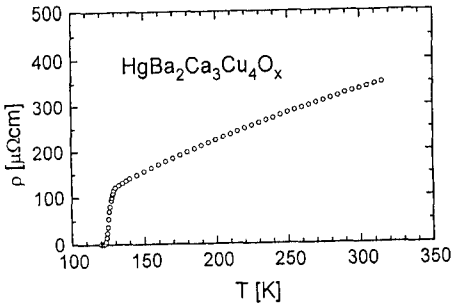

Fig.4. In-plane resistivity of HgPb-1234 single crystal vs. temperature [8].

of high T_c superconductivity.

Until now, the infinite layer samples have been synthesized only as ceramics which prohibited performing accurate measurements of both physical and structural properties. Therefore, there is a general demand for single crystals of these materials. We have obtained superconducting $CaCuO_2$ single crystals at similar conditions as Hg-12(n-1)n but starting from a $CaCuO_2$-$BaCuO_2$-CuO mixture. We have stabilized the $CaCuO_2$ phase without Sr or Li additives. Our experimental pressure of 10 kbar used for the growth of the superconducting infinite layer single crystals compound is much lower than 50 kbar reported up to now as necessary for the synthesis of this compound.

5. STRUCTURAL INVESTIGATIONS.

Crystals of $Hg_{0.8}Pb_{0.2}Ba_2Ca_3Cu_4O_{10+x}$, $Hg_{0.5}Pb_{0.5}Ba_2Ca_4Cu_5O_{12+x}$, and $CaCuO_2$ were measured on an x-ray four-circle single crystal diffractometer and the crystal structures have been refined. The crystals for x-ray experiments are black, rectangular plates with maximum dimensions of 0.5 x 0.5 x 0.03 mm^3. The main face is always (001), and the a-axes are usually running parallel to the edges. The space group of all the crystals is P4/mmm. The crystals were examined with a Gandolfi and a Buerger precession x-ray single crystal camera, using MoKα radiation (λ = 0.7107 Å).

Those crystals which showed diffraction patterns with sharp reflections and without traces of twinning or macroscopic intergrowth were selected for diffractometer measurements. The crystals were measured on a four-circle single-crystal diffractometer (Siemens P4) at 20 C, using graphite monochromatized MoKα radiation (λ = 0.71073 Å). Intensity profiles were scanned in the ω-2Θ mode and reflections were collected of the whole Ewald sphere in the range $3° < 2\Theta < 70°$. Intensity data were corrected for Lorentz polarisation effects, and analytical absorption corrections

were applied. Full-matrix least-squares refinements of structural parameters (scaling factor, extinction, position, occupation, and anisotropic thermal parameters) were performed with weighted structure factors, based on (F). No reflections have been excluded for the refinements. All structural calculations have been performed with the program SHELXTL [9].

The lattice parameters of $Hg_{0.8}Pb_{0.2}Ba_2Ca_3Cu_4O_{10.14}$ are a = b = 3.8530(5) Å and c = 18.968(3) Å and the crystal structure has been described recently [10]. The structure corresponds to the n=4 type of the Hg-12(n-1)n homologous series and has been refined to R= 0.026. Lead is incorporated at the Hg site, but it is shifted slightly from the origin in the z = 0 plane.

A reduction of electron density is observed at the Hg site and is attributed to the partial substitution by Cu or CO_3 groups. Stacking faults of 1223 or 1245 layers are observed by TEM, but not in the x-ray diffraction patterns. However, they introduce additional electron density in the Fourier maps of 1234 and it was possible to refine the amount of stacking faults to 3.8 %. Unfortunately, one of the additional electron density peaks is very close to the excess oxygen O(4) site (½, ½, 0), and may cause a wrong determination of the excess oxygen content. Without taking into account these stacking faults an excess oxygen concentration of 33 % is refined; after correction the occupation of the O(4) site is reduced to 14 %.

The lattice parameter of $Hg_{0.5}Pb_{0.5}Ba_2Ca_4Cu_5O_{12.21}$ are a = b = 3.8529(3) Å and c = 22.172(2) Å.

It represents the 5-layer member of the Hg-12(n-1)n family and the structural features are very similar to those of $Hg_{0.8}Pb_{0.2}Ba_2Ca_3Cu_4O_{10.14}$. The crystal contains 3.9 % stacking faults of 1234 or 1256 layers and the structure has been refined to R = 0.033.

The occupation of the Hg site is reduced as well, due to substitution. HgPb-1245 contains more lead than HgPb-1234, but the lead atom is also shifted slightly from the Hg position in the origin. This is in agreement with TEM observations in HgPb-1223 material [11].

The $CaCuO_2$ infinite layer structure has lattice constants a = b = 3.8556(6) Å and c = 3.1805(4) Å and was refined to R = 0.027 [3]. The structure corresponds to the central part of the Hg-12(n-1)n structures and has a full occupancy of all atom positions. The bondlengths are in agreement with those of the other Hg-12(n-1)n compounds and show systematic trends with increasing number of CuO_2 planes. The buckling of the central CuO_2 planes is smaller than that of the outer ones, indicating the approach to the ideal $CaCuO_2$ structure (d_{Cu-O} = 0) in the central part of 1234 and 1245. Table 1 compares the results from x-ray powder and single crystal refinements of the homologous series [10-14]. Ba moves to the basal plane, expressed by decreasing Ba - Ba and Hg - Ba distances. The apical oxygen atom is shifted away from Hg, and, therefore, the Ba - O bondlength decreases, too. The spacing between the CuO_2 layers increases as well, and even exceeds that of the pure $CaCuO_2$ infinite layer compound with c = 3.1805(4) Å.

Table 1. Selected bondlengths and distances in Hg-12(n-1)n compounds.

	Hg-1201 [12]	Hg-1212 [13]	Hg-1223 [13]	HgPb-1234 [10]	HgPb-1245 [14]
Hg - O (Apex)	1.950 Å	1.970 Å	1.975 Å	2.008 Å	2.031 Å
Ba - O (Apex)	2.880 Å	2.848 Å	2.837 Å	2.818 Å	2.809 Å
Hg - Ba	3.941 Å	3.907 Å	3.879 Å	3.855 Å	3.847 Å
Ba - Ba	5.662 Å	5.598 Å	5.538 Å	5.453 Å	5.432 Å
Cu - Cu	-	3.135 Å	3.156 Å	3.190 Å	3.188 Å

REFERENCES.
1. A.Schilling et al., Nature 363(1993)56.
2. M.Marezio et al., Physica B 197 (1994) 570.
3. J.Karpinski et al., Physica C 234 (1994) 10-18.
4.J.Karpinski et al., Nature 371(1994) 661.
5. B.A.Scott et al., Physica C 230 (1994) 239.
6. A.Carrington et al., Physica C 234 (1994) 1-9.
7. D.Colson et al. Physica C 233 (1994) 231.
8. J.Löhle et al. to be published.
9. G.M. Sheldrick, SHELXTL, Siemens Analytical X-ray Instruments, 1990.
10. H.Schwer et al., Physica C 234 (1995) 10.
11. Z. Iqbal et al., Phys. Rev. B 49, (1994),12322.
12. S.N. Putilin et al., Nature 362, (1993), 226.
13. L.W. Finger et al., Physica C 226, (1994), 216.
14. H. Schwer et al., Physica C, (1995) in prep.

Journal of Superconductivity, Vol. 8, No. 4, 1995

Formation and Properties of Artificially-Layered $SrCuO_2/BaCuO_2$ Superconducting Superlattices

D. P. Norton, B. C. Chakoumakos, J. D. Budai, J. R. Thompson, and D. H. Lowndes

Pulsed-laser deposition is used to synthesize artificially-layered high-temperature superconductors. Using the constraint of epitaxy to stabilize $SrCuO_2/BaCuO_2$ superlattices in the infinite layer structure, novel thin-film compounds are formed which superconduct at temperatures as high as 70 K. These results demonstrate that pulsed-laser deposition and epitaxial stabilization can be effectively used to engineer artificially-layered thin-film superconducting cuprate materials.

KEY WORDS: Pulsed-laser deposition, superconducting materials, infinite layer, superlattices, artificially-layered

1. INTRODUCTION

Since the discovery of the high-temperature superconductivity (HTSc) [1], intensive efforts have revealed numerous families of layered crystal structures containing copper oxide layers [2], with superconducting transition temperatures as high as 135 K for the Hg-containing cuprates [3]. Typically, bulk synthesis techniques have been the primary tool in the search for new HTSc materials. Recently, high-pressure synthesis methods have played a prominent role to make metastable cuprate phases [4–7]. However, thin-film growth methods offer unique advantages for the atomic engineering of new HTSc materials through the ability to form artificially layered crystal structures. Moreover, the surfaces of single-crystal substrates provide an "atomic template" that can be used to stabilize epitaxial films in metastable crystal structures. Advances in the understanding of epitaxial thin-film growth of the cuprates have heightened interest in the possibility of creating artificially layered materials [8–10]. A prelude to developing artificially-layered HTSc materials has been the epitaxial stabilization of infinite layer $(Ca,Sr)CuO_2$ single-crystal thin films [11–14]. The infinite layer $(Ca,Sr)CuO_2$ structure type, consisting of square CuO_2 layers alternately stacked with square layers of alkaline earth atoms, can be viewed as a fundamental building unit of all of the HTSc cuprates [15]. Here, we report the synthesis and properties of novel artificially-layered HTSc compounds grown as $SrCuO_2/BaCuO_2$ crystalline superlattice structures [16].

2. EXPERIMENTAL RESULTS

While previous efforts to grow multilayered cuprate structures have been restricted to sophisticated MBE-like apparatus using in situ surface analysis techniques [8, 17–19], we have formed these materials simply using pulsed-laser deposition (PLD). By sequentially depositing from $BaCuO_2$ (BCO) and $SrCuO_2$ (SCO) ablation targets in a PLD system, artificially-layered crystalline materials were constructed in which the layering sequence was controlled on nearly the atomic-layer scale. The $SrCuO_2$ and $BaCuO_2$ layers are epitaxially stabilized in the infinite layer structure, and form the building blocks for the compounds. Note that $SrCuO_2$ in the infinite layer structure is an insulator, while $BaCuO_2$ normally does not form the infinite layer structure, even by high-pressure synthesis techniques. Utilizing this approach, we have synthesized a new HTSc series, $Ba_{2+m}Sr_{n-1}Cu_{n+m+1}O_{2n+m+2+\delta}$, with T_C(onset) and T_C(resistance, R=0) as high as 70 K and 50 K, respectively. The $Ba_2Sr_{n-1}Cu_{n+1}O_{2n+2+\delta}$ series, with n = 2, 3, and 4, is structurally analogous to the recently discovered $CuBa_2Ca_{n-1}Cu_nO_{2n+2+\delta}$ high-pressure HTSc phase [4–6], and is obtained by artificially-layering two-unit cells of $BaCuO_2$ and $(n\text{-}1)$ unit cells of $SrCuO_2$ in the "infinite layer" crystal structure. A schematic of the n = 3 member is shown in Fig. 1.

The films were prepared on (100) $SrTiO_3$ substrates utilizing conventional multi-target PLD [11]. Polycrystalline, orthorhombic $SrCuO_2$ and cubic $BaCuO_2$ ablation targets were mounted in a

0896-1107/95/0800-0519$07.50/0

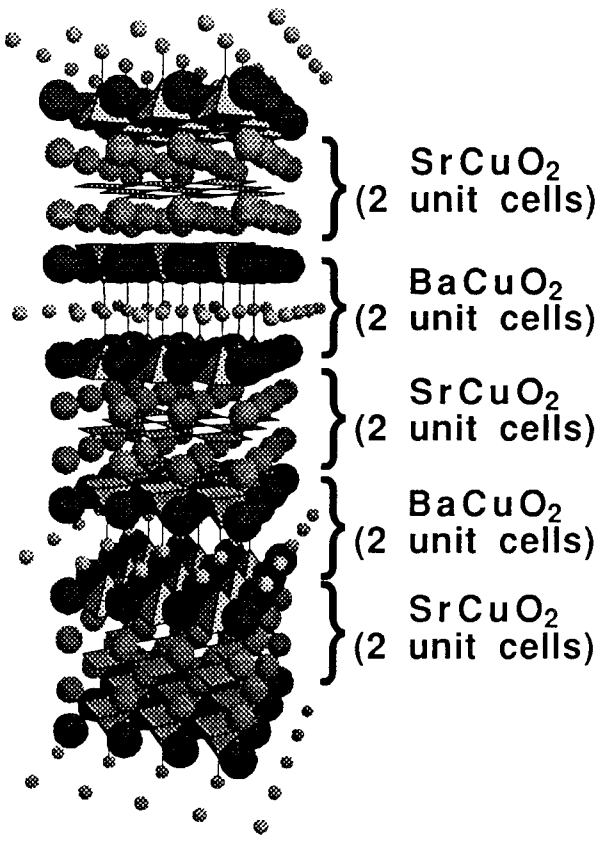

Fig. 1 Structural model of a 2×2 $SrCuO_2/BaCuO_2$ superlattice compound, also designated as $Ba_2Sr_2Cu_4O_{8+\delta}$. The Ba, Sr, and Cu atoms are represented by the large, medium, and small spheres, respectively. The CuO_4 and CuO_5 units are shown as shaded polyhedra.

multi-target carousel. The $SrCuO_2$ target was made by solid state reaction of high-purity $SrCO_3$ and CuO which was pressed and fired at 1025°C. Powder x-ray diffraction confirmed complete decomposition of the carbonates. The $BaCuO_2$ target was prepared using high-purity $BaCuO_2$ powder. (100) $SrTiO_3$ substrates were cleaned with solvents prior to being mounted with silver paint on the substrate heater. The KrF excimer laser ablation beam was focused to a 1 cm horizontal line and vertically scanned over the targets to improve film thickness uniformity. The focused laser energy density was approximately 2 J/cm^2, and the substrates, heated to 600°C, were placed 10 cm from the ablation targets. Film growth was carried out in 200 mTorr of oxygen.

Before growing the layered structures, a 9.0 nm thick $SrCuO_2$ buffer layer was grown to initiate epitaxial growth of the infinite layer structure. The average film growth rates were 0.3 Å/sec for $SrCuO_2$ and 0.43 Å/sec for $BaCuO_2$ in the infinite layer structure. The $SrCuO_2/BaCuO_2$ superlattices were grown by alternative ablation from $SrCuO_2$ and $BaCuO_2$ targets for a pre-determined number of laser shots. The $SrCuO_2$ and $BaCuO_2$ layer thicknesses were controlled by counting laser pulses, with the growth rate per laser shot calibrated from thickness measurements of $SrCuO_2$ films, and from the subsequent x-ray diffraction patterns of $SrCuO_2/BaCuO_2$ superlattice structures. Total film thickness varied from 90 to 120 nm, corresponding to 60 or more superlattice periods. After deposition, the films were cooled at ~80°C/min in 200 mTorr of oxygen, with the pressure increased to 760 Torr at 375°C.

These materials, fabricated by alternative ablation of $SrCuO_2$ and $BaCuO_2$ targets, can be nominally described either as $Ba_{2+m}Sr_{n-1}Cu_{n+m+1}O_{2n+m+2+\delta}$, or as $N\times M$ $SrCuO_2/BaCuO_2$ superlattices, where N and M are the number of infinite layer $SrCuO_2$ and $BaCuO_2$ unit cells, respectively, per superlattice period. The accurate formation of any artificially-layered phase depends on the precision with which growth of the constituent $BaCuO_2$ and $SrCuO_2$ layers can be controlled. X-ray diffraction patterns give a direct measure of the accuracy of the artificially-layered growth scheme in producing the intended structure. A x-ray diffraction pattern for a 2×2 $SrCuO_2/BaCuO_2$ superlattice is shown in Fig. 2. The corresponding schematic of the ideal atomic arrangement for this structure is shown in Fig. 1. The solid arrows indicate diffraction peaks from the artificially-layered compounds, while the asterisks designate peaks from the $SrCuO_2$ buffer layer. The vertical dashed lines show the expected locations of the (00l) peaks for an ideal artificially-layered $Ba_2Sr_2Cu_4O_{8+\delta}$ structure. The diffraction patterns clearly indicate the presence of mulitlayer modulation along the c-axis. While the diffraction peaks are close to the ideal (00l) locations, some of the peak intensities are weaker than that predicted from structure calculations with slight deviations or splitting of some of the peaks about the expected peak locations. The deviations observed in the peak locations indicate that the chemical modulation is slightly incommensurate with the structural modulation. The fact that the peak intensities are somewhat weaker than expected indicates the presence of Ba/Sr disorder. Since these thin films were formed as artificially-layered superlattices by sequentially depositing $SrCuO_2$ and $BaCuO_2$ layers, it is reasonable to assume that much of this disorder originates from substrate surface roughness and slight inaccuracies in the deposition rates. The x-ray diffraction pattern gives a c-axis lattice constant of the structural periodicity 15.7 Å, while the chemical periodicity for the same structure is 17.7 Å. Four-circle x-ray diffraction data show these

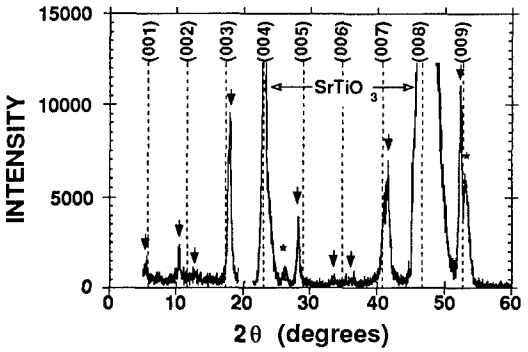

Fig. 2 X-ray diffraction pattern (Cu Kα radiation) for a $Ba_2Sr_2Cu_4O_{8+\delta}$ structure. The dashed lines indicate the nominal locations of the (00l) peaks, while the solid arrows indicate diffraction peaks due to the artificially-layered structure.

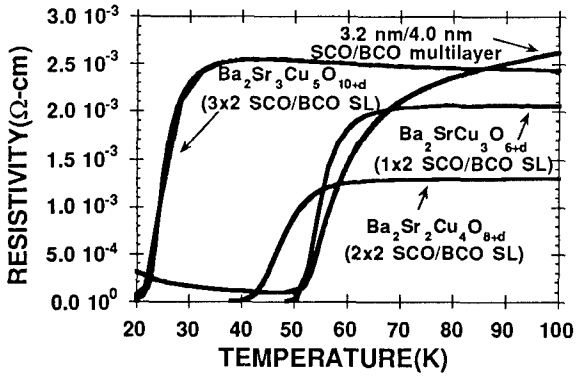

Fig. 3 Resistivity plotted as a function of temperature for the n = 2, 3, and 4 members of the $Ba_2Sr_{n-1}Cu_{n+1}O_{2n+2+\delta}$ series, as well as for the 3.2 nm/4.0 nm $SrCuO_2/BaCuO_2$ multilayer structure.

structures to be tetragonal with in-plane lattice constants of 3.9 Å, thus matching the lattice constant for the $SrTiO_3$ substrates.

In these artificially-layered structures, the $SrCuO_2$ and $BaCuO_2$ sub-units could have the ideal infinite layer structure consisting of four-fold coordinated CuO_2 planes separated by oxygen-free alkaline earth (Sr or Ba) layers, with no apical oxygen for any of the copper atoms. However, this seems unlikely as all of the hole-doped superconductors have apical oxygen on at least some of the copper atoms, and thermoelectric power measurements indicate that these materials are hole conductors [20]. The more reasonable possibility is for the Ba planes to contain some oxygen thus creating apical oxygen and increasing the Cu coordination. The schematic of the $Ba_2Sr_2Cu_4O_{8+\delta}$ structure shown in Fig. 1 assumes this to be true. It is not clear, however, whether oxygen on the Ba planes resides there at the expense of oxygen on specific Cu planes.

Figure 3 shows the resistivity for the n = 2, 3, and 4 members of $Ba_2Sr_{n-1}Cu_{n+1}O_{2n+2+\delta}$. The n = 2 member has the highest superconducting transition temperature with T_C(onset) = 70 K and T_C (R=0) = 50 K. The n = 3 member has T_C (onset) = 60 K, T_C(R=0) = 40 K, and the n = 4 member has T_C (onset) = 40 K and T_C(R=0) = 20 K. The measurement current density used was ~50 A/cm^2. Thus far, only modest attempts have been made to optimize the superconducting properties of these materials. These films are quite stable over time if stored in a dry ambient.

In addition to the $N \times M$ $SrCuO_2/BaCuO_2$ superlattices with small values for N and M, we have attempted to synthesize relatively thick $BaCuO_2$ layers in the infinite layer structure. Previous attempts to grow thick films of $BaCuO_2$ in the infinite layer structure have been unsuccessful. However, we have stabilized ~40 Å thick $BaCuO_2$ layers in the infinite layer structure within 32Å/40Å $SrCuO_2/BaCuO_2$ multilayers. The resistivity for this structure also is shown in Fig. 3. This film has a strongly metallic resistivity with a superconducting onset near 70 K. The non-zero resistivity observed for T < 50 K is presumably due to the electrically insulating 32 Å-thick $SrCuO_2$ cap layer that was grown to protect the $BaCuO_2$ layers from degradation. Significant positive magnetoresistance is observed for T ≤ 70 K, which is consistent with superconductivity. DC magnetometry revealed the presence of quasi-static persistent currents with a magnetization that was hysteretic in low magnetic fields. From the magnitude of the hysteresis for increasing versus decreasing field history, we estimate, based on the Bean critical state model [21], that the circulating critical current density is ~2×10^4 A/cm^2 at 5 K. These classical superconductive features document the fact that this multilayer structure superconducts over large areas. The magnetic signal disappeared near 36 K, somewhat below the R=0 point, due to the stringent criterion that there be well connected macroscopic paths for circulating currents. Thus, it appears that $BaCuO_2$, epitaxially-stabilized in the infinite layer structure, superconducts. Unfortunately, we were not able to determine if oxygen ordering resulted in $BaCuO_2$, or $Ba_2Cu_2O_4$ (inequivalent Cu sites). We were able to determine the c-axis lattice spacing from the (001) and (002) x-ray diffraction peaks due to the relatively thick infinite layer $BaCuO_2$.

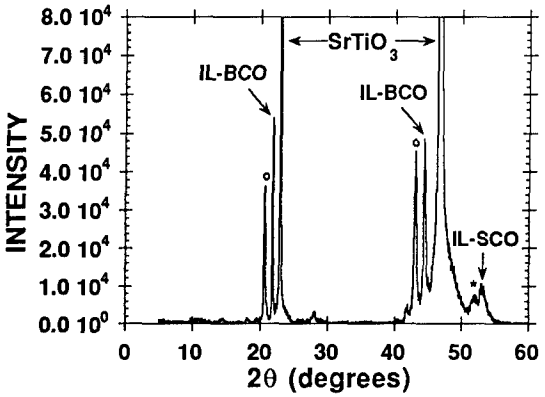

Fig. 4 X-ray diffraction pattern for the 3.2 nm/4.0 nm $SrCuO_2/BaCuO_2$ multilayer structure. The peaks due to the infinite layer $BaCuO_2$ and $SrCuO_2$ layers are indicated. Adjacent satellite peaks, designated by (o) and (*), are due to the multilayer modulation.

Figure 4 shows the x-ray diffraction pattern for this structure, indicating that the c-axis lattice spacing of the $BaCuO_2$ layers is 4.2 Å. The adjacent peaks at slightly lower angle are satellite peaks due to the $SrCuO_2/BaCuO_2$ multilayer modulation.

Note that the $n=1$ member of the $Ba_2Sr_{n-1}Cu_{n+1}O_{2n+2+\delta}$ series apparently has a value of T_c which is as high or higher than the $n > 1$ members. This behavior differs from that observed for other HTSc series, in which T_c increases as n increases. One possible explanation is that these $Ba_2Sr_{n-1}Cu_{n+1}O_{2n+2+\delta}$ films are not optimally doped, with an increase in T_c possible with an increase or reduction in the hole carrier density. Another possibility is that the use of Sr to separate the CuO_2 planes inhibits the transfer of charge from the $Ba_2Cu_2O_4$ layer into the $SrCuO_2$ layers. This latter scenario would mean that the superconducting transitions observed for all of these structures is due primarily to the $Ba_2Cu_2O_4$ layers, with little coupling in the CuO_2 planes adjacent to the Sr atoms. In fact, this interpretation is somewhat consistent with the observed behavior for $YBa_2Cu_3O_7/PrBa_2Cu_3O_7$ superlattices, where T_c decreases as the nonsuperconducting $PrBa_2Cu_3O_7$ layer thickness increases [22–24]. It also suggests that replacing Sr with Ca may increase charge transfer into adjacent CuO_2 planes and increase T_c. Additional experiments are necessary in order to fully understand the properties of these structures.

ACKNOWLEDGMENTS

We would like to thank P. H. Fleming for assistance with substrate preparation. This research was sponsored by the Division of Materials Sciences, U.S. Department of Energy under contract DE-AC05-84OR21400 with Martin Marietta Energy Systems, Inc.

REFERENCES

1. J. G. Bednorz and K. A. Muller, *Z. Phys. B, Cond. Matter* **64**, 189 (1986).
2. T. A. Vanderah, *Chemistry of Superconductor Materials*, Noyes Publications (Park Ridge, N. J., 1992)
3. A. Schilling, M. Cantoni, J. D. Guo, H. R. Ott, *Nature* **363**, 56 (1993).
4. H. Ihara et al., *Jpn. J. Appl. Phys.* **33**, L503 (1994).
5. C. -Q. Jin, S. Adachi, X. -J. Wu, H. Yamauchi, S. Tanaka, *Physica C* **223**, 238 (1994).
6. M. A. Alario-Franco, C. Chaillout, J. J. Capponi, J. -L. Thoulence, B. Souletie, *Physica C* **222**, 52 (1994).
7. Z. Hiroi, M. Takano, M. Azuma, Y. Takeda, *Nature* **364**, 315 (1993).
8. J. N. Eckstein et al., *Appl. Phys. Lett.* **57**, 931 (1990).
9. T. Terashima et al., *Phys. Rev. Lett.* **60**, 3045 (1992).
10. M. Y. Chern, A. Gupta, B. W. Hussey, *Appl. Phys. Lett.* **60**, 3045 (1992).
11. D. P. Norton, B. C. Chakoumakos, J. D. Budai, D. H. Lowndes, *Appl. Phys. Lett.* **62**, 1679 (1993).
12. C. Niu and C. M. Lieber, *J. Am. Chem. Soc.* **114**, 3570 (1992).
13. M. Yoshimoto, H. Nagata, J. Gong, H. Ohkubo, H. Koinuma, *Physica C* **185**, 2085 (1991).
14. M. Kanai, T. Kawai, S. Kawai, *Appl. Phys. Lett.* **58**, 771 (1991).
15. T. Siegrist, S. M. Zahurak, D. W. Murphy, R. S. Roth, *Nature* **334**, 231 (1988).
16. D. P. Norton, B. C. Chakoumakos, J. D. Budai, D. H. Lowndes, B. C. Sales, J. R. Thompson, and D. K. Christen, *Science* **265**, 2074 (1994).
17. T. Kawai, Y. Egami, H. Tabata, S. Kawai, *Nature* **349**, 200 (1991).
18. M. Lagues et al., *Science* **262**, 1850 (1993).
19. X. Li, T. Kawai, S. Kawai, *Jpn. J. Appl. Phys.* **33**, L18 (1994).
20. S. D. Obertelli, J. R. Cooper, J. L. Tallon, *Phys. Rev. B* **46**, 14928 (1992).
21. W. A. Fietz and W. W. Webb, *Phys. Rev.* **178**, 657 (1969).
22. D. H. Lowndes, D. P. Norton, J. D. Budai, *Phys. Rev. Lett.* **65**, 1160 (1990).
23. J. -M. Triscone et al., *Phys. Rev. Lett.* **64**, 804 (1990).
24. Q. Li et al., *Phys. Rev. Lett.* **64**, 3086 (1990).

Journal of Superconductivity, Vol. 8, No. 4, 1995

Large Bipolarons and Superconductivity

David Emin[1]

Received 5 January 1995

Superconductivity has long been speculated to result from charge carriers paired as mobile charged bosons. Although the pairing of carriers as small (single-site) bipolarons is known, small bipolarons readily localize. By contrast, large (multi-site) bipolarons, in analogy with large polarons, should be mobile. It is shown that large bipolarons can form in solids with very displaceable ions, e.g., many oxides. Large-polaronic (but not small-polaronic) carriers produce absorption spectra like the carrier-induced absorptions observed in cuprates. Redistribution of the self-trapped carriers of large bipolarons among sites of carriers' molecular orbitals in response to atomic motions lowers phonon frequencies. The dependence of the phonon zero-point energy on the spatial distribution of large bipolarons produces a phonon-mediated attraction between them. This dynamic quantum-mechanical attraction fosters the condensation of large bipolarons into a liquid. Superconductivity can result when the large-bipolarons' groundstate remains liquid rather than solidifying.

KEY WORDS: Bipolarons, infra-red absorption, mobility, liquid, superconductivity

1. INTRODUCTION

Superconductivity is defined by three properties. First, supercurrents flow without resistance. Second, superconducting carriers' orbital paramagnetism is suppressed: the Meissner effect. Third, supercurrents carry no entropy. These properties are analogous to the three properties that define the superfluidity of liquid ^{4}He: resistanceless, irrotational and entropyless flow. In both cases superflow requires that the carriers' groundstates remain fluid. However, interactions between carriers must also make the groundstate "rigid" enough to resist perturbations that would otherwise produce rotational flow and dissipation. Particles' zero-point motions enable these groundstates to retain their fluidity.

The quantum fluids responsible for superconductivity and superfluidity are not necessarily similar to one another. However for half a century it has been wondered whether superconductivity can result from a quantum fluid of mobile charged bosons comprising spatially distinct pairs of carriers.

Distinct pairs can only exist if the carrier density is small enough so that pairs do not overlap with one another. Superconductivity of distinct pairs thus requires carrier densities that are much lower than those of conventional metals. However, doped oxide-insulators' superconductivity often appears to occur at low enough carrier densities to be compatible with having distinct pairs. In addition, comparisons of electronic and magnetic measurements indicate that at least immobile (hopping-type) charge carriers pair as singlet small bipolarons in many semiconducting oxides. This paper briefly reviews how mobile pairs, large bipolarons, can form, be identified, and can condense to a liquid like that of superfluid ^{4}He. Relevant references are given in three primary works [1-3] and a recent review [4].

[1]Sandia National Laboratories
Albuquerque, NM 87185-0345

2. PRELIMINARIES

2.1 Polaron Formation

Theories of polaron and bipolaron formation have their genesis in Landau's notion of self-trapping. In particular, Landau noted that an electronic carrier can be bound in a potential well produced by displacing atoms from their carrier-free equilibrium positions. He also observed that the reduction of a carrier's energy resulting from its being bound in such a well can exceed the strain energy required to produce the potential well. The carrier is then said to be self-trapped: the formation of the potential well that traps

the carrier is stabilized by the carrier being bound in it. Because self-trapping was envisioned to occur in polar (ionic) systems, the quasiparticle comprising the self-trapped electronic carrier and the atomic displacement pattern within which it is bound came to be called a polaron. With two carriers bound in a common potential well, the quasiparticle is termed a bipolaron.

In what follows I will presume that self-trapped carriers always adjust to instantaneous atomic positions. Then the motions of these self-trapped carriers are determined by the motions of atoms. In this (adiabatic) approach a carrier's presence alters the atomic equilibrium positions and stiffnesses in its surroundings. This domain, also termed the strong-coupling regime, is valid when the binding energies of self-trapped carriers exceed characteristic phonon energies [1-4]. As will be seen later, analyses of carrier-induced absorption spectra in cuprates appear to validate use of the adiabatic theory.

Self-trapping is a nonlinear phenomena: the depth and shape of the potential well that binds the carrier depends on its wavefunction. As the carrier's wavefunction is increasingly confined, the potential well that the carrier stabilizes becomes increasingly deep. The size of an adiabatic polaron is found to be sensitive to the dimensionality of electronic motion and to details of the electron-lattice interaction.

An electron-lattice interaction is short-ranged when, as in covalent solids, an atomic displacement only affects the electronic potential in its immediate vicinity. A long-ranged electron-lattice interaction occurs in ionic solids, where, through Coulomb interactions, an ionic displacement alters the electronic potential far from the displaced ion.

A scaling argument facilitates determining how the range of the electron-lattice interaction affects polaron formation [1,4]. A polaron can exist stably when E(R), its energy as a function of its radius, R, measured in units of the lattice constant, is a minimum.

For a carrier in a deformable continuum with a short-range electron-lattice interaction:

$$E(R) = W/2R^2 - E_b/R^d, \qquad (1)$$

where W is the carrier's electronic bandwidth, d is the electronic dimensionality, and E_b is the binding energy of a polaron when its self-trapped carrier is confined to a single site, R = 1. In a multidimensional electronic system [d = 2 or 3] with a short-range electron-lattice interaction, E(R) cannot have a large-radius bound-state: an E(R) < 0 minimum at R > 1. Only a single-site, R = 1, polaron is possible. This "small" polaron's energetic stability requires $E_b > W/2$.

For a carrier embedded in a three-dimensional medium of displaceable ions [1,4]:

$$E(R) = W/2R^2 - U[1/\varepsilon_\infty - 1/\varepsilon_0]/2R, \qquad (2)$$

where U is an on-site Coulomb energy; ε_∞ and ε_0 are the medium's high-frequency (optical) and static dielectric constants, respectively. This functional has its minimum at $R = 2W/U[1/\varepsilon_\infty - 1/\varepsilon_0]$. Thus, unlike short-range interactions, this long-range electron-lattice interaction permits formation of "large" (R > 1) polarons.

Small-polaron formation in well-ordered solids requires very narrow electronic energy bands. Large polarons, however, form in broad-band ionic solids.

2.2 Polaron Motion

An adiabatic large polaron is generally viewed as moving freely, albeit slowly, with a large effective mass [1,4]. This free-carrier-like motion occurs because the binding energy of a large polaron's self-trapped carrier, -3E(R) evaluated at the R > 1 minimum, is generally much less than W. Since the energy of a large-polaron's self-trapped carrier is only fractionally changed as the large polaron moves between adjacent sites, these energy changes are also very much less than W. Therefore, a large polaron moves "coherently."

By contrast, small polarons move by hopping [1,4]. Specifically, as a small-polaron's self-trapped carrier moves between sites by following the classical motion of atoms, the energy change is at least comparable to W. Such motion is thus "incoherent." It is usually described as proceeding by a succession of thermally assisted hops between localized states centered at adjacent small-polaron sites.

In principle, small polarons can also move by a process in which atoms tunnel directly between groundstate configurations associated with a small polaron being located at adjacent sites. Since such motion requires significant atomic tunneling, the width of the associated energy band, the "small-polaron band," is always very narrow, less than the characteristic phonon energy. The disorder present in even a good

crystal generally suppresses this type of coherent motion [1,4].

3. LARGE-BIPOLARON FORMATION

For a condensate of bipolarons to be superconducting, it must be able to flow. Thus, its individual quasiparticles must move coherently. The motion of a large bipolaron, like that of a large polaron, is expected to be coherent.

Consider a situation that may be directly applicable to cuprates: a bipolaron confined to a covalently bonded plane embedded within an ionic medium. Then, the energy functional for two uncorrelated carriers in a common groundstate of reduced radius R is [1,4]:

$$E_2(R) = W/R^2 - 2U[1/\varepsilon_\infty - 1/\varepsilon_0]/R - 4E_b/R^2 + U/\varepsilon_\infty R$$

$$= (W - 4E_b)/R^2 - [1/\varepsilon_\infty - 2/\varepsilon_0]U/R. \quad (3)$$

Equation (3) is obtained by noting that having two such carriers doubles the net confinement energy and each of the two carrier's polaronic energy reduction while also introducing an intercarrier Coulomb repulsion. Rearranging terms to obtain Eq. (3)'s second equality shows that a large-bipolaron bound state is only possible if $\varepsilon_0 > 2\varepsilon_\infty$. However, Eq. (3)'s finite-radius minimum collapses to give a small bipolaron if $4E_b > W$.

To determine when a large planar bipolaron is stable with respect to dissociation into two planar large polarons, $E_2(R)$ is expressed in terms of their two-polaron energy functional:

$$2E_1(R) = W/R^2 - U[1/\varepsilon_\infty - 1/\varepsilon_0]/R - 2E_b/R^2. \quad (4)$$

After some algebraic manipulation one has:

$$E_2(R) = 2E_1(R) - 2E_b/R^2 + U/\varepsilon_0 R. \quad (5)$$

Thus, without the short-range electron-lattice interaction, $E_b = 0$, this type of large bipolaron is unstable with respect to dissociation into two separate large polarons. However, comparison of the energy minima of Eqs. (3) and (4) shows that a short-range electron-lattice interaction can stabilize the large bipolaron if $4E_b/W > [4\varepsilon_0/\varepsilon_\infty - 6]/[(\varepsilon_0/\varepsilon_\infty)^2 - 2]$. However, a large bipolaron can only form if the short-range interaction is less than that of the small-bipolaron collapse, $1 > 4E_b/W$. The unusually large values of $\varepsilon_0/\varepsilon_\infty$ in cuprates (> 20) make these materials prime candidates for stable large-bipolaron formation [1,4].

4. PROPERTIES OF LARGE BIPOLARONS

The absorption spectra of self-trapped carriers arise from their excitation from their groundstates. Our large bipolaron's self-trapped carriers have absorption spectra that are similar in shape to those of shallow impurities. In particular, as photon energy is increased above the photoionization threshold (the binding energy of the self-trapped carrier), absorption intensity first rises rapidly and then falls slowly as the ionized carrier's deBroglie wavelength drops below the self-trapped state's radius. The highly skewed carrier-induced absorption spectra observed in cuprates are like those calculated for adiabatic large-polaronic carriers [2,4]. Furthermore, application of the adiabatic (strong-coupling) approach is validated by the absorption thresholds in cuprates exceeding phonon energies. By contrast, small-polaronic carriers have absorption spectra, like those of F-centers, whose shapes differ qualitatively from those observed in cuprates [2,4].

Motion of adiabatic large polaronic carriers requires motion of the atoms producing the self-trapping. As a result, the transport effective mass of a large-polaronic carrier, m_p, is much larger than the free-electron mass. The adiabatic large-polaronic effective mass is essentially the large-polaronic binding energy divided by the square of the product of a characteristic vibrational frequency and the radius of the self-trapped state, R_p: $m_p \approx E_p/(\omega R_p)^2$ [1,2,4]. Such masses are typically several hundred electron masses. However, since the mass enhancement arises from atomic motion, it is only observable with measurements performed below vibrational frequencies. The large mass and size of a large-polaronic carrier limit its maximum kinetic energy, its "bandwidth," to a very small value [2]:

$$W_{LP} \approx (\hbar/R_p)^2/m_p \approx (\hbar\omega)^2/E_p < \hbar\omega. \quad (6)$$

As the atoms associated with an adiabatic large-bipolaron alter their positions, the self-trapped charge is shifted between atomic sites. This redistribution of charge lowers the system's energy and thereby reduces the lattice stiffness in a bipolaron's vicinity. This effect provides an interaction between large-polaronic carriers and phonons via which they scatter one another [1,2,4]. The scattering is strongest for phonon

wavevectors $\approx 1/R_p$. With sufficient vibrational dispersion, one pictures a "heavy" large-polaronic carrier being slowed as relatively "light" phonons are reflected from it. In this situation, a carrier's relaxation rate is slow, varying inversely with m_p. Notably, the large effective mass and long scattering time offset one another to give large-polaronic mobilities that, while somewhat smaller, are comparable to those of some nonpolaronic carriers.

Large-polaronic carriers can be identified by their absorption spectra, large low-frequency transport effective masses and long scattering times. Singlet bipolarons are most easily distinguished from polarons by their lack of spin. For example, bipolarons' Seebeck coefficients lack the magnetic-field dependencies that arise from carriers with spin degrees of freedom. While these features may find nonpolaronic interpretations, they are all observed in the cuprates [1,2,4].

5. LARGE-BIPOLARONIC LIQUID

Intercarrier interactions are required to produce a superconducting condensate's rigidity. There are three principal interactions between large singlet bipolarons [3,4]. First, singlet bipolarons repel one another strongly at short-range because the Pauli principle permits only two fermions to occupy the groundstate of a self-trapping well. Second, while Coulomb repulsions between bipolarons exist, their strengths are significantly reduced in materials that support our large bipolarons because these solids have very large static dielectric constants. Third, an intermediate-range phonon-mediated attraction occurs between large bipolarons because the lattice softenings they produce lower phonon energies more effectively as inter-bipolaron separations fall below phonons' wavelengths. Reducing phonon frequencies lowers a solid's low-temperature vibrational energy [3,4]. This attractive interaction is roughly equal to $-\hbar\omega(R_p/s)^4$ for $s > R_p$, where R_p is the radius of the self-trapped state and s is the separation between large bipolarons [3]. The proportionality of this attraction interaction to $\hbar$ and ω manifests both its quantum and dynamic characters.

The very large static dielectric constants of cuprates suppress the long-range Coulomb repulsion between large bipolarons. As a result, large-bipolarons in cuprates would primarily experience both a "hard-core" repulsion and an intermediate-range "phonon-mediated" attraction. Thus, a minimum of the interaction energy between a pair of large bipolarons occurs at a finite separation between them. In this situation, a gas of large bipolarons will condense into a liquid as the temperature is reduced [3,4]. Indeed, several experiments suggest that photoinduced carriers in the insulating parents of cuprate superconductors condense into liquid droplets.

A liquid of large bipolarons would be analogous to superfluid liquid ^{4}He if its groundstate remains liquid rather than solidifying. Liquidity can only be maintained through its quasiparticles' zero-point motion. Incommensurability of large bipolarons with the underlying lattice should also impede their solidification [3,4].

Several experimental findings are at least consistent with the cuprates' superconducting condensate being a large-bipolaron liquid. The observation that carriers in doped La_2NiO_4 condense into a polaronic solid rather than into a superconductor is consistent with nickelate carriers' effective masses exceeding those of cuprates. Larger effective masses are implied by the nickelates' carrier-induced absorption spectra being higher-energy versions of cuprates' spectra. Loss of superconductivity when La_2CuO_4's are doped to give one hole per eight unit cells is consistent with bipolarons ordering as a 4×4 superlattice on the underlying tetragonal structure.

ACKNOWLEDGMENT

This work was performed under the auspices of the U. S. Department of Energy and was funded in part by the Office of Basic Energy Sciences, Division of Materials Sciences contract DE-AC04-94AL85000.

REFERENCES

1. D. Emin, Phys. Rev. Lett. **62**, 1544 (1989); D. Emin and M. S. Hillery, Phys. Rev. B **39**, 6575 (1989).
2. D. Emin, Phys. Rev. B **48**, 13 691 (1993).
3. D. Emin, Phys. Rev. Lett. **72** 1052 (1994); D. Emin, Phys. Rev. B **49**, 9157 (1994).
4. D. Emin, in *Polarons and Bipolarons in High-T_c Superconductors and Related Materials*, W. Y. Liang, E. S. H. Salje and A. S. Alexandrov, eds. (Cambridge University Press, 1995).

Journal of Superconductivity, Vol. 8, No. 4, 1995

Local Polarizability, Structure, and Charge-Transfer in High-T_C Superconductors

A. R. Bishop,[1] J. T. Gammel,[1] and M. I. Salkola[1]

Using 2-band Peierls-Hubbard cluster and chain models, we illustrate the importance of polarizability and coupled charge-lattice-spin effects in complex electronic materials.

KEY WORDS: Polarizability, polarons, charge-transfer.

I. INTRODUCTION

It is by now experimentally clear [1,2] that HTC materials share with other mixed-valence perovskites the properties of competing interactions (electron-electron, electron-lattice, dimensionality) that make that whole class so rich in terms of ground states (ferroelectric, magnetic, disproportionation, complex structural transitions, *etc.*). While this has been appreciated for perovskites in a broad sense for many years, the development of refined experimental capabilities (neutron scattering, XAFS, NQR, ion-channeling, *etc.*) and the intense focus on HTC materials, have demonstrated [1,2] (a) completely new details of *local* structural variations in the form of "fine-scale structure" – various deformations of perovskites units on one to a few bond-length scales – and (b) their close correlation with optical, magnetic and superconducting degrees-of-freedom (*e.g.*, T_c and T^* in typical layered cuprate HTC compounds [2b]).

Several important lessons now seem reasonable: (1) Fine-scale "texture" is likely to be intrinsic to HTC materials and related martensitic and elastic materials, including traditional perovskite (anti)ferroelectrics ($SrTi0_3$, *etc.*); (2) The texture is composed of various in-plane and out-of-plane (c-axis) distortions (buckling, tilting, stretching) of the perovskite units (beyond a single "order parameter") and different experiments probe different aspects; (3) The texture is an intrinsic result of coupled and/or competing degrees of freedom. It can have static and dynamic components and feeds hierarchically into longer length scales (tweed, twinning, domain, *etc.*) [3]; (4) We need to understand the microscopic driving forces for fine-scale (mesoscopic) textures and their relationship to textures and macroscopic properties (superconducting, elastic, *etc.*). The notion that intrinsic structure controls function is an emerging theme in many complex electronic materials – conducting polymers, shape-memory alloys, giant magnetoresistance materials, *etc.*; (5) Charge, spin, and lattice degrees-of-freedom are strongly coupled on the fine-scales. Adiabatic (slaving) approximations must be analyzed carefully but lead naturally to various competing interactions, nonlinear potentials, and nonlinear couplings that provide model microscopic descriptions (shell models, superlattices, adiabatic polarons and bipolarons, *etc.*) for various features of texture and the related optical, electronic properties [4]. *Purely* electronic, charge-transfer, Jahn-Teller, charged-phonon, polarizability, excitonic, quantum paraelectric, *etc.*, mechanisms for superconductivity are probably illusory; and conventional global probes (LDA, Rietveld, IR, Raman) must be used and interpreted with caution.

The following two examples are paradigms for issues in this new era of complex electronic materials lying between traditional solid state physics and quantum chemistry.

II. A 3-SITE CLUSTER

Here, we summarize studies of a simple O-Cu-O cluster with *linear* electron-phonon couplings to illustrate *nonlinear* polarizability, and its structural and optical manifestations. The model was designed to represent a specific c-axis structural component of YBCO [5] but is readily applied to or modified for both intraplane and

[1]Theoretical Division, Los Alamos National Laboratory, Los Alamos, NM 87545, USA

0896-1107/95/0800-0527$07.50/0

interplane dynamical charge transfer [6].

The cluster (Peierls-Hubbard) Hamiltonian is [5]

$$H = H_{el} + H_{ph} + H_{el-ph} \, . \tag{1}$$

The electronic part is given by

$$H_{el} = \sum_a \epsilon_a n_a + \sum_{ab,\sigma} t_{ab} \left(c^\dagger_{a\sigma} c_{b\sigma} + h.c. \right) + U \sum_a n_{a\uparrow} n_{a\downarrow} . \tag{2}$$

Here, $c^\dagger_{a\sigma}$ creates a hole of spin σ at site a, $n_{a\sigma} = c^\dagger_{a\sigma} c_{a\sigma}$, $n_a = \sum_\sigma n_{a\sigma}$. Indices $a = 1, 3$ denote the axial O sites and $a = 2$ the chain Cu site. The hopping matrix element is $t_{ab} = t$ between the O and Cu sites and $t_{ab} = t'$ for an effective hopping matrix element between the O sites, $\epsilon_{1,3} = \epsilon_0$ and $\epsilon_2 = -\epsilon_0$. The cluster has two center of mass-preserving phonon modes, which are harmonic (as indicated by LDA results). One is even and the other odd under inversion; the symmetric phonon mode is Raman active and the antisymmetric one is infrared active. Using boson operators a_R and a_{IR} with bare frequencies ω_R and ω_{IR}, respectively,

$$H_{ph} = \hbar\omega_{IR} a^\dagger_{IR} a_{IR} + \hbar\omega_R a^\dagger_R a_R \, . \tag{3}$$

Measuring the site coordinates, r_a, relative to their average positions $r^{(0)}_a$: $r_a = r^{(0)}_a + z_a$, then the normal modes, $u_{IR} = \sqrt{\hbar/2M_1\omega_{IR}}(a_{IR} + a^\dagger_{IR})$ and $u_R = \sqrt{\hbar/2M_1\omega_R}(a_R + a^\dagger_R)$, are given by $u_{IR} = (z_1 - 2z_2 + z_3)/\sqrt{3}$ and $u_R = (z_1 - z_3)/\sqrt{2}$. (We have taken the ratio of the effective copper to oxygen masses as $M_2/M_1 = 4$.) We use a linear molecular-crystal type interaction:

$$\begin{aligned} H_{el-ph} = {} & \gamma_{IR} \left(a_{IR} + a^\dagger_{IR} \right) \left(n_3 - n_1 \right) \\ & + \gamma_R \left(a_R + a^\dagger_R \right) \left(n_1 + n_3 - s_0 \right) , \end{aligned} \tag{4}$$

where γ_{IR} and γ_R are the respective coupling constants. The parameter s_0 avoids artificial cluster shrinkage.

The parameters in H_{el} are taken here as $\epsilon_{1,3} = 0.307$ eV, $\epsilon_2 = -\epsilon_{1,3}$, $t = -0.634$ eV, and $U = 4.44$ eV, which are *representative* values guided by local-density calculations [7]. We use $t' \sim t/10$, $\hbar\omega_{IR} = 59.3$ meV, and $\hbar\omega_R = 71.5$ meV. γ_{IR} and γ_R, are varied so that XAFS structural experiments *and* optical data can be simultaneously reconciled with the model's predictions [5]. $\gamma_{IR} = 0.143$ eV and $\gamma_R = 0.260$ eV with $s_0 = 1.17$ lead to reasonable agreement with experiments.

Many structural and spectroscopic features of this model have been studied. For example, *energy-resolved* pair distribution function analysis has been emphasized – important because, *e.g.*, time-of-flight neutron sources [8] are now available. We summarize here only some predicted optical signatures.

Sufficiently large values of γ_{IR} *dynamically* generate a new length scale, $\delta\ell$, associated with a dynamic double-well structure in the *infrared* distortion. Here, the motion of the phonons is strongly correlated with the hole motion: polaron tunneling. As the systems moves from weak- to strong-coupling, the R active states show pronounced minima in the intermediate region, whereas the IR active states decrease in a regular fashion [5]. The minima occur close to where the double-well structure onsets. Assuming that the model parameters depend on temperature, this nonmonotonic behavior might explain the experimental observation that the Raman active state at $\sim$ 500 cm^{-1} hardens [9] whereas the IR active state at $\sim$ 580 cm^{-1} softens [10], as the temperature is decreased from 100 to 50 K.

The model's predictions are in reasonable agreement with several experiments: The Cu-O bond-length splitting $\delta\ell$ is 0.11 Å which approximately equals the XAFS result [11]; a doublet of IR active states at frequencies 526 cm^{-1} and 614 cm^{-1} is predicted in the experimentally relevant region $\sim$ 580 cm^{-1} where a broad shoulder is observed [12] below the main IR peak; see Fig. 1. Our 526 cm^{-1} state is a complicated multiphonon state involving the IR degree of freedom, whereas the 614 cm^{-1} state contains basically two bare IR phonons and one bare R one. The predicted IR and R spectra exhibit several additional features (Fig. 1): (*i*) The lowest-energy peak in the IR absorption occurs at the polaron tunneling energy $\hbar\omega_T \simeq 127\,\text{cm}^{-1}$. (*ii*) The lowest-energy features in the R spectrum are located at 317 cm^{-1} and 460 cm^{-1} of which the first is highly nonlinear, whereas the second is only a weakly renormalized bare one-R-phonon state observed experimentally at $\sim$ 500 cm^{-1}. (*iii*) There is a clear progression of R active states in intervals of $\sim$ 450 cm^{-1}, some of which are close in energy to the unassigned "state" at $\sim$ 700 cm^{-1}, observed by inelastic neutron scattering [8]; in particular, the state at 744 cm^{-1} has multiphonon character.

The anharmonic mode at 317 cm^{-1} offers intriguing possibilities for coupling to the CuO_2 plane in terms of resonant multiphonon and nonlinear excitonic mechanisms. We also emphasize that this kind of model forces us to re-examine the concept of "adiabaticity." Although the low-energy behavior as a function of γ_{IR} can be quite well described by, *e.g.*, Born-Oppenheimer approximations, multiple time scales are apparent in the time domain [13], at high energies [5], in the presence of disorder and temperature [14], *etc*: New experimental precision requires that nonadiabatic effects are modeled accurately.

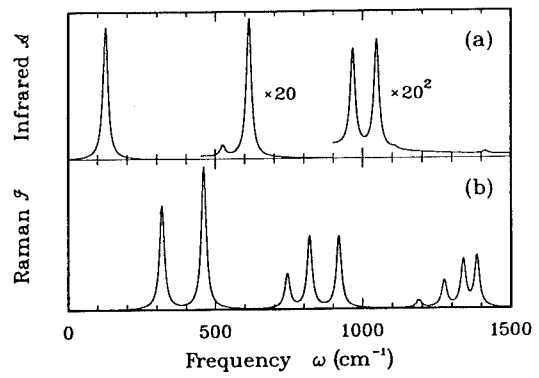

Fig. 1. The (a) IR absorption and (b) R scattering spectrum (arbitrary units) with γ_{IR}=0.143 eV and γ_R=0.260 eV (double-well regime) at zero temperature. The R spectrum is calculated at the incident photon energy of 2.5 eV. The IR spectrum is scaled up by a factor of 20 above 450 cm^{-1} and by a factor of 20^2 above 900 cm^{-1}. Lorentzian broadening with full width at half maximum of 20 cm^{-1} has been included by hand.

III. CDW-AF CROSSOVER IN A MULTIBAND PEIERLS-HUBBARD CHAIN

Including *both* electron-phonon and electron-electron interactions in *multi*band models appears [15,16] to capture important aspects of competing broken-symmetry ground states and intrinsic charge-lattice-spin "textures". We summarize a 1-D, 2-band Peierls-Hubbard model [16] that mimics the 2-D structural distortion (in-phase oxygen sublattice dimerization) found to be anomalous in HTC cuprate planes [1] and that also faithfully described quasi-1-D halogen-bridged transition chain (MX) complexes – 1-D paradigms of cuprate and bismuthate materials [16,17]. See [15] for a related 2-D study. Even at stoichiometry, the competition (e-e/e-ph) drives qualitatively new ground states beyond period-4 charge-density-wave (CDW) or spin-density-wave (AF) phases – novel magnetic phases of frustrated, superlattice (long-period) or spin-Peierls type.

The 1-D Hamiltonian is [16,17]

$$H = \sum_{l,\sigma} \Big\{ \Big(-t_0 + \alpha\delta_l \Big) \left(c^\dagger_{l,\sigma} c_{l+1,\sigma} + c^\dagger_{l+1,\sigma} c_{l,\sigma} \right) + \left[\epsilon_l - \beta_l \left(\delta_l + \delta_{l-1} \right) \right] c^\dagger_{l,\sigma} c_{l,\sigma} \Big\} \qquad (5)$$
$$+ \sum_l \left\{ U_l c^\dagger_{l,\uparrow} c_{l,\uparrow} c^\dagger_{l,\downarrow} c_{l,\downarrow} + \frac{1}{2} K \left(\delta_l - a_l \right)^2 + P\delta_l \right\} ,$$

where $c^\dagger_{l,\sigma}$ creates an electron at site l with spin σ. $M(d_{z^2})$ and $X(p_z)$ Wannier orbitals are situated on even and odd sites, respectively. Each M_2X_2 unit cell has 6 electrons (*i.e.*, 3/4 band filling). On-site energies are ϵ_l ($\epsilon_M = -\epsilon_X = \epsilon_0 \geq 0$). There is on-site ($\beta_M, \beta_X$) and inter-site ($\alpha$) e-ph coupling, on-site e-e repulsion (U_M, U_X), and pressure P. a_l is the natural M-X spring length, and δ_l is the relative displacement of sites l and $l+1$. Both HF and exact diagonalization techniques are used.

Model (5) contains many phases [16]. We focus here on intermediate to large e-e correlations (large U_M). Consider the zero-hopping limit, $t_0 = 0$. For U_M dominant, the lower, X-like band is full and nonmagnetic, while the upper, M-like band is 1/2 full with one electron per M site and uncorrelated spins. For $t_0 \neq 0$, as in the one-band case, there is an effective AF coupling between spins on neighboring metal sites, J_{MM}, driving AF order that competes with band splitting from the on-site e-ph coupling β. However, the lower band is not completely full and there are effective AF couplings between neighboring X sites, J_{XX}, and M and X sites, J_{MX}, not present in simple one-band models. When the splitting due to β is on the order of U and ϵ_0, the AF state with neighboring M-X pairs singly occupied can become the ground state. Thus, the combination of e-e and e-ph coupling in the two-band model drives, in addition to nonmagnetic CDW and BOW (bond-order-wave) phases, three (competing) spin-Peierls phases: one on the X sublattice (XAF), one on the M sublattice (MAF), and one involving M-X pairs and large lattice distortion (MXP). Since J_{MM}, J_{XX}, and J_{MX} are all antiferromagnetic ($J > 0$), the system is frustrated. When only one of the J's dominates, one can numerically check estimates of the size of the J from perturbation theory in t_0 by comparing the energies of the singlet and triplet ground states [16]. Note that the CDW phase has an entirely e-ph driven antiferromagnetic component: Even when the $X(M)$-sublattice distortion is large, some residual $M(X)$-sublattice magnetization remains.

Consider parameters where the lattice distortion is large and driven by the on-site e-ph coupling β, and/or the Hubbard U terms are large. Figure 2 presents exact diagonalization results. As U_M increases (lattice distortion decreases), there is a sharp transition from M-M charge coupling (CDW) to M-X spin coupling (MXP) to M-M spin coupling (MAF), agreeing with the $t_0 = 0$ results. For larger t_0, the couplings change more smoothly; and charge disproportionation, M-X spin coupling, and M-M spin coupling coexist, with the phase of the lattice distortion passing from CDW through MXP to BOW as the amplitude goes to zero. For large t_0, even for $U_M = 0$, the CDW phase shows a strong tendency towards antiferromagnetic order driven by valence fluctuations.

The crossover between the period-4 CDW and MAF phases is accompanied by long-period superlattice phases [18] when $|\beta_X/\beta_M| > 1$ or the *intersite* e-ph coupling α is large. Superlattices may be viewed as ordered arrays

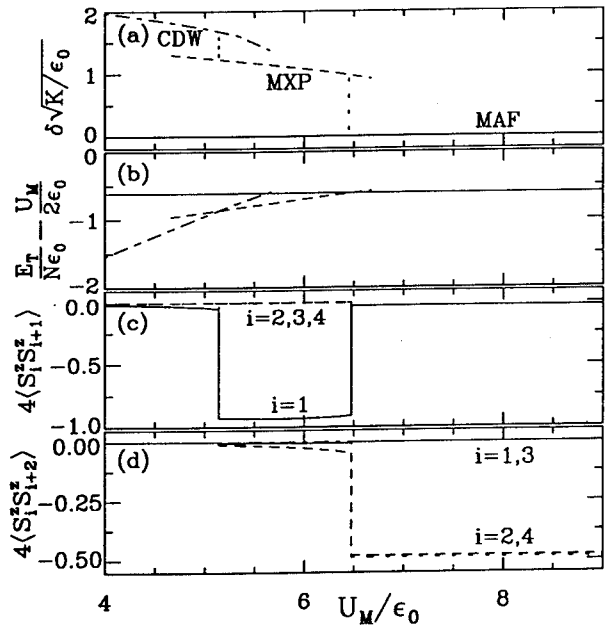

Fig. 2. Exact diagonalization, 16-site ring: (a) lattice distortion amplitude, (b) total energy E_T, and (c) NN and (d) NNN spin correlations as a function of U_M/ϵ_0 for MAF, CDW, and MXP phases at t_0/ϵ_0=0.5, β_X/β_M=1, U_X/U_M=1, $\beta_M^2/K\epsilon_0$=7−3$U_M/4\epsilon_0$. For finite systems lattice distortion strongly pins competing phases.

of discommensuration (bipolaron) defects with respect to nearby commensurate (period-4) order. Considering the effective J's discussed above, it is natural to view such states in terms of ANNNI-like models. Hole doping into these soft crossover stoichiometric phases is especially intriguing.

SUMMARY

We have entered an age of complex electronic materials characterized by competing interactions and intimately coupled degrees-of-freedom (charge, spin, lattice). Growing experimental evidence points to the pervasive consequence of intrinsic fine-scale (mesoscopic) structure ("texture"), whose microscopic origins and macroscopic functionality must be understood. Impressive advances in experimental probes for static and dynamic local variations in structure, charge, and spin provide the opportunity to address issues of, *e.g.*, polarizability, polaron structure, and dynamics in previously unavailable detail.

Concerning HTC materials, *the* pairing mechanism remains speculative. However, it seem increasingly likely that charge-transfer/excitonic fluctuations play an important role [19,20]. Globally ordered phases, whether AF or (anti)ferroelectric or CDW (equivalently ordered arrays of polarons/bipolarons) are of course not superconductivity. We need to be close to phase boundaries to take advantage of charge, spin, or lattice *fluctuations*. It is tempting to use 2-fluid phenomenologies – *e.g.*, in YBCO, strong c-axis *e*-ph coupling/charge-transfer driving in-plane fine structure ("flat" electronic bands) that controls both CDW and superconducting tendencies of in-plane carriers. However, suitably extended Peierls-Hubbard models can quite generally, and self-consistently, describe competitions between superconductivity and (anti)ferrodistortions (CDW, polaron lattice, antiferroelectric). The driving force for such competitions could be Hubbard "V" [19,20], *etc.*; but the involvement of charge transfer-metal insulator crossovers [1,16], and explicit electron-lattice coupling seems highly beneficial and indicated by experiment [1,2]. Detailed descriptions of which lattice distortions are most important are best left to experimental guidance. However, we now face the aesthetically pleasing possibility of unifying superconductivity in cuprates and bismuthates [20] – and also possibly quasi-1-D analogs [16,17].

We are grateful for discussions with many colleagues, particularly A. Bussmann-Holder, J. Mustre de Leon, H. Röder, Z. Tesanovic, and S. A. Trugman.

REFERENCES

1. See, *e.g.*, T. Egami *et al.*, these proceedings; A. Bianconi *et al.*, these proceedings.
2. a) *Lattice Effects in High-T_c Superconductors*, eds. Y. Bar-Yam *et al.* (World Scientific, 1992); b) A. R. Bishop, in *Strongly Correlated Electronic Materials*, eds. K. Bedell *et al.* (Addison-Wesley 1994).
3. *e.g.*, J. A. Krumhansl, in [2].
4. *e.g.*, A. Bussmann-Holder, A. R. Bishop, *Phys. Rev. B* (in press).
5. M. I. Salkola *et al.*, *Phys. Rev. B* **49**, 3671 (1994); *ibid.* (in press).
6. I. Batistic *et al.*, *Phys. Rev. B* **40**, 6896 (1989).
7. W. Pickett, *Rev. Mod. Phys.* **61**, 433 (1989).
8. *e.g.*, M. Arai *et al.*, *Phys. Rev. Lett.* **69**, 359 (1992).
9. E. Altendorf *et al.*, *Physica* **C175**, 44 (1991).
10. H. Obki and E. Salje, *Physica* **C171**, 547 (1990).
11. J. Mustre de Leon *et al.*, *Phys. Rev. Lett.* **65**, 1675 (1990).
12. *e.g.*, D. Born *et al.*, *Phys. Rev. B* **37**, 1574 (1988).
13. M. I. Salkola and A. R. Bishop, preprint (1994).
14. M. Spicci *et al.*, *J. Phys.: Condens. Matter* **6**, L361 (1994).
15. K. Yonemitsu, A. R. Bishop, and J. Lorenzana, *Phys. Rev. B* **45**, 5530 (1992); **47**, 8065 (1993).
16. H. Röder *et al.*, *Phys. Rev. Lett.* **70**, 3498 (1993).
17. J. T. Gammel *et al.*, *Phys. Rev. B* **45**, 6408 (1992); *Physica* **B163**, 458 (1990).
18. I. Batistic *et al.*, *Phys. Rev. B* **44**, 13228 (1991).
19. C. M. Varma *et al.*, *Sol. State Comm.* **62**, 681 (1987); V. J. Emery, *Phys. Rev. Lett.* **58**, 2794 (1987); P. Littlewood, *Phys. Rev. B* **42**, 10075 (1990).
20. Z. Tesanovic, A. R. Bishop, and R. L. Martin, *Sol. State Comm.* **68**, 337 (1988); A. R. Bishop *et al.*, *Z. Physik B* **76**, 17 (1989).

Journal of Superconductivity, Vol. 8, No. 4, 1995

Carrier relaxation through localized states in metallic and insulating $YBa_2Cu_3O_{7-\delta}$

D.Mihailovic[1], T.Mertelj[1], I.Poberaj[1], J.Demsar[1] and C.Chen[2]

The temperature dependence of photoexcited carrier relaxation in insulating and metallic $YBa_2Cu_3O_{7-\delta}$ and $La_{1.85}Sr_{0.15}CuO_4$ suggests that carriers relax towards equilibrium by hopping between localized states. The implication is that in the optimally doped superconducting phase, localized states and extended states co-exist. The findings confirm the polaronic interpretation of the MIR band in the optical conductivity.

KEY WORDS: Carrier relaxation; non-equilibrium phonons; localized states

1. INTRODUCTION

The study of non-equilibrium phonons in semiconductors using ultrafast laser spectroscopy has been very extensive in the past decades because of the valuable and detailed information it gives about scattering processes of elementary excitations[1]. However, apart from a recent study of amorphous Si[2] in disordered or self-localized carrier systems there have so far been no such studies. In a recent work[3], we have found that the methods can be usefully applied to high-T_c superconductors where we have investigated the photoinduced insulator-to-metal transition with Stokes/anti-Stokes Raman scattering. Qualitatively at least, we have been able to show that coupling of PE carriers to certain *c*-axis phonons is significant and the coupling changes at the I-M transition.

More recently, we have been studying the temperature dependence of the carrier relaxation rate through measurements of the *T*-dependence of the non-equilibrium occupation number n_{neq} in $YBa_2Cu_3O_{7-\delta}$ for $0 < \delta < 1$ and $La_{1.85}Sr_{0.15}CuO_4$ and La_2CuO_4 for different phonons and here we report on the present state of these measurements.

In a crystalline semiconductor, the intra-band energy relaxation of hot carriers proceeds via Fröhlich or deformation potential scattering with phonons and is relatively temperature independent[4] for carriers significantly out of equilibrium. On the other hand, relaxation via localized states is expected to be strongly temperature dependent and so carrier relaxation experiments can distinguish between localized and extended states in the material under study. On the basis of the present measurements we propose that the temperature-activated behaviour of the phonon shake-off is *direct evidence* for the existence of localized states in the cuprates, including the metallic phase of $YBa_2Cu_3O_{7-\delta}$ and $La_{1.85}Sr_{0.15}CuO_4$.

2. EXPERIMENTAL DETAILS

The experiments entail measurement of the Stokes and anti-Stokes Raman scattered intensities for two different O phonons using 1.5 laser pulses at a photon energy of 2.33 eV. From these intensities we can determine the non-equilibrium occupation number of each

[1] *Jozef Stefan Institute, University of Ljubljana, 61 111 Ljubljana, Slovenia*
[2] *Clarendon Laboratory, University of Oxford, Oxford OX1 3PU, U.K.*

0896-1107/95/0800-0531$07.50/0

phonon from $n_{neq} = (I_S/I_A - 1)^{-1} - n_{eq}$ where the equilibrium occupation number n_{eq} for each phonon of frequency ω at any temperature is given by the Bose-Einstein distribution function at temperature T. The experimental set-up is similar to the one used previously[3], with two important improvements. A Princeton Instruments nitrogen-cooled CCD detector was used instead of a intensified diode array to enable us to have longer accumulations with very weak anti-Stokes Raman signals. Also, additional stabilization was added to the mode-locked laser set-up, significantly improving the pulsewidth jitter and intensity stability of the Raman stabilized pulse compressor. As a result we have been able to perform temperature-dependence measurements of the Stokes/anti-Stokes ratio from the planar 340 cm^{-1} mode for $\delta \sim 0.1$ in addition to the much stronger apical O(4) mode.

3. EXPERIMENTAL RESULTS

In Figure 1 we show first the temperature-dependence of n_{neq} for $YBa_2Cu_3O_{7-\delta}$ with δ = 0.75 and for two different phonons (the 340 and 470 cm^{-1} Raman-active modes).

The data are plotted on an Arrhenius plot, where we observe a very pronounced temperature-dependence of n_{neq}.

There are two ways to fit the data. The first is to assume an activated law $n_{neq} = A \exp[-E_0/k_BT]$ above about 100 K and a departure from this behaviour below 100 K. The value of the activation energies obtained from the fit are 34 ± 8 meV and 64 ± 8 meV for the plane-buckling 340 cm^{-1} mode and the apical O(4) c-axis vibration at 470 cm^{-1}. The departure from an activated law at low-temperatures can be ascribed to variable-range hopping (VRH) which we could expect in a disordered or self-localized system at low temperatures. A fit (not shown) to the VRH model where $n_{neq} \propto \exp[-(T_0/T)^{1/4}]$ gives rather good agreement with DC transport

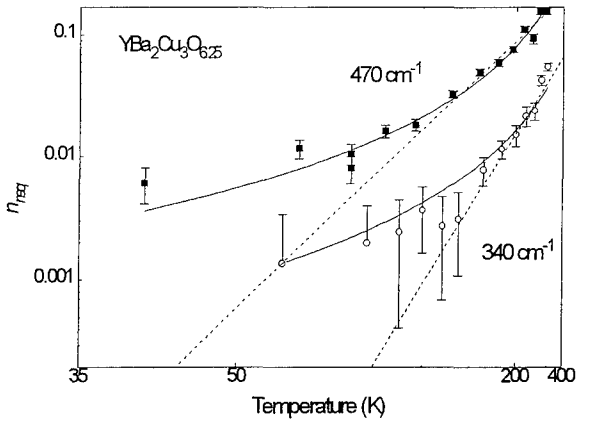

Figure 1. The non-equilibrium occupation number for the 340 and 470 cm^{-1} phonons in $YBa_2Cu_3O_{7-\delta}$ ($\delta \sim 0.75$) as a function of temperature. The straight lines are power law fits, while the dashed lines are simple activated law fits. There is a clear deviation from simple activated behaviour below 100K.

measurements on $Pr_{1-x}Y_xBa_2Cu_3O_7$: the value $T_0 = 3000 \pm 1000$ K obtained from our fit are within experimental error of the value T_0 = 2150 - 2400 K obtained by Jiang et al.[5] on insulating $Pr_{1-x}Y_xBa_2Cu_3O_7$. The value of the most probable hopping distance $R = 0.4\ \xi\ (T_0/T)^{1/4}$ is about 15-20 Å at 20 K, a reasonable value for VRH model to be appropriate.

The alternative is to fit the data to a power law with $n_{neq} = BT^2$ where the the carrier relaxation is dependent on the square of the temperature as discussed for a case of a disordered semiconductor by Long[6] with reasonable agreement over the whole temperature range (shown in solid lines in Figure 1). The scatter in the data prevents us from deciding which is a better fit, and we hope that we will be able to improve the experimental technique in the future sufficiently to be able to analyse the all-important low-temperature behaviour.

The same experiments were repeated also on single crystals of $YBa_2Cu_3O_{7-\delta}$ with $\delta \sim 0.1$. The results were cross-checked on crystals

grown by three different labs (G.Collin-Orsay, H.Noel-Toulouse/Grenoble and C.Chen-Oxford) and we found no significant differences between the different crystals. The data are shown in Figure 2, plotted separately for clarity for the 340 cm^{-1} plane-buckling vibration and for the apical O(4) vibration at 500 cm^{-1}. Again the data is fitted with an activated model and a power law. The activation energies obtained are now rather close to each other : 70 and 64 ± 8 meV for the two modes respectively.

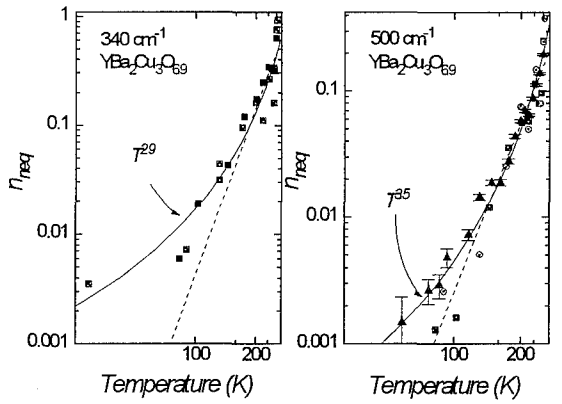

Figure 2. The temperature dependence of the phonon occupation number for the 340 and 500 cm^{-1} modes in $YBa_2Cu_3O_{7-\delta}$ ($\delta \sim 0.1$). The dashed line is a simple activated fit to the data, while the solid line is a power law fit. Again, a clear deviation from the activated fit is observed at the lowest temperatures. The different symbols correspond to measurements on single crytals grown by different labs.

Again we see departure from the simple activated behaviour at low tempereatures, but we refrain from fitting the data to the VRH model as there are not enough data points to make a reliable fit. The exponents of the power law are 2.9 and 3.5 respectively, which are significantly above 2 expected for relaxation through localized states.

The most recent data we have are on single crystals of La_2CuO_4 and $La_{1.85}Sr_{0.15}CuO_4$. Due to lack of space we do not show the data, but it is significant that we observe qualitatively the same behaviour as in the $YBa_2Cu_3O_{7-\delta}$ samples. The occupation numbers were measured for the apical O vibration at 420 cm^{-1} in both La_2CuO_4 and $La_{1.85}Sr_{0.15}CuO_4$. In both samples we see activated behavour above 100 K, with $E_0 \sim 60 \pm 10$ meV and 68 ± 10 meV for $La_{1.85}Sr_{0.15}CuO_4$ and La_2CuO_4 respectively. There were so far insufficient data for a fit below 100 K for the La series.

4. DISCUSSION

Assuming that carrier relaxation proceeds by emission of phonons, then the energy loss rate R is directly proportional to the number of phonon emitted, i.e. non-equilibrium phonon occupation number, n_{neq}. Here we have made an assumption that the phonon lifetime does not change significantly with temperature. This is justified because the linewidth does not change significantly with temperature below 300 K, and moreover, if we take into account the slight narrowing with cooling, this gives a negligible correction to the data. It is not necessary to assume that phonon emission is the only relaxation channel, indeed other mechanisms could (in principle) add to the relaxation. However, the activation energy measured is the total activation energy required to move the carrier, not just the phonon part.

In the process of photoexcitation both a hole and an electron are emitted and both are expected to relax towards equilibrium emitting phonons. Since we are investigating different phonons in the Raman spectra, it is possible to discuss also which electronic states are responsible for the relaxation. The in-plane vibration at 340 cm^{-1} involves displacements along the c axis, but nevertheless it is coupled to the in-plane states, as it involves buckling of the plane, which modulates strongly the transfer integral between Cu and O. The apical O on the other hand is much closer to the chain Cu(1) ion than the plane Cu(2), and its p_z orbital is hybridized with the chain Cu d states.

Carriers coupled to both phonons appear to have similar activation energies in $YBa_2Cu_3O_{6.9}$ which suggests that it is one and the same carrier which is coupled to both phonons. In $YBa_2Cu_3O_{6.25}$ on the other hand, the carriers coupled to one mode appear to be different than the other, judging by the difference in E_0. The origin of this differnce is not presently understood in detail.

5.CONCLUSION

The present experiments were performed to determine the T-dependence of the carrier relaxation rate by measuring the phonon shake-off. They clearly indicate that the shake-off shows strong T-dependence which cannot be understood in terms of semiconductor-like intra-band relaxation. The explanation proposed here is that the relaxation proceeds via localized states and is similar on both sides of the I-M transition.

The behaviour can be modelled in the same way as in disordered semiconductors with simple activated carrier hopping above about 100 K and VRH below this temperature, behaviour that has already been observed in transport measurements, albeit only in the insulating phase[5]. The alternative power law fits expected in disordered semiconducor[6] may describe the data quite well especially for the insulating material. However, the exponent is grater than 2 (in the metallic phase), which does not agree with the disordered polaron hopping model, we presently prefer to use the description of activated hopping above 100 K with possible deviation below this temperature because of another relaxation mechanism.

The presence of localized states within 2 eV of E_F in the metallic phase of the cuprates does not exclude the simultaneous presence of "free" carriers as well. The Fermi surface anisotropy takes care of that, the flat, "extended van Hove" bands in photoemission and the mid-infrared feature observed in the $\sigma(\omega)$ of all the optimally doped materials being indication of carriers with large effective mass m^*, while the Drude-like carriers seen in the $\sigma(\omega)$ below 500 cm^{-1} being indication of nearly-free-carriers. The interplay between the two makes for interesting possibilities for constructing a superconductivity mechanism.

ACKNOWLEDGMENTS

We wish to acknowledge G.Collin and H.Noel for single crytals of $YBa_2Cu_3O_{7-\delta}$. Part of the funding for this work has been provided by the European Commission which we gratefully acknowledge.

[1] See for example chapter on relaxation processes in *"High Excitation and Short Pulse Phenomena"* Ed. M.H.Pilkhun (North Holland, 1985)
[2] A.J.Scholten, A.V.Akimov and J.I.Dijkhuis, Phys.Rev.B **47**, 13910 (1993)
[3] D.Mihailovic and I.Poberaj, Phys.Rev.B **50**,6426 (1994)
[4] K.Seeger *"Semiconductor Physics"* sect. 6.11 - 6.12 (Springer, 1985)
[5] Wu.Jiang, J.L.Peng, J.J.Hamilton and R.L.Greene, Phys.Rev.B **49**, 690 (1994)
[6] A.R.Long, Adv.Phys. **31**, 553 (1982), S.R.Elliott, Adv. Phys. **36**, 135 (1987)

Easy access to vital information on COMPACT DISK!

NATO Science & Technology Disk

NATO-PCO DATABASE & AGARD AEROSPACE DATABASE

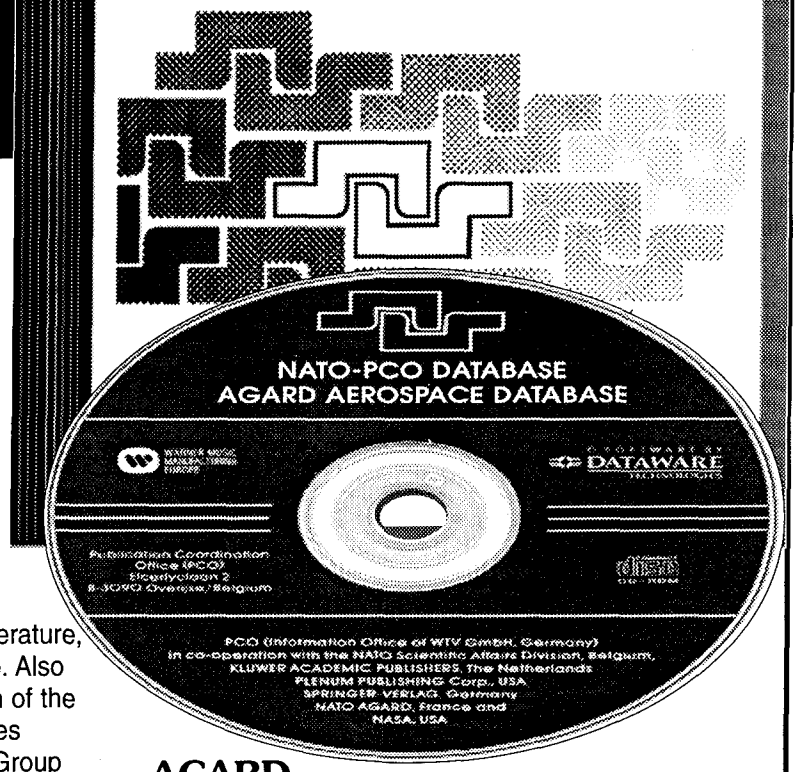

Two important databases for scientists and engineers working in universities, research institutes, and industry

IFI/Plenum Data Corporation is pleased to announce the enhanced version of the NATO Science and Technology Disk—the computer-readable compact disk (CD-ROM). It contains the first major update of the NATO-PCO database containing over *40,000* bibliographic records of non-military scientific/technical literature, sponsored by the NATO Science Committee. Also featured *for the first time* is a special version of the AGARD Aerospace Database, which provides access to proceedings of NATO's Advisory Group for Aerospace Research and Development. The easy-to-follow menu option of the retrieval software offers simple and fast access to the well-structured data.

The CD-ROM can be used with standard Personal Computer equipment (PC XT/AT or 100% compatible, minimum 512 KByte RAM and with MS-DOS/PC-DOS version 3.0 and above) including a CD-ROM drive.

NATO-PCO Database

The NATO-PCO Database covers *over 20 years* of non-military scientific/technical meetings and publications in the NATO Advanced Study Institutes Series. It contains *full* references—complete with keywords and/or abstracts—to more than 40,000 contributions from renowned international scientists. The Database covers a broad spectrum of disciplines, including • life sciences • ecology • medicine • chemistry • geosciences • astronomy • mathematical and physical sciences • behavioral sciences • materials sciences • engineering • systems and computer sciences.

AGARD Aerospace Database

This unique bibliographic database, generated by PCO in cooperation with NASA (USA) and AGARD (France), provides vital information on *thousands* of AGARD-sponsored publications—conference proceedings, AGARDographs (major works of long-lasting interest), lecture series, reports, and advisory reports published from about 1960-1991. The Database includes significant details not only of the publications themselves, but also of the papers contained within them, up to 40 or more in conference proceedings. AGARD's coverage includes • aerospace medicine • avionics • flight mechanics • electromagnetic wave propagation • fluid dynamics • guidance and control • propulsion and energetics • structures and materials • and technical information.

The price for the CD-ROM *containing both databases* is $790.00 excluding tax. Annual updates are planned.

For more information on the NATO SCIENCE and TECHNOLOGY DISK, please contact:

IFI/Plenum Data Corp.
3202 Kirkwood Hwy.
Suite 203
Wilmington, DE 19808
1-800-331-4955

Instructions to Contributors

1. Manuscripts, in quadruplicate and in English, should be submitted to one of the Co-Editors:

   for submission of theoretical papers:

   Dr. Vladimir Kresin
   Lawrence Berkeley Laboratories
   2-200 University of California
   Berkeley, California 94720

   for all others:

   Drs. Stuart A. Wolf and Donald U. Gubser
   Journal of Superconductivity
   P.O. Box 160
   Bowie, Maryland 20719-0160

2. Submission is a representation that the manuscript has not been published previously and is not currently under consideration for publication elsewhere. A statement transferring copyright from the authors (or their employers, if they hold the copyright) to Plenum Publishing Corporation will be required before the manuscript can be accepted for publication. The Co-Editors will supply the necessary forms for this transfer. Such a written transfer of copyright, which previously was assumed to be implicit in the act of submitting a manuscript, is necessary under the U.S. Copyright Law in order for the publisher to carry through the dissemination of research results and reviews as widely and effectively as possible.
3. Type double-spaced, and submit the original and three copies (including, where possible, copies of all illustrations and tables). All copies must be dark, sharp, and clear. Computer-generated manuscripts *must* be of letter quality (*not* dot-matrix).
4. A title page is to be provided and should include the title of the article, author's name (no degree), author's affiliation, and suggested running head. The affiliation should comprise the department, institution (usually university or company), city, and state (or nation) and should be typed as a footnote to the author's name. The suggested running head should be less than 80 characters (including spaces) and should comprise the article title or an abbreviated version thereof. For office purposes, the title page should include the complete mailing and telephone number of the one author designated to review proofs.
5. An abstract is to be provided, preferably no longer than 100–150 words.
6. A list of 4–5 key words is to be provided directly below the abstract. Key words should express the precise content of the manuscript, as they are used for indexing purposes.
7. All sections should be numbered with Arabic numerals (such as **1. INTRODUCTION**). Subsections should be identified with section and subsection numbers (such as **6.1. Second-Value Subheading**). If applicable, an independent single-number system (one for each category) should be used to label all theorems, lemmas, propositions, corollaries, definitions, remarks, examples, etc. The label (such as **Theorem 4**) should be typed with paragraph indentation, followed by a period and the theorem itself.
8. Mathematical notation should be typewritten wherever possible. If handwritten notation must be used, it should be clear and legible, with any necessary explanatory notes located in the margin. Equations should be numbered consecutively with Arabic numerals in parentheses placed flush right, and should be thusly referred to in the text [such as Eqs. (2) and (6)].
9. Illustrations (photographs, drawings, diagrams, and charts) are to be numbered in one consecutive series of Arabic numerals. The captions for illustrations should be typed on a separate sheet of paper. All illustrations must be complete and final, i.e., camera-ready. Photographs should be large, glossy prints, showing high contrast. Drawings should be prepared with india ink. Either original drawings or good-quality photographic prints are acceptable. Identify figures on the back with author's name and number of the illustration. Reproduction of illustrations in color is possible by special arrangement, with the total cost, which is significant, borne by the author.
10. Tables should be numbered (with Roman numerals) and referred to by number in the text. Each table should be typed on a separate sheet of paper.
11. List references numerically at the end of the paper. Use the appropriate Arabic numeral in square brackets for citation in the text. Where there are three or more authors, only the first author's name is given in the text, followed by *et al.* References should include (in this order): initials and last names of *all* authors, name of publication, volume number, starting page or inclusive pages, and year published. The style and punctuation of the references should conform to that used in the journal—illustrated by the following examples:

    Journal Article

    1. T. Ōgushi, Y. Hakuraku, Y. Honjo, G. N. Suresha, S. Higo, Y. Ōzono, I. Kawano, and T. Numata, *J. Low Temp. Phys.* **70**, 485 (1988).

    Book

    2. E. W. Collings, *Applied Superconductivity, Metallurgy, and Physics of Titanium Alloys*, Vol. 2 (Plenum Press, New York, 1986).

    Contribution to a Book

    3. C. W. Chu, P. H. Hor, R. L. Meng, L. Gao, Z. J. Huang, Y. Q. Wang, and J. Bechtold, in *Novel Superconductivity*, S. A. Wolf and V. Z. Kresin, eds. (Plenum Press, New York, 1987), pp. 581–597.

12. Footnotes should be avoided. When their use is absolutely necessary, footnotes should be numbered consecutively using Arabic numerals and should be typed at the bottom of the page to which they refer. Place a line above the footnote, so that it is set off from the text. Use the appropriate superscript numeral for citation in the text.
13. After a manuscript has been accepted for publication and after all revisions have been incorporated, manuscripts may be submitted to the Editor's Office on **personal-computer disks**. Label the disk with identifying information—kind of computer used, kind of software and version number, disk format and file name of article, as well as abbreviated journal name, authors' last names, and (if room) paper title. Package the disk in a disk mailer or protective cardboard. **The disk *must* be the one from which the accompanying manuscript (finalized version) was printed out**. The Editor's Office cannot accept a disk without its accompanying, matching hard-copy manuscript. Disks will be used on a case-by-case basis—where efficient and feasible.
14. **The journal makes no page charges.** Reprints are available to authors, and order forms with the current price schedule are sent with proofs.

JOURNAL OF SUPERCONDUCTIVITY

Volume 8, Number 4 **August 1995**

Special Issue: University of Miami Workshop on High-Temperature Superconductivity, Part I of II

Because of the great number of articles in this issue, the contents listing has been placed at the front of the issue rather than here, which is its usual position